New Dithienylpyrrole-containing bipyridine ligands and corresponding Ruthenium complexes. Electronic properties and applications to photosensitization in Dye-Sensitized Solar Cells

Sajida Noureen

FACULTE DES SCIENCES ET TECHNOLOGIE

Ecole Doctorale Lorraine de Chimie et Physico-Chimie Moléculaire (SESAMES)

THÈSE

présentée pour l'obtention du titre de

DOCTEUR de l'Université de Lorraine

Mention Chimie

par

Sajida Noureen

Nouveaux ligands polypyridiniques à motifs Dithiénylpyrroles et complexes de Ruthénium correspondants. Propriétés électroniques et applications en photosensibilisation dans les cellules solaires à colorants (DSSC)

Soutenue le 4 Juin 2012
devant le jury suivant :

Rapporteurs	Mme Valérie HEITZ	Professeur, Université de Strasbourg
	M. J.A.G. WILLIAMS	Professeur, Université de Durham (Royaume Uni)
Examinateurs	M. M. BELEY	Professeur, Université de Lorraine
	M. S. CARAMORI	Assistant Professor, Université de Ferrara (Italie)
	M. A. MONARI	Maitre de Conférence, Université de Lorraine
	M. P.C. GROS	Directeur de Recherche CNRS, Université de Lorraine Directeur de Thèse

UMR CNRS - UHP 7565 (SRSMC)- Groupe Synthèse Organométallique et Réactivité
Faculté des Sciences et Technologie – Université de Lorraine
BP 239, 54506 Vandoeuvre-lès-Nancy Cedex

FACULTE DES SCIENCES ET TECHNOLOGIE

Ecole Doctorale Lorraine de Chimie et Physico-Chimie Moléculaire (SESAMES)

THÈSE

présentée pour l'obtention du titre de

DOCTEUR de l'Université de Lorraine

Mention Chimie

par

Sajida Noureen

New Dithienylpyrrole-containing bipyridine ligands and corresponding Ruthenium complexes. Electronic properties and applications to photosensitization in Dye-Sensitized Solar Cells

Soutenue le 4 Juin 2012
devant le jury suivant :

Rapporteurs	Mme Valérie HEITZ	Professeur, Université de Strasbourg
	M. J.A.G. WILLIAMS	Professeur, Université de Durham (Royaume Uni)
Examinateurs	M. M. BELEY	Professeur, Université de Lorraine
	M. S. CARAMORI	Assistant Professor, Université de Ferrara (Italie)
	M. A. MONARI	Maitre de Conférence, Université de Lorraine
	M. P.C. GROS	Directeur de Recherche CNRS, Université de Lorraine Directeur de Thèse

UMR CNRS - UHP 7565 (SRSMC)- Groupe Synthèse Organométallique et Réactivité
Faculté des Sciences et Technologie – Université de Lorraine
BP 239, 54506 Vandoeuvre-lès-Nancy Cedex

Acknowledgements

I am very grateful to the Islamia University of Bahawalpur, Pakistan (IUB), my alma mater and my institution of work, for a full financement of my PhD studies. I find myself very lucky to be among those faculty members who were selected under the Faculty Development Program (FDP) of the university, as the university is trying to come at par with the other world class institutions. The governing board of the university is greatly admired for providing equal opportunity to all the competing candidates.

I am indebted to Professor Yves Fort, Director of SRSMC for his generous acceptance of my candidature and the way he welcomed me to his lab and introduced me to my supervisor, Dr. Philippe Gros.

I am immensely pleased to place on record my profound gratitude and heartfelt thanks to Dr. Philippe Gros. It is a real pleasure to work with such a polite, honest and open-minded person. In the beginning he used to guide me just like kids as I had a little training in organic synthesis. His patience while instructing is remarkable. We experienced together all the ups and downs of routine work, the shared happiness of success and the depression of failure whenever things used to go wrong. I would also acknowledge his constant support and help to manage with my deficiency of French language throughout my PhD. Specially, the French summary would not have come to life without his efforts. No doubt, without his active involvement, this thesis could not have been completed in a comparatively short duration of less than three years.

My success equally owes itself to Prof. Marc Beley who co-supervised my work. He is infact a very caring and kind person. He taught and guided me in every aspect of my PhD work since the day I started. He is not only a good teacher but a very sincere friend also. He always kept his door open to any of my questions and problems, and always provided smart solutions for any practical problem I had during my research. I really learned many chemistry techniques from him.

I, gratefully acknowledge prof. Carlo A. Bignozzi, Dr. Roberto Argazzi and Dr. Stefano Caramori for their collaboration to evaluate photophysical properties and photovoltaic applications and valuable explanations. I am also grateful to Dr. Antonio Monari and Prof. Xavier Assfeld for their collaboration to carry out computational analysis.

This thesis could not have been completed in time without the timely technical help by Brigitte Fernette for NMR, Stéphane Parant for UV-Vis, Sandrine Adach for elemental analysis and François Dupire for Mass Spectrometry. The CRM2 lab is also acknowledged for their help in solving the crystal structures of certain compounds.

I would like to acknowledge my colleagues Olivier, Zein, Naoual, Thibaut, Adeline, Tioga, Dominique and Fabian for many good experiences throughout the last three years. I had some very nice former colleagues in the form of Thanh Chau and Fredo whose company was a great fun. They were always ready to help me and used to take great care of mine. Specially the funny gestures of Fredo shall always make me laugh. He was a very lively person. In fact, the whole team at SOR is worth admiring and I find myself lucky to be among so cooperative and sincere colleagues.

I feel short of a proper expression to express my gratitude for my parents. However, I can simply say that my existence and success owes to them. It is a moment of great pride and honor for me while submitting this manuscript as it is a fulfillment of their cherished dream. It is certainly due to their silent prayers that things become easy for me. My sisters have been my best and I love them and thank them for all their encouragements and support. The moral support and care of my in laws is worth high esteem.

And finally my husband Maqsood Ahmed, for his love and support. He is simply the best.

List of Abbreviations

AcOH	acetic acid
AM	air mass
APCI	Atmospheric-pressure chemical ionization
bpy	bipyridine
CE	counter electrode
Cps	counts per seconds
CT	Charge transfer
CTTS	charge transfer to solvent
CV	cyclic voltammetry
dcbpy	dicarboxy bipyridine
DFT	Density functional theory
DIBAL-H	diisobutylaluminium hydride
DMF	Dimethylformamide
DMSO	Dimethyl sulfoxide
dppe	1,2-Bis(diphenylphosphino)ethane
DSSCs	Dye-sensitized solar cells
DTB	4,4-ditertiobutyl-2,2'-bipyridine
DTP	dithienylpyrrole
ECD	electrochromic device
EQE	external quantum efficiency
eV	electron volt
ff	fill factor
FTIR	Fourier transform infrared
FTO	Fluorine doped tin oxide
FWHM	Full width at half maximum
HOMO	highest occupied molecular orbital
HRMS (ESI)	high-resolution mass spectrometry (Electrospray ionization)
G	global
GC-MS	Gas chromatography–mass spectrometry
ILCT	intraligand charge transfer
IMVS	intensity-modulated photovoltage spectroscopy
IPCE	incident photon-to-current conversion efficiency
J/V curve	Current/Voltage curve
LC	ligand-centered
LDA	lithium diisopropylamide
LHE	light-harvesting efficiency
LLCT	ligand-to-ligand charge transfer
LMCT	ligand-to-metal charge transfer
LiTMP	Lithium tetramethylpiperidine
LUMO	lowest unoccupied orbital
MC	metal-centered

MLCT	metal-to-ligand charge transfer
NBS	*N*-Bromosuccinimide
NLO	non-linear optics
NTO	Natural Transition Orbitals
OFEDs	organic field-effect transistors
OLEDs	organic light-emitting diodes
ORTEP	Oak Ridge Thermal Ellipsoid Plot Program
OSCs	organic solar cells
PCM	polarizable continuum model
PE	photoelectrode
PMII	1-propyl-3-methyl-imidazolium iodide
p-TsOH	*p*-Toluenesulfonic acid
PV	photovoltaic
SAMs	self-assembled monolayers
SCE	Saturated calomel electrode
SNS	2,5-di(2-thienyl)- 1*H*-pyrrole
SVD	singular value decomposition
TA	Transient absorption
TBA	Tetrabutylammonium
t-BuOK	Potassium *tert*-butoxide
t-Bupy	4-*t*-Butyl pyridine
TCSPC	time correlated single photon counting
TDDFT	time dependent density functional theory
TLC	Thin layer chromatography
TMEDA	Tetramethylethylenediamine
TMS	Tetramethylsilane
TMSCl	Trimethylsilyl chloride
TW	terawatts
UV-Vis	Ultraviolet visible
V_{OC}	open-circuit potential
XRD	X-ray diffraction

Table of Contents

Index of Ligands and Complexes

DTP_1 Series Ligands

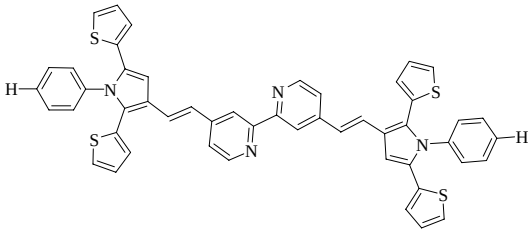

bpy(DTP_1-H)

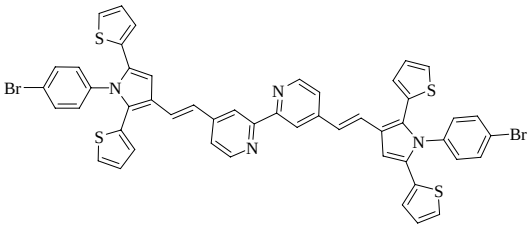

bpy(DTP_1-Br)

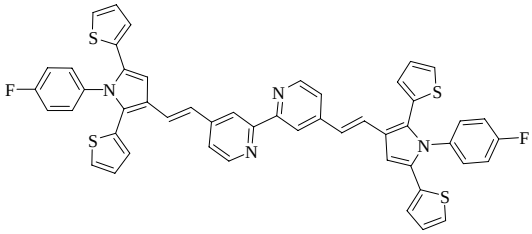

bpy(DTP_1-F)

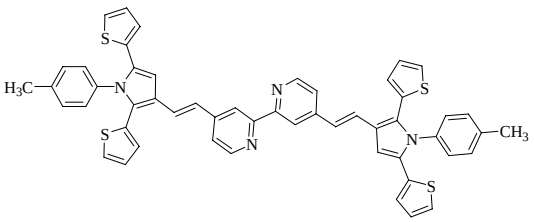

bpy(DTP_1-Me)

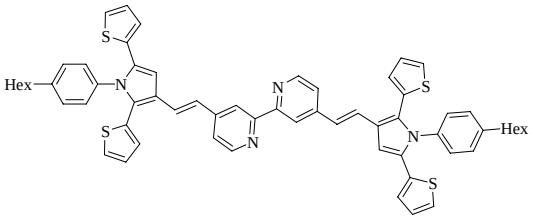

bpy(DTP_1-Hex)

DTP_2 Series Ligands

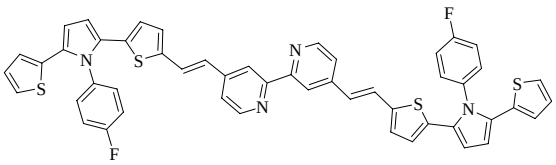

bpy(DTP_2-F)

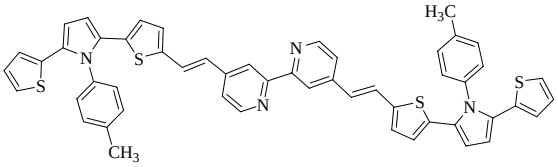

bpy(DTP_2-Me)

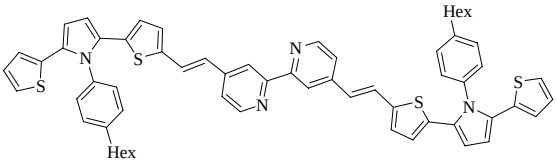

bpy(DTP_2-Hex)

Homoleptic complexes of DTP_1 Series Ligands

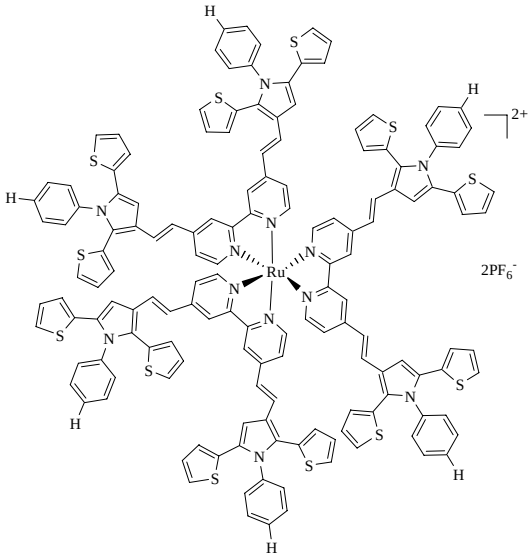

Ru[bpy(DTP_1-H)]$_3$ (PF_6)$_2$

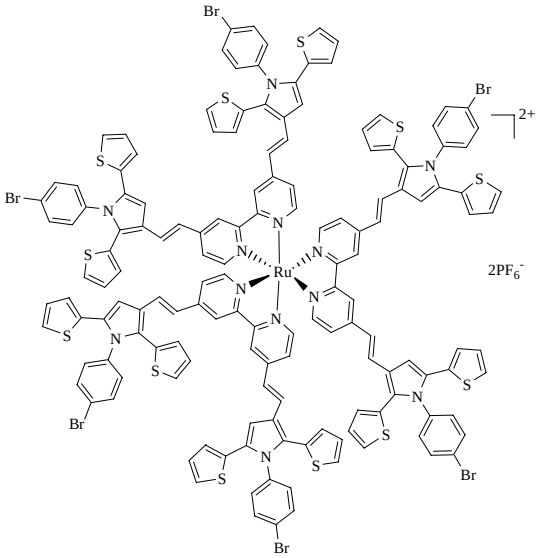

Ru[bpy(DTP_1-Br)]$_3$ (PF_6)$_2$

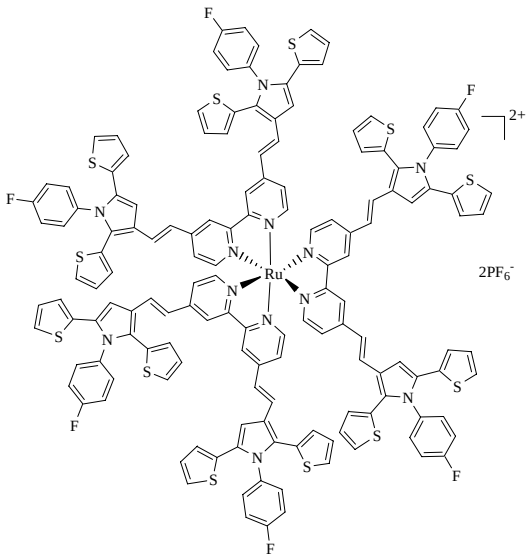

Ru[bpy(DTP$_1$-F)]$_3$ (PF$_6$)$_2$

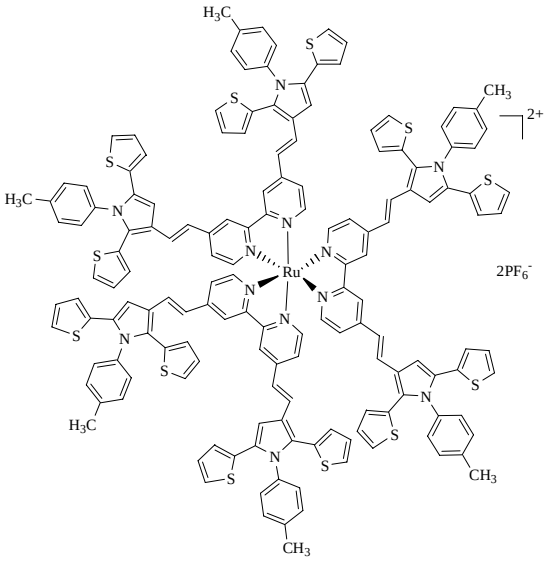

Ru[bpy(DTP$_1$-Me)]$_3$ (PF$_6$)$_2$

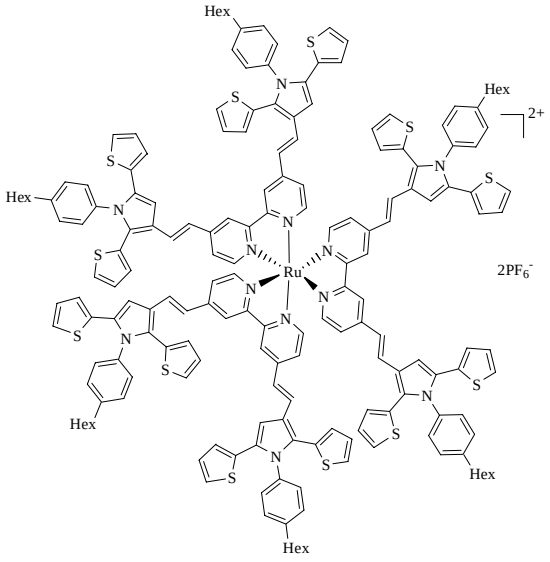

Ru[bpy(DTP$_1$-Hex)]$_3$ (PF$_6$)$_2$

Homoleptic complexes of DTP_2 Series Ligands

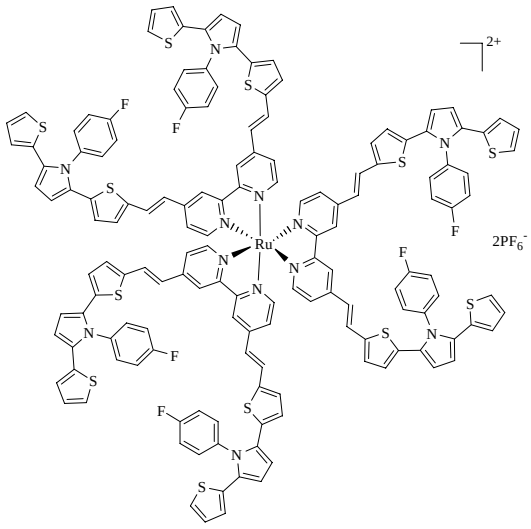

$Ru[bpy(DTP_2\text{-}F)]_3\ (PF_6)_2$

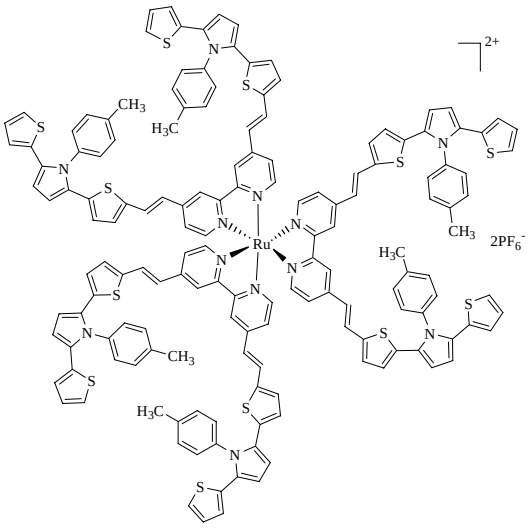

$Ru[bpy(DTP_2\text{-}Me)]_3\ (PF_6)_2$

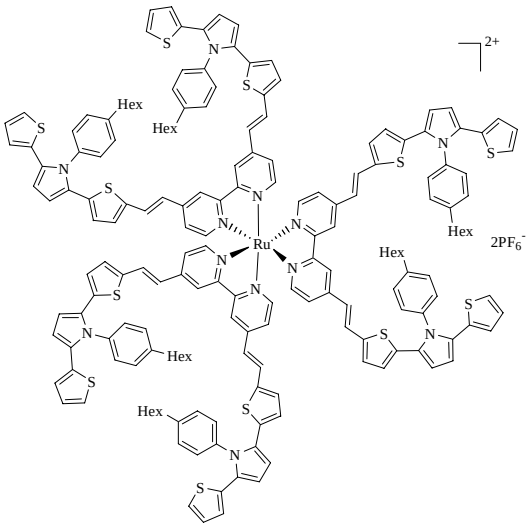

$Ru[bpy(DTP_2\text{-}Hex)]_3\ (PF_6)_2$

Bis-heteroleptic complexes

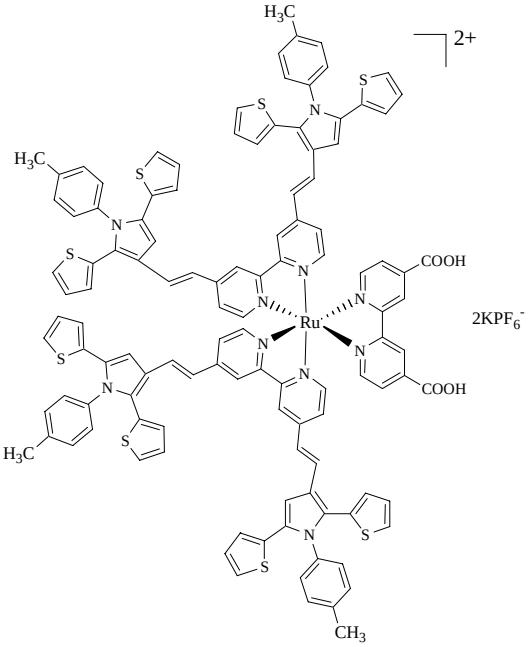

[Ru{bpy(DTP$_1$-Me)}$_2$(dcbpy)](PF$_6$)$_2$

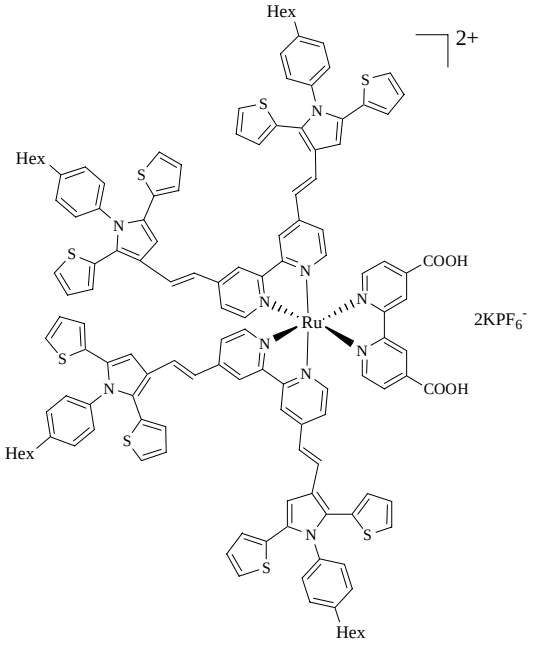

[Ru{bpy(DTP$_1$-Hex)}$_2$(dcbpy)](PF$_6$)$_2$

Tris-heteroleptic complexes of DTP$_1$ Series Ligands

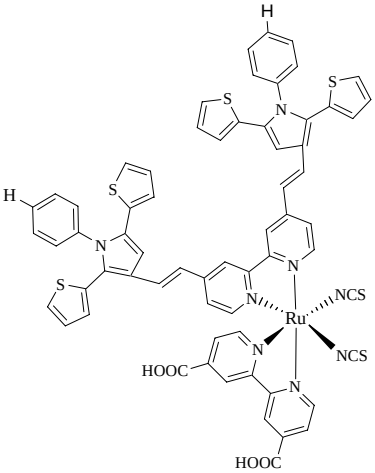

[Ru{bpy(DTP$_1$-H)}(dcbpy)(NCS)$_2$]

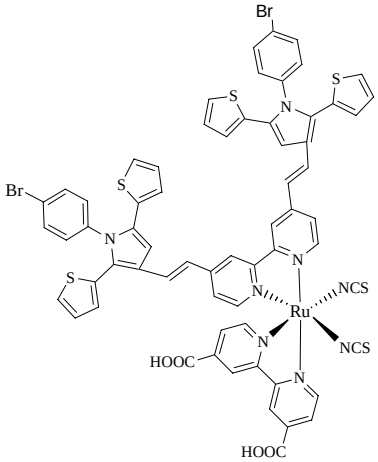

[Ru{bpy(DTP$_1$-Br)}(dcbpy)(NCS)$_2$]

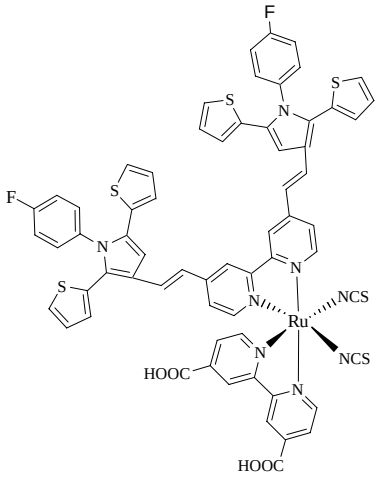

[Ru{bpy(DTP$_1$-F)}(dcbpy)(NCS)$_2$]

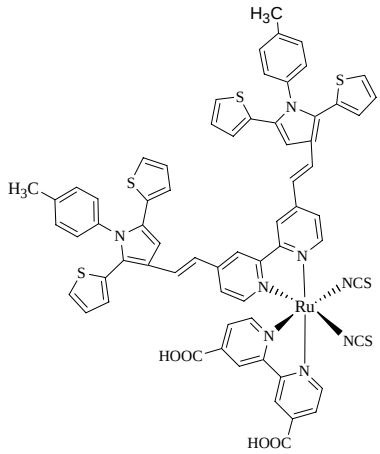

[Ru{bpy(DTP$_1$-Me)}(dcbpy)(NCS)$_2$]

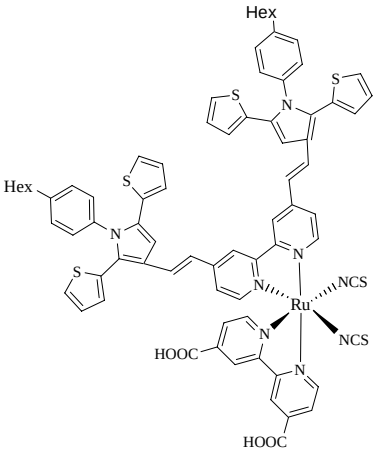

[Ru{bpy(DTP$_1$-Hex)}(dcbpy)(NCS)$_2$]

Tris-heteroleptic complexes of DTP$_2$ Series Ligands

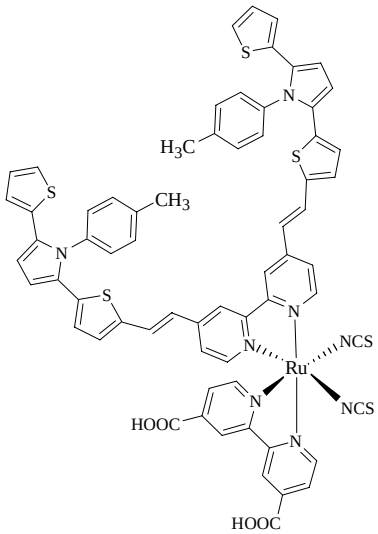

[Ru{bpy(DTP$_2$-Me)}(dcbpy)(NCS)$_2$]

Chapitre No: 1

Introduction en français

La consommation énergétique mondiale est de 4.1×10^{20} joules/an soit 13 térawatts (TW) Essentiellement basée sur les énergies fossiles. Cette demande est appelée à tripler d'ici la fin du siècle. Le développement de sources d'énergie propres et renouvelable est donc le grand challenge pour nos sociétés modernes **[1-3].**

La source primaire d'énergie la plus propre et abondante qui vient à l'esprit est évidemment le soleil qui apporte 120000 TW de radiation à la surface de la terre et donc bien au delà des besoins humains. Les technologies utilisées jusqu'ici pour exploiter cette source à base de panneaux photovoltaïques restent de prix élevé et à applications limitées ce qui a considérablement limité de développement à grande échelle. C'est pourquoi, il est indispensable de développer des technologies moins couteuses et plus performantes pour rendre les énergies renouvelables accessibles à une large population.

1.1. Les cellules classiques à jonction P-N

Dans les cellules conventionnelles à semi conducteur solide, les électrons et les trous sont séparés par création d'un champ électrique à la jonction P-N. La jonction P-N est obtenue en combinant des blocs de semiconducteurs dopés de façon opposée [**4**]. Par exemple, silicium dopé au bore (type p contenant les trous) et silicium dopé au phosphore (type n contenant les électrons).

Figure 1.1: Structure d'une cellule silicium dopé

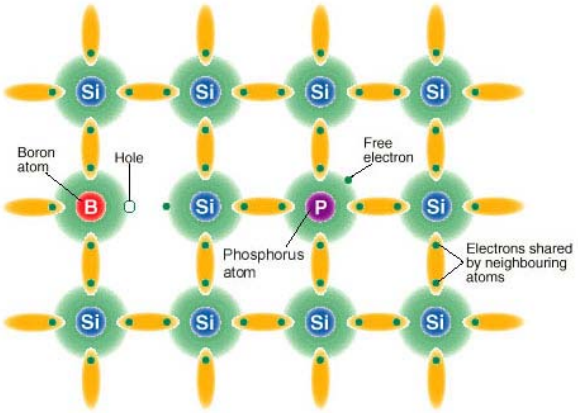

Figure 1.2: Fonctionnement d'une cellule conventionnelle

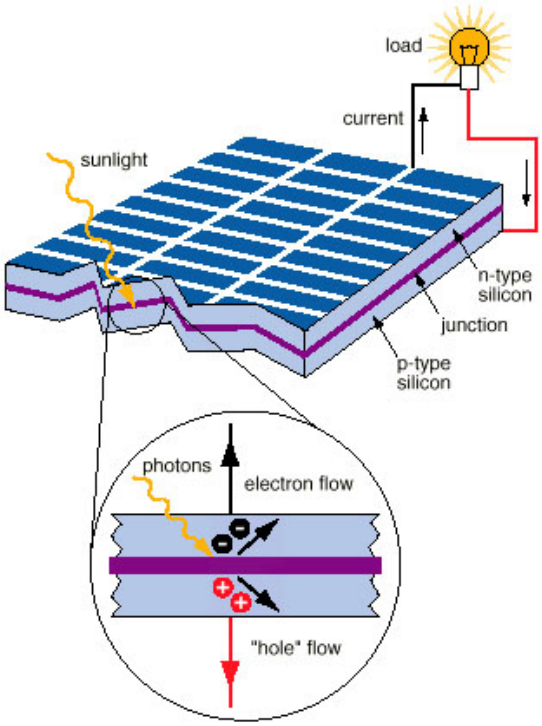

1.2. Les trois générations de cellules

Les cellules solaires peuvent être classées en trois générations **[3]**. **Les cellules de première génération.** Elles utilisent du silicium de très haute pureté (monocristallin) et représentent 90% de l'offre actuelle. Le coût est très dépendant du prix du matériau silicié **[3, 5].**

Les cellules de seconde génération. Elles utilisent la technologie couche mince. Les plus efficaces sont les cellules CIGCS (Cd-In-Ga-Se) et Cd-Te. Elles deviennent compétitives avec une apparence attrayante et la possibilité d'utilisation en support flexible **[6].**

Les cellules de troisième génération. Ces dernières années de nouveaux concepts sont apparus : les cellules solaires à colorant "dye-sensitized solar cells" (DSSCs), les cellules

polymères et les cellules nanocristallines. L'objectif est de produire des cellules à grande échelle à coût faible.

Les DSSC ont focalisé l'attention en raison de leur efficacité de conversion de la lumière solaire en électricité, de leur couleur ou encore esthétique et surtout faible coût de production. Elles sont basées sur la photosensibilisation d'oxydes métalliques nanocristallins par adsorption of de colorants. Depuis les travaux pionniers de O'Regan et Grätzel en 1991 **[7],** les progrès ont été considérables faisant de ces cellules une alternative très sérieuse à tel point qu'elles ont pu être mises sur le marché par G24 Innovations Limited (G24i) qui les fabrique à grande échelle. Plus récemment les chercheurs se sont focalisés sur le côté fondamental de compréhension du rôle de chaque composant de la cellule et de leurs interactions.

1.3. Fonctionnement des DSSC

Le fonctionnement d'une DSSC est assuré par 5 composants (voir schéma de principe Fig.1.3):

1. Un support conducteur transparent.
2. Un film nanocristallin semiconducteur (en général TiO_2)
3. Un photosensibilisateur (Dye) adsorbé à la surface du semiconducteur
4. Un électrolyte contenant un médiateur (usuellement I^-/I_3^-).
5. Une contre électrode pour régénération du médiateur (Pt).

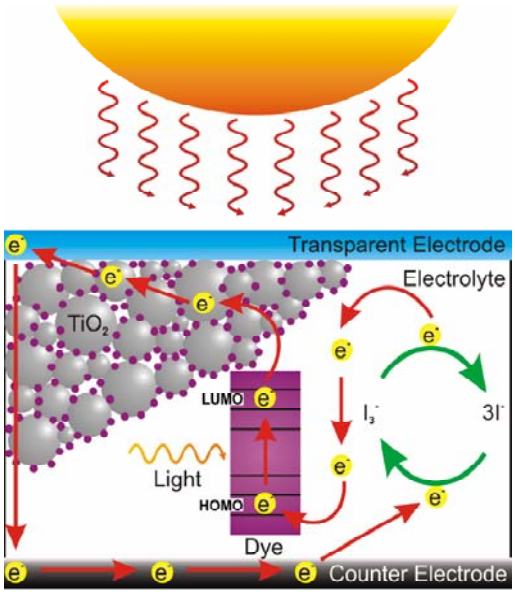

Figure 1.3: Schéma de principe d'une DSSC.

La première étape est l'absorption d'un photon par le colorant D (Eq. 1), qui conduit à la forme excitée D^* qui injecte alors un électron dans la bande de conduction du semiconducteur, produisant alors une oxydation du colorant en D^+ (Eq. 2). Les électrons transitent alors jusqu'à la contre electrode pour réduire le médiateur (Eq. 3) qui à son tour régénère le colorant (Eq. 4). Ceci complète le circuit **[8].**

$$D_{(adsorbed)} + hv \rightarrow D^*_{(adsorbed)} \quad \textbf{(1)}$$

$$D^*_{(adsorbed)} \rightarrow D^+_{(adsorbed)} + e^-_{(injected)} \quad \textbf{(2)}$$

$$I_3^- + 2e^-_{(cathode)} \rightarrow 3I^-_{(cathode)} \quad \textbf{(3)}$$

$$D^+_{(adsorbed)} + \frac{3}{2}I^- \rightarrow D_{(adsorbed)} + \frac{1}{2}I_3^- \quad \textbf{(4)}$$

Ce processus donne lieu également à des recombinaisons diminuant les performances de la cellule telles que la recombinaison des électrons injectés avec, soit le colorant oxydé (Eq. 5) ou avec la forme oxydée du médiateur à la surface du semiconducteur (Eq. 6).

$$D^+_{(adsorbed)} + e^-_{(TiO_2)} \rightarrow D_{(adsorbed)} \quad \textbf{(5)}$$

$$I_3^- + 2e^-_{(TiO_2)} \rightarrow 3I^-_{(anode)} \quad \textbf{(6)}$$

L'IPCE (incident photon-to-current conversion efficiency, aussi appelée EQE (external quantum efficiency) est une caractéristique importante de la cellule. Elle permet, dans des cellules identiques de comparer la capacité des colorants à collecter les photons. Elle se définit par le rapport entre le nombre d'électrons générés par la lumière dans le circuit externe et le nombre de photons incidents en fonction de la longueur d'onde d'excitation (Eq. 7) **[9].**

$$\mathrm{IPCE}(\lambda) = \frac{\text{Photocurrent density}}{\text{Wavelength} \times \text{Photon flux}} = \mathrm{LHE}(\lambda) \times \varphi_{inj} \times \eta_{coll} \quad \textbf{(7)}$$

LHE(λ) représente l'efficacité de la collecte à la longueur d'onde λ , φ_{inj} est le rendement quantique d'injection dans la bande conduction et η_{coll} est l'efficacité de la collecte

Le rendement global *(η)* de la DSSC est alors déterminé selon l'équation 8 impliquant la densité de photocourant en court-circuit Jsc, le photovoltage en circuit ouvert Voc, le facteur de forme *ff*, et la puissance de la lumière incidente I_S **[10].**

$$\eta_{global} = \frac{J_{SC} \cdot V_{OC} \cdot ff}{I_S} \qquad \textbf{(8)}$$

On voit ici qu'en plus des propriétés du semiconducteur et du médiateur redox, les propriétés photophysiques et électrochimiques du photosensibilisateur seront en grande partie responsables des performances de la cellule. En effet, son potentiel d'oxydation déterminera la Voc maximale et les propriétés d'absorption détermineront le courant de court circuit **[8]**.

1.3.1. Les photosensibilisateurs

La photosensibilisation de TiO_2 a été étudiée à l'aide de nombreux colorants organiques ou inorganiques. Le colorant idéal doit absorber la majeure partie des les longueurs d'onde du spectre solaire jusqu'à environ 920 nm. Il doit être adsorbé très efficacement à la surface du semiconducteur et injecter les électrons avec un rendement quantique très élevé. Son potentiel redox doit être suffisamment élevé pour pourvoir être régénéré efficacement par le médiateur. Enfin, il doit être stable pour pouvoir supporter 10^8 cycles redox sous irradiation solaire soit 20 ans d'exposition **[11].**

Les colorants à base de complexes métalliques sont les plus utilisés tels que les complexes polypyridiniques de ruthénium ou d'osmium, les porphyrines métalliques, les quantum dots inorganiques. Les colorants organiques naturels et synthétiques se développent également. Les colorants inorganiques présentent en général une meilleure stabilité thermique et chimique.

Les complexes à base de ruthénium **[12]** présentent les caractéristiques les plus adaptées qui sont un large spectre d'absorption, un positionnement adéquat des niveaux d'énergie des états excités et fondamentaux, des durées de vie à l'état excité relativement longues et une bonne stabilité (électro) chimique.

1.3.2. Les complexes de ruthenium

Le premier complexe performant a été découvert en 1993 il s'agit du N3 [bis(isothiocyanato)-bis(2,2'-bipyridyl-4,4'-carboxylate) ruthenium(II)] **[13].** Il absorbe jusqu'à 800 nm. Les

performances du N3 on été surpassées ensuite par le N749 [tri(isothiocyanato)-2,2',2''-terpyridyl-4,4',4''-tricarboxylate) ruthenium(II)] aussi appelé « black dye » **[14].**

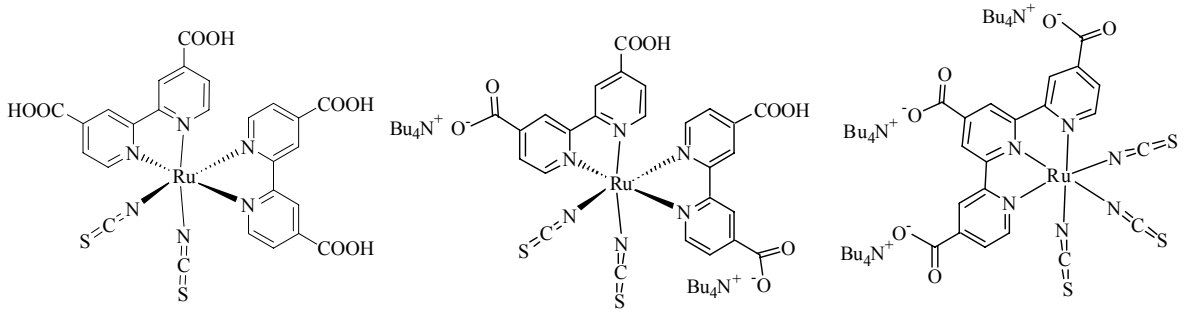

N3 **N719** **N749**
Black dye

Des améliorations ont ensuite été apportées par déprotonnation de certaines fonctions carboxyliques du N3. Le complexe doublement déprotonné $(Bu_4N)_2[Ru(dcbpyH)_2(NCS)_2]$, appelé N719 montre une meilleure efficacité que le N3 **[15].**

Le groupe de Gratzel a étudié la modification du ligand bipyridine (alkyl, alkoxy, phenylene, etc.) avec l'objectif d'accrître le coefficient d'extinction molaire, de supprimer l'agrégation du colorant à la surface de TiO_2 et d'optimiser les potentiels redox. Le complexe amphiphile Z907 se montre très stable thermiquement. En combinaison avec l'acide hexadecyl phosphonique comme coadsorbeur, 7 % d'efficacité ont été obtenus sur un longue période **[16].** L'introduction de systemes π-délocalisés permet d'optimiser la fenêtre d'absorption, le complexe Z9103-portant le methoxystyryl donne une efficacité de 10.2 % **[17].**

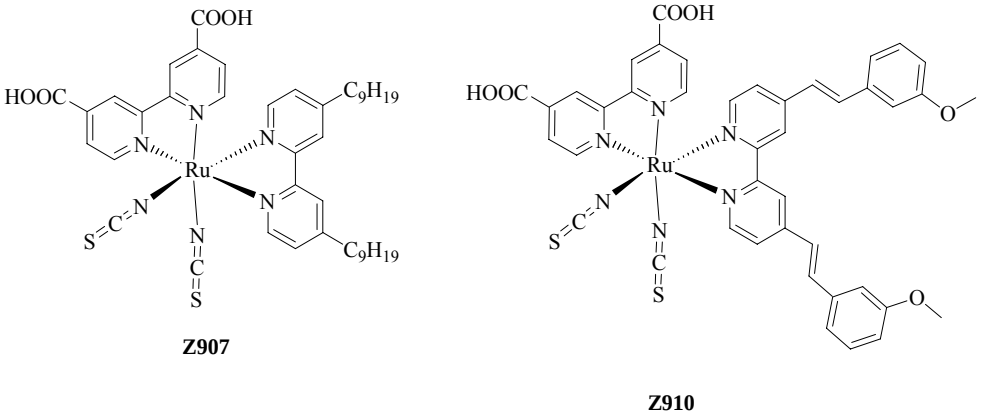

Z907 **Z910**

Nazeeruddin et coll. Ont également introduit de la delocalisation au niveau de la function carboxylique K9 and K23 **[18]** génèrent des photo-courants plus importants que Z907 et montrent une absoption étendue dans le proche infra rouge.

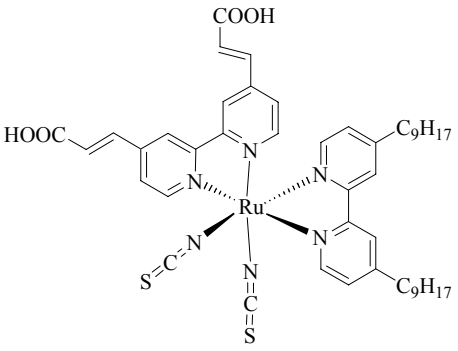

K9

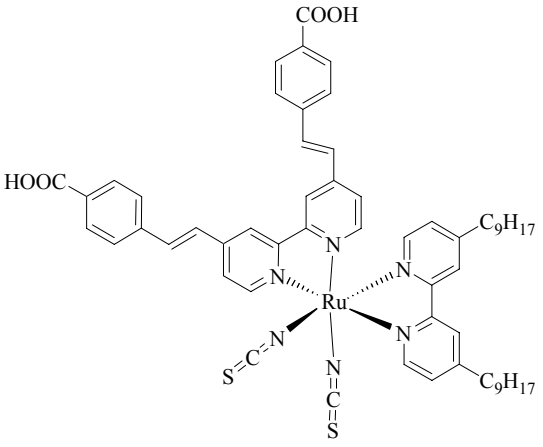

K23

De nouvelles familles de colorants à haut coefficient d'absorption molaire ont été décrites récemment par Wang et coll **[19].** le colorant C101 a permis d'atteindre un rendement de 11%. Ko et coll. ont introduit des antennes de type fluorene qui contribuent grandement à accroître l'absorbance **[20].** JK56 donne un IPCE de 83% IPCE et un rendement de 9.2%.

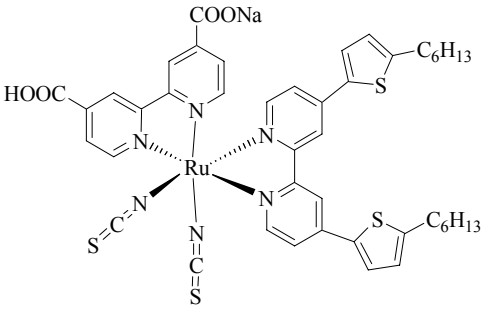

C101

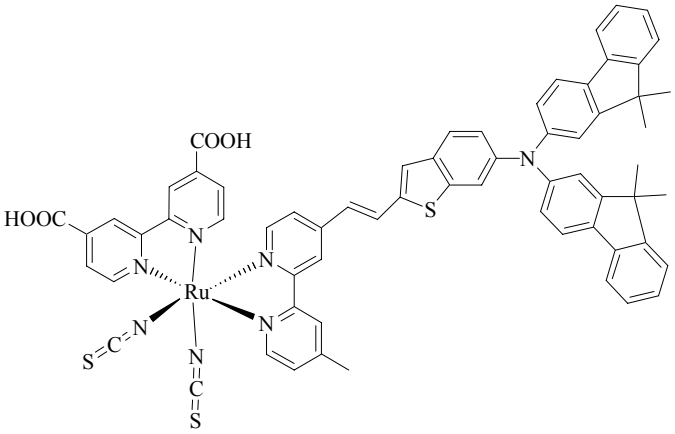

JK56

De nombreux travaux ont consisté à essayer de remplacer le ruthenium par d'autres métaux tels que l'osmium **[21],** le rhénium **[22],** le fer **[23],** le platine **[24]** ou encore le cuivre **[25].** Mais jusqu'à présent, les complexes de ruthénium offrent les meilleures performances et stabilité et sont les seuls à permettent d'atteindre les 10% de rendement.

1.3.3. Travaux antérieurs du groupe

Le groupe SOR a développé de nouveaux colorants à base de ligands N-pyrrolo-bipyridine. Des complexes homoléptiques, bis- et tris-hétéroleptiques ont été préparés et caractérisés **[26]**.

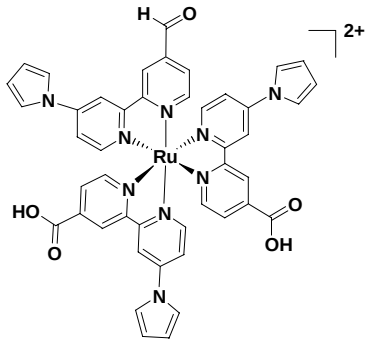

SOR_1

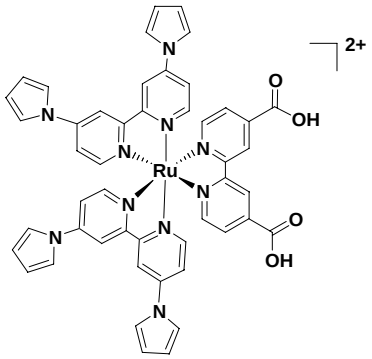

SOR_2

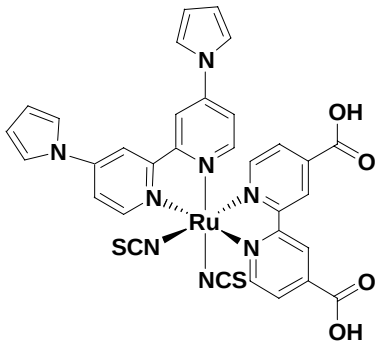

SOR_3

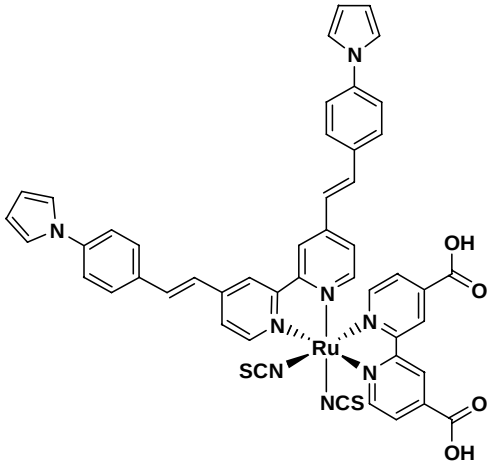

SOR_4

Parmi ces complexes, les colorant SOR_3 et SOR_4 sont les plus prometteurs pour plusieurs raisons. Le pyrrole lié par son azote à la bipyridine apporte des effets électroniques donneurs ce qui accroît le niveau énergétique de l'orbitale HOMO du métal permettant à la transition MLCT d'opérer à basse énergie et donc de produire un effet bathochrome sur le spectre d'absorption.

De plus, la π-délocalisation dans le colorant SOR_4 permet d'obtenir une fenêtre spectrale très élargie même meilleure que celle de N3 ($Ru(dcbpy)_2(NCS)_2$).

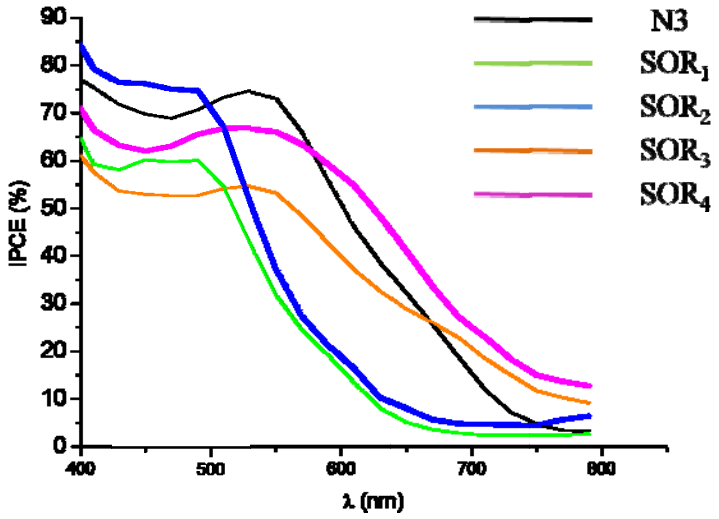

Figure 1.5: Courbes IPCE des complexes à base de pyrroles développés par le groupe

De plus, nous avons montré en utilisant la spectroscopie laser que le motif pyrrolostyryle permet d'assurer une protection de surface limitant la recombinaison des électrons injectés avec la forme oxydée du médiateur.

A partir de ces premiers résultats, nous allons poursuivre dans l'optimisation de la structure des colorants en prenant en compte les caractéristiques suivantes :

1. Il est impératif de diminuer l'énergie nécessaire au transfert MLCT. Des motifs thiophènes donneurs seront incorporés à nos ligands en synthétisant des motifs mixtes pyrrole-thiophène **[27].**
2. Afin d'accroître les coefficient d'extinction molaire, les nouveaux motifs seront liés aux bipyridines par des systèmes conjugués **[28].**
3. L'objectif est que les nouveaux substituants des bipyridines puissent jouer le rôle d'antennes collectrices de photons dont le domaine d'absorption sera complémentaire de celui du complexe métallique **[29].**

1.4. Références

[1] Service, R.F. *Science*, 2005, ***309***, 548.

[2] U.S. Energy Information Administration (EIA) "International Energy Outlook 2010", (2010) Web site: http://www.eia.doe.gov/oiaf/ieo/index.html

[3] Kalyanasundaram, K. *Dye sensitized solar cells*, EPEL press: Switzerland, 2010.

[4] Nelson, J. *The Physics of Solar Cells*; Imperial College Press: London, 2003.

[5] Green, M.A. *Third Generation Photovoltaics: Advanced Solar Energy Conversion.* Springer- Verlag: Berlin, Germany, 2004.

[6] Wronski, C.R. *Conference Record of the 28th IEEE Photo*Voltaic *Specialists Conference, Anchorage, AK*; IEEE: New York, 2000.

[7] O'Regan*, B.;* Grätzel*,* M. *Nature 1991*, 353, 737.

[8] Nazeeruddin, M.K.; Baranoff, E.; Grätzel, M. *Solar energy*, 2011, **85**, 1175.

[9] Hagfeldt, A.; Grätzel, M. *Chem. Rev.* 1995, **95**, 49.

[10] Nazeeruddin, M.K.; Kay, A.; Rodicio, I.; Humphry-Baker, R.; Muller, E.; Liska, P.; Vlachopoulos, N.; Grätzel, M. *J. Am. Chem. Soc.* 1993, **115**, 6382.

[11] Hagfeldt, A.; Grätzel, M. *Accounts of Chemical Research*, 2000, **33(5)**, 269.

[12] (a) Haque, S.A.; Palomares, E.; Cho, B.M.; Green, A.N.M.; Hirata, N.; Klug, D.R.; Durrant, J.R.; *J. Am. Chem. Soc.* 2005, **127**, 3456. (b) Klein, C.; Nazeeruddin, M.K.; Liska, P.; Di Censo, D.; Hirata, N.; Palomares, E.; Durrant, J.R. M. Grätzel, *Inorg. Chem.* 2005, **44**, 178. (c) Nazeeruddin, M.K.; Klein, C.; Liska, P.; Grätzel, M. *Coord. Chem. Rev.* 2005, **249**, 1460. (d) Nazeeruddin, M.K.; Wang, Q.; Cevey, L.; Aranyos, V.; Liska, P.; Figgemeier, E.; Klein, C.; Hirata, N.; Koops, S.; Haque, S.A.; Durrant, J.R.; Hagfeldt, A.; Lever, A.B.P.; Grätzel, M. *Inorg. Chem.* 2006, **45,** 787.; (e) Hirata, N.; Koops, S.; Haque, S.A.; Durrant, J.R.; Hagfeldt, A.; Lever, A.B.P.; Grätzel, M. *Inorg. Chem.* 2006, **45,** 787. (f) Schmidt-Mende, L.; Kroeze, J.E.; Durrant, J.R.; Nazeeruddin, M.K.; Grätzel, M. *Nano Lett.* 2005, **5**, 1315. (g) Wang, P.; Klein, C.; Humphry-Baker, R.; Zakeeruddin, S.M.; Grätzel, M. *J. Am. Chem. Soc.* 2005, **127**, 808. (h) Barolo, C.; Nazeeruddin, M.K.; Fantacci, S.; Di Censo, D.; Comte, P.; Liska, P.; Viscardi, G.; Quagliotto, P.; De Angelis, F.; Ito, S.; Grätzel, M. *Inorg. Chem.* 2006, **45,** 4642. (i) Martineau, D.; Beley, M.; Gros, P.C.; Cazzanti, S.; Caramori, S.; Bignozzi, C.A. *Inorg. Chem.* 2007, **46**, 2272.

[13] Nazeeruddin, M.K.; Kay, A.; Rodicio, I.; Humphry-Baker, R.; Muller, E.; Liska, P.; Vlachopoulos, N.; Grätzel, M. *J. Am. Chem. Soc.* 1993, **115**, 6382.

[14] (a) Grätzel, M. *Prog. Photovoltaics Res. Appl*., 2000, **8**, 171. (b) Nazeeruddin, M.K.; Péchy, P.; Renouard, T.; Zakeeruddin, S.M.; Humphry-Baker, R.; Comte, P.; Liska, P.; Cevey, L.; Costa, E.; Shklover, V.; Spiccia, L.; Deacon, G.B.; Bignozzi, C.A.; Grätzel, M.; *J. Am. Chem. Soc.* 2001, **123(8)**, 1613.

[15] Nazeeruddin, M.K.; Humphry-Baker, R.; Grätzel, M.; Wöhrle, D.; Schnurpfeil, G.; Schneider, G.; Hirth, A.; Trombach, N. *Journal of Porphyrins and Phthalocyanines*, 1999, **3(3)**, 230.

[16] (a) Wang, P.; Zakeeruddin, S.M.; Exnar, I.; Grätzel, M. *Chem. Commun.* 2002, 2972. (b) Wang, P.; Zakeeruddin, S.M.; Humphry-baker, R.; Moser, J.E.; Gratzel, M. *Adv. Mater. (Weinheim, Ger.)* 2003, **15**, 2101.

[17] Wang, P.; Zakeeruddin, S.M.; Moser, J.E.; Humphry-Baker, R.; Comte, P.; Aranyos, V.; Hagfeldt, A.; Nazeeruddin, M.K.; Grätzel, M. *Adv. Mater.* 2004, **16**, 1806.

[18] Jang, S.R.; Yum, J.H.; Klein, C.; Kim, K.J.; Wagner, P.; Officer, D.; Grätzel, M.; Nazeeruddin, M.K. *J. Phys. Chem. C* 2009, **113**, 1998.

[19] (a) Arakawa, H.; Yamaguchi, T.; Agatsuma, S.; Takanori, S.; Koishi, Y. *Proceedings of the 23rd European Photo*Voltaic *Solar Energy Conference, Valencia, Spain*; 2008. (b) Cao, Y.M.; Bai, Y.; Yu, Q.J.; Cheng, Y.M.; Liu, S.; Shi, D.; Gao, F.F.; Wang, P. *J. Phys. Chem. C* 2009, **113**, 6290.

[20] (a) Jung, I.; Choi, H.; Lee, J.K.; Song, K.H.; Kang, S.O.; Ko, J.; *Inorg. Chim. Acta* 2007, **360**, 3518. Choi, H.; Baik, C.; (b) Kim, S.; Kang, M.S.; Xu, X.; Kang, H.S.; Kang, S.O.; Ko, J.; Nazeeruddin, M.K.; Grätzel, M. *New J. Chem.* 2008, **32**, 2233.

[21] (a) Hoertz, P.G.; Thompson, D.W.; Friedman, L.A.; Meyer, G.J. *J. Am. Chem. Soc.* 2002, **124**, 9690. (b) Sauve, G.; Cass, M.E.; Doig, S.J.; Lauermann, I.; Pomykal, K.; Lewis, N.S. *J. Phys. Chem. B* 2000, **104**, 3488. (c) Chiorboli, C.; Rodgers, M.A.J.; Scandola, F. *J. Am. Chem. Soc.* 2003, **125**, 483. (d) Kuciauskas, D.; Monat, J.E.; Villahermosa, R.; Gray, H.B.; Lewis, N.S.; McCusker, J.K. *J. Phys. Chem. B* 2002, **106**, 9347. (e) Altobello, S.; Argazzi, R.; Caramori, S.; Contado, C.; Da Fre, S.; Rubino, P.; Chone, C.; Larramona, G.; Bignozzi, C.A. *J. Am. Chem. Soc.* 2005, **127**, 15342. (f) Verma, S.; Kar, P.; Das, A.; Palit, D.K.; Ghosh, H.N. *J. Phys. Chem. C* 2008, **112**, 2918.

[22] Hasselmann, G.M.; Meyer, G.J. *J. Phys. Chem. B* 1999, **103**, 7671.

[23] (a) Ferrere, S. *Chem. Mater.* 2000, **12**, 1083. (b) Ferrere, S. *Inorg. Chim. Acta* 2002, **329**, 79.

[24] (a) Islam, A.; Sugihara, H.; Hara, K.; Singh, L.P.; Katoh, R.; Yanagida, M.; Takahashi, Y.; Murata, S.; Arakawa, H. *Inorganic Chemistry*, 2001, **40(21)**, 5371. (b) Geary, E.A.M.; Hirata, N.; Clifford, J.; Durrant, J.R.; Parsons, S.; Dawson, A.; Yellowlees, L.J.; Robertson, N. *Dalton Trans.* 2003, 3757. (c) Geary, E.; Yellowlees, L.J.; Jack, L.A.; Oswald, I.D.H.; Parsons, S.; Hirata, N.; Durrant, J.R.; Robertson, N. *Inorg. Chem.* 2005, **44**, 242.

[25] (a) Alonso-Vante, N.; Nierengarten, J.-F.; Sauvage, J.-P. *J. Chem. Soc., Dalton Trans.* 1994, 1649. (b) Bessho, T.; Constable, E.C.; Grätzel, M.; Redondo, A.H.; Housecroft, C.E.; Kylberg, W.; Nazeeruddin, M.K.; Neuburger, M.; Schaffner, S. *Chem. Commun.* 2008, 3717. (c) Sakaki, S.; Kuroki, T.; Hamada, T. *J. Chem. Soc., Dalton Transac.* 2002, 840.

[26] (a) Martineau, D.; Beley, M.; Gros, P.C.; Cazzanti, S.; Caramori, S.; Bignozzi, C.A. *Inorg. Chem.* 2007, **46**, 2272. (b) Grabulosa, A.; Beley, M.; Gros, P.C.; Cazzanti, S.; Caramori, S.; Bignozzi, C.A. Inorg. Chem. 2009, **48**, 8030. (c) Grabulosa, A.; Martineau, D.; Beley, M.; Gros, P.C.; Cazzanti, S.; Caramori, S.; Bignozzi, C.A. *Dalton Trans.* 2009, 63.

[27] (a) Jiang, K.-J.; Masaki, N.; Xia, J.; Noda, S.; Yanagida, S. *Chem. Commun*. 2006, 2460. (b) Shi, D.; Pootrakulchote, N.; Li, R.; Gui, J.; Wang, Y.; Zakeeruddin, S. M.; Grätzel, M.; Wang, P. *J. Phys. Chem. C* 2008, **112**, 17046.

[28] (a) Klein, C.; Nazeeruddin, M.K.; Liska, P.; Di Censo, D.; Hirata, N.; Palomares, E.; Durrant, J.R. M. Grätzel, *Inorg. Chem.* 2005, **44**, 178. (b) Renouard, T.; Fallahpour, R.-A.; Nazeeruddin, M.K.; Humphry-Baker, R.; Gorelsky, S.I.; Lever, A.B.P.; Grätzel, M. *Inorg. Chem*. 2002, **41**, 367. (c) Wang, P.; Klein, C.; Humphry-Baker, R.; Zakeeruddin, S.M.; Grätzel, M. *J. Am. Chem. Soc.* 2005, **127**, 808.

[29] (a) Gilat, S. L.; Adronov, A.; Frechet, J. M. J. *Angew. Chem., Int. Ed.* 1999, **38**, 1422. Adronov, A.; Frechet, J. M. J. *Chem. Commun*. 2000, 1701. (b) Ambroise, A.; Kirmaier, C.; Wagner, R. W.; Loewe, R. S.; Bocian, D. F.; Holten, D.; Lindsey, J. S. *J. Org. Chem.* 2002, **67**, 3811**.** (c) Li, F.; Yang, S. I.; Ciringh, Y.; Seth, J.; Martin, C. H.; Singh, D. L.; Kim, D.; Birge, R. R.; Bocian, D. F.; Holten, D.; Lindsey, J. S. *J. Am. Chem. Soc.* 1998, **120**, 10001.

Chapter No: 1

Introduction

1.1. The combustion of fossil fuels

Increasing global population have increased the energy demand that have already led to environmental degradation of the planet on an unprecedented scale. Today, about 20×10^{12} kg of carbon dioxide are put into the atmosphere every year, mainly by burning of fossil fuel **[1].**

Global mean surface temperature has increased by 0.3-0.6° C since the late 19th century and the global sea level has risen by 10-25 cm, most likely due to human activities. Depending on future emission scenarios and the actual climate sensitivity, it may increase by another 0.6-7.0° C by the year 2100 **[2].**

The consequences of this temperature change have already increased the frequency and severity of natural disasters **[1].** Moreover, the reserves of fossil fuels are limited; for example, the constantly growing oil and gas prices give indication that the exhaustion of crude oil maybe not so far in the future.

1.2. Background, motivation and current status of solar energy utilization

The world now uses energy at a rate of approximately 4.1×10^{20} joules/yr, equivalent to a continuous power consumption of 13 trillion watts, or 13 terawatts (TW). Even with aggressive conservation and energy efficiency measures, due to rapid technology development and economic growth world-wide, the world demand for energy is projected to more than double by 2050 (25-30 TW) and to more than triple by the end of the century (40-50 TW). Finding sufficient supplies of clean energy for the future is one of society's most daunting challenges **[3].**

Our primary source of clean and abundant energy is the sun. The sun deposits 120,000 TW of radiation on the surface of the Earth, far exceeding human needs even in the most aggressive energy demand scenarios. The technologies to utilize the enormous energy potential

that lies in the sun have existed for several decades already but the still high price of the photovoltaic (PV) panels and the stability of current PV devices for only limited variety of applications have hindered the large scale usage of solar power. This is why development of new, more advanced, cheaper and efficient solar energy technologies is called for, to bring this form of renewable energy available to even large number of customers.

The sun emits light with a range of wavelengths from the ultraviolet and visible to the infrared. It peaks in the visible, resembling the spectrum of a blackbody at a temperature of 5250 K. It is, however, influenced by atmospheric absorption and the position of the sun. When skies are clear, the maximum radiation strikes the earth's surface when the sun is directly overhead, having the shortest path length through the atmosphere. The path length is called the *air mass* (AM) and can be approximated by AM = 1/cos φ, where φ is the angle of elevation of the sun. The standard solar spectrum used for efficiency measurements of solar cells is AM 1.5 G (global), giving that φ = 42°. This spectrum is normalized so that the integrated irradiance (the amount of radiant energy received from the sun per unit area per unit time) is 1000 W m^{-2} **[4]**.

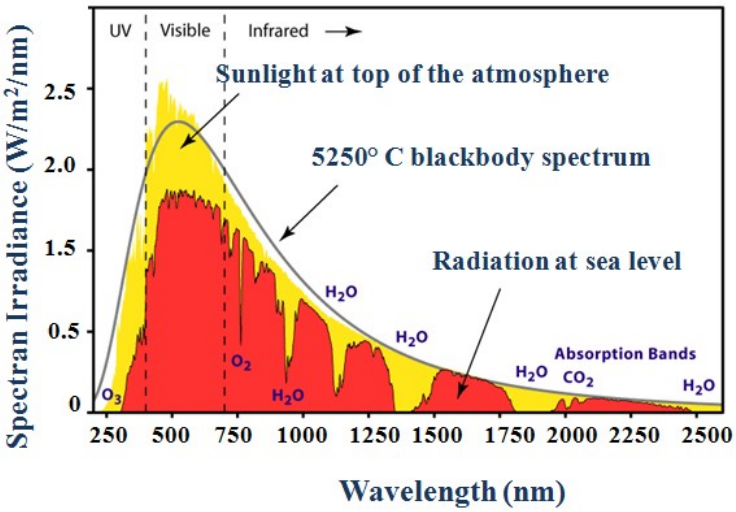

Figure 1.1: The standard AM 1.5 global solar spectrum.
(Source: http://rredc.nrel.gov/solar/spectra/am1.5/.)

1.3. Classical P-N junction cells

In conventional, solid semiconductor solar cells, electrons and holes are driven apart by internal electric field in the device. This field forms around the P-N junction, which is the core of

all solid semiconductor photovoltaics. P-N junction is created by combining blocks of oppositely doped semiconductors **[4]**. For example silicon doped with boron and silicon doped with phosphorus. The former is called P-type silicon, due to boron's valency of three, which is one electron less than that of silicon's and thus results in electron depletion (positive "holes") in silicon's valence band. Analogously, the latter is called N-type silicon, due to phosphorus' valency of five, which results in excess electrons on silicon's conduction band. When these blocks are brought to physical contact, the "extra" electrons in the N-type silicon flow to fill the "holes" in the P-type silicon, thus leaving behind ionized dopant atoms, as well as creating those in the P-side, when boron's valency of three exceeds by one. These ionized dopants then create the internal electric field that affects in the so-called depletion region around the P-N junction. When an electron-hole pair is generated in this region, the internal electric field sweeps the charge carriers on the opposite sides of the junction, thus preventing recombination energetically, the same can be understood by "bending" of the valence and conduction bands.

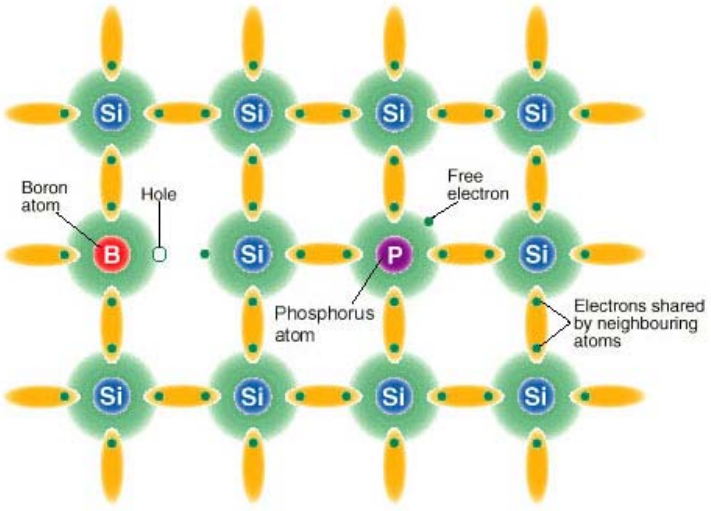

Figure 1.2: Silicon Crystal Lattice with Dopant Atoms.

In an undoped semiconductor, the Fermi level is located in the middle of the band gap. When the semiconductor is doped with atoms with "extra" electrons, the Fermi level shifts upwards and analogously, when the dopant causes electron depletion, the Fermi level moves lower. When the oppositely doped blocks are brought to contact, the flow of electrons from the N-side to the P-side shifts the N-side conduction band lower and correspondingly, the flow of holes from the P-side to the N-side moves the P-side valence band higher on electronic energy

scale. As a result of this, the Fermi levels match throughout the junction. Because of this band "bending", it is energetically favorable for the photogenerated charge carriers to move across the junction, i.e. electrons created on the P-side flow "downwards" to the N-side and holes created in the N-side move "upwards" to the P-side.

Typically, either N- or P-side is doped heavier so the depletion region reaches further in this side and the most of the charge carriers can be collected there. This offers also the benefit that the junction itself can be brought close to the solar cell surface, thus maximizing the amount of absorbed photons.

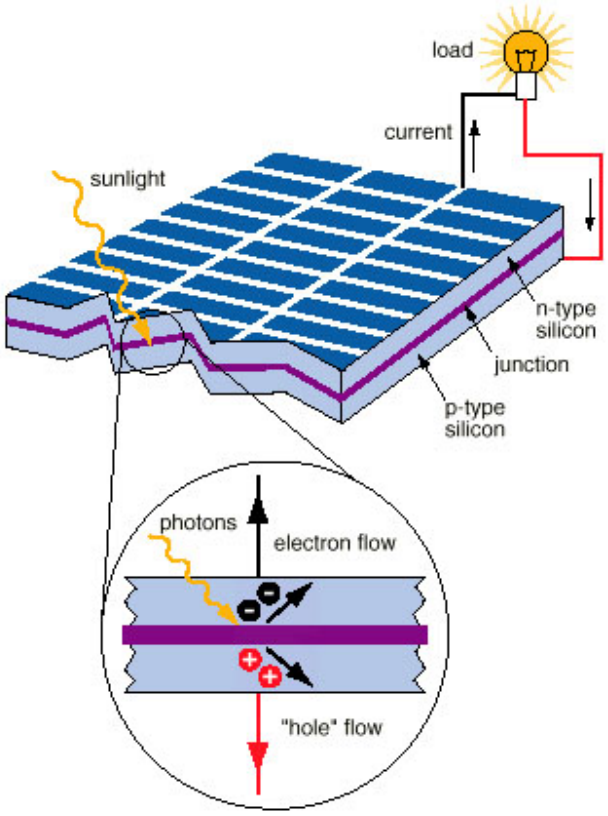

Figure 1.3: The Photovoltaic Effect in a Solar Cell

1.4. Generations of solar cell

Based on the nature of material, maximum conversion efficiency obtainable and the associated cost of photovoltaic power, Martin Green has grouped various photovoltaic solar cells into three major categories **[5].**

The conventional solar cells of today, the **first generation solar cells** are based on highest purity silicon material with least structural defects (such as single crystals). Silicon-based systems make up around 90% of the current PV market. The production cost is presently around $3/Wp (Watt peak), but is highly dependent on the price of the silicon material **[5, 6].**

The **second generation solar cells** are based on low energy, intensive preparation techniques such as vapor deposition and electroplating. Most efficient examples of solar cells made up of multi crystalline or amorphous silicon, Cd-In-Ga-Se (CIGS), and CdTe, are based on thin film technologies. They are becoming a competitive class of PVs, doubling production from 2006 to 2007. The advantages of thin film solar cells include the ease of manufacture permitting a reduction of the production cost to about $1/Wp, a wider range of applications with attractive appearance, and possibilities of using flexible substrates. The most established thin-film technology is amorphous silicon (a-Si) **[7].**

In the last few decades, new concepts of solar cells were conceived and realized. These technologies mainly include dye-sensitized solar cells (DSSCs), polymer solar cells, and nanocrystalline solar cells, all of which are now known as **third generation** photovoltaics. The goal for the third generation solar cells is to deliver electricity at a large scale competitive price, that is, less than $0.5/Wp.

DSSCs have attracted considerable attention in recent years because of their high incident solar light-to-electricity conversion efficiency, colourful and decorative natures, and low cost of production. DSSCs are based on the sensitization of mesoporous, nanocrystalline metal oxide films to visible light by the adsorption of metal complexes or organic molecular dyes. Following its discovery in 1991 **[8]**, research on the DSSCs has progressed remarkably, rendering it a credible chemical alternative to solid-state silicon-based devices. Due to their high efficiency and stability, DSSCs were the first organic photovoltaic products to reach the market. G24 Innovations Limited (G24i), a U. K. company founded in 2006, uses DSSCs technology to manufacture and design solar modules. Over the past few years, considerable progress has been made in understanding the function of various components of dye-sensitized solar cells.

1.5. Working principles of DSSC

A schematic representation of components and operating principles of a dye-sensitized solar cell are shown in Figure 1.4.

The actual DSSC contains five components:

1. a mechanical support coated with Transparent Conductive Oxides.
2. The nanocrystalline semiconductor film electrode, usually TiO_2
3. a sensitizer (D) adsorbed onto the surface of the semiconductor.
4. an electrolyte containing a redox mediator, usually the I^-/I_3^- couple.
5. a counter electrode capable of regenerating the redox mediator like platinum.

The first step is the absorption of a photon by the dye D Eq. (1), leading to the excited dye D^* which injects an electron into the conduction band of the semiconductor, leaving the dye in the oxidized state D^+ Eq. (2). The injected electron flows through the semiconductor network to arrive at the back contact and then through the external load to the counter electrode to reduce the oxidized form (I^-) of redox mediator Eq. (3) which in turn regenerates the sensitizer Eq. (4). This completes the circuit. Under illumination, the device constitutes a regenerative and stable photovoltaic energy conversion system **[9].**

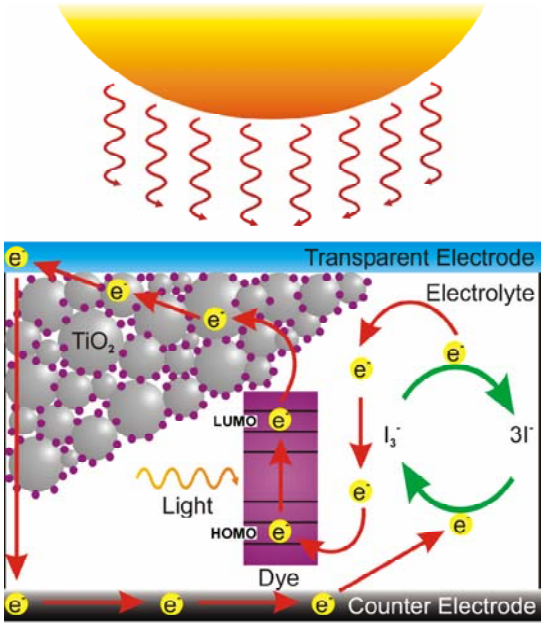

Figure 1.4: The structure and operating principle of the DSSC

$$D_{(adsorbed)} + hv \rightarrow D^{*}_{(adsorbed)} \quad \textbf{(1)}$$

$$D^{*}_{(adsorbed)} \rightarrow D^{+}_{(adsorbed)} + e^{-}_{(injected)} \quad \textbf{(2)}$$

$$I_3^- + 2e^-_{(cathode)} \rightarrow 3I^-_{(cathode)} \quad \textbf{(3)}$$

$$D^{+}_{(adsorbed)} + \frac{3}{2}I^- \rightarrow D_{(adsorbed)} + \frac{1}{2}I_3^- \quad \textbf{(4)}$$

Some undesirable reactions resulting losses into the cell efficiency may also occur. They are the recombination of the injected electrons either with oxidized dye Eq. (5) or with the oxidized redox couple at the TiO_2 surface Eq. (6).

$$D^{+}_{(adsorbed)} + e^{-}_{(TiO_2)} \rightarrow D_{(adsorbed)} \quad \textbf{(5)}$$

$$I_3^- + 2e^-_{(TiO_2)} \rightarrow 3I^-_{(anode)} \quad \textbf{(6)}$$

The total efficiency of the dye-sensitized solar cell depends on optimization and compatibility of each of these constituents, in particular on the semiconductor film along with the dye spectral responses **[10]**. A very important factor is the high surface area and the thickness of the semiconductor film which leads to increased dye loading, thus optical density resulting in efficient light harvesting **[11]**.

The incident photon-to-current conversion efficiency (IPCE), sometimes referred as the "external quantum efficiency" (EQE), is an important characteristic of a device. In particular, using devices with same architecture, it is possible to compare the light-harvesting performance of sensitizers. It is defined as the number of electrons generated by light in the external circuit divided by the number of incident photons as a function of excitation wavelength as in Eq. (7) **[12].**

$$\mathrm{IPCE}(\lambda) = \frac{\text{Photocurrent density}}{\text{Wavelength} \times \text{Photon flux}}$$

$$= \mathrm{LHE}(\lambda) \times \varphi_{inj} \times \eta_{coll} \quad \textbf{(7)}$$

Where LHE(λ) is the light-harvesting efficiency at wavelength λ , φ_{inj} is the quantum yield for electron injection from the excited sensitizer in the conduction band of the TiO_2, and η_{coll} is the efficiency for the collection of electrons.

The overall conversion efficiency *(η)* of the dye sensitized solar cell is determined by the photocurrent density *(J_{SC})*, the open-circuit potential *(V_{OC})*, the fill factor *(ff)* of the cell and the intensity of the incident light *(I_S)*, Eq. (8) **[13]**.

$$\eta_{global} = \frac{Jsc \cdot Voc \cdot ff}{I_S} \qquad \textbf{(8)}$$

The open-circuit photo-voltage is determined by the energy difference between the Fermi level of the solid under illumination and the Nernst potential of the redox couple in the electrolyte. However, the experimentally observed open-circuit potential *(V_{OC})* for various sensitizers is smaller than the difference between the conduction band edge and the redox couple. This is generally due to the competition between electron transfer and charge recombination pathways. Knowledge of the rates and mechanisms of these competing reactions are vital for the design of efficient sensitizers and thereby improvement of the devices **[14-17].**

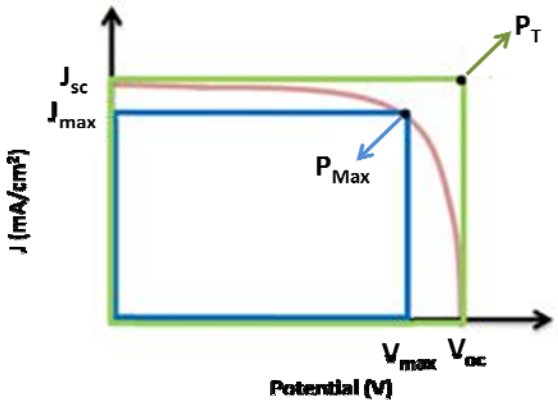

Figure 1.5: Getting fill factor from the J-V curve

The fill factor *(ff)* is defined as the ratio of the maximum power P_{max} obtained with the device and the theoretical maximum power, that is $P_T = J_{SC} . V_{OC}$.

J_{SC} is the short circuit current and V_{OC} is the open-circuit voltage. The fill factor *(ff)* can take values between 0 and 1. It reflects electrical and electrochemical losses occurring during operation of the DSSC.

It can be seen that the photophysical and electrochemical properties of the sensitizer will mainly define the performances of the device. First through the oxidation potential which sets the maximum open-circuit voltage possible and second through the absorption properties, which dictate the short circuit current. Finally, overall electron transfer dynamics will influence losses **[18].**

1.6. Key Components of DSSC

Detailed description about the development of following three components of DSSC will be covered in this topic.

1.6.1. Semiconductor
1.6.2. Electrolyte
1.6.3. Dye/Sensitizer

1.6.1. Semiconductor

Research on wide band gap oxide semiconductors sensitized with dyes began already in the late 1800's, related to photography. Moser observed that the photoelectric effect on silver plates was enhanced in the presence of erythrosine dye **[19]** and confirmed by Rigollot in 1893 (Rigollot, 1893). Systematic mechanistic studies started only in the late 1960's with the work of dye-sensitization process on ZnO **[20-22]** and SnO_2 **[23-25]** electrodes carried out by Memming et al. Most of these early studies were fundamental in nature, aimed to understand electron–transfer processes involving valence and conduction bands of a semiconductor immersed in a redox electrolyte. Gerischer combined the stability of large band gap semiconductors with the photosensitivity to light in the visible region by dye adsorption onto semiconductor surface. Though these works were still on their preliminary stage, the dye-sensitized cells obtained were characterized by poor dye anchorage (mostly physisorbed) on the semiconductor surface and low conversion efficiencies restricted by the limited and weak light absorption (in the order of 1 to 2%) of the dye monolayer on the planar surface. But the basic problem was the belief that only smooth semiconductor surfaces could be used. The light-harvesting efficiency for a monomolecular layer of dye sensitizer, even for phthalocyanines and porphyrins, which have among the highest extinction coefficients known, with far less than 1% of the AM 1.5 G spectrum **[26]**. Attempts to harvest more light by using multilayers of dyes were in general unsuccessful. Incremental improvements were then achieved both in the chemisorption of sensitizers **[27, 28]**, electrolyte redox chemistry and the judicious selection of photoelectrode materials **[29-35]** . Several studies have addressed the use of alternative metal oxides including SnO_2 , ZnO , and Nb_2O_5 **[36-37] .**

Most semiconductors underwent serious photocorrosion or even normal corrosion in the dark, thus a stable, wide band-gap semiconductor, TiO_2, became the material of choice. Grätzel, Augustynski, and co-workers presented results on dye-sensitized fractal-type TiO_2 electrodes with high surface area in 1985 **[38]**.

The key to the breakthrough for DSSC in 1991 was the use of a mesoporous TiO_2 electrode **[8]**. The semiconductor material that forms the core of the photoelectrode (PE) should be chemically stable and inert towards the electrolyte species, it should have a lattice structure suitable for dye bonding, its conduction band should be located slightly below the LUMO level of the dye in order to facilitate efficient electron injection, and it should be available in nanostructured form to enable high enough dye loading. Due to low-cost, abundance in the market, nontoxicity, and biocompatiblity, as it is also used widely in health care products as well as in paints, TiO_2 fulfills these requirements and becomes the best choice in semiconductor till now.

TiO_2 exists in three crystalline forms, anatase, rutile, and brookite, of which rutile is the thermodynamically most stable form but anatase structure is the most suitable for DSSC applications. Because it has a larger band gap (3.2 vs 3.0 eV for rutile) energy, a higher conduction band edge energy, E_c and absorbs only below 388 nm making it invisible to most of the solar spectrum **[39]**.

1.6.2. Electrolyte

The electrolyte is a crucial part of all DSSC. It is responsible for the inner charge carrier between electrodes, it is the hole transporting material. It endlessly regenerates the dye at the photoelectrode with the charge collected at the counter electrode (CE).

The properties of electrolyte have much effect on the conversion efficiency and stability of the solar cells. The electrolyte used in DSSC is divided into three types: liquid electrolyte, quasi-solid state electrolyte, and solid electrolyte. Liquid electrolyte could be divided into organic solvent electrolyte and ionic liquid electrolyte according to the solvent used.

The demands on the liquid redox electrolytes are that they should be chemically stable, have low viscosity in order to minimize transport problems, and be a good solvent for the redox couple components and various additives but at the same time not cause significant dissolution of

adsorbed dye or even the semiconducting material of the electrodes. Because many organometallic sensitizing dyes are sensitive toward hydrolysis, water and reactive protic solvents are normally not optimal choices. Finally, the redox electrolyte should be compatible with a suitable sealing material to avoid losses by evaporation or leakage.

Organic solvent electrolytes were widely used and investigated in DSSC for their low viscosity, fast ion diffusion, high efficiency, ease of design, and high pervasion into nanocrystalline film electrode **[40, 41]**. The composition of the electrolytes includes organic solvent, redox couple, and additive.

Organic solvents used in organic liquid electrolytes include nitriles such as acetonitrile, valeronitrile, 3-methoxypropionitrile, and esters such as ethylene carbonate (EC), propylene carbonate (PC), γ-butyrolactone.

So far the triiodide/iodide I_3^-/I^- couple has been the most efficient and commonly used redox mediator in DSSCs, due to the fast regeneration of the oxidized dye provided by I^- on a nanosecond time scale **[42, 43].**

$$I^- \rightleftharpoons I + e^- \quad \textbf{(9)}$$

$$2I \rightleftharpoons I_2 \quad \textbf{(10)}$$

$$I_2 + I^- \rightleftharpoons I_3^- \quad \textbf{(11)}$$

Thus, iodide (I^-) is the reduced species of both the total reaction and the charge-transfer reaction. In contrast to this, triiodide I_3^- is the oxidized species of the total reaction, but elementary iodine (I) is the oxidized species of the charge transfer reaction. The first two reactions are fast reactions and we can assume that the ions involved are always in equilibrium.

Br^-/Br_2 couple, $SCN^-/(SCN)_2$ couple and $SeCN^-/(SeCN)_2$ couple are also shown in the literature **[44, 45]**. A two electron redox couple based on 5-mercapto-1-methyltetrazole ions and its oxidized dimer has been tested recently reaching impressive overall conversion efficiencies of 6.4% **[46]** although some concerns exist regarding the stability of this class of mediator due to the radicals involved in the reaction **[47]**. Kinetically fast, one-electron, couples, such as ferrocene/ferrocenium (Fc/Fc^+) **[48-50]**, cobalt complexes [Co(II)/Co(III)] **[51-53]**, copper complexes [Cu(I)/(II)] **[54]**, and mediator mixtures **[55]**, have been used with some interesting results for DSSCs, despite their high rate of recombination with the electrons.

Additives play a central role in the enhancement of photoelectrochemical performance of DSSCs. Most additives are understood at a fairly phenomenological level, and their effects are often attributed to modification of redox couple potential, band shifts of the semiconducting electrode material, effects of surface blocking, or surface dye organization. Most additives that have been reported contain an electrondonating nitrogen heterocycle, such as 4-*tert*-butylpyridine (TBP).

4-*tert*-Butylpyridine (TBP) was first applied in DSSC by Grätzel and co-workers in 1993, demonstrating a remarkable increase in *V*oc of these cells in combination with LiI-based electrolytes **[55]**. On the basis of intensity-modulated photovoltage spectroscopy (IMVS) measurements, it was shown that TBP shifts the titania band edge toward higher energies **[56]**.

The increase in *V*oc was due to the suppression of the back electron transfer at the dyed-TiO_2/electrolyte junction. Such a back transfer originates from the reduction of triiodide by the electron on the semiconductor, as is considered to be an essential factor for decreasing the device efficiency. The back electron transfer occurred on the surface of TiO_2, unable to be covered by dye molecules, and thus triiodide anions were adsorbed. With the addition of TBP or other pyridine derivatives in the electrolyte, the basic pyridine molecules were expected to adsorb onto the bare TiO_2 surface due to its Lewis acidity, thus preventing the invasion of triiodide and decrease the undesirable electron transfer from the TiO_2 triiodide.

The effects of large series of different types of nitrogen-donating additives including pyrimidines, aminotriazoles, quinolines, benzimidazoles, alkylaminopyridines, and alkylpyridines, etc **[57-64]** and it was observed that the molecular size of the derivatives was strongly related to the suppression effect. The smaller the size of the derivatives used in the electrolytes, the higher was the *V*oc of the corresponding cells, which was due to the effective adsorption on TiO_2 for smaller sizes of the derivatives. Sulfur containing groups as donors, such as aminothiazoles have also been investigated. The interaction between iodine and different nitrogen-donating additives were investigated at density-functional and perturbation- theory levels and found to be of the expected donor-acceptor type **[65-68].**

The commonly used additives in the electrolytes of DSSC include tetrabutylammoniumhydroxide (TBAOH) **[69]**, 4-tert-butylpyridine (TBP) **[70, 71]**, 2-propylpyridine (2PP) **[72]** or methylbenzimidazole (MBI) **[73]**. Additionally, these additives also enhance the cell's long-term stability and suppress dark current.

The best results have always been obtained with the triiodide/iodide (I_3^- /I$^-$) redox couple in an organic matrix, generally acetonitrile.

1.6.3. Dye/Sensitizer

In DSSC, the dye molecules "sensitize" the semiconductor TiO_2 to visible radiations that would otherwise be transmitted as TiO_2 absorbs only below 388 nm. The dye molecules are therefore generically referred to a "sensitizers".

The sensitization of TiO_2 with a wide variety of inorganic and organic dyes/sensitizers for light harvesting has been investigated. Dye sensitizers serve as an electron pump in the sensitization in DSSC, whose properties will have much effect on the light harvesting efficiency and the overall photoelectric conversion efficiency. The ideal sensitizer for DSSC should absorb all light below a threshold wavelength of about 920 nm. In addition, it should be firmly grafted to the semiconductor oxide surface and inject electrons to the conduction band with a quantum yield of unity. Its redox potential should be sufficiently high that it can be regenerated rapidly via electron donation from the electrolyte or a hole conductor. Finally, it should be stable enough to sustain at least 10^8 redox turnovers under illumination corresponding to about 20 years of exposure to natural light **[74]**.

The sensitizers used in DSSC can be divided into two types: organic dye and inorganic dye according to the structure. Inorganic dye includes metal complexes, such as polypyridyl complexes of ruthenium and osmium, metal porphyrin, phthalocyanine and inorganic quantum dots, while organic dye includes natural as well as synthetic organic dyes. Compared with organic dye, inorganic dyes have higher thermal and chemical stability **[75-83]**.

Among the metal complexes, Ru complexes **[84-100]** have shown the best photovoltaic properties so far in terms of broad absorption spectrum, suitable excited and ground state energy levels, relatively long excited-state lifetime, and good (electro) chemical stability. Several Ru complexes used in DSSCs have reached more than 10% solar cell efficiency under standard measurement conditions.

Among Ru complexes, polypyridyl ruthenium complexes **[101-120]** are widely used and investigated for their high stability, outstanding redox properties and good response to natural visible sunlight. They may be divided into carboxylate polypyridyl ruthenium complex,

phosphonate ruthenium complex, and polynuclear bipyridyl ruthenium complex. The difference between the first two types of sensitizers lies in the anchoring group i.e. carboxylate group or phosphonate group, which enables the electron injection into the conduction band of the semiconductor. The first two types of sensitizers are different from the last type in the number of metal centers.

1.7. Classical Ruthenium based Sensitizers

Ru complexes with carboxylated bipyridine ligands were first used for sensitization of TiO_2 single crystals in 1979 **[121]** and then in 1985 a similar dye was used, with three carboxylated bipyridine ligands, to obtain the first reported efficient dye-sensitized solar cell with an IPCE of 44% **[52]**.

The first high-performance polypyridyl ruthenium complex was the so-called N3 [bis(isothiocyanato)-bis(2,2'-bipyridyl-4,4'-carboxylate) ruthenium(II)] reported in 1993 **[122]**. N3 has two bipyridine and two thiocyanate (NCS) ligands. It absorbs radiations up to 800 nm, due to the loosely-attached NCS groups. N3 results were only surpassed more than 5 years later by another ruthenium complex, the N749 [tri(isothiocyanato)-2,2',2''-terpyridyl-4,4',4''-tricarboxylate) ruthenium(II)] also called as black dye, first introduced in 1997 **[9, 123, 124]** which has achieved the absorption up to 860 nm.

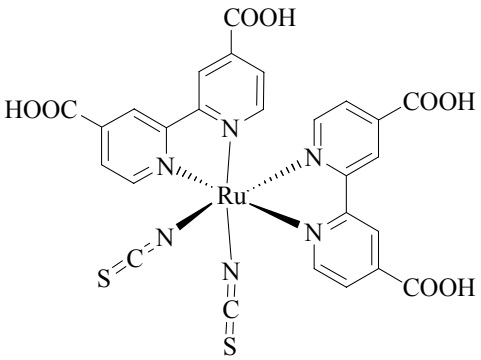

N3

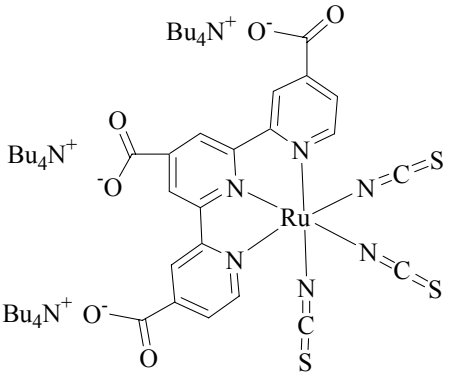

N749
Black dye

Nazeeruddin et al.**, [125]** investigated the effect exerted by the proton content of the N3 dye on the performance of DSSC. The doubly protonated form, $(Bu_4N)_2[Ru(dcbpyH)_2(NCS)_2]$, named N719 exhibited an improved power conversion efficiency. It means that N719 dye has the

same structure as N3 dye but has TBA^+ (tetrabutylammonium) instead of H^+ at two carboxyl groups.

Grätzel and co-workers focused on adjusting the ancillary 2,2′-bipyridyl ligand with different substituents (alkyl, alkoxy, phenylene, etc.) to increase the molar extinction coefficient, suppress dye aggregation on the semiconductor, and optimize the redox potential of the photosensitizer. The amphiphilic heteroleptic ruthenium sensitizer, Z907, demonstrated prominent thermal stability due to the introduction of two hydrophobic alkyl chains on the bipyridyl ligand. In combination with hexadecyl phosphonic acid as a coadsorber, the dye maintained 7% power conversion efficiency under a long-term thermal stress measurement**[126-128]**.

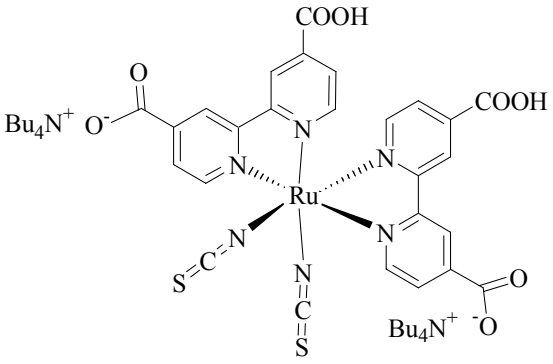

N719

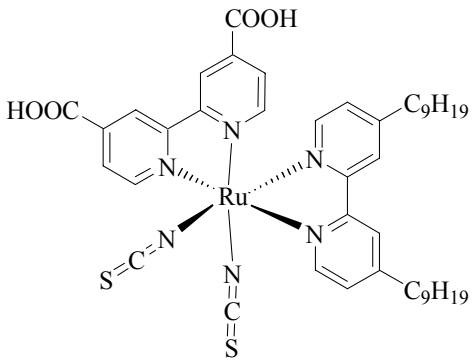

Z907

To further extend the π-conjugated system of the bipyridine and enhance the harvesting of solar light, 3-methoxystyryl was introduced into the ancillary ligand to obtain a novel Ru dye, Z910, which exhibited prominent efficiency (10.2%) and impressive stability. The study demonstrated that enhancing the molar extinction coefficient is a good strategy to improve the photovoltaic performance of Ru dyes **[129]**.

Through introduction of the tri(ethylene oxide) methyl ether (TEOME) into the 2,2′-bipyridine ligand, a novel ion coordinating sensitizer, NaRu(4-carboxylic acid-4′-carboxylate)(4,4′-bis[(tri(ethylene glycol) methyl ether) methyl ether]-2,2′-bipyridine)-(NCS)2 (coded as K51), was obtained **[130]**. This study revealed that the ion coordinating sensitizer, when incorporated in a DSSC, using a nonvolatile electrolyte or hole-transporting material, exhibited a simulated full-sun power conversion efficiency of 7.8% or 3.8%, respectively.

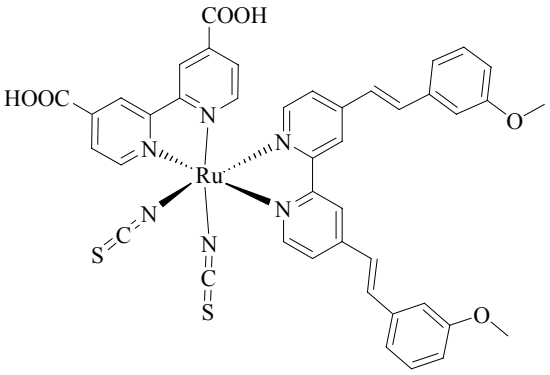

Z910

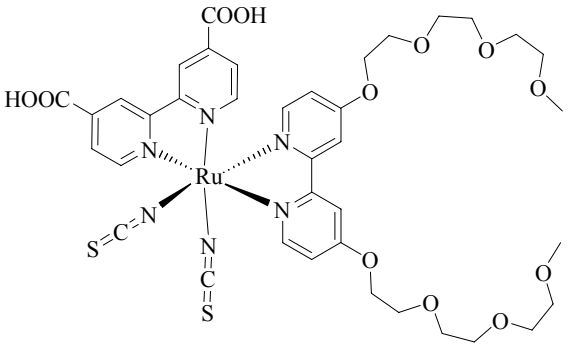

K51

Nazeeruddin and co-workers reported two new photosensitizers, K9 and K23 **[131]** which showed high short-circuit photocurrents in thin film DSSCs in comparison with the Z907 due to increased molar extinction coefficients and enhanced spectral response in the visible and near-IR regions.

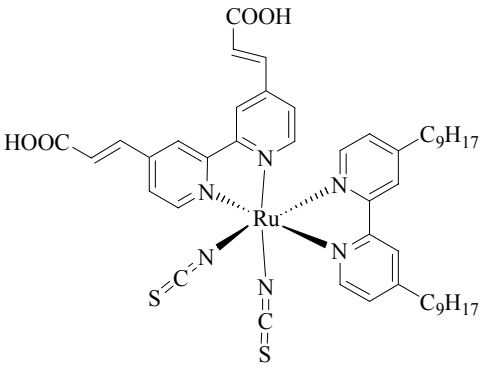

K9

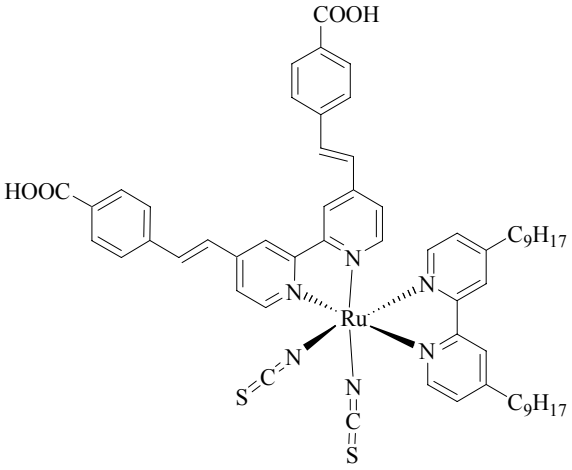

K23

A family of high molar extinction coefficient heteroleptic polypyridyl ruthenium sensitizers was reported by Wang and co-workers **[132-134]** featuring conjugated electron-rich units in their ancillary ligands, such as alkyl thiophene, alkyl furan, alkyl selenophene, or alkyl thieno[3,2-*b*]thiophene. C101 achieved several new DSSC benchmark levels under AM 1.5 illumination: it gave 11.0 % efficiency with an acetonitrile based electrolyte.

Ko and co-workers introduced organic antenna groups into Ru complexes, which significantly increased the extinction coefficient **[135,136]**. Among these dyes JK56 yielded 83% IPCE and 9.2% power conversion efficiency under AM 1.5 G (N719, 8.9%).

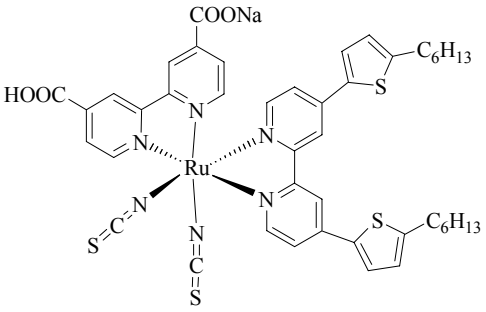

C101

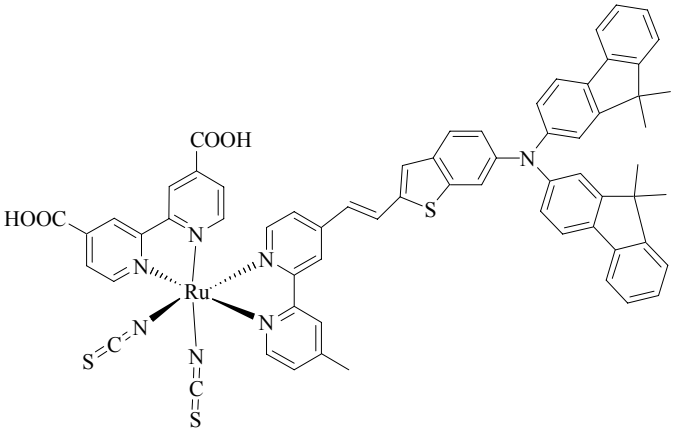

JK56

Many attempts have also been made to construct sensitizers with other metal ions, such as Os **[137-142]**, Re **[143]**, Fe **[144, 145]**, Pt **[146, 147]**, and Cu **[148-150]**.

But to date, the best photovoltaic performance both in terms of conversion yield and long-term stability has so far been achieved with polypyridyl complexes of ruthenium and the only ones so far to achieve over 10% efficiency under standard conditions.

1.8. Previous results of our group

A Series of N-pyrrolo-bipyridine ligands was synthesized by our group. Homoleptic, bis-heteroleptic and tris-heteroleptic complexes of these ligands were synthesized and characterized by us **[151-153]**.

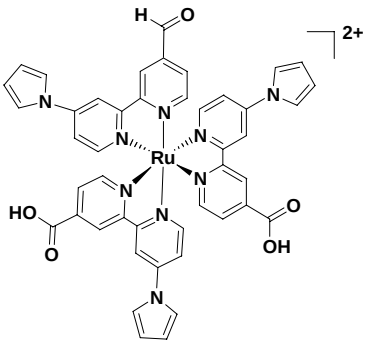

SOR_1

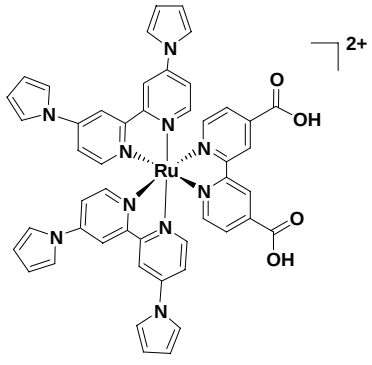

SOR_2

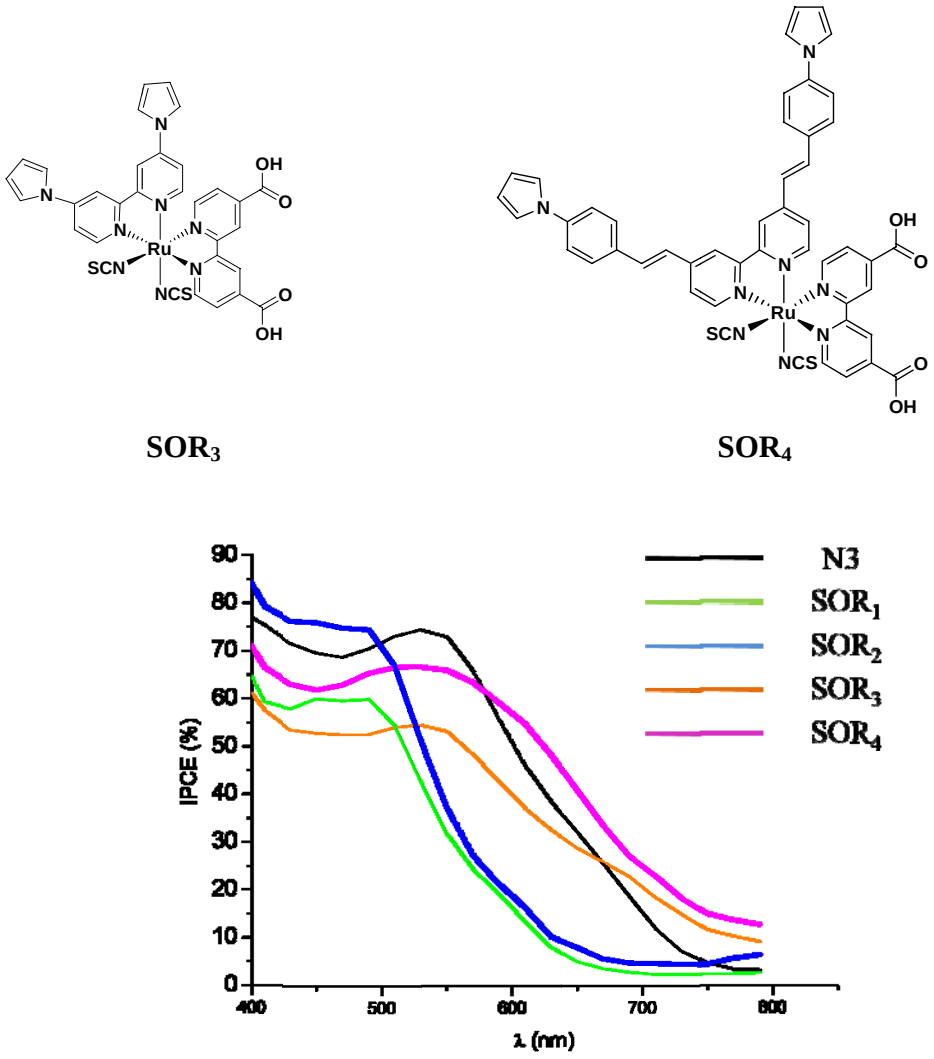

Figure 1.5: IPCE curves of pyrrole-based complexes developed in SOR group

Among them, SOR_3 (having an extended pyrrole ligand) and SOR_4 (also contained a styryl group) have been found as the most promising for several reasons. The pyrrole bound by its nitrogen atom to the bipyridine ligand brings electron-donating effects. The consequence is an increase of the HOMO energy level, allowing the MLCT transition to occur at lower energy and thus leading to red-shifted absorption of light. Additionally, π-electrons of pyrrole contribute to an increase of the molar extinction coefficient. The π-delocalization in SOR_4 led to an extended absorption domain even better than those of the standard dye N3 ($Ru(dcbpy)_2(NCS)_2$). In Fig. 1.5 black curve represents standard dye N3.

By taking these exciting and promising results into account, we further aimed to obtain more efficient dyes. For this purpose the structural and physical properties of the dyes are clearly important, especially the conjugation across the donor and anchoring groups, and good electronic coupling between the lowest unoccupied molecular orbital (LUMO) of the dye and the conduction band of TiO_2, which is very important for high electron-transfer rates.
Thus, in order to exploit such sensitizers, following points are worth considering.

1. It is necessary to lower the energy of the charge-transfer transition. Electron rich heteroaromatic ring e.g. thiophene possess smaller resonance energy in comparison with that of benzene (thiophene, 29 $kcalmol^{-1}$; benzene, 36 $kcalmol^{-1}$). It is well established that thiophene group substituted to an ancillary polypyridyl ligand in ruthenium sensitizers causes a red shift and increases an absorption coefficient of the MLCT band **[154-157].**

2. It is also well known that increasing the conjugation length of the ligand improves the molar extinction coefficient **[158].**

3. Introduction of organic antenna groups into Ru complexes is also carried out during last years in order to harvest photons over a large spectral window**.** The role of antenna is to maximize the absorption cross section of the light source, in terms of both absorption coefficients and the window of the wave lengths that are collected. A variety of elegant structures have been prepared and significant light-harvesting efficiencies have been achieved with antenna systems **[159-162].**

1.9.References

[1] United Nations Environment Programme (UNEP) "Global Environment Outlook (GEO)-2000", Earth- scan Publications Ltd., London (2000). Web site: www.unep.org.

[2] Intergovernmental Panel on Climate Change (IPCC) "Second Assessment Report - Climate Change 1995", (1995) Web site: www.meto.gov.uk

[3] Service, R.F. *Science*, 2005, ***309***, 548.

[4] Nelson, J. *The Physics of Solar Cells*; Imperial College Press: London, 2003.

[5] Kalyanasundaram, K. *Dye sensitized solar cells*, EPEL press: Switzerland, 2010.

[6] Green, M.A. *Third Generation Photovoltaics: Advanced Solar Energy Conversion.* Springer- Verlag: Berlin, Germany, 2004.

[7] Wronski, C.R. *Conference Record of the 28th IEEE Photo*Voltaic *Specialists Conference, Anchorage, AK*; IEEE: New York, 2000.

[8] O'Regan, B.; Grätzel, M. *Nature,* 1991, **353**, 737.

[9] Nazeeruddin, M.K.; Péchy, P.; Renouard, T.; Zakeeruddin, S.M.; Humphry-Baker, R.; Comte, P.; Liska, P.; Cevey, L.; Costa, E.; Shklover, V.; Spiccia, L.; Deacon, G.B.; Bignozzi, C.A.; Grätzel, M.; *J. Am. Chem. Soc.* 2001, **123(8)**, 1613.

[10] Barbe, C.J.; Arendse, F.; Comte, P.; Jirousek, M.; Lenzmann, F.; Shklover, V.; Grätzel, M. *J. Am. Chem. Soc.* 1997, **80**, 3157.

[11] Rothenberger, G.; Comte, P.; Grätzel, M. *Solar Energy Mater. Solar Cells*, 1999. **58**, 321.

[12] Hagfeldt, A.; Grätzel, M. *Chem. Rev.* 1995, **95**, 49.

[13] Nazeeruddin, M.K.; Zakeeruddin, S.M.; Humphry-Baker, R.; Jirousek, M.; Liska, P.; Vlachopoulos, N.; Shklover, V.; Fischer, C.H.; Grätzel, M. *Inorg. Chem.* 1999, **38**, 6298.

[14] Cahen, D.; Hodes, G.; Grätzel, M.; Guilemoles, J.F.; Riess, I. *J. Phys. Chem. B*, 2000, **104**, 2053.

[15] Van de Lagemaat, J.; Frank, A.J. *J. Phys. Chem. B,* 2000, 104.

[16] Ferber, J.; Luther, J. *J. Phys. Chem. B*, 2001, **105**, 4895.

[17] Hagfeldt, A.; Boschloo, G.; Sun, L.; Kloo, L.; Pettersson, H. *Chem. Rev.* 2010, **110***,* 6595.

[18] Nazeeruddin, M.K.; Baranoff, E.; Grätzel, M. *Solar energy*, 2011, **85**, 1175.

[19] Moser, J. *Monatsh. Chem.* 1887, **8,** 373.

[20] Gerischer, H.; Tributsch, H. *Berich. Buns. Gesell.* 1968, **72**, 437.

[21] Tributsch, H.; Gerischer, H. *Berich. Buns. Gesell.* 1969*,* **73***,* 251.

[22] Gerischer, H.; Schoppel, H.R.; Pettinge, B. *J. Electrochem. Soc.* 1972, **119**, 230.

[23] Memming, R. *Faraday Discuss.* 1974, 261.

[24] Memming, R.; Schroppel, F. *Chem. Phys. Lett.* 1979, **62**, 207.

[25] Memming, R.; Schroppel, F.; Bringmann, U. *J. Electroanal. Chem.* 1979, **100**, 307.

[26] Hasselman, G.M.; Watson, D.F.; Stromberg, J.R.; Bocian, D.F.; Holten, D.; Lindsey, J.S.; Meyer, G.J. *J. Phys. Chem. B,* 2006, **110**, 25430.

[27] Tsubomura, H.; Matsumura, M.; Noyamaura, Y.; Amamyiya, T. *Nature,* 1976, **261**, 402.

[28] Clark, W.D.K.; Sutin, N. *J. Am. Chem. Soc.* 1977, **99**, 4676.

[29] Gerischer, H. *Photochem. Photobiol.* 1972, **16**, 243.

[30] Gerischer, H. *Electroanal. Chem. Interfac. Electrochem.* 1975, **58**, 263.

[31] Memming, R. *Photochem. Photobiol.* 1972, **16**, 325.

[32] Jayadevaiah, T.S. *Appl. Phys. Lett.* 1974, **25**, 399.

[33] Tsubomura, H.; Matsumura, M.; Noyamaura, Y.; Amamyiya, T. *Nature,* 1976, **261**, 402.

[34] Fujishima, A.; Watanabe, T.; Tatsuoki, O.; Honda, K. *Chem. Lett.* 1975, **4**, 13.

[35] Hamnett, A.; Dare-Edwards, M.P.; Wright, R.D.; Seddon, K.R.; Goodenough, J.B. *J. Phys. Chem.,* 1979, **83**, 3280.

[36] Rensmo, H.; Keis, K.; Lindstrom, H.; Sodergren, S.; Solbrand, A.; Hagfeldt, A.; Lindquist, S.E.; Wang, L.N.; Muhammed, M. *J. Phys. Chem. B* 1997, **101**, 2598.

[37] Zhang, Q.F.; Dandeneau, C.S.; Zhou, X.Y.; Cao, G.Z. *Adv. Mater.* 2009, **21**, 4087.

[38] Desilvestro, J.; Grätzel, M.; Kavan, L.; Moser, J.; Augustynski, J. *J. Am. Chem. Soc.* 1985, **107**, 2988.

[39] Goncalves, L.M.; de Zea Bermudez, V.; Ribeiroa, H.A.; Mendes. A.M. *Energy Environ. Sci.*, 2008, **1**, 655.

[40] Grätzel, M. *Nature*, 2001, **414 (6861)**, 338.

[41] Grätzel, M. *Journal of Photochemistry and Photobiology A*, 2004, **164(1-3)**, 3.

[42] Heimer, T.A.; Heilweil, E.J.; Bignozzi, C.A.; Meyer, G.J. *Journal of Physical Chemistry A*, 2000, **104(18)**, 4256.

[43] Montanari, I.; Nelson, J.; Durrant, J.R. *Journal of Physical Chemistry B*, 2002, **106 (47)**, 12203.

[44] Oskam, G.; Bergeron, B.V.; Meyer, G.J.; Searson, P.C. *Journal of Physical Chemistry B*, 2001, **105(29)**, 6867.

[45] Bergeron, B.V.; Marton, A.; Oskam, G.; Meyer, G.J. *Journal of Physical Chemistry B*, 2005, **109(2)**, 937.

[46] Barnes, P.R.F.; Anderson, Y.A.; Mindaugas, J.; Lingxuan, L.; Xiaoe, L.; Palomares, E.; Fornelli, A.; O'Regan, B.C. *Phys. Chem. Chem. Phys.* 2011, **13**, 3547.

[47] Wang, M.K.; Chamberland, N.; Breau, L.; Moser, J.E.; Humphry-Baker, R.; Marsan, B.; Zakeeruddin, S.M.; Grätzel, M. *Nat. Chem.* 2010, **2**, 385.

[48] Gregg, B.A.; Pichot, F.; Ferrere, S.; Fields, C.L. *J. Phys. Chem. B* 2001, **105**, 1422.

[49] Hamann, T.W.; Farha, O.K.; Hupp, J.T. *J. Phys. Chem. C* 2008, **112**, 19756.

[50] Feldt, S.M.; Gibson, E.A.; Gabrielsson, E.; Sun, L.; Boschloo, G.; Hagfeldt, A. *J. Am. Chem. Soc.* 2010, **132**, 16714.

[51] Nusbaumer, H.; Moser, J.E.; Zakeeruddin, S.M.; Nazeeruddin, M.K.; Grätzel, M. *J. Phys. Chem. B* 2001, **105**, 10461.

[52] Nusbaumer, H.; Zakeeruddin, S.M.; Moser, J.E.; Grätzel, M. *Chem. Eur. J.* 2003, **9**, 3756.

[53] Sapp, S.A.; Elliott, C.M.; Contado, C.; Caramori, S.; Bignozzi, C.A. *J. Am. Chem. Soc.* 2002, **124(37)**, 11215.

[54] Brugnati, M. ; Caramori, S.; Cazzanti, S.; Marchini, L.; Argazzi, R.; Bignozzi, C.A. *Int. J. Photoenergy* 2007, 80756.

[55] Cazzanti, S.; Caramori, S.; Argazzi, R.; Elliott, C.M.; Bignozzi, C.A. *J. Am. Chem. Soc.* 2006, **128**, 9996.

[56] Schlichthorl, G.; Huang, S.Y.; Sprague, J.; Frank, A.J. *J. Phys. Chem. B* 1997, **101**, 8141.

[57] Kusama, H.; Arakawa, H. *J. Photochem. Photobiol., A* 2003, **160**, 171.

[58] Kusama, H.; Arakawa, H. *Int. Conf. Photochem., Nara, Japan* 2003, 103.

[59] Kusama, H.; Arakawa, H. *J. Photochem. Photobiol., A* 2004, **162**, 441.

[60] Kusama, H.; Arakawa, *J. Photochem. Photobiol., A* 2004, **165**, 157.

[61] Kusama, H.; Arakawa, *Sol. Energy Mater. Sol. Cells* 2004, **81**, 87.

[62] Kusama, H.; Arakawa, *Sol. Energy Mater. Sol. Cells,* 2004, **82**, 457.

[63] Kusama, H.; Arakawa, *Sol. Energy Mater. Sol. Cells* 2005, **85,** 333.

[64] Kusama, H.; Konishi, Y.; Sugihara, H.; Arakawa, H. *Sol. Energy Mater. Sol. Cells* 2003, **80**, 167.

[65] Kusama, H.; Arakawa, H.; Sugihara, H. *J. Photochem. Photobiol., A* 2005, **171**, 197.

[66] Kusama, H.; Sugihara, H. *J. Comput. Chem.* 2005, **26**, 1372.

[67] Kusama, H.; Sugihara, H. *Sol. Energy Mater. Sol. Cells* 2006, **90**, 953.

[68] Kusama, H.; Sugihara, H. *J. Photochem. Photobiol., A* 2006, **181**, 268.

[69] Tributsch, H. *Coord. Chem. Rev.*, 2004, **248**, 1511.

[70] Yanagida, M.; Yamaguchi, T.; Kurashige, M.; Hara, K.; Katoh, R.; Sugihara, H.; Arakawa, H. *Inorg. Chem.*, 2003, **42**, 7921.

[71] Boschloo, G.; Haggman, L.; Hagfeldt, A. *J. Phys. Chem. B,* 2006, **110**, 13144.

[72] Kay, A.; Grätzel, M. *Sol. Energy Mater. Sol. Cells*, 1996, **44**, 99-117.

[73] Figgemeier, E.; Hagfeldt, A. *Int. J. Photoenergy*, 2004, **6**, 127.

[74] Hagfeldt, A.; Grätzel, M. *Accounts of Chemical Research*, 2000, **33(5)**, 269.

[75] Kamat, P.V.; Ford, W.E. *Chemical Physics Letters*, 1987, **135(4-5)**, 1987.

[76] Kay, A.; Grätzel, M. *The Journal of Physical Chemistry*, 1993, **97(23)**, 6272.

[77] Liu, D.; Kamat, P.V. *Journal of Physical Chemistry*, 1993, **97(41)**, 10769.

[78] Das, S.; Rajesh, C.S.; Suresh, C.H.; Thomas, K.G.; Ajayaghosh, A.; Nasr, C.; Kamat, P.V.; George, M.V. *Macromolecules*, 1995, **28(12)***,* 4249.

[79] Rehm, J.M.; McLendon, G.L.; Nagasawa, Y.; Yoshihara, K.; Moser, J.; Grätzel, M. *Journal of Physical Chemistry*, 1996, **100(23)**, 9577.

[80] Paw, W.; Cummings, S.D.; Mansour, M.A.; Connick, W.B.; Geiger, D.K.; Eisenberg, R. *Coordination Chemistry Reviews*, 1998, **171(1)**, 125.

[81] He, J.; Hagfeldt, A.; Lindquist, S.-E.; Grennberg, H.; Korodi, F.; Sun, L.; Åkermark, B. *Langmuir*, 2001, **17(9)**, 2743.

[82] Islam, A.; Sugihara, H.; Hara, K.; Singh, L.P.; Katoh, R.; Yanagida, M.; Takahashi, Y.; Murata, S.; Arakawa, H. *Inorganic Chemistry*, 2001, **40(21)**, 5371.

[83] Odobel, F.; Blart, E.; Lagrée, M.; Villieras, M.; Boujtita, H.; El Murr, N.; Caramori, S.; Bignozzi, C.A. *Journal of Materials Chemistry*, 2003, **13(3)**, 502.

[84] Haque, S.A.; Handa, S.; Peter, K.; Palomares, E.; Thelakkat, M.; Durrant, J.R. *Angew. Chem., Int. Ed.* 2005, **44,** 5740.

[85] Klein, C.; Nazeeruddin, M.K.; Liska, P.; Di Censo, D.; Hirata, N.; Palomares, E.; Durrant, J.R. M. Grätzel, *Inorg. Chem.* 2005, **44**, 178.

[86] Nazeeruddin, M.K.; De Angelis, F.; Fantacci, S.; Selloni, A.; Viscardi, G.; Liska, P.; Ito, S.; Takeru, B.; Grätzel, M. *J. Am. Chem. Soc.* 2005, **127**, 16835.

[87] Nazeeruddin, M.K.; Klein, C.; Liska, P.; Grätzel, M. *Coord. Chem. Rev.* 2005, **249**, 1460.

[88] Nazeeruddin, M.K.; Wang, Q.; Cevey, L.; Aranyos, V.; Liska, P.; Figgemeier, E.; Klein, C.; Hirata, N.; Koops, S.; Haque, S.A.; Durrant, J.R.; Hagfeldt, A.; Lever, A.B.P.; Grätzel, M. *Inorg. Chem.* 2006, **45,** 787.

[89] Schmidt-Mende, L.; Kroeze, J.E.; Durrant, J.R.; Nazeeruddin, M.K.; Grätzel, M. *Nano Lett.* 2005, **5**, 1315.

[90] Wang, P.; Klein, C.; Humphry-Baker, R.; Zakeeruddin, S.M.; Grätzel, M. *J. Am. Chem. Soc.* 2005, **127**, 808.

[91] Barolo, C.; Nazeeruddin, M.K.; Fantacci, S.; Di Censo, D.; Comte, P.; Liska, P.; Viscardi, G.; Quagliotto, P.; De Angelis, F.; Ito, S.; Grätzel, M. *Inorg. Chem.* 2006, **45,** 4642.

[92] Chen, C.-Y.; Lu, H.-C.; Wu, C.-G.; Chen, J.-G.; Ho, K.-C. *Adv. Funct. Mater.* 2007, **17**, 29.

[93] Chen, C.-Y.; Wu, S.-J.; Li, J.-Y.; Wu, C.-G.; Chen, J.-G.; Ho, K.-C. *Adv. Mater. (Weinheim, Ger.)* 2007, **19**, 3888.

[94] Chen, K.S.; Liu, W.H.; Wang, Y.H.; Lai, C.H.; Chou, P.T.; Lee, G.H.; Chen, K.; Chen, H.Y.; Chi, Y.; Tung, F.C.; *Adv. Funct. Mater.* 2007, **17,** 2964.

[95] Ghosh, S.; Chaitanya, G.K.; Bhanuprakash, K.; Nazeeruddin, M.K.; Grätzel, M.; Reddy, P.Y. *Inorg. Chem.* 2006, **45,** 7600.

[96] Jang, S.-R.; Lee, C.; Choi, H.; Ko, J.J.; Lee, J.; Vittal, R.; Kim, K.-J. *Chem. Mater.* 2006, **18**, 5604.

[97] Mazille, F.; Fei, Z.F.; Kuang, D.B.; Zhao, D.B.; Zakeeruddin, S.M.; Grätzel, M.; Dyson, P.J. *Inorg. Chem.* 2006, **45**, 1585.

[98] Kuang, D.; Ito, S.; Wenger, B.; Klein, C.; Moser, J.-E.; Humphry- Baker, R.; Zakeeruddin, S.M.; Grätzel, M. *J. Am. Chem. Soc.* 2006, **128,** 4146.

[99] Kuang, D.B.; Klein, C.; Ito, S.; Moser, J.E.; Humphry-Baker, R.; Evans, N.; Duriaux, F.; Gratzel, C.; Zakeeruddin, S.M.; Grätzel, M. *Adv. Mater.* 2007, **19**, 1133.

[100] Faiz, J. ; Philippopoulos, A.I. ; Kontos, A.G.; Falaras, P.; Pikramenou, Z. *Adv. Funct. Mater.* 2007, **17**, 54.

[101] Murakoshi, K.; Kano, G.; Wada, Y.; Yanagida, S.; Miyazaki, H.; Matsumoto, M.; Murasawa, S. *J. Electroanal. Chem*. 1995, **396**, 27.

[102] Huang, S.Y.; Schlichthorl, G.; Nozik, A.J.; Grätzel, M.; Frank, A.J. *J. Phys. Chem. B* 1997, **101,** 2576.

[103] Ihara, M.; Tanaka, K.; Sakaki, K.; Honma, I.; Yamada, K. *J. Phys. Chem*. *B* 1997, **101**, 5153.

[104] Zaban, A.; Ferrrere, S.; Sprague, J.; Gregg, B.A. *J. Phys. Chem. B*. 1997, **101**, 55.

[105] Argazzi, R.; Bignozzi, C.A.; Heimer, T.A.; Meyer, G.J. *Inorg. Chem.* 1997, **36**, 2.

[106] Argazzi, R.; Bignozzi, C.A; Hasselmann, G.M.; Meyer, G.J. *Inorg. Chem*. 1998, **37**, 4533.

[107] Schlichthorl, G.; Park, N.G.; Frank, A.J. *J. Phys. Chem. B* 1999, **103,** 782.

[108] Ferrere, S.; Gregg, B.A. *J. Am. Chem. Soc.* 1998, **120**, 843.

[109] Jing, B.; Zhang, H.; Zhang, M.; Lu, Z.; Shen, T. *J. Mater. Chem*. 1998, **8**, 2055.

[110] Nasr, C.; Hotchandani, S.; Kamat, P.V. *J. Phys. Chem*. *B* 1998, **102**, 4944.

[111] Salafsky, J.S.; Lubberhuizen, W.H.; Van Faassen, E.; Schropp, R.E.I. *J. Phys. Chem. B* 1998, **102**, 766.

[112] Sughihara, H.; Sing, L.P.; Sayama, K.; Arakawa, H.; Nazeeruddin, M.K.; Grätzel, M. *Chem. Lett.* 1998, 1005.

[113] Bando, K.K.; Mitsuzuka, Y.; Sugino, M.; Sughihara, H.; Sayama, K.; Arakawa, H. *Chem. Lett.* 1999, 853.

[114] Franco, G.; Gehring, J.; Peter, L.M.; Ponomarev, E.A.; Uhlendorf, I. *J. Phys. Chem. B* 1999, **103**, 692.

[115] Langdon, B.T.; MacKenzie, V.J.; Asunskis, D.J.; Kelly, D.F. *J. Phys. Chem. B* 1999, **103**, 11176.

[116] Lemon, B.I.; Hupp, J.T.; *J. Phys. Chem. B* 1999, **103**, 3797.

[117] Kelly, C.A.; Farzad, F.; Thompson, D.W.; Stipkala, J.M.; Meyer, G.J. *Langmuir* 1999, **15**, 7047.

[118] Schwarzburg, K.; Willig, F. *J. Phys. Chem. B* 1999, **103**, 5743.

[119] Solbrand, A.; Henningsson, A.; Sodergren, S.; Lindstrom, H.; Hagfeldt, A.; Lindquist, S.-E. *J. Phys. Chem. B* 1999, **103**, 1078.

[120] Thompson, D.W.; Kelly, C.A.; Farzad, F.; Meyer, G.J. *Langmuir* 1999, **15**, 650.

[121] Anderson, S.; Constable, E.C.; Dare-Edwards, M.P.; Goodenough, J.B.; Hamnett, A.; Seddon, K.R.; Wright, R.D. *Nature* 1979, **280**, 571.

[122] Nazeeruddin, M.K.; Kay, A.; Rodicio, I.; Humphry-Baker, R.; Muller, E.; Liska, P.; Vlachopoulos, N.; Grätzel, M. *J. Am. Chem. Soc.* 1993, **115**, 6382.

[123] Nazeeruddin, M.K.; Péchy, P.; Grätzel, M. *Chem. Commun.*, 1997, 1705.

[124] Gratzel, M. *Prog. Photovoltaics Res. Appl*., 2000, **8**, 171.

[125] Nazeeruddin, M.K.; Humphry-Baker, R.; Grätzel, M.; Wöhrle, D.; Schnurpfeil, G.; Schneider, G.; Hirth, A.; Trombach, N. *Journal of Porphyrins and Phthalocyanines*, 1999, **3(3)**, 230.

[126] Wang, P.; Zakeeruddin, S.M.; Exnar, I.; Grätzel, M. *Chem. Commun.* 2002, 2972.

[127] Wang, P.; Zakeeruddin, S.M.; Moser, J.E.; Nazeeruddin, M.K.; Sekiguchi, T.; Grätzel, M. *Nat. Mater.* 2003, **2**, 498.

[128] Wang, P.; Zakeeruddin, S.M.; Humphry-baker, R.; Moser, J.E.; Grätzel, M. *Adv. Mater. (Weinheim, Ger.)* 2003, **15**, 2101.

[129] Wang, P.; Zakeeruddin, S.M.; Moser, J.E.; Humphry-Baker, R.; Comte, P.; Aranyos, V.; Hagfeldt, A.; Nazeeruddin, M.K.; Grätzel, M. *Adv. Mater.* 2004, **16**, 1806.

[130] Kuang, D.; Ito, S.; Wenger, B.; Klein, C.; Moser, J.-E.; Humphry- Baker, R.; Zakeeruddin, S.M.; Grätzel, M. *J. Am. Chem. Soc.* 2006, **128,** 4146.

[131] Jang, S.R.; Yum, J.H.; Klein, C.; Kim, K.J.; Wagner, P.; Officer, D.; Grätzel, M.; Nazeeruddin, M.K. *J. Phys. Chem. C* 2009, **113**, 1998.

[132] Arakawa, H.; Yamaguchi, T.; Agatsuma, S.; Takanori, S.; Koishi, Y. *Proceedings of the 23rd European Photo*V*oltaic Solar Energy Conference, Valencia, Spain*; 2008.

[133] Gao, F.F.; Cheng, Y.M.; Yu, Q.J.; Liu, S.; Shi, D.; Li, Y.H.; Wang, P. *Inorg. Chem.* 2009, **48**, 2664.

[134] Cao, Y.M.; Bai, Y.; Yu, Q.J.; Cheng, Y.M.; Liu, S.; Shi, D.; Gao, F.F.; Wang, P. *J. Phys. Chem. C* 2009, **113**, 6290.

[135] Jung, I.; Choi, H.; Lee, J.K.; Song, K.H.; Kang, S.O.; Ko, J.; *Inorg. Chim. Acta* 2007, **360**, 3518.

[136] Choi, H.; Baik, C.; Kim, S.; Kang, M.S.; Xu, X.; Kang, H.S.; Kang, S.O.; Ko, J.; Nazeeruddin, M.K.; Grätzel, M. *New J. Chem.* 2008, **32**, 2233.

[137] Hoertz, P.G.; Thompson, D.W.; Friedman, L.A.; Meyer, G.J. *J. Am. Chem. Soc.* 2002, **124**, 9690.

[138] Sauve, G.; Cass, M.E.; Coia, G.; Doig, S.J.; Lauermann, I.; Pomykal, K.E.; Lewis, N.S. *J. Phys. Chem. B* 2000, **104**, 6821.

[139] Kuciauskas, D.; Monat, J.E.; Villahermosa, R.; Gray, H.B.; Lewis, N.S.; McCusker, J.K. *J. Phys. Chem. B* 2002, **106**, 9347.

[140] Chiorboli, C.; Rodgers, M.A.J.; Scandola, F. *J. Am. Chem. Soc.* 2003, **125**, 483.

[141] Altobello, S.; Argazzi, R.; Caramori, S.; Contado, C.; Da Fre, S.; Rubino, P.; Chone, C.; Larramona, G.; Bignozzi, C.A. *J. Am. Chem. Soc.* 2005, **127**, 15342.

[142] Verma, S.; Kar, P.; Das, A.; Palit, D.K.; Ghosh, H.N. *J. Phys. Chem. C* 2008, **112**, 2918.

[143] Hasselmann, G.M.; Meyer, G.J. *J. Phys. Chem. B* 1999, **103**, 7671.

[144] Ferrere, S. *Chem. Mater.* 2000, **12**, 1083.

[145] Ferrere, S. *Inorg. Chim. Acta* 2002, **329**, 79.

[146] Geary, E.A.M.; Hirata, N.; Clifford, J.; Durrant, J.R.; Parsons, S.; Dawson, A.; Yellowlees, L.J.; Robertson, N. *Dalton Trans.* 2003, 3757.

[147] Geary, E.; Yellowlees, L.J.; Jack, L.A.; Oswald, I.D.H.; Parsons, S.; Hirata, N.; Durrant, J.R.; Robertson, N. *Inorg. Chem.* 2005, **44**, 242.

[148] Alonso-Vante, N.; Nierengarten, J.-F.; Sauvage, J.-P. *J. Chem. Soc., Dalton Trans.* 1994, 1649.

[149] Sakaki, S.; Kuroki, T.; Hamada, T. *J. Chem. Soc., Dalton Transac.* 2002, 840.

[150] Bessho, T.; Constable, E.C.; Grätzel, M.; Redondo, A.H.; Housecroft, C.E.; Kylberg, W.; Nazeeruddin, M.K.; Neuburger, M.; Schaffner, S. *Chem. Commun.* 2008, 3717.

[151] Martineau, D.; Beley, M.; Gros, P.C.; Cazzanti, S.; Caramori, S.; Bignozzi, C.A. *Inorg. Chem.* 2007, **46**, 2272.

[152] Grabulosa, A.; Beley, M.; Gros, P.C.; Cazzanti, S.; Caramori, S.; Bignozzi, C.A. Inorg. Chem. 2009, **48**, 8030.

[153] Grabulosa, A.; Martineau, D.; Beley, M.; Gros, P.C.; Cazzanti, S.; Caramori, S.; Bignozzi, C.A. *Dalton Trans.* 2009, 63.

[154] Jiang, K.-J.; Masaki, N.; Xia, J.; Noda, S.; Yanagida, S. *Chem. Commun*. 2006, 2460.

[155] Shi, D.; Pootrakulchote, N.; Li, R.; Gui, J.; Wang, Y.; Zakeeruddin, S. M.; Grätzel, M.; Wang, P. *J. Phys. Chem. C* 2008, **112**, 17046.

[156] Gao, F.; Wang, Y.; Zhang, J.; Shi, D.; Wang, M.; Humphry-Baker, R.; Wang, P.; Zakeeruddin, S.M.; Grätzel, M. *Chem. Commun.* 2008, 2635.

[157] Gao, F.; Wang, Y.; Shi, D.; Zhang, J.; Wang, M.; Jing, X.; Humphry- Baker, R.; Wang, P.; Zakeeruddin, S.M.; Grätzel, M. *J. Am. Chem. Soc.* 2008, **130**, 10720.

[158] Renouard, T.; Fallahpour, R.-A.; Nazeeruddin, M.K.; Humphry-Baker, R.; Gorelsky, S.I.; Lever, A.B.P.; Grätzel, M. *Inorg. Chem*. 2002, **41**, 367.

[159] Li, F.; Yang, S. I.; Ciringh, Y.; Seth, J.; Martin, C. H.; Singh, D. L.; Kim, D.; Birge, R. R.; Bocian, D. F.; Holten, D.; Lindsey, J. S. *J. Am. Chem. Soc.* 1998, **120**, 10001.

[160] Gilat, S. L.; Adronov, A.; Frechet, J. M. J. *Angew. Chem., Int. Ed.* 1999, **38**, 1422.

[161] Adronov, A.; Frechet, J. M. J. *Chem. Commun*. 2000, 1701.

[162] Ambroise, A.; Kirmaier, C.; Wagner, R. W.; Loewe, R. S.; Bocian, D. F.; Holten, D.; Lindsey, J. S. *J. Org. Chem.* 2002, **67**, 3811.

Chapter No: 2

Plan of Work

From the previous results of our group, we have noticed that the extended π-delocalization led to an extended absorption domain even better than N3 that is considered as standard dye so far. By taking these promising results into account we further aimed to obtain more efficient sensitizers.

Thus, in order to exploit such sensitizers,

1. We aimed to introduce thiophene ring in new class of ligands (resonance energy = 29 $kcalmol^{-1}$) to lower the energy of the charge-transfer transition.
2. We aimed to prepare ligands with extended conjugation length to improve the molar extinction coefficient.
3. In current study we are interested to incorporate some antenna type system in ligands to enhance light-harvesting efficiencies.

In order to get all above characteristics, we planned to incorporate dithienylpyrrole (DTP) moiety with different electron donating or electron withdrawing substituents, in our new class of ligands. DTP was planned to attach with bipyridine through different sites that can be thiophene ring, pyrrole ring or phenyl ring.

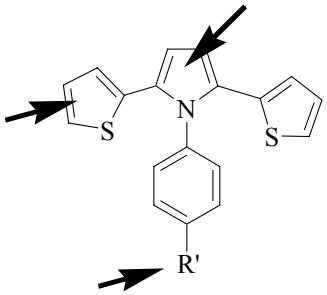

DTP

R’ = Electron donating group (methyl, hexyl)/electron withdrawing group (F, Br)

In current study we targeted to obtain complexes that are described in Figure 2.1.

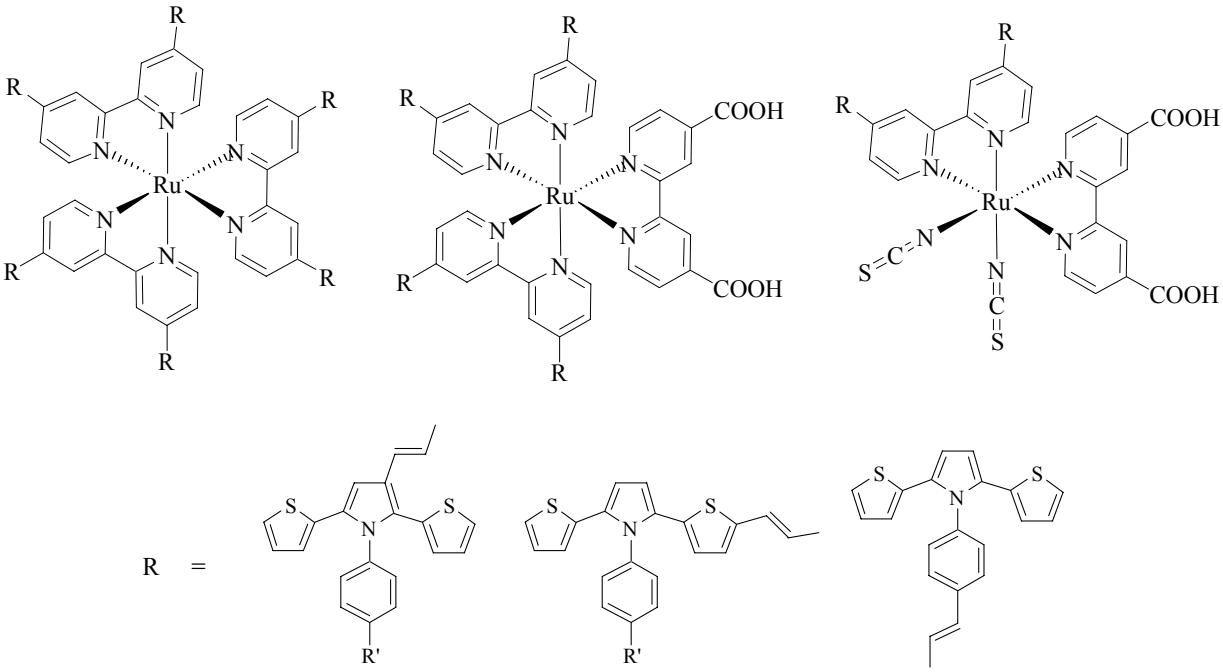

Figure 2.1: Structures of Ruthenium complexes targeted in current study

Retrosynthetic approach

In order to obtain targeted complexes, it is important to design synthetic scheme, so by following that targets can be achieved in efficient manner. Retrosynthetic approach is helpful in this regards (Scheme 2.1)

As shown, the new ligands can be obtained by a Wadsworth-Emmons reaction between DTP bearing carboxaldehyde at the appropriate position and bipyridyldiphosphonate. The aldehyde can be introduced on DTP moiety by using various formylation methods such as Vilsmeier-Haack reaction or lithiation reactions. Parent DTP moiety can be built by Paal-Knorr reaction between dithienyldiketone and an appropriate aniline derivative.

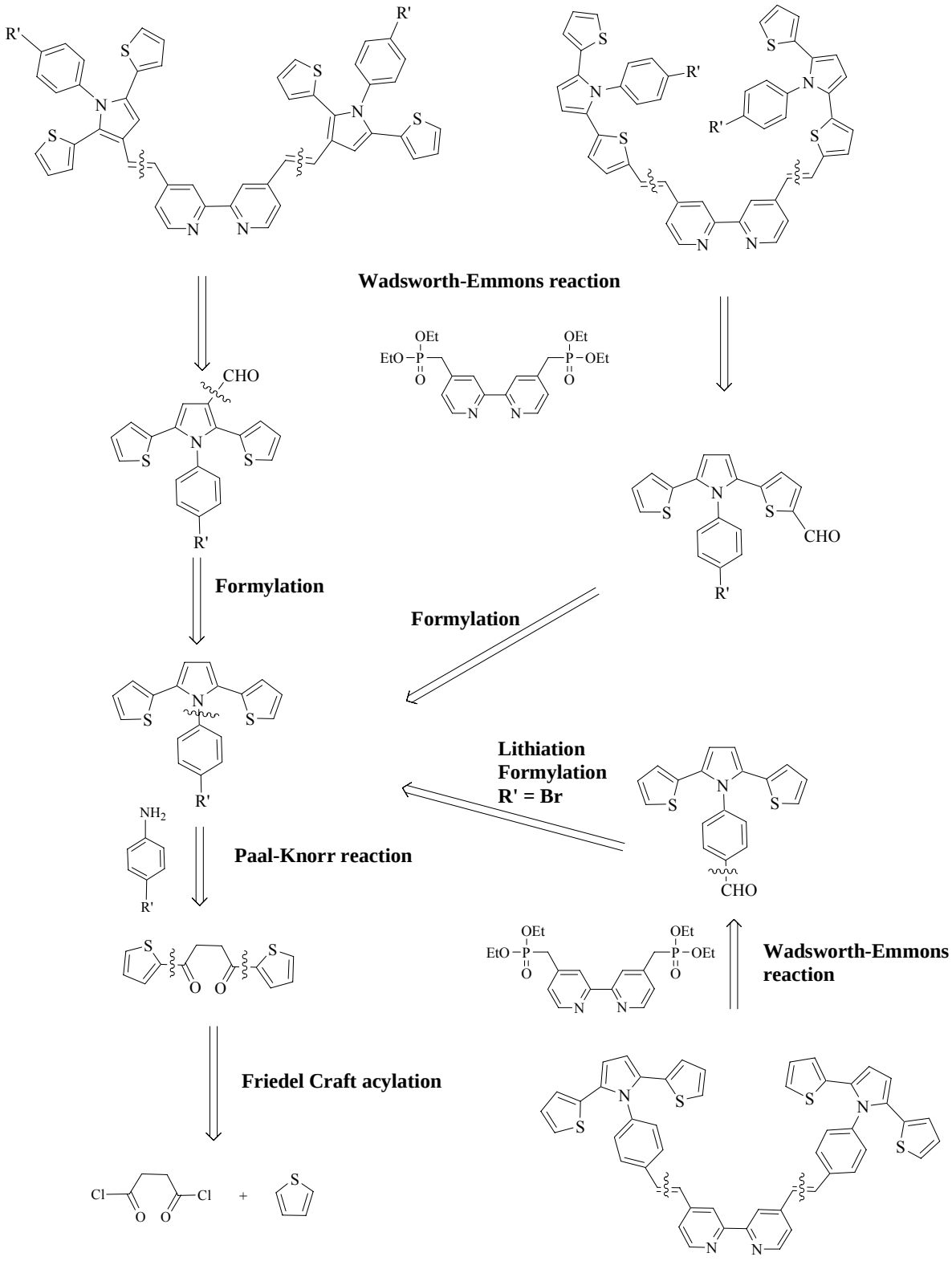

Scheme 2.1: Retrosynthetic approach for the synthesis of ligands

In the current study, we targeted the complexes that are shown in Figure 2.2. In the beginning homoleptic complexes can be prepared to evaluate the photophysical properties. Then bis-heteroleptic complexes can be synthesized having carboxylic acid groups to ensure anchoring at the surface of TiO_2 film and finally tris-heteroleptic complexes can be achieved to study the effect of additional ligand that is thiocyanate.

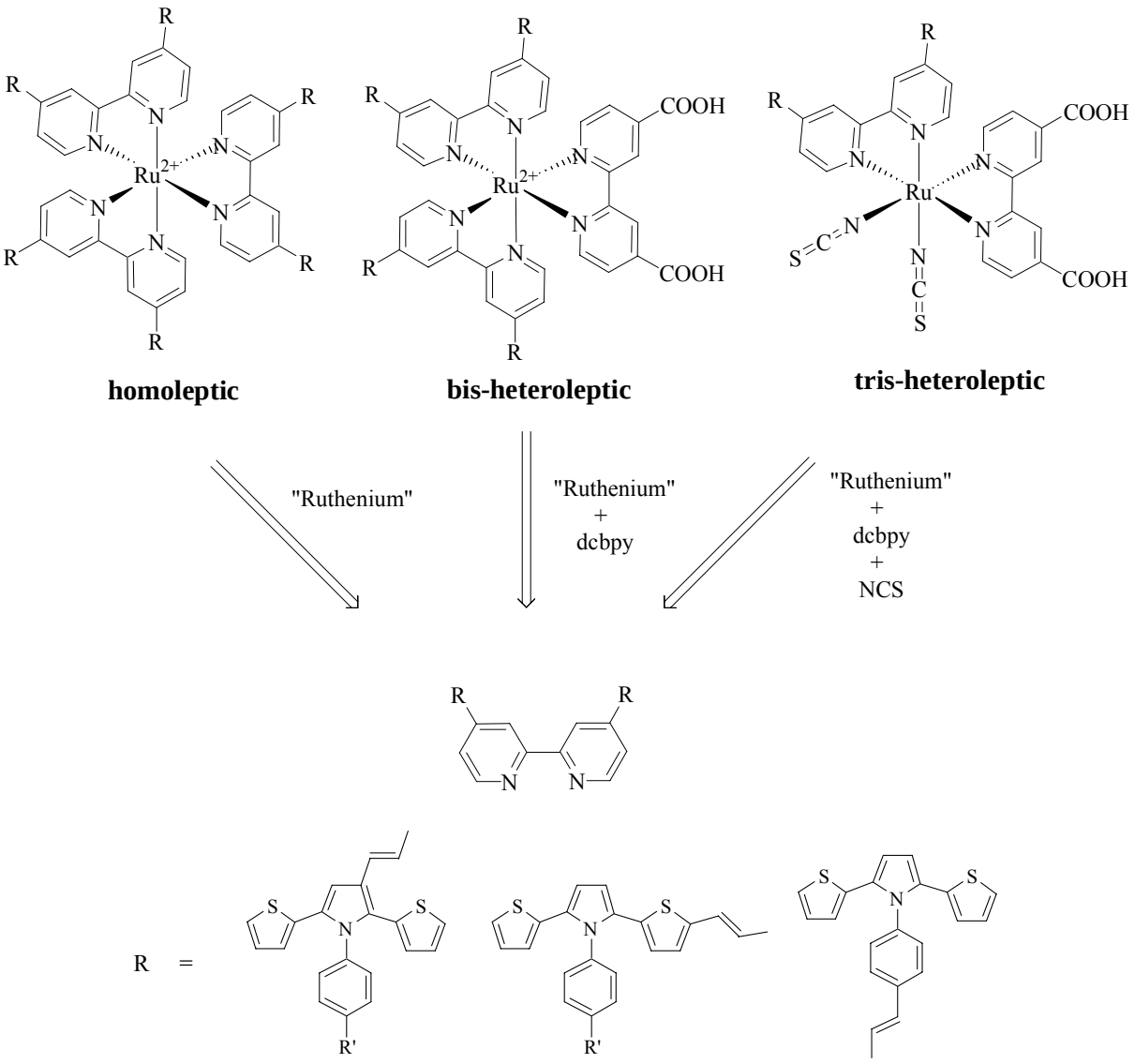

Scheme 2.2: Access to different families of complexes

Photophysical and electrochemical characterization of each complex will be carried out. Complexes bearing carboxylic acidic functional groups will be the subject of photoelectrochemical measurements and we will attempt to develop solar cells from them.

Chapter No: 3

Dithienylpyrroles (DTP)

By considering the desired characteristics in new series of ligands, we decided to examine the effect of mixed pyrrole-based compounds, dithienyl pyrrole (DTP) moieties. We explored literature to see to what extent work has been done in this area.

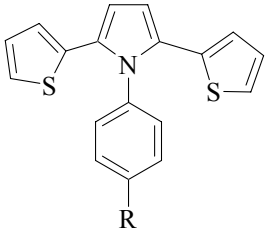

DTP

Ferraris and Skilies in 1987 first proposed the use of poly 2,5-di(2-thienyl)- 1*H*-pyrrole (SNS) derivatives as a route to well defined co-polymers that are not easily achieved through oxidative copolymerization of momomer mixture, even if the monomer oxidation potential are very similar **[1]**. SNS derivatives were chosen as polymer precursor for several reasons.

1. The functionalization of ter-heteroatom unit by the use of the Paal-Knorr reaction seemed an attractive one step procedure for introducing various bridges into the monomer.
2. The oxidation potential of the SNS derivatives is lower (about 0.7 V vs SCE) than that of their ter-thiophene analogues (about 0.95 V vs SCE) **[2]**.
3. Good quality films of poly SNS can easily generated on platinium from various solvents **[3, 4].**

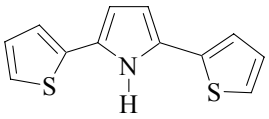

SNS

The majority of work on the anodic polymerization of 2,5-di-(2-thienyl)-pyrrole (SNS) has been devoted to the study of optical, electrical, structural and electrochemical properties of the obtained soluble conducting polymer **[5].**

In 2002, Just et al., reported the synthesis of less geometrically and sterically constrained structures by using N, N'- disubstituted SNS derivatives **[6]**.

Development of π–conjugated polymers and oligomers has been a significant subject of many recent studies because of the numerous optical, electrochemical and electrical properties of these compounds. In particular, poly- and oligothiophenes appear to be promising candidates on account of their high chemical and electrochemical stability. Since unsubstituted poly- and oligothiophenes become less soluble in regular organic solvents, alkyl chains are often introduced into the thiophene ring to improve their solubility. However, these chains cause another problem, that is, the co-planarity of the π–conjugated system is decreased **[7, 8, 9]**. An acceptor-donor-acceptor type of non-linear optics has already being reported **[10], 1** which have an electron-donating terthiophene-based π–system at the center and electron-accepting ketene dithioacetal *S,S*-dioxide moieties at both ends. Although the compound **1** (R_1=Me, R_2=*p*-Tol) showed excellent properties but its low solubility in regular organic solvents prevented further research and development. In order to solve this dilemma, Ogura et al., focused their attention on a 1-aryl-2,5-di(2-thienyl)pyrrole (DTP) system as an elementary unit. This new system was expected to have some advantageous points: (i) the central aryl group stands perpendicular to the π–system such that the co-planarity is affected to a lesser extent to cause a bathochromic shift in its UV-vis. absorption spectrum. (ii) the perpendicular aryl group impedes the stacking of the π–systems and as a result increases their solubility; (iii) various aryl groups can be employed in order to evolve the physical properties of **1**. Ogura et al., reported a synthetic route leading to 1-aryl-2,5-di(2-thienyl)pyrroles and their oligomers as well as their physical properties, including third order optical non-linearity **[11]**.

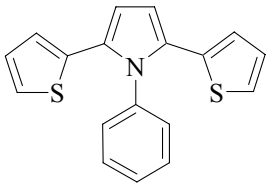

DTP

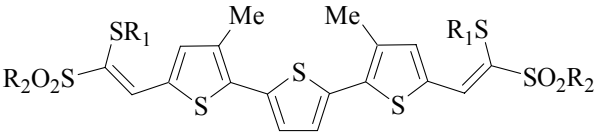

1

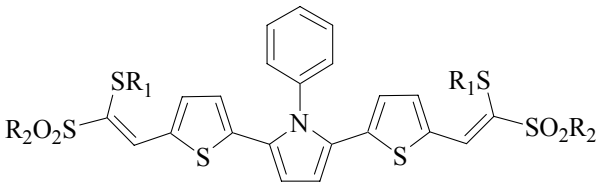

2

1-aryl-2,5-di(2-thienyl)pyrrole system was employed as the central donor site. Among various derivatives of **2** (Ar = *o*-, *m*-, or *p*-methoxyphenyl, phenyl, *p*-chlorophenyl; R_1 =R_2=Me, *p*-tolyl, *p*-methoxyphenyl, or *p*-chlorophenyl), derivative (Ar = *m*-methoxyphenyl, R_1 = R_2 = *p*-tolyl) gave best results for the third-order non-linear optics with relatively lower molecular weight **[10]**.

The ability to tune the color constitutes, one of the important goals in the design of electrochromic devices. Organic materials are attractive for such purposes since a wide range of colors can result from variations in molecular structure **[12, 13]**. Although there have been reports of multicolor electrochromic materials, it is unusual for one conducting polymer to exhibit an electrochromic change covering the entire visible region **[14, 15, 16].** A simple method of achieving a wide range color change might result from a combination of two electrochromic conducting polymers or an electro-chromic polymer with another electrochromic material, each covering a different color change region **[17]**.

In 1998, Meeker et al., tried to determine whether is it possible to obtain color changes by making blends of two polymers exhibiting different electrochromic properties since this method might lead to more facile modifications of the color. To test this they chose poly(*N*-vinylcarbazole), PVK, an electrochromic material that is green in the doped state and colorless in the neutral state, and another polymer poly(*N*-phenyl-2-(2′-thienyl)-5-(5″-vinyl-2″-thienyl)pyrrole), PSNPhS, whose color changes from yellow to reddish brown when oxidized.

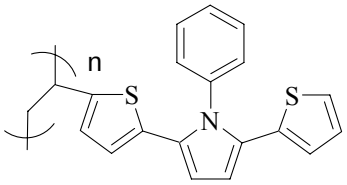

PSNPhS

The electrochromic properties of these polymer blends were studied and their reflectance spectra were analyzed. The electrochromic properties of these blends were found to be controlled by modifying the ratio of the individual components of the blends, which provides a simple and effective technique for tailoring the color. Furthermore these blends

successfully generated the desired range of brown, tan, and green colors often found in natural vegetation and soils **[18]**.

Audebert et al., 2002 reported conjugated electroactive polymers (2,5-dithienylpyrrole derivatives) based on an azo dye i.e. 4-[(2,2'-bis thienyl)-N-pyrrolyl]azobenzene **(3)** and bis-4,4'-[(2,2'-bisthienyl)-N-pyrrolyl]azobenzene **(4)**.

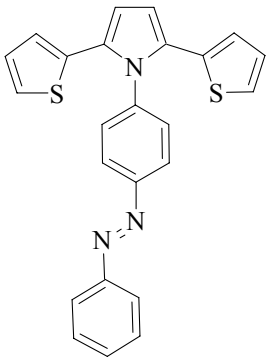

3

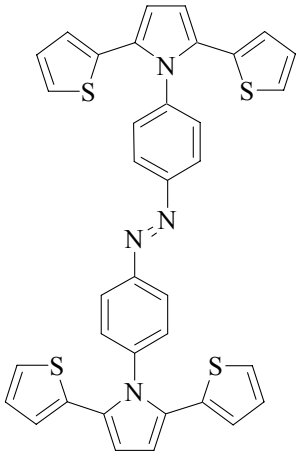

4

The first results obtained from spectroscopic, electrochemical measurements, as well as the theoretical calculations, have demonstrated an extended conjugation brought about by the azo moiety in the pyrrole derivatives. In the case of 2, 5-dithienylpyrrole derivatives, no stabilizing effect through the conjugation with the azo group has been observed, leading to oxidation localized on the polymerizable units. Therefore, it seems unfortunately unlikely that in conjugated polymers of this kind, a high conjugation may be achieved between the main chain and the functional group. However, this feature remains to be confirmed by further studies **[19]**. Analogous to previous work of Audebert et al., on *N*-azo pyrroles and 2,5-dithienylpyrroles, Thompson and his colleagues presented a new class of fully conjugated monomers, which contain a pendant photochromic salicylidene-aniline functionality. Monomers **5** and **6** were found to electropolymerize to yield electroactive films, which displayed an electrochromic response upon oxidation changing from yellow to green to gray-blue **[20]**.

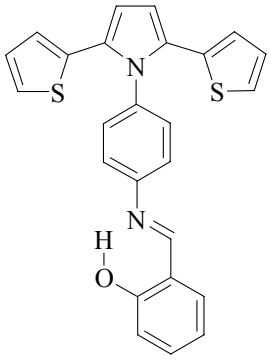

5

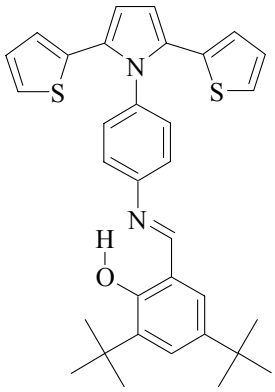

6

Ogura et al., 2002 reported 1-aryl-(2-thienyl)-5-[5-(tricyanoethenyl)-2-thienyl]pyrroles, a new class of π-conjugated compounds comprised of a stronger π-electron-withdrawing tricyanoethenyl substituent and a conjugated thiophene-pyrrole-thiophene skeleton which shows gold- or bronze-like metallic lusters and have possibility of applications in novel functional materials. Their metallic color relies on the substitutent on the central *N*-phenyl ring of **7**. When a small substituent is located at the *para*-position of the *N*-phenyl group, gold-like lustrous crystals were formed. The derivatives of **7** having a longer alkyl chain at the *para* position of the aryl ring gave bronze-like crystals **[21].** Crystals with red-violet metallic luster were obtained in the case that heteroatom combined methyl substituents (OMe, SMe, and NMe_2) are introduced into the *para* position of the central aryl group **[22]**.

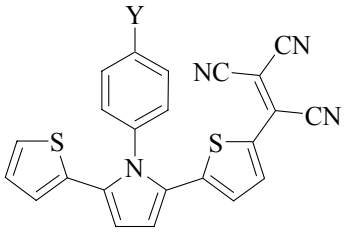

7

Interestingly, X-ray structural analysis revealed that, in these crystals, the molecules are arranged into a planar sheet-like, flat lane-like, or heaving ribbon-like structure via the interatomic C-H···N hydrogen bond between the *cyano* group and the olefinic hydrogen (CN···H-C-C) to make their π-system get close to each other. One characteristic feature of these metal-lustrous crystals is that they dissolve easily in common organic solvents and are quickly deposited from the resultant solution upon evaporation. However, this property is disadvantageous when they are utilized as a metal-lustrous pigment.

In order to develop gold-like lustrous crystals that are sparingly soluble in common organic solvents, Ogura et al., designed a 1-aryl-2,5-bis[5-(tricyanoethenyl)-2-thienyl]-pyrrole **(8)** π -system having two tricyanoethenyl groups that would play an important role in

the intermolecular interaction, and it was found that 1-(*p*-substituted phenyl)-2,5-bis[5-(tricyanoethenyl)-2-thienyl]pyrroles form insoluble gold-like lustrous crystals when the *p* substituent is relatively small, like cyano and methyl groups. Notably, these crystals show a higher melting point of more than 300°C, and, especially, the melting point of the crystals of (Y=CN) is 394°C. The essential motif present in these crystals is an infinite, intermolecular network of CN···H-C-C interactions which organize the molecules to arrange regularly into a planar sheet. The number of CN···H-C-C interactions that originate from the unique effect of two tricyanoethenyl groups make the crystals sparingly soluble in organic solvents including DMF and DMSO. This property promises the crystals to be utilized as an organic pigment with gold-like metallic luster, which was on-going subject **[23]**.

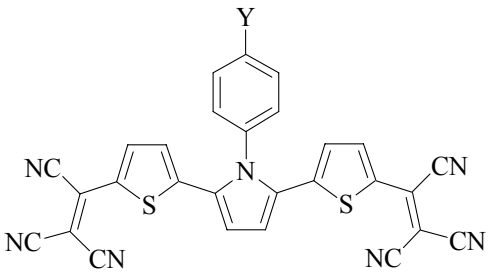

8

As a part of further investigation, the group of Ogura also synthesized the compound bearing two tricyanoethenyl groups **(9)**, and found that crystallization of compound from its DMF solution results in formation of bronze-like microcrystals with inclusion of DMF. Further studies have revealed that gold-like inclusion crystals can be formed by effective inclusion of synthesized with various electron-donating aromatic molecules such as toluene, *p*-xylene, anisole, dimethoxybenzenes, and indene. Apart from this inclusion phenomenon they also report the relationship between crystal appearance and crystal structure **[23]**.

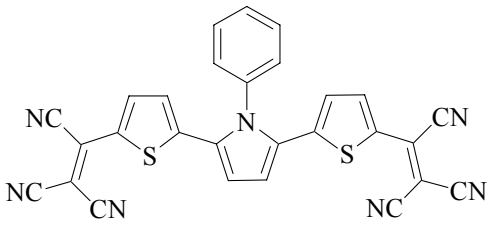

9

Due to the attachment of two powerful electron-withdrawing tricyanoethenyl groups to 1-phenyl-2,5-di(2-thienyl)- pyrrole skeleton leads to a new versatile construction element which proved useful in crystalline inclusion and π-conjugated compound supramolecular chemistry. The inclusion crystals show gold-like metallic lustre, suggesting that the origin of the metallic lustre is not exclusively limited to the tricyanoethenyl derivative itself, but

possibly also to the crystalline inclusion compound containing tricyanoethenyl derivative. Based on the structural features of the inclusion crystals, it was interpreted that the essential origin of the gold-like metallic lustre is due to the co-planar sheet-like crystal arrangement being extremely favorable to the sidewise intermolecular π–π contact (CN···C=C) between the host molecules. It was also noteworthy that the aromatic guest molecules suitable for the crystalline inclusion are all electron-donating. Combined with the fact that the electron-deficient quinone and 2,3-dichloro-5,6-dicyano-1,4-benzoquinone (DDQ) molecule cannot be included, so, it can be infered that electrostatic forces also play a role in these supramolecular architectures **[23]**.

Nakazaki et al., 2003 reported a thienyl substituted derivative, 4-[2', 5'-bis(2"-thienyl)-1'-pyrrolyl]phenylNN (*N*-TPN), along with other pyrrole derivatives, with aim to prepare conductive high spin polymers. Pyrrole derivatives were selected as spin carrying monomers because of their low oxidation potentials.

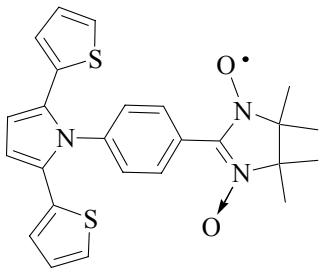

(*N*-TPN)

From analysis of pyrrolylNN electronic structure based on the perturbational MO method and electrochemical evidence for the electronic structure, it was found that N-TPN would be an effective building block for the preparation of a conductive magnetic macromolecule **[24]**.

Due to its unique three-dimensional structure and high degree of π-electron delocalization, C_{60} and its functional derivatives are widely studied. In particular, C_{60}-based thin films have potential applications in photoconductivity, superconductivity upon doping with alkali metals, nonlinear optics, and biological activity. Self-assembly is a superior approach to achieve thin-film materials because self-assembled monolayers (SAMs) are formed spontaneously by chemisorption, yielding robust and well-defined structures on chosen substrates. Kim et al., reported a newly synthesized rigid C_{60}-tethered 2,5-dithienylpyrrole triad, described its synthesis, electrochemical properties, and highly efficient photocurrent generation in SAMs. The π-conjugated 2,5-dithenylpyrrole was chosen as a donor segment, whereas the C_{60} acts as an acceptor. The phenylethynyl moiety was chosen to provide a rigid framework in the molecular structure for forming a stable and conducting

footing in the SAM. This design strategy is readily applicable to materials for highly efficient photovoltaic devices **[25]**.

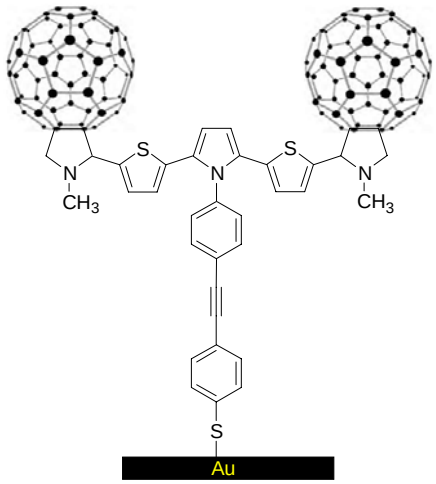

Figure 2.1: the C_{60}s and the chromophores are spatially separated

Conjugated donor-acceptor molecules based on 9-cyanoanthracene have been prepared by Lin and co-workers. Two series of 9-cyanoanthracene compounds, namely, biaryls (9-phenyl-10-anthronitriles, PANs) and biarylethynes (9-phenylethynyl-10-anthronitriles, PEANs) have been synthesized. The donors used for this purpose were methoxy- (ie., anisole, An-), *p*-*N*,*N*-(dimethylamino)- (DMA-), *p*-(2,5- dithienyl)pyrrolyl- (DTP-), and *N*,*N*-di-*p*-anisylamino- (An_2N-) substituted phenyls, and the acceptor was the anthronitrile (AN) moiety. The approach was to provide the fluorophore AN with incremental electron-donating strength at the phenyl moiety from no donor to weak (OMe) to strong (NMe_2) donors and high-spin donors [*N*-(2,5-dithienylpyrrolyl)phenyl- (DTP-P) and *N*,*N*-di-*p*-anisylaminophenyl- (An_2N-P)]. From photophysical measurements, electrochemical measurements and density functional calculations no electronic communication between the DTP donor and AN acceptor was established whereas in other system it was observed in different ranges **[26]**.

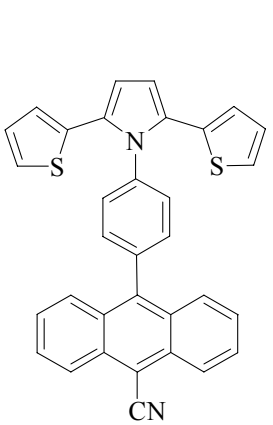

DTP-PAN

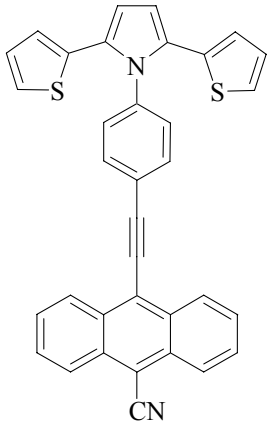

DTP-PEAN

The oxidation potentials of 2,5-bis(2-thienyl)-1*H*-(pyrrole) (SNS) derivatives are quite low (about 0.7V vs Ag/Ag^{+}) due to the conjugation of SNS into the aromatic system and the presence of heteroatoms (S and N) in the main chain **[27]**. An electrochromic material sustains reversible and persistent changes of its optical properties upon applied potential. An electroactive or photoactive moiety are introduced along this SNS backbone to tune the band gap and thus to gain useful properties **[28, 29]**. Koyuncu et al., synthesized a new conducting 2,5-bis (2-thienyl)-1*H*-(pyrrole) (SNS) polymer containing electroactive carbazole subunits **(10)** via chemical and electrochemical processes. CV measurements showed two separate redox processes which were observed at +0.84V and +1.43 V, via one-electron stepwise oxidation processes of SNS and carbazole moiety, respectively. The polymer coated onto ITO–glass surface by electro-oxidative process gives uniform film that exhibits electrochromism among three different colors (orange, green and blue). Chemical polymerization product exhibits a high thermal stability and narrow molecular weight distribution. The results anticipate that this kind of polymers can be used for designing electrochromics based on the use of one molecule for the generation of three basic colors **[30]**.

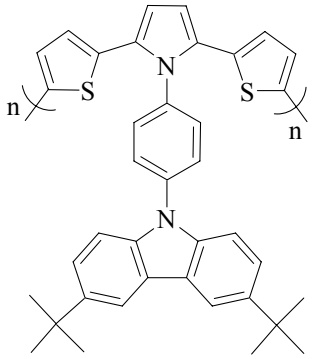

10

So, 2,5-bis-dithienyl-1*H*-pyrrole (SNS) derivatives are very important electroactive polymer for electrochromic applications **[31]**.

The synthesis of the monomer, 4-(2,5-di(thiophen-2-yl)-1H-pyrrol-1-yl)benzenamine ($SNS-NH_2$) and its electrochemical polymerization and characterization was reported by Yildiz and co-workers **[32]**. Tuncagil et al., reported the use of $SNS-NH_2$ matrix as a bacterial biosensing platform. *G. oxydans* cells were entrapped on this novel conducting polymer behind a dialysismembrane onto the surface of graphite electrode. The measurement was based on the respiratory activity of the cells. As well as the optimization and characterization, application of the proposed system on real samples was carried out **[33]**.

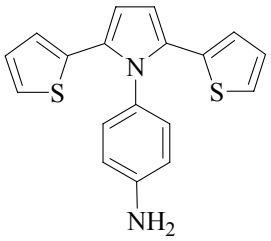

SNS-NH_2

So it is concluded that the use of conducting polymers in the area of bioanalytical sciences is of great interest since their compatibility opens up the possibility of using them in different biosensing applications **[34, 35]**.

Immobilization is a technique which comprises attachment of enzyme to a solid matrix without loss of catalytic activity. Thus enzyme immobilization on solid support materials becomes a very effective way to stabilize them.

Selebi et al., investigated the immobilization of invertase via electrochemical method in poly(2,5-di(thiophen–2-yl)-1-p-tolyl-1H-pyrrole-co-pyrrole) (DTTP). Optimum pH, temperature and kinetic parameters were examined for the immobilized enzymes. Also, operational stability and shelf life of the enzyme electrodes were determined.

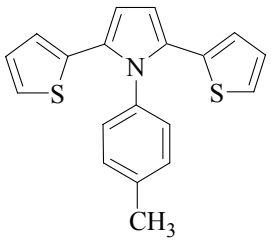

DTTP

Fujii et al. have reported the use of thiophene–pyrrole mixed oligomers in organic field-effect transistors (OFETs) with mobilities exceeding values of $10^{-2}cm^2V^{-1}s^{-1}$ **[36]**. Homogeneous oligothiophenes have been synthesized with a multitude of chemical variants for use in device applications, such as OFETs, OLEDs (organic light-emitting diodes), organic photovoltaics, and optically pumped organic lasers.

Given this diverse spectrum of applications for the related oligothiophenes, Oliva et al., studied of a new series of thiophene–pyrrole co-oligomers [Hex265T, TPT, Hex2-TPT, Hex2-TTPTT, TPT-p(HP) , Hex2-TPT-p(HP) , Hex2-TTPTT-p(HP)].

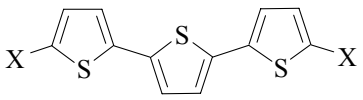

3T (X=H)
Hex2-3T (X=C_6H_{13})

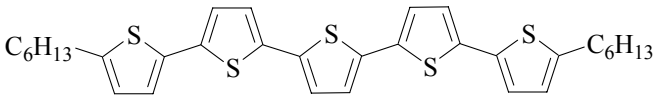

Hex2-5T

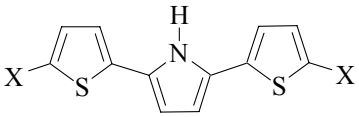

TPT (X=H)
Hex2-TPT (X=C_6H_{13})

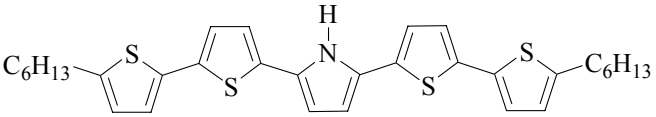

Hex2-TTPTT

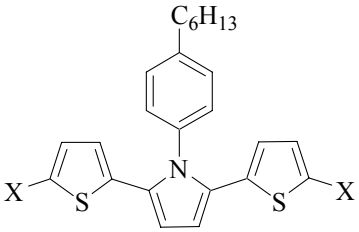

TPT-p(HP) (X=H)
Hex2-TPT-p(HP) (X=C_6H_{13})

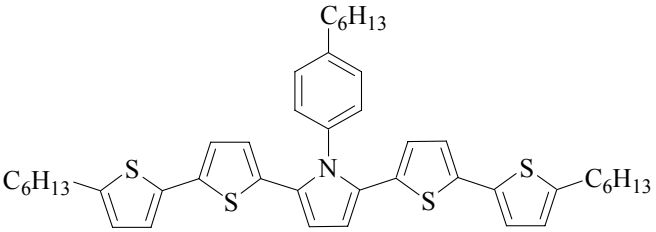

Hex2-TTPTT-p(HP)

The approach includes studying the electronic absorption and emission spectra, the electrochemical properties, and the vibrational Raman spectra in combination with their theoretical estimation. In-depth comparison between the co-oligomers and the homogeneous oligo-thiophenes of the same length and substitution pattern (3T, Hex2-3T and Hex2-5 T) was carried out. Both neutral and oxidized species were included in study. The pyrrole inclusion improved both the oxidation capacity and the luminescence properties relative to their homogeneous oligothiophenes. On the other hand, the addition of hexyl and hexyl–phenyl groups might improve the processability and chemical stability, two key requirements for the successful implementation in useful devices. The inclusion of five-membered rings of a different nature caused the molecular π-conjugated backbone to be slightly distorted, while conserving good redox and luminescence responses. Overall, this study sheds light on the potential of mixed thiophene–pyrrole oligomers for use in organic electronics **[37]**.

Yavuz et al., synthesized a new monomer, 4- (2,5-di-2-thiophen-2-y l-pyrrol-1-yl) - phthalonitrile (SNS-PN), containing an acceptor group bonded to a high-spin donor.

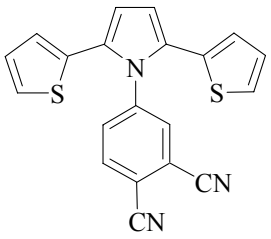

SNS-PN

The corresponding polymer P(SNS-PN) was obtained electrochemically and its characterization was performed using cyclic voltammetry (CV) and Fourier transform infrared (FTIR) techniques. The shifts in the oxidation potential of the polymer film make P(SNS-PN) also a candidate in cation sensing, besides its use in organic lasers and electroluminescent materials **[38]**.

In 2010, Sefer et al., reported the synthesis of 3-(2,5-di-2-thienyl-1*H*-pyrrol-1-yl)-9-ethyl-9 H-carbazole (SNSC) monomer and its electrochemical polymerization onto indium tin oxide (ITO)/glass surface to produce a polymeric electrochromic material exhibiting a high contrast ratio in the NIR region (Δ T = 50% at 1000 nm). Further, electrochemical and optical band gap were calculated by using their oxidation and reduction onset potentials and absorption edges, respectively. Finally, an electrochromic device (ECD) constructed from it represents a very short response time (about 0.3 s), high redox stability and a high coloration efficiency (1216 cm^2C^{-1}).

Finally, electrochemical and optical behavior exhibited that the SNSC polymer having the low oxidation potential may be used as donor unit for the conjugated donor–acceptor low band gap polymers, which is one of the most important issues in optoelectronic technologies such as organic solar cells (OSCs) for high photon to current conversion efficiency and organic light-emitting diodes (OLEDs) **[39]**.

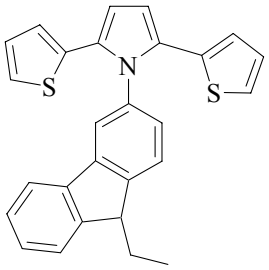

SNSC

Wang et al., reported three SNS derivatives i.e. SNS-1, SNS-2, SNS-3. Longer conjugate moieties and new functional group (amino group) were introduced to the central pyrrole ring of the SNS monomer, which made the polymer chains softer and easily modified.

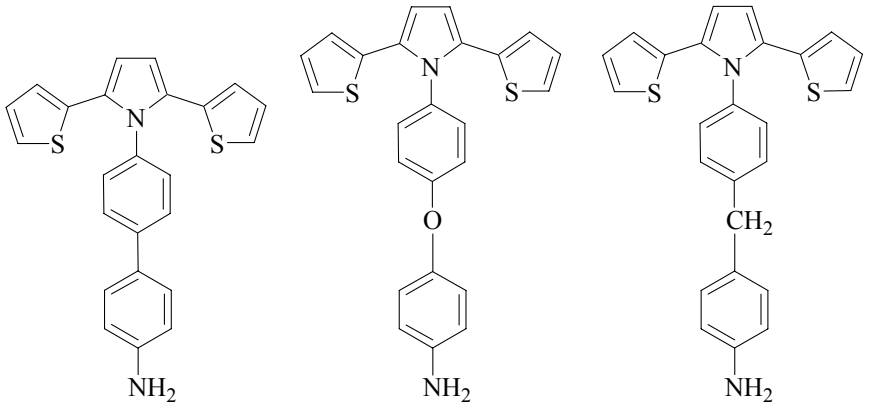

SNS-1 **SNS-2** **SNS-3**

Moreover, their corresponding polymer films were prepared by electropolymerization, and their spectroelectrochemical, electrochromic behavior were also studied and compared. It was found that the three polymer films performed similar spectroelectrochemical properties. All the three polymer films showed a stable, well-defined reversible redox process and multicolor electrochromic behavior (mainly yellow in the reduced state, grey in the intermediate state and blue in the oxidized state) which can make them amenable for electrochromic devices **[40]**.

Wang and his co-workers further synthesized double SNS hybrid polymer materials, 2SNS-1, 2SNS-2 and 2SNS-3 and corresponding polymer fims.

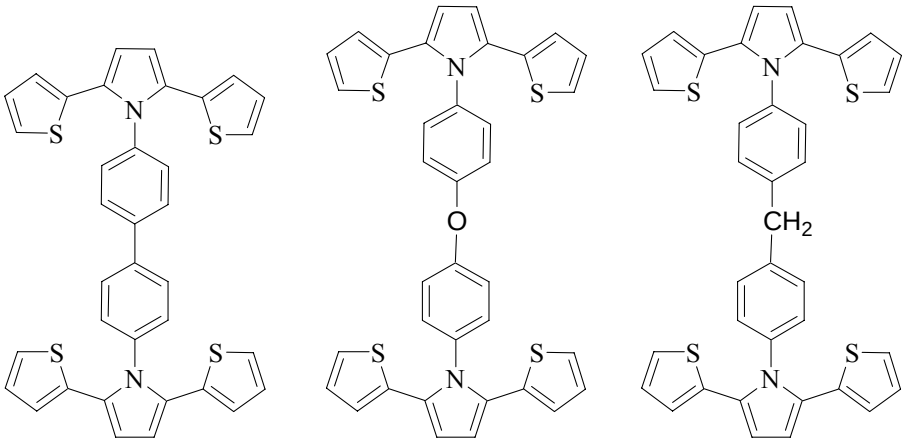

2SNS-1 **2SNS-2** **2SNS-3**

Their spectroelectrochemical, electrochromic and fluorescent properties were investigated and compared. All of the three polymer films exhibited stable, well-defined, reversible redox processes, low optical band gaps, thermal stabilities, smooth layer structures, multicolor electrochromic behaviors and fluorescence **[41]**.

Overall it can be concluded that despite appropriate oxidation capability and enhanced luminescence properties dithienylpyrrole (DTP) have been studied to a lesser extent and have limited applications in organic electronic applications than oligothiophenes essentially due to lack of efficient synthetic routes.

It is evident from the above examples that the DTP moieties have not been bound to a bipyridine ligand yet and their effect on the electronic properties of the corresponding complexes are unexplored.

So, it can be a potential candidate to bind to bipyridine in order to prepare new series of ligands. As in this way it is possible to incorporate thiophene ring in the system that can be helpful to decrease the energy of the charge-transfer transition and conjugation length can be extended as well. Moreover the DTP moiety can be used as antenna function to enhance harvesting of photons over a wide spectral range.

So, we aim to synthesize different series of DTP-based bipyridine ligands (on the basis of connectivity), with different electron donating and electron withdrawing substituents. From these ligands homoleptic, bis-heteroleptic and tris-heteroleptic ruthenium complexes were planned to prepare.

References

[1] Ferraris, J.P.; Skiles, G.D. *Polymer*, 1987, **28**, 179.

[2] Ferraris, J.P.; Newton, M.D. *Polymer*, 1992, **33**, 391.

[3] Ferraris J.P.; Hanlon, T.R. *Polymer*, 1989, **30**, 1319.

[4] Brillas, E.; Carrasco, J.; Figueras, A.; Urpi, F.; Otero, T.F. *J. electroanal. Chem*. 1995, **392**, 55.

[5] Carrasco, J.; Figueras, A.; Otero, T.F.; Brillas, E. ; *Synth. Met*., 1993, **61,** 253.

[6] Just, P.E.; Chane-Ching, K.I.; Lacaze, P.C. *Tetrahedron*, 2002, **58**, 3467.

[7] McCullough, R.D.; Lowe, R.D.; Jayaraman, M.; Anderson, *D. J. Org. Chem.* 1993, **58**, 904.

[8] Home, J.C.; Blanchard, G.J.; LeGoff, *E. J. Am. Chem. Soc.* 1995, **117**, 9551.

[9] Barbarella, G.; Zambianchi, M.; Bongini, A.; Antolini, *L. J. Org. Chem.* 1996, **61**, 4708.

[10] Ogura, K.; Miokawa, M.; Fujita, M.; Ashitaka, H.; Morita, K.; Suehiro, T.; Mito, A. *Nonlinear Optics,* 1995, **13**, 253.

[11] Ogura, K.; Yanai, H.; Miokawa, M.; Akazome, M. *Tetrahedron Lett.*, 1999, **40**, 8887.

[12] Mastragostino, M. In Applications of Electroactive Polymers; Scrosati, B., Ed.; Chapman and Hall: London, 1993.

[13] Monk, P.M.S.; Mortimer, R.J.; Rosseinsky, D.R. Electro-chromism: Fundamentals and Applications; VCH: New York, 1995.

[14] Stilwell, D.E.; Park S. *J. Electrochem. Soc*. 1989, **136,** 427.

[15] Wanatabe, A.; Mori, K.; Mikuni, M.; Nakamura, Y.; Matsuda, M. *Macromolecules,* 1989, **22**, 3323.

[16] Reddinger, J.L.; Sotzing, G.A.; Reynolds, J.R.J. *Chem. Soc., Chem. Commun.*, 1996, 1777.

[17] Morita, M. *Makromol. Chem.* 1993, **194**, 2361.

[18] Meeker, D.L.; Mudigonda, D.S.K.; Osborn, J.M.; Loveday, D.C.; Ferraris, J.P. *Macromolecules*, 1998, **31**, 2943.

[19] Audebert, P.; Sadki, S.; Miomandre, F.; Hapiot, P.; Chane-Ching, K. *New J. Chem.*, 2003, **27**, 798.

[20] Thompson, B.C.; Abboud, K.A.; Reynolds, J.R.; Nakatanib, K.; Audebert, P. *New J. Chem*., 2005, **29**, 1128.

[21] Ogura, K.; Zhao, R.; Yanai, H.; Maeda, K.; Tozawa, R.; Matsumoto, S.; Akazome, M. *Bull. Chem. Soc. Jpn*., 2002, **75**, 2359.

[22] Zhao, R.; Akazome, M.; Matsumoto, S.; Ogura, K. *Tetrahedron,* 2002, **58**, 10225.

[23] Ogura, K.; Zhao, R.; Jiang, M.; Akazome, M.; Matsumotoa, S.; Yamaguchic, K. *Tetrahedron Lett.*, 2003, **44**, 3595.

[24] Nakazaki, J.; Chung, I.; Matsushita, M.M.; Sugawara, T.; Watanabe, R.; Izuoka, A.; Kawada, Y. *J. Mater. Chem.*, 2003, **13**, 1011.

[25] Kim, K.S.; Kang, M.S.; Ma, H.; Jen, A.K.-Y. *Chem. Mater*. 2004, **16**, 5058.

[26] Lin, J.H.; Elangovan, A.; Ho, T.I. *J. Org. Chem.* 2005, **70**, 7397.

[27] Cihaner, A.; Algi, F.; *Electrochim. Acta*, 2008, **53**, 2574.

[28] Cihaner, A.; Algi, F. *Electrochim Acta,* 2008, **54**, 665.

[29] Cihaner, A.; Algi, F. *Electrochim Acta*, 2008, **54**, 786.

[30] Koyuncu, S.; Zafer, C.; Sefer, E.; Baycan Koyuncu, F.; Demic, S.; Kaya, I.; Ozdemir, E.; Icli, S. *Synth Metals*., 2009, **159**, 2013.

[31] Varis, S.; Ak, M.; Akmedov, I.M.; Tanyeli, C.; Toppare, L.J. *Electroanal Chem*., 2007, **603**, 8.

[32] Yildiz, E.; Camurlu, P.; Tanyeli, C.; Akhmedov, I.M.; Toppare, I.M. *J. Electroanal. Chem*. 2008, **612**, 247.

[33] Tuncagila, S.; Odacib, D.; Yildiz, E.; Timurb, S.; Topparea, L. *Sensor Actuat B-Chem*., 2009, **137,** 42

[34] Balci, Z.; Akbulut, U.; Toppare, L.; Alkan, S.; Bakir, U; Yagci, Y. *J. Macr. Sci., Pure and Appl. Chem.*, 2002, **39(3)**, 183.

[35] Altan, G.; Alkan, S.; Toppare, L.; Yagcı, Y. *React. Funct. Polym*., 2003, **57**, 57.

[36] Fujii, M.; Nishinaga, T.; Iyoda, M. *Tetrahedron Letters*, 2009, **50**, 555.

[37] Oliva, M.M.; Pappenfus, T.M.; Melby, J.H.; Schwaderer, K.M.; Johnson, J.C.; McGee, K.A.; Filho, D.A.S.; Bredas, J.-L.; Casado, J.; Lopez Navarrete, J. T. *Chem. Eur. J.*, 2010, **16**, 6866.

[38] Yavuz, A.; Bezgin, B.; Onal, A.M.; J. Appl. Polym. Sci. 2009, **114**, 2685.

[39] Sefer, E.; Koyuncu, F.B.; Oguzhan, E.; Koyuncu, S. *J. Polym. Sci., Part A: Polym. Chem.* 2010, **48**, 4419.

[40] Wang, G.; Fu, X.; Huang, J.; Wu, C.L.; Wu, L.; Deng, J.; Du, Q.; Zou, X. *Electrochimica Acta,* 2011, **56**, 6352.

[41] Wang, G.; Fu, X.; Huang, J.; Wu, L.; Deng, J. *J. electroanal. Chem*. 2011, **611**, 351.

Chapter No: 4

Ruthenium Complexes

Ruthenium was discovered in 1844 in Tartu, Estonia, by Karl Karlovich Klaus, who named this new metal Ruthenia, the Latin name for Russia **[1].** Ruthenium(II) complexes with 2,2'-bipyridine ligands constitute a huge field of research because of their stability, interesting redox and photochemical properties and applications in several areas like nanocrystalline TiO_2-based solar cells, biosensors, and molecular wires. The choice of ruthenium metal is of particular interest for a number of reasons:

i. Because of its octahedral geometry, specific ligands can be introduced in a controlled manner.
ii. The photophysical, photochemical, and the electrochemical properties of these complexes can be tuned in a predictable way.
iii. It is a unique metal due to its ability to form complexes that cover the widest range of oxidation states theoretically allowed for a transition metal, from 8 in $[RuO_4]$ to –2 in $[Ru(CO)_4]^{2-}$, it possesses stable and accessible oxidation states from I to III. The most common are the Ru^{II} and Ru^{III} oxidation states **[2, 3]**.

The kinetic stability of the ruthenium complexes formed in a broad range of oxidation states, the reversible nature of most of their redox pairs and the wide range of well known synthetic reactions for their preparation make these complexes very attractive for use in a wide range of studies. Here, attention has been particularly focused on the study of Ru^{II} complexes.

4.1.Properties of Ruthenium polypyridyl complexes

Ruthenium polypyridyl complexes are extremely versatile with wide ranging photophysical, photochemical and redox properties, which can be optimized for a particular purpose. They have played and are still playing a key role in the development of photochemistry, photophysics, photocatalysis, electrochemistry and electron and energy

transfer. Their unique combination of chemical stability, redox properties, excited-state reactivity, luminescence emission and long excited-state lifetimes has attracted the attention of many researchers **[4, 5]**.

The bonding properties of ruthenium complexes can be explained by crystal field theory and molecular orbital theory. From the point of view of crystal field theory, the properties of ruthenium complexes arise from electrostatic interactions between the metal ion and chelating ligands, which result in the splitting of d-orbital energies.

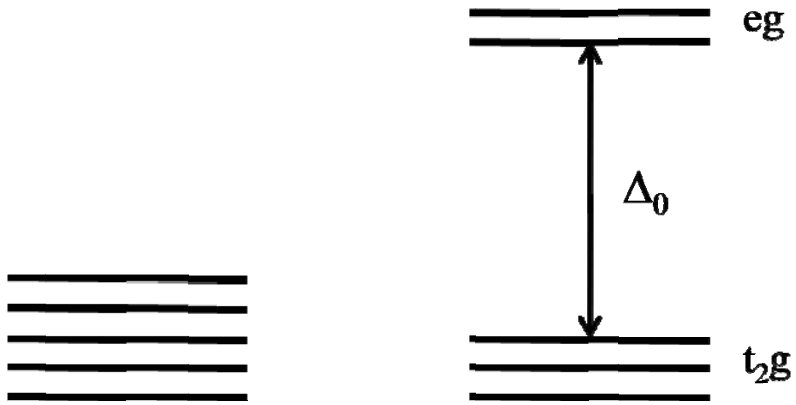

Figure 4.1: Schematic picture of the splitting between the t_2g and eg orbitals occurring when ligands are coordinated to the metal. The ligand field strength parameter Δ_0 is also indicated.

From the point of view of molecular orbital theory, the properties of ruthenium can be explained by the charge transfer between the metal and chelating ligands as a result of the interactions between the s, p and d atomic orbitals of the metal centre with those of the chelating ligands that have an appropriate geometry.

Polypyridyl complexes of Ru^{II} have a d^6 electronic configuration and a preferred octahedral geometry. Surrounding the metal ion, polypyridine ligands interact with ruthenium through σ -donor orbitals located on the nitrogen atoms and π -donor and π*-acceptor molecular orbitals delocalised on the aromatic rings **[6]**. The spectroscopic and electrochemical properties of ruthenium complexes are usually described through a simplified linear combination of atomic orbitals (Figure 4.1) **[7]**.

Each molecular orbital is denominated as metal (M) or ligand (L) in agreement with its prevalent localisation. The molecular orbital diagram for an octahedral complex of a transition metal such as Ru^{II} indicates that different transitions between the different chelating ligand and metal orbitals can take place upon the absorption of light. These transitions can be classified as

1. Metal-centered transitions (MC), also called ligand field or d-d transitions, when the electrons are promoted from a π_M metal orbital to σ^*_M orbital.
2. Ligand-centred (LC) or $\pi - \pi^*$ ligand-to-ligand transitions or intraligand transitions, for transitions between molecular orbitals predominately localised on the chelating ligands.
3. Charge transfer (CT) transitions between molecular orbitals with different localization, which cause the displacement of the electronic charge from the ligands to the metal or *vice versa*. Charge transfer transitions can be more specifically distinguished into metal-to-ligand charge transfer (MLCT), or ligand-to-metal charge transfer transitions (LMCT).

Electronic transitions that occur to a lesser extent are those from a metal-centred orbital to a solvent orbital (charge transfer to solvent, CTTS) or between two orbitals predominantly localized on different ligands on the same metal centre (ligand-to-ligand charge transfer, LLCT) **[7]**.

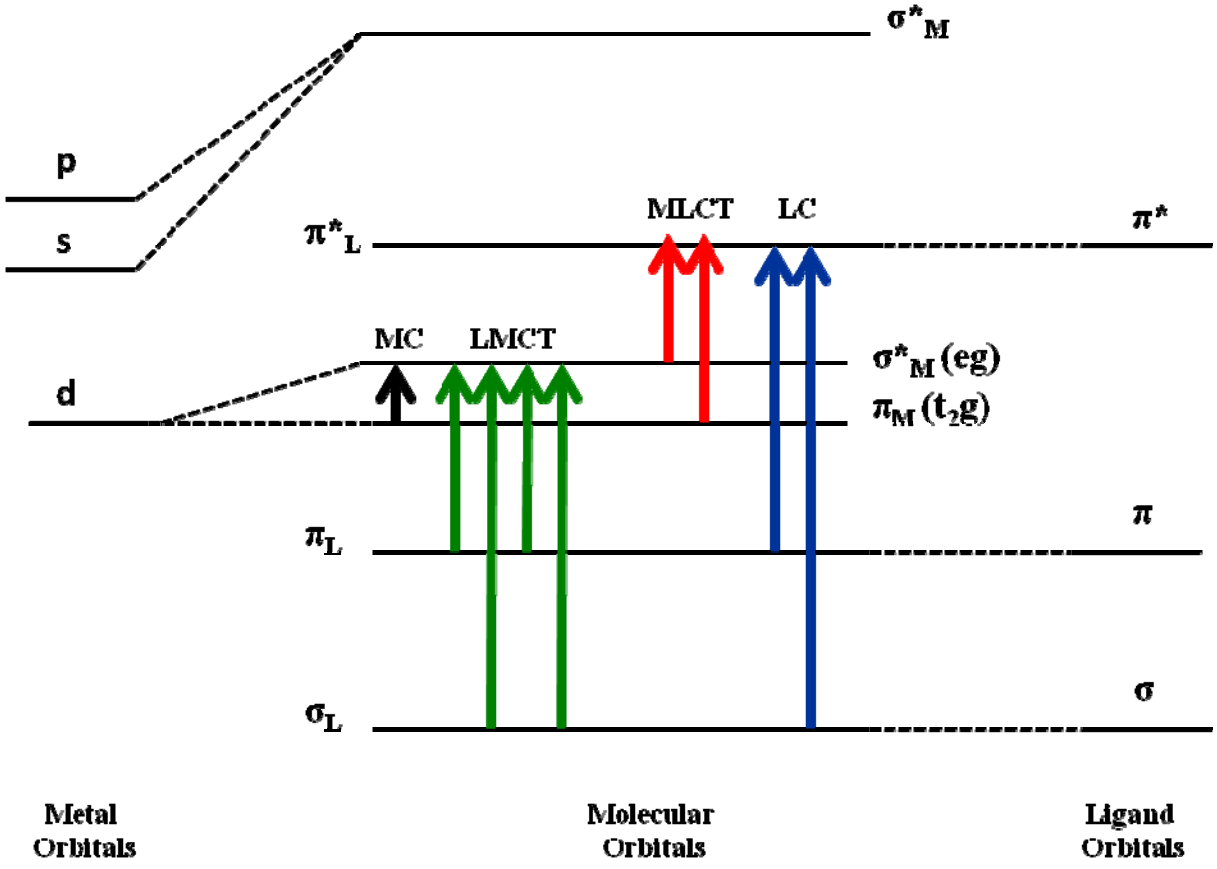

Figure 4.2: Simplified molecular orbital diagram showing different electronic transitions for a transition-metal complex in an octahedral geometry.

The light absorption processes are only allowed for transitions in which the ground and the excited state have the same spin value. These transitions can be observed as intense bands in the absorption spectra of the molecules. On the other hand, transitions from the ground state to excited states with different spin values are considered forbidden and can rarely be observed in absorption spectra. The MC, MLCT and LC transitions of an octahedral transition-metal complex are related to the ligand field strength, the redox potential of the metal complex and the intrinsic properties of the ligands, respectively **[8]**. For this reason, changes in the molecular structure of the ligands attached to the ruthenium metal ion can dramatically vary the relative energy positions of the excited states, with the consequent change in their photophysical properties **[9]** .

The metal-to-ligand charge transfer (MLCT) transition present in the ruthenium complex plays an important role in the light-harvesting process. Absorption and fluorescence spectra of these complexes are generally dominated by $d\pi_{Ru(II)} \rightarrow \pi^*_{bpy/terpy}$-based transitions. This transition leads to efficient charge separation, which consequently facilitates the charge injection process while suppressing unwanted charge recombination. To ensure fast and efficient electron injection, the energy levels of the dye, the $\pi^*_{bpy/terpy}$- based lowest unoccupied molecular orbital (LUMO) must be higher than that of the TiO_2 conduction band edge. For efficient regeneration process, the $d\pi_{Ru(II)}$-based highest occupied molecular orbital (HOMO) must align below the oxidation potential of the redox mediator. Energies of the electronic transitions and the corresponding energy gap between highest occupied molecular orbitals (HOMO) and lowest unoccupied molecular orbitals (LUMO) can be tuned with appropriate substitution of the polypyridyl ligand (bpy or terpy) with suitable electron donor or acceptor functionalities **[10-13]**. The absorption band can be extended into a longer-wavelength region by destabilizing the metal t_{2g} orbital using a strong donor ligand or by introducing a ligand with a low-lying π^*-level molecular orbital **[14, 15].**

The behaviour of excited species is usually represented in a Jablonski diagram (Figure 4.2). In most ruthenium polypyridyl complexes, three states are involved in the photochemical activation process: a singlet ground state and a singlet and triplet excited state.

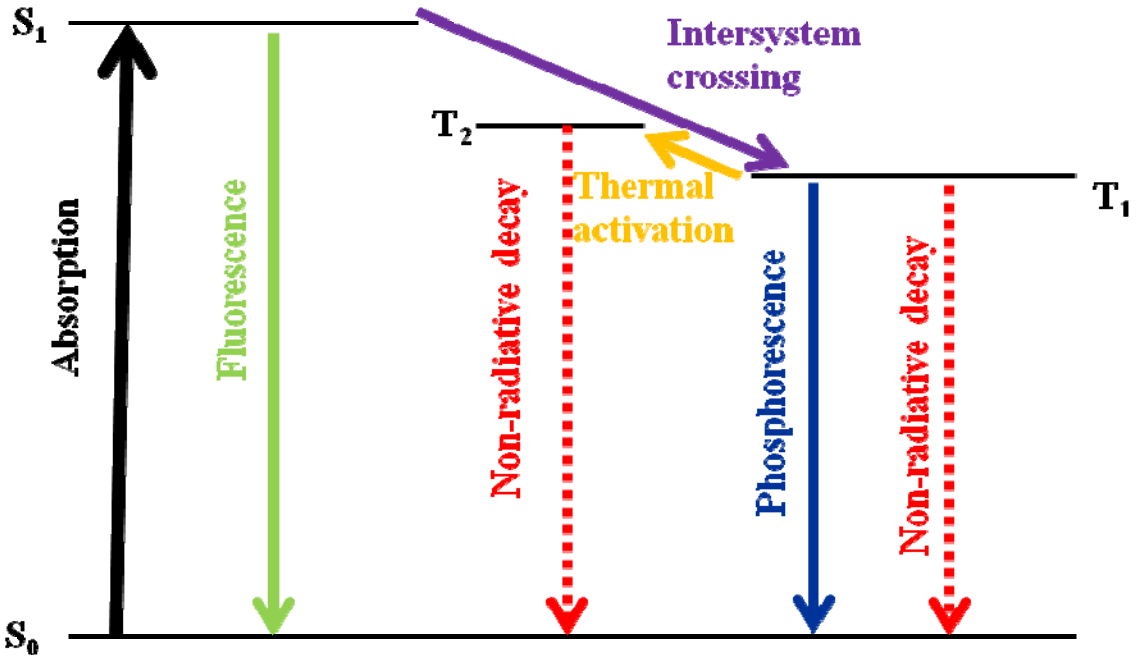

Figure 4.3: Jablonski diagram for ruthenium polypyridyl complexes.

The multiplicity of the ground state for most ruthenium (II) polypyridyl complexes is a singlet (S_0), and the absorption of a photon leads to promotion of an electron from an occupied orbital to a higher energy unoccupied orbital with the same spin multiplicity (S_1) . However, the lowest excited state is often a triplet (T_1) and, although it cannot be populated with excited electrons directly by light absorption, it can be through the deactivation of higher excited states. The S_1 state rapidly decays by intersystem crossing to T_1 because of strong spin-orbital coupling in metal complexes **[4]**. The quantum yield for the formation of the lowest triplet excited state is often equal to 100 %, which yields a short-lived fluorescence. Photo-excited state deactivation occurs though both a radiative (phosphorescence) and a non-radiative pathway.

Most ruthenium bipyridyl complexes show a lowest excited state as a triplet T_1, whose deactivation results in an intense long lived luminescence. However, at high temperatures, non-radiative deactivation can take place via thermally activated T_2 metal-centered excited state **[2, 16]**.

The behaviour of ruthenium terpyridyl complexes is completely different from their bipyridyl analogues **[17]**. No emission is detected at room temperature in ruthenium terpyridyl complexes because of non-radiative relaxation of the excited state (T_1) by transition from a T_2 metal centered excited state to the ground state. However, when the temperature decreases, the transition is less efficient and some luminescence can be observed. Furthermore, the

optical properties of these complexes can be modified by introduction of substituents on the ligands, which allows improvement in the luminescence quantum efficiency and/or life-time **[12]**.

The observed excited state lifetimes (τ) of the ruthenium polypyridyl complexes depends on the rate constants for radiative (k_r) and non-radiative (k_{nr}) decays to the ground state. The term k_{nr} includes the non-radiative decays from the excited state T_1 and the thermally activated excited state T_2 to the ground state. The thermal population of the metal-centered T_2 state can be described by the Arrhenius equation: $k_t \cdot (e^{-Ea/RT})$, where k_t is the prefactor for the thermally activated process and E_a is the activation energy barrier to the T_2 state (Equation 1) **[18]**. The relationship between the emission quantum yield (Φ) and k_r is given by (Equation 2), η_{isc} is the efficiency of intersystem crossing, normally considered unity.

$$1/\tau = k_r + k_{nr} \quad \textbf{(1)}$$

$$\Phi = \eta_{isc} \, . \, k_r \, . \, k_{nr} \quad \textbf{(2)}$$

Ru^{II} polypyridyl complexes are octahedral and diamagnetic, with a t_{2g}^6 configuration. The energy available to $*[Ru(NN)_3]^{2+}$ for energy-transfer processes is 2.12 eV, and its reduction and oxidation potentials are +0.83 and –0.79 V (in CH_3CN Vs SCE) **[19]** making $*[Ru(NN)_3]^{2+}$ at the same time a good energy donor, a good electron acceptor and a good electron donor **[4]**. The oxidation of a d^6 Ru^{II} polypyridine complex involves removal of an electron from the HOMO, usually a π_M (t_{2g}) metal-centered orbital, with the formation of paramagnetic low-spin d^5 Ru^{III} complexes, which are inert to ligand substitution (Equation 3).

$$[Ru^{II}(NN)_3]^{2+} \rightarrow [Ru^{II}(NN)_3]^{3+} + e^- \quad \textbf{(3)}$$

On the other hand, the reduction of a Ru^{II} polypyridyl complex may involve the introduction of one electron into the lowest-unoccupied molecular orbital, either into a metal-centered (σ^*_M) or a ligand-centered orbital (π^*_L), depending on their relative energy level arrangement. Generally, polypyridine ligands co-ordinated to ruthenium metal ions are easily reduced, and the reduction takes place on the ligand (Equation 3). In this case, ruthenium metal ions maintain their d^6 low-spin configuration. These species are usually inert, and the reduction reaction is reversible. However, when the lowest energy empty orbital is a metal-centered orbital, the electron is added to the metal-centered orbital. The reduction of these complexes produces an unstable low-spin d^7 electronic configuration, which leads to a rapid ligand dissociation, and makes the reaction irreversible (Equation 4).

$$[Ru^{II}(NN)_3]^{2+} + e^- \rightarrow [Ru^{II}(NN)_2(NN^-)]^{2+} \quad \textbf{(4)}$$

$$[Ru^{II}(NN)_3]^{2+} + e^- \rightarrow [Ru^{I}(NN)_3]^{+} \rightarrow [Ru^{I}(NN)_2]^{+} + NN \quad \textbf{(5)}$$

Thus, (polypyridine) ruthenium (II) complexes serve as excellent candidates for use as an electron source/sink in molecular electronic applications. In order to unequivocally direct this energy/ electron transfer to a specific target, a linker or a bridge is required. A wide variety of bridges have been reported with the most common being oligophenylenes **[20]**, oligo(phenylethylenes) **[21]** and oligothiophenes **[22-26]**. Due to their stability, coplanarity and ease of derivitisation, oligothiophenes have gained prominence within the field of molecular electronics and have found applications in organic light emitting diodes and organic field-effect transistors.

However, the attachment of a linker of any kind to one of the 2, 2'-bipyridine ligands will affect the properties of the resulting $[Ru(bpy)_2(L)]^{2+}$ complex. Steric effects between the bridge and the auxiliary bipyridine ligands may alter the coordination symmetry of the metal core **[27]**. So, through a judicious choice of ligands, it is possible to "fine-tune" the ground-state redox properties and excited-state energies **[28-35].**

Ruthenium polypyridyl complexes have an extensive and well-known synthetic chemistry. Their compounds show high stability and flexibility with a wide range of mono-, bi-, tri- and tetradentate ligands. Furthermore, ligands can be exchanged sequentially, by removing some of them while maintaining the presence of others **[4]**.

One of the most common synthetic precursors for ruthenium mononuclear polypyridyl complexes is the commercially available $RuCl_3 \cdot xH_2O$. Some important precursors in the synthesis of homoleptic and heteroleptic complexes such as $[Ru(CO)_2Cl_2]_n$, $[Ru(DMSO)_4Cl_2]$ (DMSO = dimethylsulfoxide), $[Ru(\eta^6\text{-arene})Cl_2]_2$, $[Ru(COD)Cl_2]_n$ (COD = 1,5-cyclooctadiene) can be synthesized in one step from $RuCl_3 \cdot xH_2O$.

In coming sections synthetic procedures for homoleptic, bis-heteroleptic and tris-heteroleptic Ru complexes will be described.

4.2. Homoleptic Complexes

4.2.1. Introduction

Homoleptic complex is a metal compound with all ligands identical. The term uses a homo prefix to indicate that something is the same for all.

A common drawback to the bis-heteroleptic and tris-heteroleptic approach is the multistep reaction pathway needed for sequential introduction of the appropriate ligands around the metal often implying selectivity concerns and separations by size-exclusion chromatography. At first glance, homoleptic complexes appear more attractive by offering a straightforward access to dyes from adequately designed ligands without any complicated separation procedures.

So, it is an attractive approach to prepare homoleptic complexes first to investigate MLCT transitions and other photophysical and electrochemical properties.

4.2.2. Synthetic procedures

The first synthesis of a homoleptic ruthenium complex was reported in 1936 by Burstall, corresponds to the complex $[Ru(bpy)_3]Cl_2$ **[36]**. The heating at reflux of $RuCl_3 \cdot xH_2O$ with an excess of a bipyridyl compound (NN) results in the formation of ruthenium homoleptic tris(bidentate) ligand.

$$RuCl_3 \cdot xH_2O + \quad bpy(8\ eq.) \xrightarrow[\text{no solvent}]{\text{250-260° C, 4.5 h}} [Ru(bpy)_3]Cl_2$$

Scheme 4.1: Synthesis of homoleptic complexes by Burstall, 1936

In 1966 Palmer and piper refluxed bipyridine and $RuCl_3.3H_2O$ for 72 hr in 95 % ethanol. Resulting $Ru(bipy)_3^{2+}$ was then precipitated as the iodide from the diluted aqueous solution by addition of KI in excess. Contrary to the previously mentioned procedure reported by Burstall, greater than 95% yield was obtained in this case. So, this high yield and the simplicity of the procedure make this a superior preparation of $Ru(bipy)_3^{2+}$ compared to other methods in the literature **[37]**.

In 1973 Braddock and Meyer prepared $Ru(terpy)_2^{2+}$, $Ru(phen)_3^{2+}$, and $Ru(bipy)_3^{2+}$ by heating at reflux a mixture of $RuCl_3.nH_2O$ and stoichiometric amounts of the appropriate

ligands for about 3 hr in of N,N-dimethylformamide (DMF). All complexes were obtained in satisfactory yields **[38]**.

$$RuCl_3 \cdot xH_2O \; + \; bpy(3\ eq.) \xrightarrow{DMF,\ reflux,\ 3\ h} [Ru(bpy)_3]Cl_2$$

Scheme 4.2: Synthesis of homoleptic complexes by Braddock and Meyer, 1973

The synthesis of such complexes was extended to the incorporation of a wide range of bidentate ligands with the addition of a reducing agent such as phosphinic acid or hydroxylamine hydrochloride to the reaction mixture **[39].** The reduction of $RuC1_3.3H_2O$ with freshly prepared NaH_2PO_2 followed by a short time reflux with bipyridine in H_2O is also reported **[40].**

The use of Dichlorotetrakis(dimethyl sulfoxide) ruthenium(II) formulated as $[Ru(DMSO)_4Cl_2]$ where (DMSO = dimethylsulfoxide) and cis-Dichlorobis(2,2'-bipyridine)ruthenium(II) dihydrate instead of $RuC1_3.3H_2O$ is also reported **[41]**.

It is noted that synthesis of these complexes is often time consuming. In 1991 Greene and Mingos introduced the microwave-assisted reaction, an interesting alternative to previous synthetic routes, which offers a convenient synthetic procedure and reduction in the reaction time. $[Ru(bipy)_3](PF_6)_3$, $[Ru(terpy)_2](PF_6)_2$, $[Ru(phen)_3](PF_6)_2$ and $[Ru(bipy^*)_3]\ (PF_6)_2$ were obtained after only 20 seconds of microwave exposure to the mixture of $RuC1_3.3H_2O$, MeOH, dry Et_3N and ligand but the yields were slightly less satisfactory **[42]**.

$$RuCl_3 \cdot xH_2O \; + \; 4\ bpy \xrightarrow[2)\ KPF_6\ treatment]{1)\ \mu W/600\ W/\ MeOH\text{-}Et_3N,\ 20\ s + 20\ s\ (autoclave)} [Ru(bpy)_3](PF_6)_2$$

Scheme 4.3: Synthesis of homoleptic complexes by Greene and Mingos, 1991

The use of microwave reactors is a rapidly expanding area of synthetic chemistry in both organic and inorganic syntheses. The technique offers several advantages over traditional synthesis especially in the synthesis of ruthenium and osmium complexes, which typically require many hours of refluxing in high boiling solvents to effect a reaction. Similar reactions, when performed in a microwave reactor, can occur in a matter of minutes.

Efficient and rapid synthesis of many ruthenium polypyridine complexes using microwave irradiation has been reported. For example, $Ru(bpy)_3^{2+}$ was prepared by microwave heating of a ruthenium chloride solution with 3 equiv of 2,2'-bipyridine in ethylene glycol for 15 minutes in 95 % yield, which is slightly higher than the literature value of 86 % **[43]**. Martineau et al., reported the method that provided the homoleptic complexes in high yields (78-95 %) after 3 minutes of microwave irradiation (250 W) at 196 °C in ethylene glycol **[44].**

4.3. Bis-Heteroleptic Complexes

4.3.1. Introduction

The trisheteroleptic $RuL(dcbpy)(NCS)_2$ complexes (L=bipyridine, dcbpy=4,4'-dicarboxy-2,2'-bipyridine) have been widely studied. This family of complexes was reported to absorb light within a wide domain with high molar extinction coefficients **[45-48]**, the most popular being **N3** ($Ru(dcbpy)_2(NCS)_2$ **[49, 50]** and **N719** which is obtained by deprotonation of one dcbpy in **N3 [51]**.

The thiocyanate ligands are usually considered as the most fragile part of ruthenium complex. Firstly, it is a monodentate ligand, so it is easier to decoordinate it than a bidentate ligand like bipyridine. Secondly, it is an ambidentate ligand which can bind to a metal through either the nitrogen or the sulfur atoms. For solar cell applications, it has been postulated that the N-bound thiocyanate isomer is preferable. Although charge transfer from electrolyte to dye could happen in several other ways **[52, 53],** it has been suggested that the N-bound isomer promotes charge transfer from the iodide redox mediator, which can interact with the soft, sulfur end of the ligand **[54, 55]**.

NCS ligands tune the spectral and redox properties of the complexes by destabilizing the metal t_{2g} orbital. Although the NCS is a suitable donor ligand, it can undergo photosubstitution or photodegradation reactions, which decrease the long-term stability of the complexes. The occurrence of these reactions can be reduced through the replacement of NCS ligands with other donor ligands, such as bidentate ligands **[14]**.

Thus approach using bisheteroleptic $[RuL2(dcbpy)]^{2+}$ complexes remain of interest in the quest for stable and efficient dyes.

4.3.2. Synthetic procedures

Since ruthenium (II) can accommodate three bidentate ligands, the use of two different ligands A and B leads to the formation of mixed complexes of the types Ru (AAB) and Ru(ABB). Thus in 1980's nearly all the mixed bidentate ligand complexes of ruthenium (II) that have been examined have been of these two types **[56-59]**. In a number of cases these complexes have properties that differ significantly from those of either of the two parent systems Ru(AAA) or Ru(BBB).

A widely used synthetic approach involves the introduction of two chelate ligands by direct reaction of $RuCl_3 \cdot xH_2O$ with two equivalents of the bidentate ligand, to obtain a $[Ru(L_1)_2Cl_2]$ complex. Other precursors used in the synthesis of such complexes are $Ru(COD)Cl_2$ **[60]** and $Ru(DMSO)_4Cl_2$ **[61]**. Subsequent introduction of a second ligand to the $[Ru(L)_2Cl_2]$ complex in an appropriate medium results in the formation of $[Ru(L_1)_2(L_2)]^{2+}$.

The bis-heteroleptic complexes were prepared by Sullivan et al., in 1978 in two steps. $Ru(bpy)_2Cl_2$ was prepared in a first step by using the following reaction scheme and then in a second step, a slight excess of ligand was reacted with $Ru(bpy)_2Cl_2$ according to the conditions described in scheme. The addition of a saturated aqueous solution of NH_4PF_6 to the reaction mixture precipitated the complex as its bis(hexafluorophosphate)salt **[62]**.

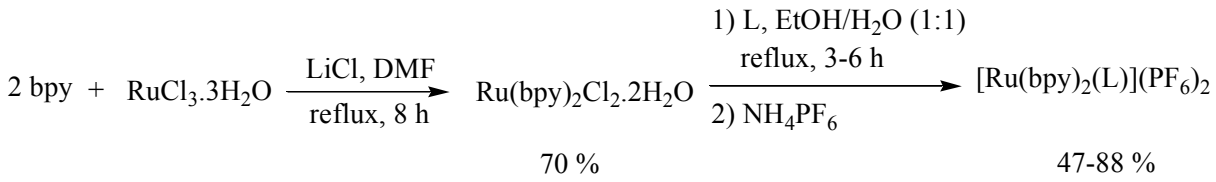

Scheme 4.4: Synthesis of bis-heteroleptic complexes by Sullivan et al., 1978

For second step use of different ratios of ethanol/water and different reaction times are also reported **[63].**

The use of $[Ru(bpy)_2(CH_3COCH_3)_2]^{2+}$ as an intermediate proved to be easier and more efficient for the synthesis of some of the dicationic complexes **[61]**.

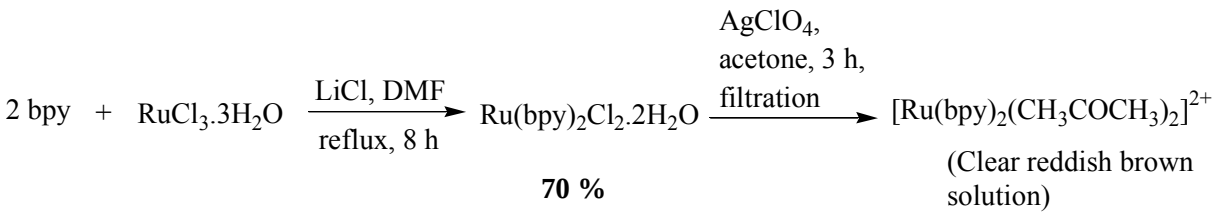

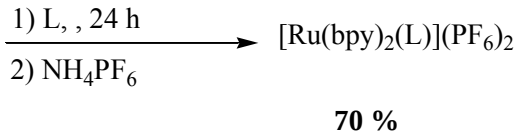

Scheme 4.5: Synthesis of bis-heteroleptic complexes by Sullivan et al., 1978

Rau and his co-workers reported the synthesis of bis-heteroleptic complex by using $Ru(COD)Cl_2$ (cod = cyclooctadiene) synthon under microwave irradiation **[59].**

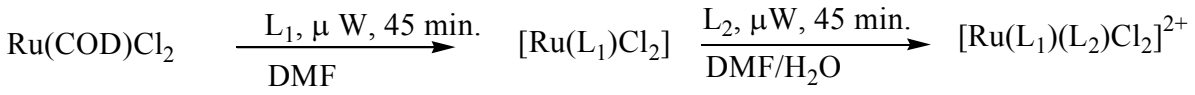

Scheme 4.6: Synthesis of bis-heteroleptic complexes by Rau et al., 2004

Martineau et al., reported two step method to prepare bis-heteroleptic complexes. First step was very efficient and was performed in microwave whereas second step was classical thermal step **[64]**.

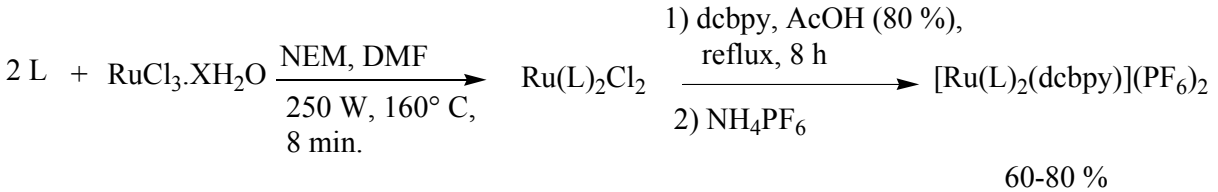

Scheme 4.7: Synthesis of bis-heteroleptic complexes by Martineau et al., 2007.

4.4. Tris-Heteroleptic Complexes

4.4.1. Introduction

Heteroleptic ruthenium complexes have emerged as a promising class of sensitizers for DSSC applications **[65, 66, 67]**. These complexes contain a 4,4'-dicarboxy-2,2'-bidpyridine (dcbpy) ligand for anchoring on the titanium oxide (TiO_2) surface (anchoring ligand), a second bipyridine ligand used as an antenna for improving the light harvesting performances (ancillary ligand) and two thiocyanate ligands that tune the photo- and electrochemical properties of the dyes to relevant levels by destabilizing the metal t_{2g} orbital. Anchoring ligands are also responsible for providing the intimate electronic coupling between their excited-state wave functions and the conduction band of the semiconductor. This particular design leads to complexes with significantly improved extinction coefficients in the visible part of the absorption spectrum. State of the art DSSCs achieve more than 11% energy conversion, allied to good performance under any atmospheric condition and under one sun illumination (AM 1.5) are actually obtained **[68]**.

Thiocyanate (SCN^-) has been successfully used as an ancillary ligand in many ruthenium sensitizers **[50-73]**. Such Ru(II) polypyridyl complexes, however, suffer from the lability of the thiocyanate ligand, which decreases the dye's stability **[74, 75]**. Attempts to use alternative ligands have led to limited success so far.

To accelerate the discovery and improvement of better performing sensitizers, easily accessible strategies for the functionalization of bipyridyl derivatives are required.

4.4.2. Synthetic procedures

There have been two early reports of a ruthenium tris(diimine) complex with three different ligands. In one case no experimental details were reported **[29]** and in the other case $Ru(CO)_2(bpy)(phen)[PF_6]_2$ was treated with di-2- pyridylamine (dpa) to provide $Ru(bpy)(phen)(dpa)\ [PF_6]_2$ **[76]**.

Most of the earlier attempts to develop general synthetic routes to tris-heteroleptic complexes have met with limited success **[2, 77, 78]**.

In 1987 Thummel et al., reported the detailed synthesis of tris-heteroleptic complex. They refluxed an equimolar solution of $[Ru(bpy)Cl_2]_2$ and L_1 in 15 mL of 1:1 $EtOH/H_2O$ for 24 h. The solution was cooled and same number of moles L_2 was added, and then

reflux was continued another 48 h. After cooling, an aqueous solution of NH_4PF_6 (2 equiv) was added. The resulting precipitate was collected, dried, and chromatographed **[79]**.

Two synthetic routes for the synthesis of $[Ru(L_1)(L_2)(L_3)]^{2+}$ complexes with $[Ru(CO)_2(Cl)_2]_n$ as a starting material have been extensively studied by Black, Deacon and Thomas. The first step in both methodologies is the introduction of one chelate ligand. The subsequent decarbonylation step differs. In the first method, the labile CO ligands are substituted by the application of heat, while in the second, decarbonylation takes place by irradiation with UV light **[80-87]**.

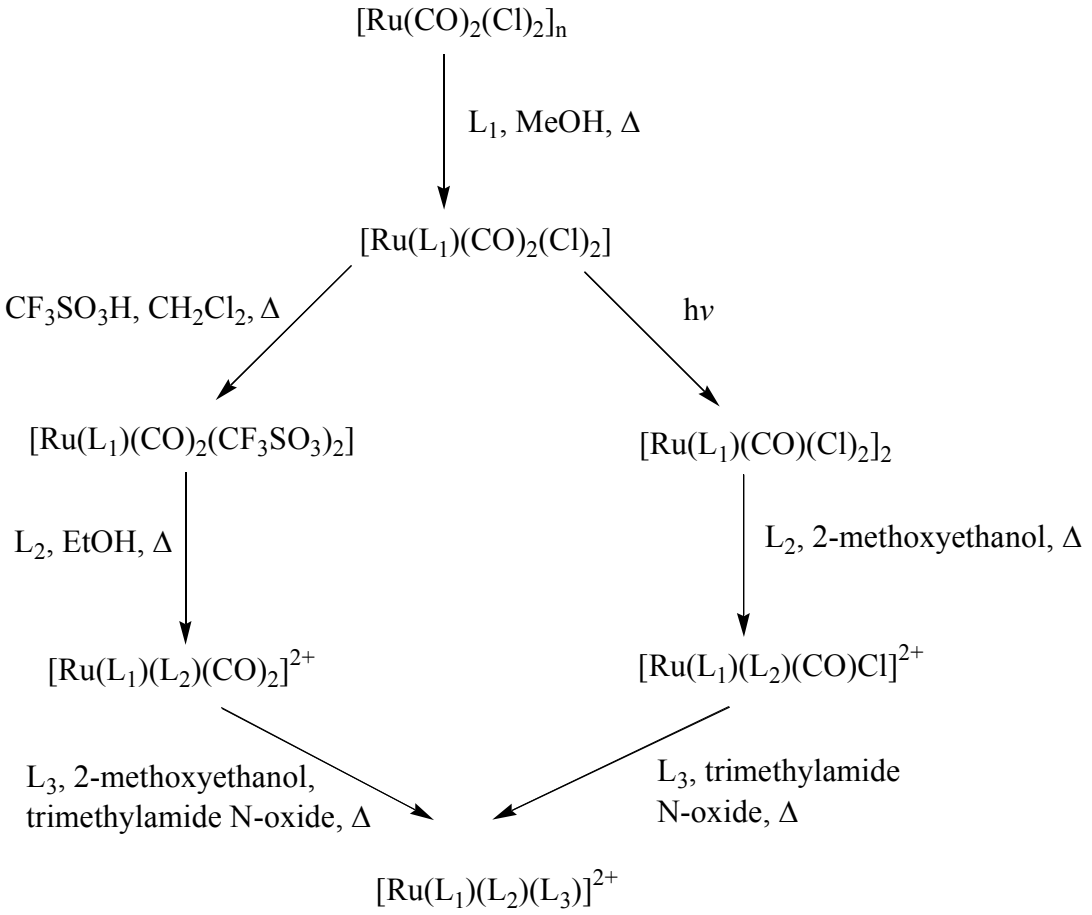

Scheme 4.8: Synthesis of Tris-Heteroleptic complexes $[Ru(L_1)(L_2)(L_3)]^{2+}$

Zakeeruddin et al., carried out reaction between $RuCl_2(DMSO)_4$ and ligands and it relies on $Ru(L_1)(L_2)Cl_2$ as a synthetic intermediate for tris-$[Ru(L_1)(L_2)\ )(NCS)]^{2+}$ complexes **[88].**

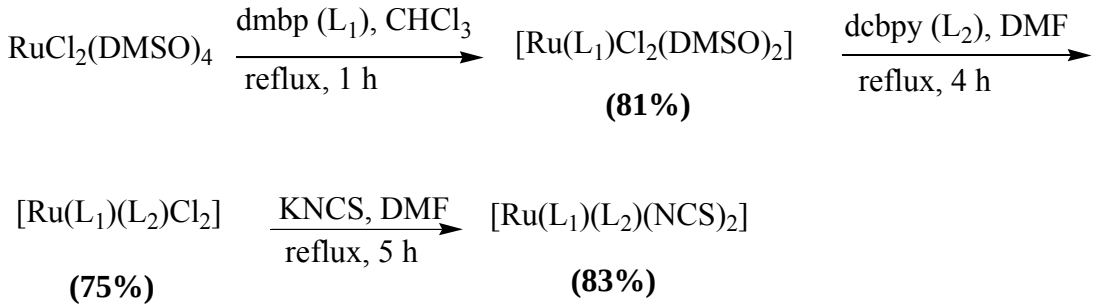

Scheme 4.9: Synthesis of Tris-Heteroleptic complexes by Zakeeruddin et al., 1998

In 2001, Freedman et al., reported a method by using η^6-benzeneruthenium-μ-dichloro dimer, $[BzRuCl_2]_2$ synthon **[89]**. This method is adventageous in the sense that all of the synthetic reactions take place under relatively mild conditions that avoid ligand-scrambling reactions and reagents used during reactions required no special purification.

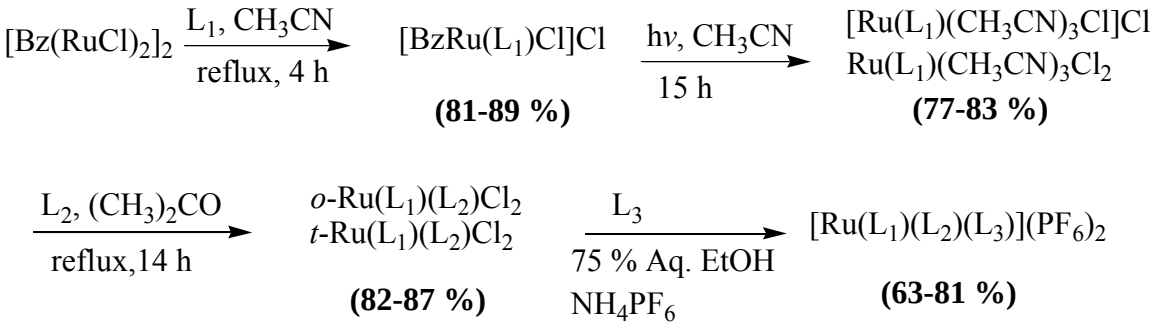

Scheme 4.10: Synthesis of Tris-Heteroleptic complexes by Freedman et al., 2001

Most commonly employed one pot synthesis of tris-Heteroleptic complexes, starting from $[Ru(p\text{-cymene})Cl_2]_2$ synthon, followed by sequential addition of ligands at each step are reported in following scheme.

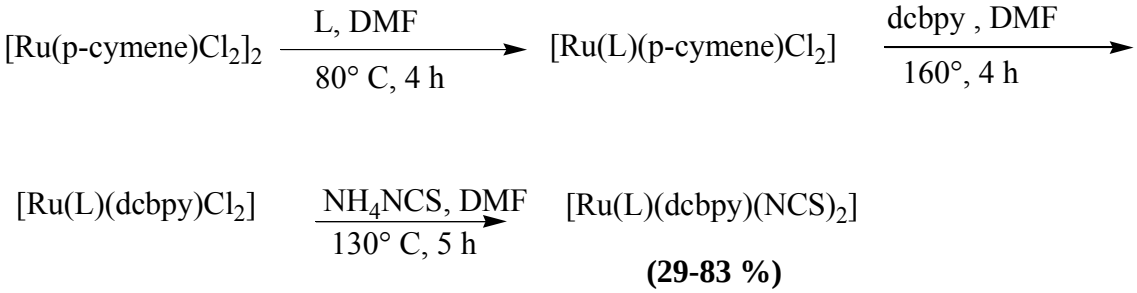

Scheme 4.11: Synthesis of Tris-Heteroleptic complexes **[90-95]**

Kuang et al., reported the synthesis of tris-Heteroleptic complexes **[96]** described in the following scheme. Instead of commonly employed one pot synthesis method, they

refluxed the mixture of ligand and [Ru(*p*-cymene)Cl_2]$_2$ in ethanol for 4 hours. Then after evaporation of solvent they continue next steps in DMF.

$$[Ru(p\text{-cymene})Cl_2]_2 \xrightarrow[\text{reflux, 4 h}]{\text{L, EtOH}} [Ru(L)(p\text{-cymene})Cl_2] \xrightarrow[140°, 4\ h]{\text{dcbpy , DMF}}$$

$$[Ru(L)(dcbpy)Cl_2] \xrightarrow[140°\ C, 4\ h]{NH_4NCS, DMF} [Ru(L)(dcbpy)(NCS)_2]$$

Scheme 4.12: Synthesis of Tris-Heteroleptic complexes by Kuang et al., 2006

Rapid and efficient synthesis of heteroleptic complex by microwave method was reported by Sun and his co-workers **[97]**.

$$Ru(DMSO)_2Cl_2 \xrightarrow[105°\ C, 1\ atm, 8\ min.]{\text{dcbpy, DMF}} Ru(dcbpy)DMSO_2Cl_2 \xrightarrow[105°\ C, 1\ atm\ 16\ min.]{\text{dcbpy , DMF}}$$

$$Ru(dcbpy)_2Cl_2 \xrightarrow[115°\ C, 8\ min.]{NH_4NCS, DMF} Ru(dcbpy)_2NCS_2$$

Scheme 4.13: Synthesis of Tris-Heteroleptic complexes by Sun et al., 2010

From literature survey it is evident that synthesis of homoleptic and bis-heteroleptic and tris-heteroleptic ruthenium complexes under microwave conditions is a quick and efficient approach. So we planned to prepare our new series of complexes under microwave conditions in order to save time and to obtain better yield.

4.5. References

[1] Griffith, W. P. *Chem. Soc. Rev.* 1992, **21**, 179.

[2] Juris, A.; Campagna, S.; Balzani, V.; Gremaud, G. *Inorg. Chem.* 1988, **27**, 3652.

[3] Wagenknecht, P.S.; Ford, P.C. *Coord. Chem. Rev*. 2011, **255**, 591.

[4] Juris, A.; Balzani, V.; Barigelletti, F.; Campagna, S.; Belser, P.; Von Zelewsky, A. *Coord. Chem. Rev.* 1988, **84**, 85.

[5] Balzani, V.; Juris, A. *Coord. Chem. Rev.* 2001, **211,** 97.

[6] Campagna, S.; Puntoriero, F. ; Nastasi, F. ; Bergamini, G.; Balzani, V. ; *Top. Curr. Chem.* 2007, **280**, 117.

[7] Balzani, V.; Juris, A. Venturi, M.; Campagna, S.; Serroni, S. *Chem. Rev*. 1996, **96**, 759.

[8] Crosby, G.A. *Acc. Chem. Res*. 1975, **8**, 231.

[9] Kalyanasundaram, K. Nazeeruddin, M.K. *Chem. Phys. Lett*. 1992, **193**, 292.

[10] Kalyanasundaram, K. *Coord. Chem. Rev.*, 1982, **46**, 159.

[11] Kalyanasundaram, K.; Grätzel, M. *Coord. Chem. Rev.*, 1998, **177**, 347.

[12] Maestri, M.; Armaroli, N.; Balzani, V.; Constable, E.C.; Thompson, A.M.W.C. *Inorg. Chem*. 1995, **34**, 2759.

[13] Verma, S.; Kar, P.; Das, A.; Ghosh. H.N. *Dalton Trans*. 2011, **40**, 9765.

[14] Funaki, T.; Yanagida, M.; Komatsuzaki, N.O.; Kasuga, K.; Kawanishi, Y.; Kurashige, M.; Sayama, K.; Sugihara, H. *Inorg. Chem. Commun.,* 2009, **12**, 842.

[15] Funaki, T.; Yanagida, M.; Komatsuzaki, N.O.; Kasuga, K.; Kawanishi, Y.; Sugihara, H. *Inorganica Chimica Acta*, 2009, **362**, 2519.

[16] Reynal, A.; Palomares, E. *Eur. J. Inorg. Chem.* 2011, 4509.

[17] Hofmeier, H. Schubert, U.S. *Chem. Soc. Rev*. 2004, **33**, 373.

[18] Wang, X.-Y.; Del Guerzo, A.; Schmehl, R.H. *J. Photochem. Photobiol. C: Photochem. Rev*. 2004, **5**, 55.

[19] Balzani, V.; Bergaminia, G.; Marchionia, F.; Ceronia, P. *Coord. Chem. Rev.* 2006, 1254.

[20] Welter, S.; Salluce, N.; Benetti, A.; Rot, N.; Belser, P.; Sonar, P.; Grimsdale, A.C.; Mullen, K.; Lutz, M.; Spek, A.L.; Cola, L.D. *Inorg. Chem.* 2005, **44**, 4706.

[21] Barbieri, A.; Ventura, B.; Barigelletti, F.; Nicola, A.D.; Quesada, M.; Ziessel, R. *Inorg. Chem.* 2004, ***43,*** 7359.

[22] Fichou, D. (Ed.), *Handbook of Oligo- and Polythiophenes*,Wiley-VCH, Weinheim, 1998.

[23] Horowitz, G. *Adv. Mater.*1998, **10(5)**, 365.

[24] Barbarella, G.; Favaretto, L.; Zambiachani, M.; Pudova, O.; Arbizzani, C.; Bongini, A.; Mastragostino, M. *Adv. Mater.* 1998, **10,** 551.

[25] Facchetti, A.; Deng, Y.; Wang, A.; Koide, Y.; Sirringhaus, H.; Marks, T.J.; Friend, H.R. *Angew. Chem. Int. Ed.* 2000, **39,** 4547.

[26] Funahashi, M.; Hanna, J.-I. *Adv. Mater.* 2005, **17,** 594.

[27] Onggo, D.; Scudder, M.L.; Craig, D.C.; Goodwin, H.A. *J. Mol. Struct.* 2005, **738**, 129.

[28] Buckingham, D.A.; Dwyer, F.P.; Goodwin, H.A.; Sargeson, A.M. *Aust. J. Chem*. 1964, **17**, 325.

[29] Creutz, C.; Chou, M.; Netzel, T.L.; Okumura, M.; Sutin, N. *J. Am. Chem. Soc*. 1980, **102**, 1309.

[30] Allen, G.H.; Sullivan, B.P.; Meyer, T.J. *J. Chem. Soc., Chem. Commun*. 1981, 793-794.

[31] Kober, E.M.; Sullivan, B.P.; Dressick, W.J.; Caspar, J.V.; Meyer, T.J. *J. Am. Chem. Soc*. 1980, **102**, 7383.

[32] Kober, E.M.; Meyer, T.J. *Inorg. Chem*. 1982, **21**, 3967.

[33] Johnson, S.R.; Westmoreland, T.D.; Caspar, J.V.; Barqawi, K.R.; Meyer, T.J. *Inorg. Chem*. 1988, **27**, 3195.

[34] Anderson, P.A.; Deacon, G.B.; Haarmann, K.H.; Keene, F.R.; Meyer, T.J.; Reitsma, D.A.; Skelton, B.W.; Strouse, G.F.; Thomas, N.C.; Treadway, J.A.; White, A.H. *Inorg. Chem*. 1995, **34**, 6145.

[35] Anderson, P.A.; Keene, F.R.; Meyer, T.J.; Moss, J.A.; Strouse, G.F.; Treadway, J.A. *J. Chem. Soc., Dalton Trans.* 2002, 3820.

[36] Burstall, F.H. *J. Chem. Soc.* 1936, 173.

[37] Palmer, R.A.; Piper, T.S. *Inorg. Chem*. 1966, **5**, 864.

[38] Braddock, J.N.; Meyer, T.J. *J. Am. Chem. Soc.* 1973, **95**, 3158.

[39] Crosby, G.A.; Watts, R.J. *J. Am. Chem. Soc.* 1971, **93**, 3184.

[40] Lin, C.T.; Bottcher, W.; Chou, M.; Creutz, C.; Sutin, N. *J. Am. Chem. Soc.* 1976, **98**, 6536.

[41] Elliott, C.M.; Hershenhart, E.J. *J. Am. Chem. Soc*. 1982, **104**, 7519.

[42] Greene, D.L.; Mingos, D.M.P. *Transition Metal Chemistry*, 1991, **16**, 71.

[43] Matsumura-Inoue, T.; Tanabe, M. *Chem. Lett.* 1994, **12**, 2443.

[44] Martineau, D.; Beley, M.; Gros, P.C. *J. Org. Chem*., 2006, **71**, 566.

[45] Nazeeruddin, M.K.; Zakeeruddin, S.; Lagref, J.-J.; Liska, P.; Comte, P.; Barolo, C.; Viscardi, G.; Schenk, K.; Grätzel, M. *Coord. Chem. Rev*. 2004, **248**, 1317.

[46] Nazeeruddin, M.K.; Wang, Q.; Cevey, L.; Aranyos, V.; Liska, P.; Figgemeier, E.; Klein, C.; Hirata, N.; Koops, S.; Haque, S.A.; Durrant, J.R.; Hagfeldt, A.; Lever, A.B.P.; Grätzel, M. *Inorg. Chem.* 2006, **45**, 787.

[47] Wang, P.; Zakeeruddin, S.M.; Moser, J.E.; Humphry-Baker, R.; Comte, P.; Aranyos, V.; Hagfeldt, A.; Nazeeruddin, M.K.; Grätzel, M. *Adv. Mater*. 2004, **16**, 1806.

[48] Ito, S.; Ha, N.-L.C.; Rothenberger, G.; Liska, P.; Comte, P.; Zakeeruddin, S.M.; Pechy, P.; Nazeeruddin, M.K.; Grätzel, M. *Chem. Commun.* 2006, 4004.

[49] Benko, G.; Kallioinen, J.; Korppi-Tommola, J.E.I.; Yartsev, A.P.; Sundstrom, V. *J. Am. Chem. Soc*. 2002, **124**, 489.

[50] Grätzel, M. *J. Photochem. Photobiol., A* 2004, **164**, 3.

[51] Nazeeruddin, M.K.; Kay, A.; Rodicio, I.; Humphry-Baker, R.; Mueller, E.; Liska, P.; Vlachopoulos, N.; Grätzel, M. *J. Am. Chem. Soc.* 1993, **115**, 6382.

[52] Clifford, J.N.; Palomares, E.; Nazeeruddin, M.K.; Gra□tzel, M.; Durrant, J.R. *J. Phys. Chem. C* 2007, **111**, 6561.

[53] Ardo, S.; Meyer, G.J. *Chem. Soc. Rev.* 2009, **38**, 115.

[54] Hamann, T.W.; Ondersma, J.W. *Energy Environ. Sci.* 2011, **4**, 370.

[55] Tuikka, M.; Hirva, P.; Rissanen, K.; Korppi-Tommola, J.; Haukka, M. *Chem. Commun.* 2011, **47**, 4499.

[56] Belser, P.; von Zelewsky, A. *Helv. Chim. Acta* 1980, **63**, 1675.

[57] Juris, A,; Balzani, V.; Belser, P.; von Zelewsky, A. *Helv. Chim. Acta* 1981, **64**, 2175.

[58] Balzani, V.; Juris, A,; Barigelletti, F.; Belser, P.; von Zelewsky, A. Sci. Pap. *Inst. Phys. Chem. Res. (Jpn.)* 1984, **78**, 78.

[59] Thummel, R.P.; Decloitre, Y.D. *Inorg. Chim. Acta* 1987, **128**, 245.

[60] Rau, S.; Bernhard, S.; Grubing, A.; Schebesta, S.; Lamm, K.; Vieth, J.; Gorls, H.; Walther, D.; Rudolph, M.; Grummt, U.W.; Birkner, E. *Inorg. Chim. Acta*, 2004, **357**, 4496.

[61] Johansson, O.; Wolpher, H.; Borgstrom, M.; Hammarstrom, L.; Bergquist, J.; Sun, L.; Akermark, B. *Chem. Commun.* 2004, 194.

[62] Sullivan, B.P.; Salmon, D.J.; Mayor, T.J. *Inorg. Chem.*, 1978, **17**, 3334.

[63] Ioachim, E.; Medlycott, E.A.; Skene, W.G.; Hanan, G.S. *Polyhedron*, 2007, **26**, 4929.

[64] Martineau, D.; Beley, M.; Gros, P.C.; Cazzanti, S.; Caramori, S.; Bignozzi, C.A. *Inorg. Chem.* 2007, **46**, 2272.

[65] Chen, C.-Y.; Wu, S.-J.; Wu, C.-G.; Chen, J.-G.; Ho, K.-C. *Angew. Chem., Int. Ed*. 2006, **45**, 5822.

[66] Chen, C.-Y.; Wu, S.-J.; Wu, C.-G.; Chen, J.-G.; Ho, K.-C. *Adv. Mater.* 2007, **19**, 3888.

[67] Gao, F.; Wang, Y.; Zhang, J.; Shi, D.; Wang, M.; Humphry-Baker, R.; Wang, P.; Zakeeruddin, S.-M.; Grätzel, M. *Chem. Commun.* 2008, 2635.

[68] Klein, C.; Baranoff, E.; Nazeeruddin M.K.; Grätzel, M. *Tetrahedron Letters*, 2010, **51**, 6161.

[69] Nazeeruddin, M. K.; Péchy, P.; Renouard, T.; Zakeeruddin, S. M.; Humphry-Baker, R.; Comte, P.; Liska, P.; Cevey, L.; Costa, E.; Shklover, V.; Spiccia, L.; Deacon, G. B.; Bignozzi, C. A.; Grätzel, M. *J. Am. Chem. Soc*. 2001, **123**, 1613.

[70] Nazeeruddin, M. K.; De Angelis, F.; Fantacci, S.; Selloni, A.; Viscardi, G.; Liska, P.; Ito, S.; Takeru, B.; Grätzel, M. *J. Am. Chem. Soc.* 2005, **127**, 16835.

[71] Wang, P.; Zakeeruddin, S.M.; Moser, J.E.; Nazeeruddin, M.K.; Sekiguchi, T.; Grätzel, M. *Nat. Mater.* 2003, **2**, 402.

[72] Wang, P.; Klein, C.; Humphry-Baker, R.; Zakeeruddin, S.M.; Grätzel, M. *J. Am.Chem. Soc.* 2005, **127**, 808.

[73] Chang, W. C.; Chen, H. S.; Li, T. Y.; Hsu, N. M.; Tingare, Y. S.; Li, C. Y.; Liu, Y. C.; Su, C.; Li, W. R. *Angew. Chem., Int. Ed.* 2010, **49**, 8161.

[74] Bessho, T.; Yoneda, E.; Yum, J. H.; Guglielmi, M.; Tavernelli, I.; Imai, H.; Rothlisberger, U.; Nazeeruddin, M. K.; Grätzel, M. *J. Am. Chem. Soc.* 2009, **131**, 5930.

[75] Wu, K.L.; Hsu, H.C.; Chen, K.; Chi, Y.; Chung, M.W.; Liu, W.H.; Chou, P.T. *Chem. Commun*. 2010, **46**, 5124.

[76] Black, D.; Deacon, G.; Thomas, N. *Aust. J. Chem*. 1982, **35**, 2445.

[77] Von Zelcwsky, A.; Gremaud, G. *Helv. Chim. Acta* 1988, **71**, 1108.

[78] Ross, H.B.; Boldaji, M.; Rillema, D.P.; Blanyon, C.B.; White, R.P. *Inorg. Chem*. 1989, **28**, 1013.

[79] Thummel, R.P.; Lefoulon, F.; Chirayil, S. *Inorg. Chem.*, 1987, **26**, 3072.

[80] Black, D.; Deacon, G. ; Thomas, N. *Transition Met. Chem*. 1980, **5**, 317.

[81] Black, D.; Deacon, G.; Thomas, N. *Inorg. Chim. Acta* 1981, **54**, L143.

[82] Black, D.; Deacon, G.; Thomas, N. *Inorg. Chim. Acta* 1982, **65**, L75.

[83] Thomas, N.; Deacon, G. *Synth. React. Inorg. Met. Org. Chem.* 1986, **16**, 85.

[84] Kepert, C.; Deacon, G.; Spiccia, L. *Inorg. Chim. Acta,* 2003, **355**, 213.

[85] Kepert, C.; Sahely, N.; Deacon, G.; Spiccia, L.; Fallon, G.; Skelton, B.; White, A. *Inorg. Chem*. 2004, **43**, 2818.

[86] Kepert, C.; Deacon, G.; Spiccia, L.; Skelton, B.; White, A. *Dalton Trans*. 2004, 1766.

[87] Pearson, P.; Kepert, C.; Deacon, G.; Spiccia, L.; Warden, A.; Skelton, B.; White, A. *Inorg. Chem*. 2004, **43**, 683.

[88] Zakeeruddin, S. M.; Nazeeruddin, M. K.; Humphry-Baker, R.; Grätzel, M. *Inorg. Chem*. 1998, **37**, 5251.

[89] Freedman, D.A.; Evju, J.K.; Pomije, M.K.; Mann, K.R. *Inorg. Chem.* 2001, **40**, 5711.

[90] Kim, J.-J.; Choi, H.; Kim, C. Kang, M.-S.; Kang, H.S.; Ko, J. *Chem. Mater.* 2009, **21**, 5719.

[91] Song, H.-K.; Park, Y.H.; Han, C.-H.; Jee, J.-G. *J. Ind. Eng. Chem.* 2009, **15**, 62.

[92] Willinger, K.; Fischer, K.; Kisselev, R.; Thelakkat, M. *J. Mater. Chem.* 2009, **19**, 5364.

[93] Willinger, K.; Fischer, K.; Kisselev, R.; Thelakkat, M. *J. Mater. Chem.* 2009, **19**, 5364.

[94] Chandrasekharam, M.; Rajkumar, G.; Rao, C.S.; Suresh, T.; Reddy, M.A.; Reddy, P.Y.; Soujanya, Y.; Takeru, B., Ho, Y. J.; Nazeeruddin, M.K.; Grätzel, M. *Synt. Met.* 2011, **161**, 1098.

[95] Han, W.-S.; Han, J.-K.; Kim, H.-Y.; Choi, M.J.; Kang, Y.-S. ; Pac, C.; Kang, S.O. *Inorg. Chem*. 2011, **50**, 3271.

[96] Kuang, D.; Ito, S.; Wenger, B.; Klein, C.; Moser, J.-E.; Humphry- Baker, R.; Zakeeruddin, S.M.; Grätzel, M. *J. Am. Chem. Soc.* 2006, **128,** 4146.

[97] Sun, Y.; Machala, M.L.; Castellano, F.N. *Inorg. Chim. Acta*, 2010, **363**, 283.

Chapitre No: 5

Synthèse et propriétés des ligands

Résumé en français

Dans ce chapitre est décrite la synthèse de nouveaux ligands bipyridine portant le motif dithienylpyrrole (DTP). L'objectif est de lier la bipyridine en différentes positions du DTP pour étudier les effets électroniques sur les propriétés spectroscopiques et électrochimiques des ligands obtenus. Deux familles ont été préparées à partir de précurseurs DTP carboxaldéhydes et de diphosphonates bipyridiniques selon une réaction de Wadsworth-Emmons.

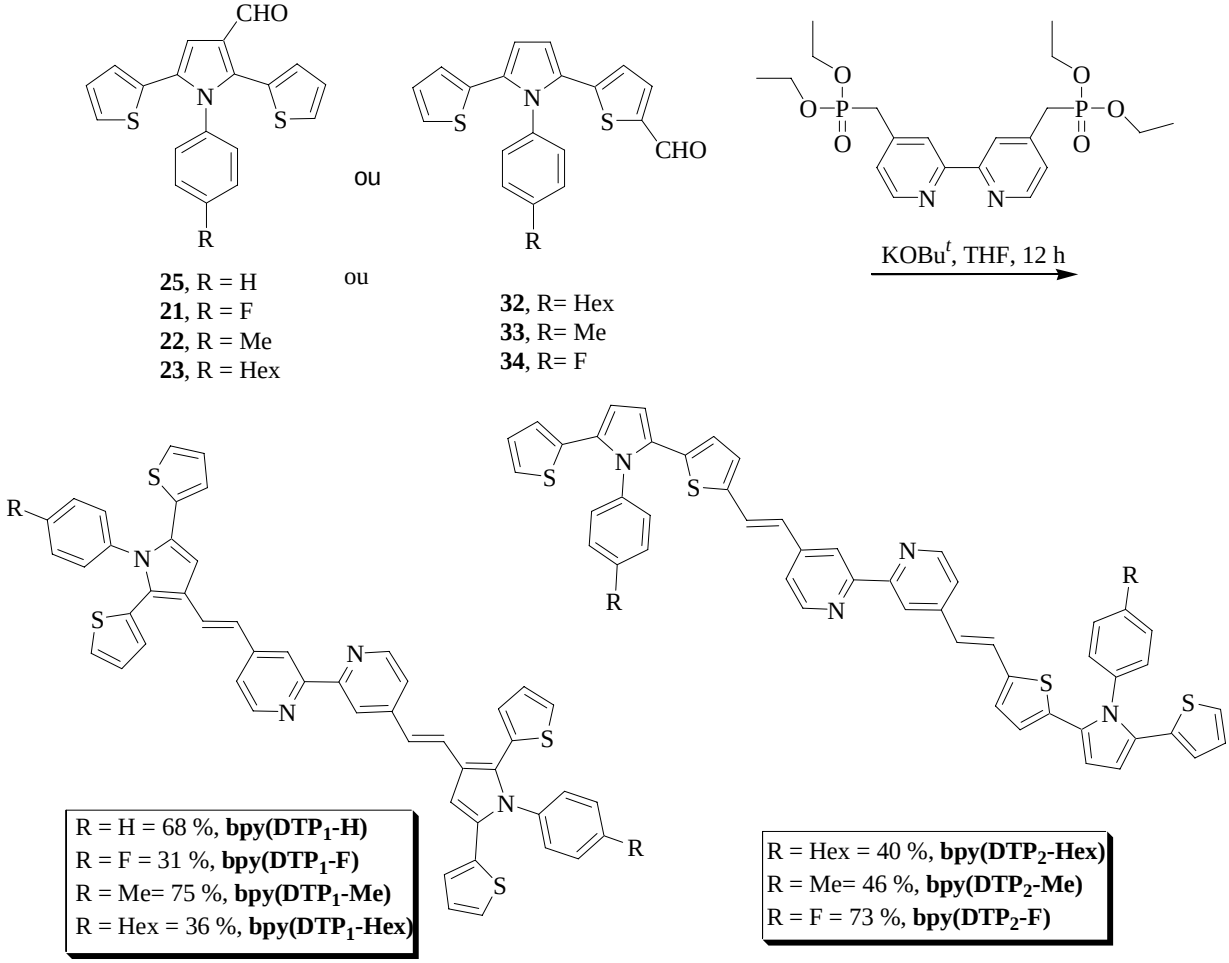

Cette nouvelle famille de ligands a été caractérisée par spectroscopie UV-Vis, électrochimie, photophysique et calculs théoriques.

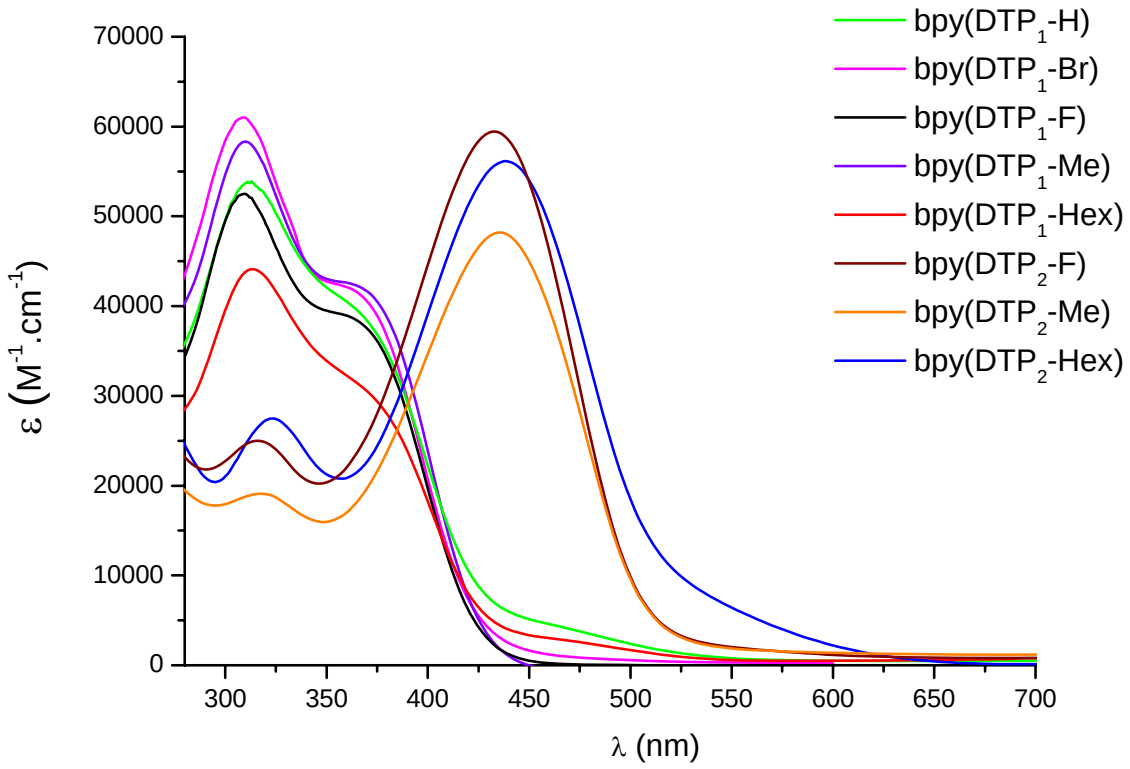

Les propriétés électroniques sont tès fortement modifiées selon que la bipyridine est liée au pyrrole (**bpy(DTP$_1$-R)**) ou au thiophene (**bpy(DTP$_2$-R)).** Le spectre UV-Vis montre clairement un très fort effet bathochrome pour la série (**bpy(DTP$_2$-R)**. Les coefficients d'extinction molaire sont élevés dans tous les cas.

La spectroscopie transitoire (laser) ainsi que les calculs théoriques DFT ont permis de mettre an evidence clairement une plus forte délocalisation π dans la série **bpy(DTP$_2$-R)**. Compte-tenu des coefficients d'extinction molaires élevés et de la possibilité de moduler les propriétés électroniques par la délocalisation, ces nouveaux ligands sont prometteurs et seront à la suite engagés dans la coordination du ruthénium pour la préparation de nouveaux complexes photoactifs homoléptiques, bis-hétéroleptiques et tris-hétéroleptiques.

Chapter No: 5

Synthesis and Properties of Ligands

Nitrogen-containing heterocycles are one of the most important class of ligands in coordination chemistry **[1-3].** 2,2'-bipyridines are nitrogen-containing organo-materials with a large spectrum of applications in materials chemistry. They readily form complexes with transition metals in which they can interact with the metals via both σ-donating nitrogen atoms and π-accepting molecular orbitals **[4]**. The resulting complexes are very stable due to the formation of a five-membered chelate. 4,4'-π-conjugated-2,2'-bipyridines have been explored in materials chemistry since last two decades due to their excellent performance in the areas of non-linear optics (NLO) **[5-11]**, light-emitting diode devices **[12]**, electrochemistry **[13, 14]** and solar cells **[15-17]**.

In present study we are interested to prepare series of ligands by attaching DTP moiety through different sites (pyrrole or thiophene) via styryl bond to 2,2'-bipyridines.

5.1. Synthesis of DTP moiety

Friedel Craft acylation of thiophene with succinyl chloride resulted in 1,4-dithienyl-butanedione **1 [18]**, which is a convenient starting material for the preparation of DTP moiety which in turn can serve as precursors of ligands and complexes which can show electrical conductivity and particular photophysical properties **[19]**.

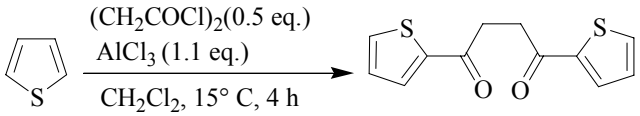

1, 65 %

The Paal-Knorr reaction that involves cyclocondensation, is a well-established and valuable tool for the preparation of pyrroles and related heterocycles. The DTP moiety can be built by Paal-Knorr reaction between **1** and substituted anilines under acidic conditions. 1,4-dicarbonyl compound provides the four carbon atoms with their substituents and amine provide the pyrrole nitrogen with its substituents **[20, 21]**.

This reaction is acid-catalysed (activation of the ketone functions) but the acidity of the medium must be adjusted in order to avoid total protonation of the amine function. This is why the literature indicates various reaction conditions involving different media: benzene or toluene with propionic acid **[22, 23]**, benzene with glacial acetic acid **[24-26]**, toluene with glacial acetic acid **[27, 28],** benzene and *p*-TsOH **[29],** toluene and *p*-TsOH **[18, 27]** or toluene in the presence of titanium tetrachloride as cooperative Lewis acid **[30]**.

Among several methods of Paal-Knorr reaction, two are most commonly employed. One method involves the reflux of **1** and the corresponding aniline derivative (4 eq.) in toluene-acetic acid, 3:1 (v/v) solution until the completion of reaction **[27, 28]** whereas other method involves the reflux of the mixture of **1**, corresponding aniline derivative (4 eq.), and *p*-TsOH.H_2O in toluene (5-24 h) under dean stark conditions **[18, 27]**.

2 was obtained in good yield by reaction between **1** and 4-bromoaniline by following acetic acid and toluene (3:1) conditions.

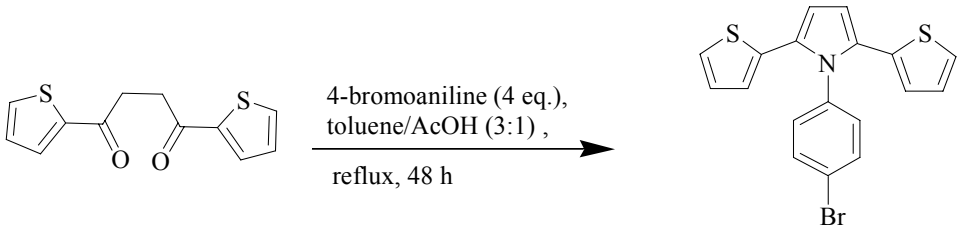

2, 65%

5.1.1. Functionalization of DTP

2 is a very important precursor as it has many reactive sites for functionalization. Bromo group can be functionalized by adding aldehyde group whereas alkyl chains can be introduced at thiophene rings.

Thus, the metallation routes, such as halogen-metal exchange and deprotonation were adopted in the beginning for the functionalization of **2.**

5.1.1.1. Halogen-metal exchange

n-BuLi was used as metallating agent to metallate the phenyl ring (Br-Li exchange) and trimethylsilyl chloride (TMSCl) was used to trap the metalated intermediate.

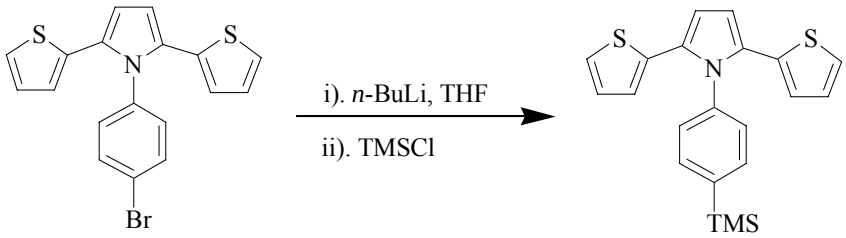

2

Different reaction conditions were tried. All tried conditions along with obtained results are given in **table 5.1**. It is evident that **2** was reduced by using 1 eq. *n*-BuLi but silylation did not take place at the phenyl ring but only at thiophene and when amount of *n*-BuLi was increased then phenyl ring was also silylated but the deprotonation of thienyl protons was observed as the main reaction. Thus it appeared that metallation with *n*-BuLi was not regioselective.

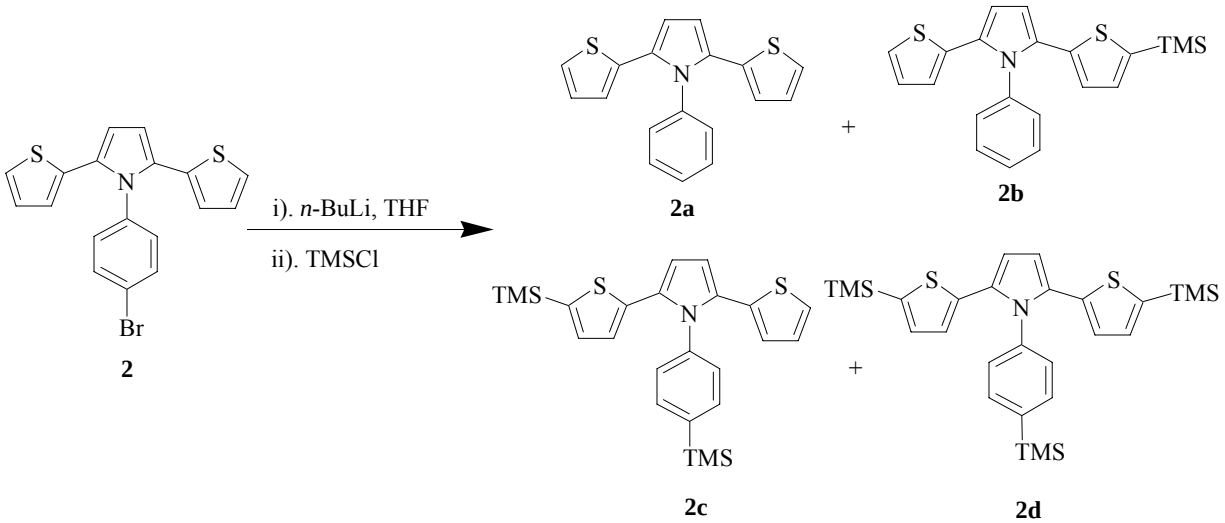

2 **2a** **2b** **2c** **2d**

Table 5.1: *n*-BuLi as metallating agent to metallate the phenyl ring

S.No.	Conditions	Results (%)[a]			
		2a	2b	2c	2d
1	1. *n*-BuLi (1 eq.), THF, -78° C, 2 h 2. TMSCl (1.5 eq.), -78° C, 1 h	70	30	-	-
2	1. *n*-BuLi (2 eq.), THF, -78° C, 2 h 2. TMSCl (2.5 eq.), -78° C, 1 h	10	35	55	-
3	1. *n*-BuLi (3 eq.), THF, -78° C, 2 h 2. TMSCl (3.5 eq.), -78° C, 1 h	3	32	65	-
4	1. *n*-BuLi (4 eq.), THF, -78° C, 2 h 2. TMSCl (4.5 eq.), -78° C, 1 h	10	50	20	20

[a] determined by GC-MS

Then other metallating agents with lower basicity were used to attempt Br-metal exchange. Grignard reagents were found to be good candidates for this purpose whereas water was used to trap metallated species in this case **(table 5.2)**.

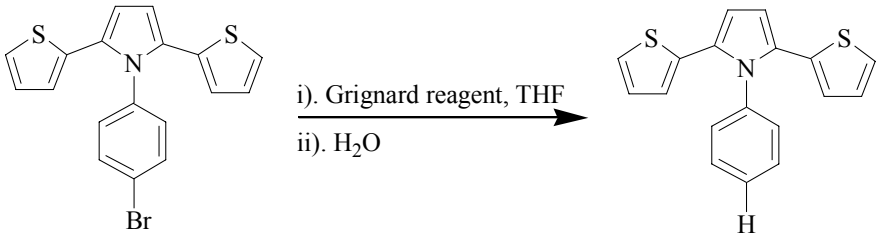

2

Table 5.2: Grignard reagent employed for Br-metal exchange

S.No.	Grignard reagents and Conditions	Results[a]
1	1. *i*-PrMgCl.LiCl (1 eq.), -5° C (1 h), r.t. (30 min) 2. H_2O (0°C)	n.r.
2	1. *i*-PrMgCl.LiCl (2 eq.), -5° C (1 h), r.t. (30 min) 2. H_2O (0°C)	n.r.
3	1. Mg (2 eq.), r.t. (1 h) 2. H_2O (0°C)	n.r.

n.r. = no reaction; [a] determined by NMR spectra

Unfortunately, no reaction occurred in any case. So it was concluded that metallation was not possible to carry out at **2**.

5.1.1.2. Deprotonation

As Br-Li exchange did not take place by using various metallating agents, it was planned to deprotonate thienyl protons first to introduce hexyl chains in order to increase solubility and then perform Br-Li exchange, so that thienyl protons would not be available and bromine atom would be the only available site for functionalization.

Lithium 2,2,6,6-Tetramethylpiperidine (LiTMP) was used as the deprotonating agents for this purpose.

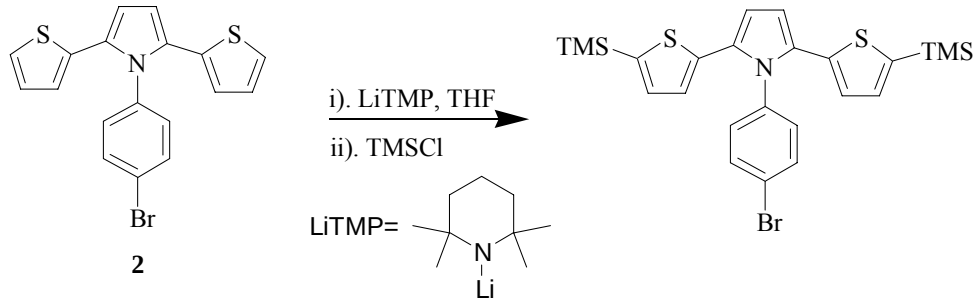

Table 5.3: LiTMP as deprotonating agent

S.No.	Deprotonating agents and Conditions	Results[a]
1	1. LiTMP (1 eq.)-78 ° C (1 h), -40° C (30 min) 2. TMSCl, -78° C, 1 h	n.r.
2	1. LiTMP (2 eq.), -78 ° C (1 h), -40° C (30 min) 2. TMSCl, -78° C, 1 h	n.r.
3	1. LiTMP (4 eq.), -78 ° C (1 h), -40° C (30 min) 2. TMSCl, -78° C, 1 h	n.r.

n.r. = no reaction; [a] determined by NMR spectra

As shown in table 5.3, deprotonation did not take place even by using a large excess of the base (4 eq.)

When no fruitful results were achieved then a possibility was considered that perhaps during the reaction, deprotonation may occur but electrophilic trapping was not efficient. To check this, CH_3OD was used as an electrophile in order to ensure efficient trapping of metallated species. All reaction conditions attempted for this purpose are reported in **table 5.4.**

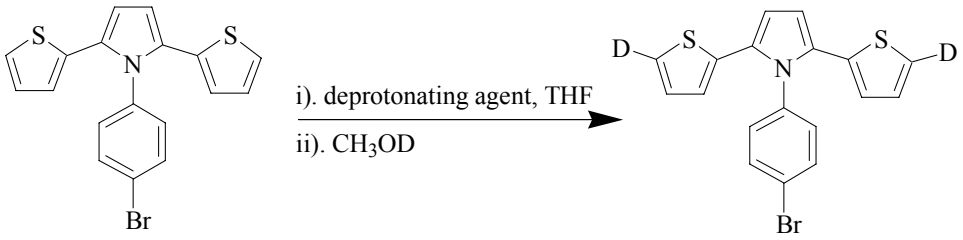

2

Table 5.4: Different conditions employed for deprotonation by using LiTMP as deprotonating agent

S.No.	Deprotonating agents and Conditions	Results[a]
1	LiTMP (1 eq.), -78 ° C (2 h)	n.r.
2	LiTMP (2.5 eq.), -78 ° C (1 h)	n.r.
3	LiTMP (2.5 eq.), 0 ° C (1 h)	n.r.
4	LiTMP (2.5 eq.), -78° C (1 h), 0° C (1 h)	n.r.
5	LiTMP (2 eq.), -40° C (2 h)	n.r.
6	LiTMP (2 eq.), -78 ° C (2 h)	n.r.
7	LiTMP (2 eq.), -40° C (2 h)	n.r.
8	LiTMP (4 eq.), -78 ° C (2 h)	n.r.
9	LiTMP (4 eq.), -40 ° C (2 h)	n.r.
10	LiTMP (5 eq.), 0 ° C (1 h)	n.r.

n.r. = no reaction; [a] determined by ^{1}H NMR spectroscopy

But no reaction took place by following all the conditions reported in **table 5.4.** Starting material was recovered at the end of reaction in each case.

Since Br-Li exchange and deprotonation were found to be unsuccessful, so other approaches were considered for the functionalization of **2.**

5.1.1.3. Paal-Knorr reaction

It was planned to prepare DTP moiety substituted with nitrile group via Paal-Knorr reaction, so that aldehyde group can be obtained by the reduction of nitrile. After protection of aldehyde group deprotonation of thiophene ring may take place to introduce alkyl chain.

3 was synthesized in 60 % yield by reaction between **1** and *p*-aminobenzonitrile in xylene in presence of *p*-TsOH.H_2O. Reduction of nitrile **[18]** was carried out by using diisobutylaluminium hydride (DIBAL-H) to obtain aldehyde in 92 %. Then protection of aldehyde group was attempted by its reaction with ethylene glycol but the formed product was insoluble in every solvent including DMSO. So it was not possible to characterize the product and consequently to carry out further work.

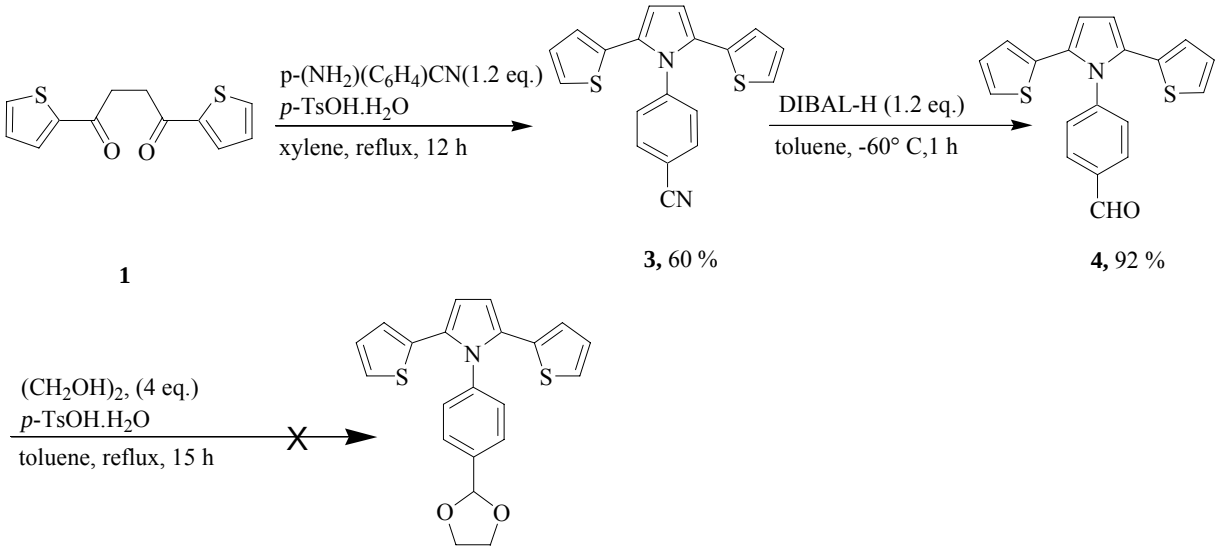

5.1.1.4. Introduction of alkyl chains on DTP

Taking into account the above results the new plan was designed that alkyl chains should be introduced into the DTP system first to induce solubility before further functionalization.

Friedel Craft acylation between 2-bromo thiophene and succinyl chloride resulted 1,4-Bis(5-bromo-2- thienyl)-1,4-butanedione **(5)**. Then the mixture of **5**, ethylene glycol and *p*-TsOH.H_2O in toluene was refluxed for 48 h in order to get diprotected diketone **(6) [31]** by following reaction scheme. The diprotected diketone was separated from the monoprotected species by fractionated recrystallization from hexane.

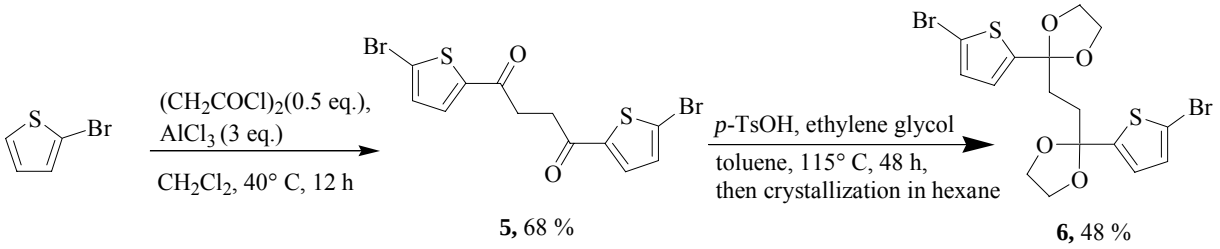

5, 68 %

6, 48 %

6 was expected to be highly versatile because of its possibility of further functionalization by, e.g. metalation and/or coupling reactions at the bromo-substituted carbon atoms. So it was planned to carry out Br-Li exchange first followed by coupling to introduce hexyl chain.

For Br-Li exchange 2.5 eq. *n*-BuLi was added into the solution of **6** in anhydrous THF at -78° C. Reaction was carried out for 2 h. Instead of adding alkyl halide, deuteration was carried out first in order to check whether exchange occurred or not. But NMR spectrum revealed that no exchange took place and starting material was recovered at the end. Same reaction was repeated at -40° C but no reaction occurred. Co-ordination of BuLi by dioxolane oxygens possibly occurred. Further attempts with large amounts of BuLi did not improve the results.

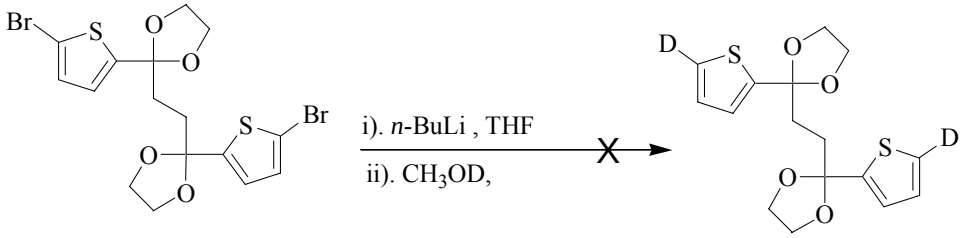

6

Then Isopropylmagnesium chloride (*i*-PrMgCl) was used for the purpose of exchange then addition of hexyl iodide was carried out but no reaction occurred and starting material was recovered as such at the end.

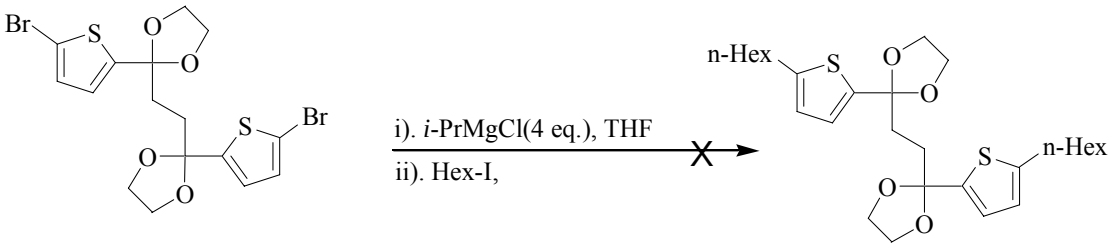

6

Kumada coupling between **6** and Grignard reagent in presence of Ni catalyst was carried out to introduce alkyl chains. But this approach was not successful either.

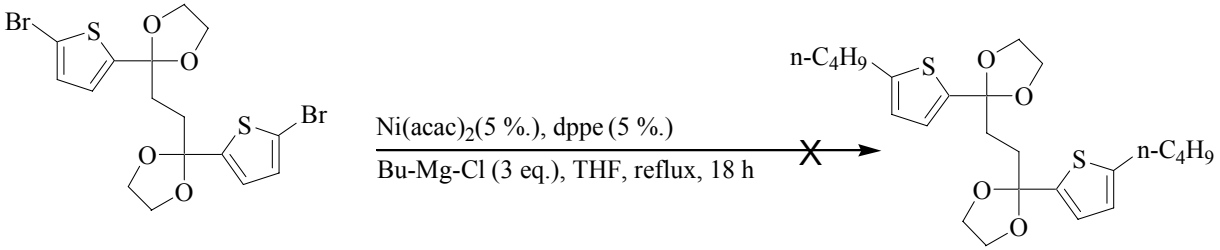

6

Thus it was decided to first introduce alkyl chains on the diketone in order to avoid problems.

1 ,4- Bis(5-hexyl-2-thienyl)-1,4-butanedione **(7) [32]** was then prepared in moderate yield by Friedel Craft acylation between 2-Hexyl thiophene and succinyl chloride in presence of $AlCl_3$.

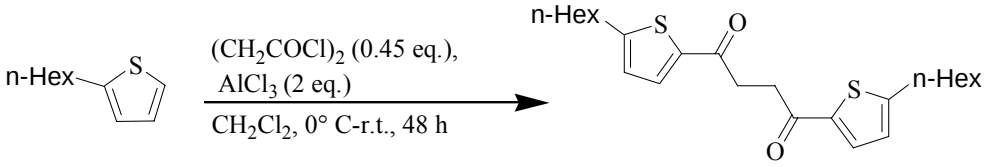

7, 30 %

Paal-Knorr reaction between **7** and *p*-aminobenzonitrile in presence of *p*-TsOH.H_2O was then planned. By using DIBAL-H, nitrile group can be reduced further into aldehyde **[18]** that finally can be subjected to ligand synthesis.

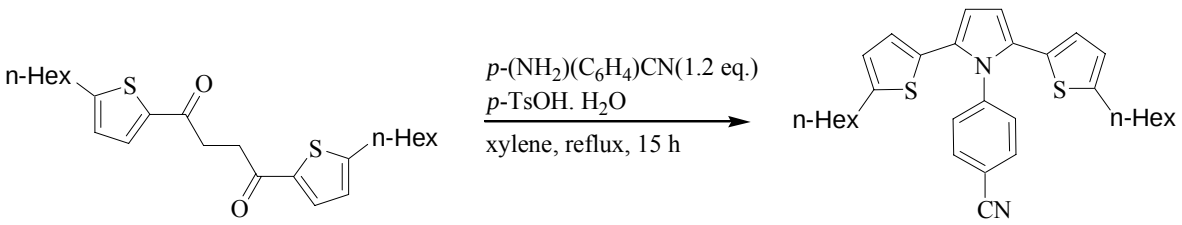

7

8, 2 %

Unfortunately **8** was obtained but yield was very low (ca. 2 %). Major portion of **7** was recovered unreacted. Paal Knorr reaction was repeated by using other reaction conditions. Toluene/acetic acid (3:1) was used and the reaction mixture was refluxed for 48 h. But same low yield was resulted. Microwave method (250 W, 160° C, 10-30 min.) was also used but no improvement was obtained. With such a low yield it was not possible to carry out further steps. So modification in synthetic route was made.

7 was planned to react with 4-bromoaniline by following acetic acid and toluene (3:1) conditions of Paal Knorr reaction. And then bromine lithium exchange can be performed by using BuLi and the treatment of lithiated compound with DMF can introduce aldehyde group at this position.

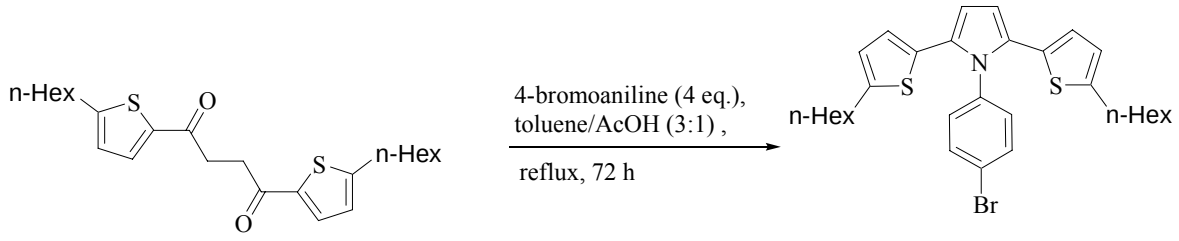

7 **9,** 5 %

But like in previous case, **9** was also obtained in very small yield (5 %). Reaction time was extended upto 72 h but no improvement was found. Same reaction was carried out by using *p*-TsOH (30 mol %) and xylene instead of toluene and acetic acid but same results were obtained. Microwave synthesis was also tried by using 3.5 eq. of 4-bromoaniline and acetic acid as solvent. Reaction was carried out at 130° C and 150 W for 20 minutes but low yield was obtained.

Then **7** was subjected to Paal Knorr reaction with aniline substituted with electron donating group (hexyl) instead of electron withdrawing group (Br, CN).

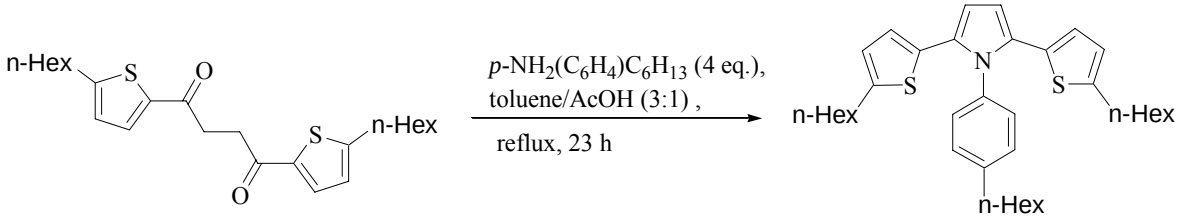

7 **10,** 55 %

10 was obtained in good yield (55 %). It was concluded that it was impossible to perform Paal-Knorr reaction from **7** with aniline substituted by electron withdrawing group (Br, CN) but only with aniline substituted with electron donating group (hexyl). A lower nucleophilicity of the aniline combined with a weaker electrophilicity of ketones could be the reason for such an absence of reactivity.

Then it was planned to subject **5** to Paal-Knorr reaction with *p*-aminobenzonitrile in presence of *p*-TsOH.H_2O that can be treated further with DIBAL-H to reduce nitrile into aldehyde. Before doing metallation to introduce hexyl chains at thiophene rings it was planned to protect aldehyde and the resulting compound can be subjected to metallation. After completion of metallation, alkylation can be carried out. Then deprotection can be done and resulting aldehyde can be subjected to ligand synthesis.

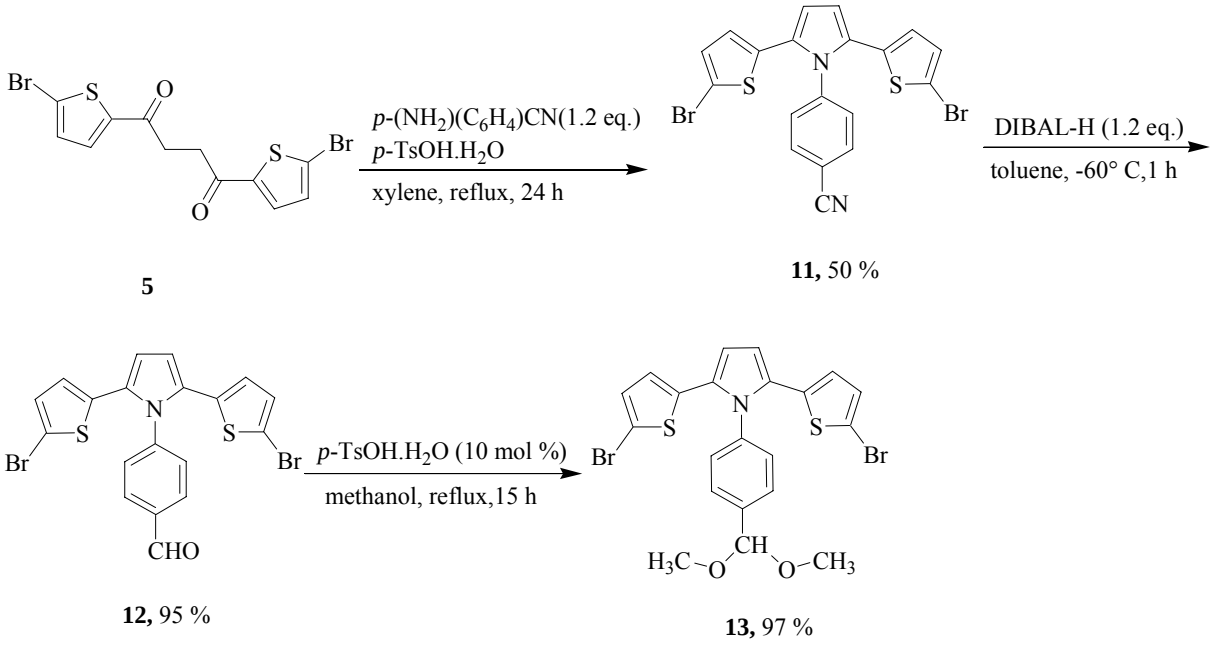

5 underwent Paal–Knorr reaction with *p*-aminobenzonitrile and **11** was obtained in acceptable yield (50 %), then by the reduction of nitrile group into aldehyde, **12** was isolated in 95 % yield. Aldehyde group was successfully protected by using methanol and *p*-TsOH giving **13** in 97 % yield.

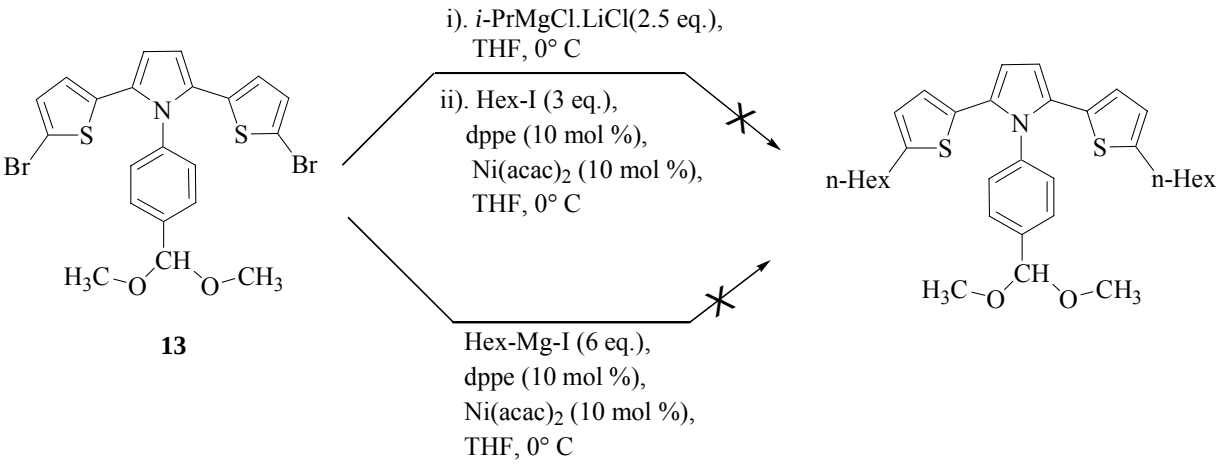

Kumada coupling between the Grignard reagent prepared from **13** by using *i*-PrMgCl.LiCl and hexyl iodide was carried out in the presence of Ni catalyst and 1,2-Bis(diphenylphosphino)ethane (dppe) but this approach was not successful. Hexyl magnesium iodide was prepared and 6 equivalents were added into the solution of **13**, dppe and nickel

acetylacetonate in THF at 0° C, then mixture was allowed to react at room temperature. NMR spectrum revealed that 40 % deprotection of aldehyde group was observed but no coupling occurred.

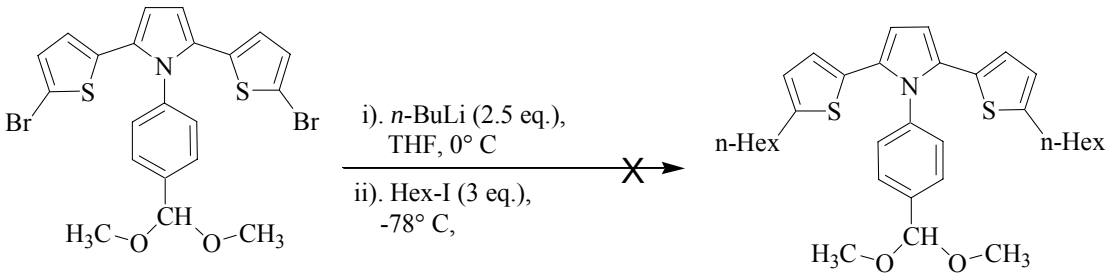

13

Then **13** was subjected to metallation, by using 2.5 eq. *n*-BuLi as metallating agent and THF as solvent. Reaction was carried out at -40° C. Reaction progress was monitored by TLC after one hour. Starting material was no more located that clearly indicated the completion of metallation. For alkylation temperature of reaction mixture was decreased to -78° C and 1-iodohexane was introduced. Temperature was gradually raised to room temperature and allowed to react overnight. But alkylation did not occur. Same reaction was also attempted by using 1-bromohexane. But no reaction took place. 35-50 % deprotection of aldehyde was confirmed by NMR spectra in each case.

Deprotection of protected aldehyde during the reaction was the major problem. In order to overcome this, some other protecting group was planned to use. For this purpose ethylene glycol was used in presence of *p*-TsOH.H_2O (2.5 mol %) as catalyst and toluene as solvent. The mixture was refluxed for 15 h, and dean stark apparatus was used to trap water. **14** was obtained in 90 % yield.

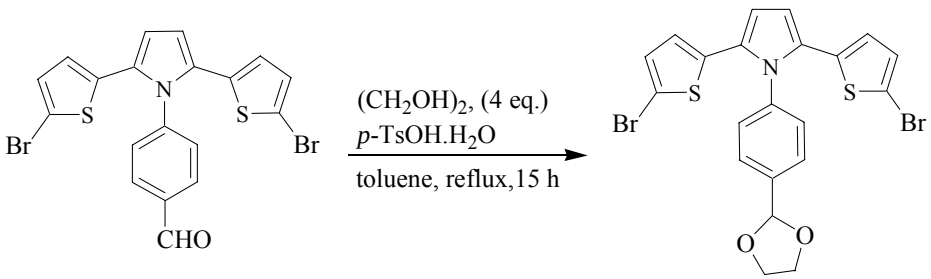

12 **14,** 90 %

14 was reacted with *i*-PrMgCl.LiCl at 0° C to exchange bromine atoms. And then this was added dropwise into the mixture of hexyl iodide, dppe and nickel acetylacetonate into THF and allowed to react overnight at room temperature. But coupling did not take place.

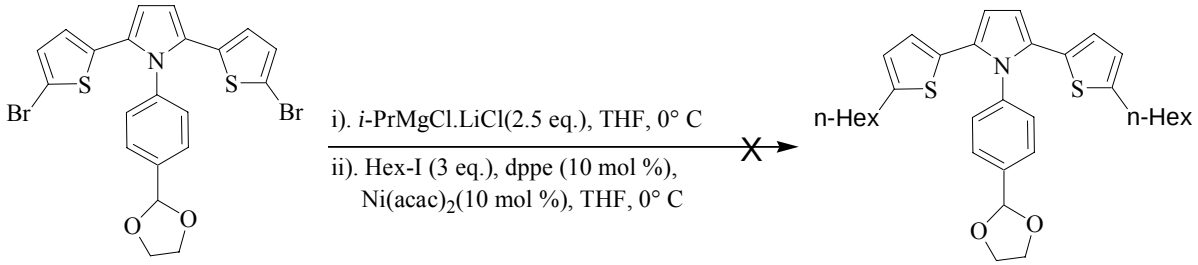

14

When all early attempts to functionalize **2** on the phenyl ring were not successful then it was planned to introduce carboxaldehyde on the heteroaromatic rings i.e. thiophene or pyrrole.

5.1.1.5. Introduction of aldehyde on heteroaromatic rings of DTP

The Vilsmeier-Haack reagent ($POCl_3$+DMF) has attracted the attention of synthetic organic chemists since its discovery in 1927 **[33]** and Vilsmeier-Haack reaction has emerged as an efficient and economical tool for the formylation of heterocycles **[34-36]**. In order to introduce the carboxaldehyde at heteroaromatic ring Vilsmeier-Haack formylation was chosen.

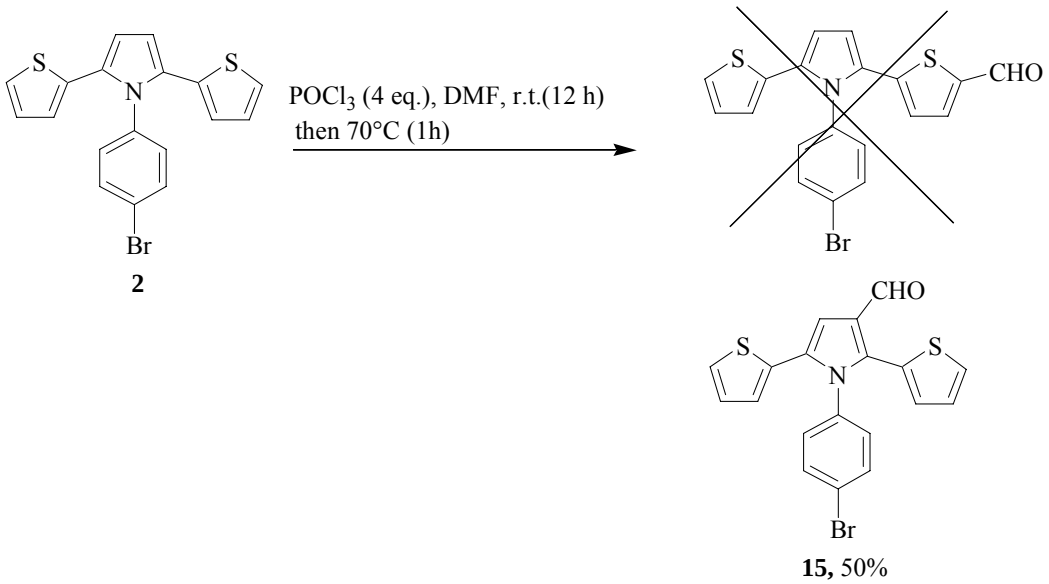

2

15, 50%

As shown, Carboxaldehyde was introduced exclusively on the pyrrole ring of **2**, in acceptable yield (50 %) and this fact was revealed by NMR spectra. The extremely high reactivity of a pyrrole ring creates the possibility of introducing an aldehyde into the β-position of

the pyrrole ring even with the free α-positions of thiophene rings. **15** was subjected to ligand synthesis in order to study the electronic properties of DTP moiety.

5.2. Synthesis of bpy(DTP$_1$-Br) ligand

The synthetic strategies to obtain styryl substituted bipyridine includes either the classical Knoevenagel Condensation between the deprotonated 4,4'-dimethyl-2,2'-bipyridine and an aromatic aldehyde or Wadsworth-Emmons reaction between the Tetraethyl[4,4'-diphosphonate-2,2'-bipyridine] and an aldehyde. Wadsworth-Emmons reaction is a well-known synthetic route for the preparation of 4,4'-bis-styryl-2,2'-bipyridines with predominantly *E*-selectivity of the C=C vinyl bond.

The key precursor of Wadsworth-Emmons reaction, Tetraethyl[4,4'-diphosphonate-2,2'-bipyridine] **(16)** was prepared from commercially available compound 4,4'-dimethyl-2,2'-bipyridine in three steps **[37, 38]**. In first step, 4, 4'-bis [(trimethylsilyl)methyl]-2,2'-bipyridine derivative **bpySi** (99 %) was obtained by deprotonation of 4,4'-dimethyl-2,2'-bipyridine by lithium diisopropylamide (LDA) followed by trapping of the resulting di-anion with trimethylsilyl chloride (TMSCl), then **bpySi** was subjected to chlorination with hexachloroethane in the presence of a dry fluoride source (CsF) in acetonitrile at 60° C for 16 h to afford 4,4'-bis(chloromethyl)-2,2'-bipyridine **bpyCl** (85 %). **bpyCl** was reacted with NaH and triethylphosphite at 80° C for 6 h and **16** was obtained (55 %).

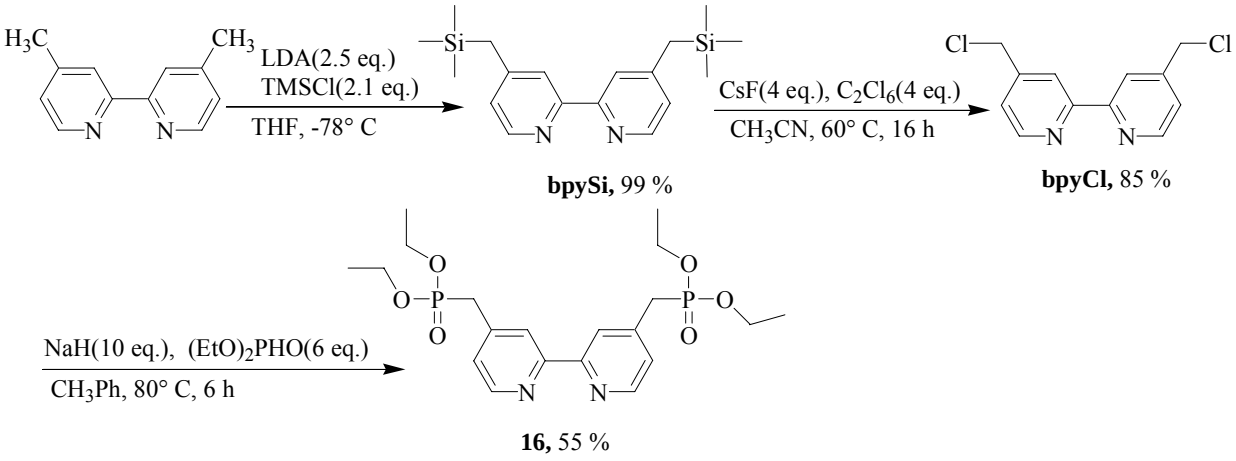

Finally, the Wadsworth–Emmons reaction between **16** and **15** in the presence of *t*-BuOK in THF at room temperature afforded the ligand **bpy(DTP$_1$-Br)** in 38 % yield. ^{1}H NMR, ^{13}C

NMR and mass spectrometry data confirmed the ligand. Structure of ligand was also verified by single crystal X-ray diffraction (XRD) analysis. Crystals of sufficient quality were obtained by slow evaporation of dichloromethane solution.

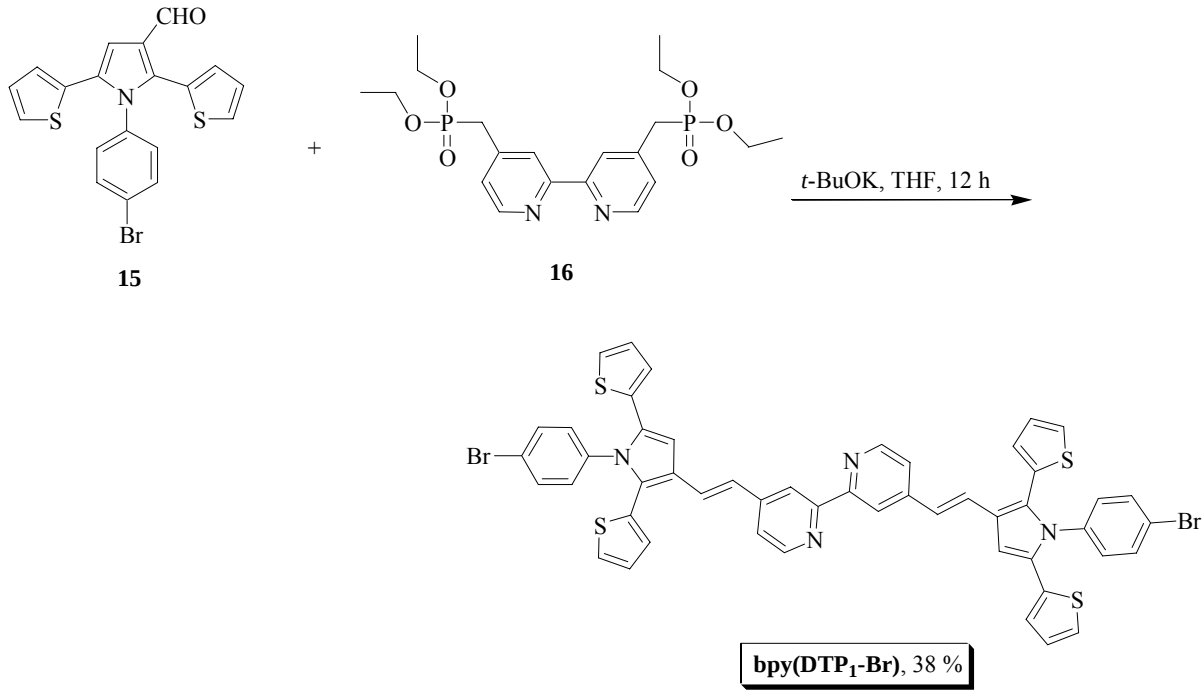

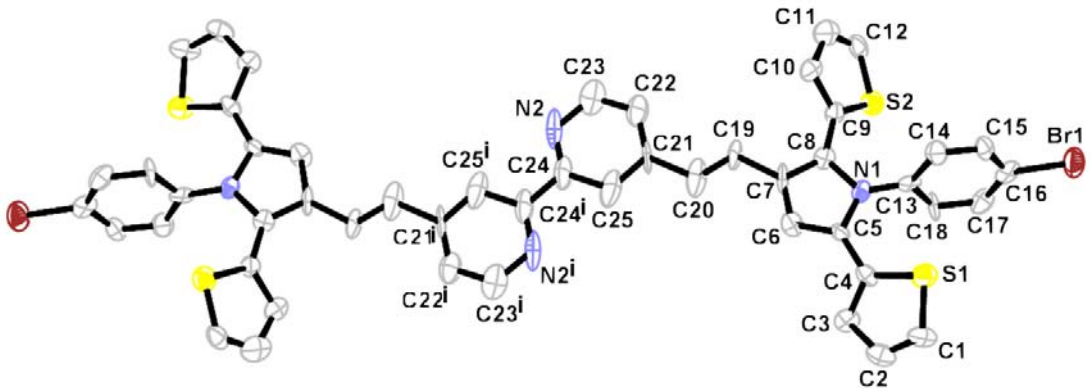

Figure 5.1: An ORTEP diagram of the bpy(DTP$_1$-Br) showing the thermal ellipsoids and atom numbering scheme. The thermal ellipsoids are drawn at 50% probability level. Symmetry code: (i) -X+2, -Y, -Z+1
(Coll. M. Ahmed, C. Jelsch, C. Lecomte; CRM2).

5.3. Synthesis of other DTP carboxaldehyde moieties

Then, we planned to prepare a series of ligands (DTP_1-R) with electron withdrawing (F, Br) and electron donating (methyl, hexyl) substituent to obtain ligands with different electronic effects. Ligand without any substituent was also planned to prepare in order to clearly understand the contribution of electron withdrawing and electron donating substituents.

1 underwent cyclocondensation reaction with appropriate anilines. Cyclocondensation reaction with non-substituted aniline was also performed to obtain DTP moiety without any substituent.

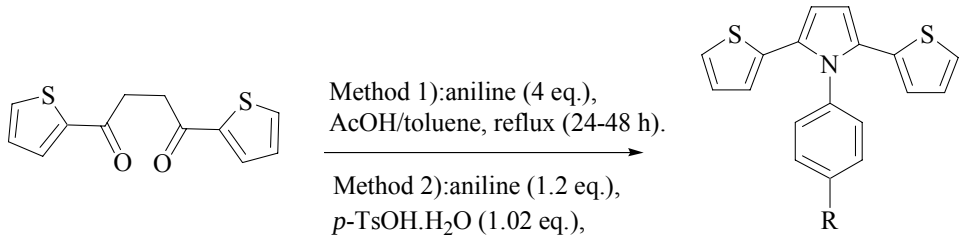

1

17, R=H, 94%
18, R=F, 68%
19, R=Me, 70%
20, R=Hex, 55%

17 was obtained in excellent yield (94 %) by following the conditions of method **2**. Whereas **18-20** were obtained in good yield (55-70 %) by following method **1** conditions.

Then all DTP compounds **(17-20)** underwent Vilsmeier-Haack formylation to introduce the carboxaldehyde. **21-23** were obtained in acceptable yields (52-65 %).

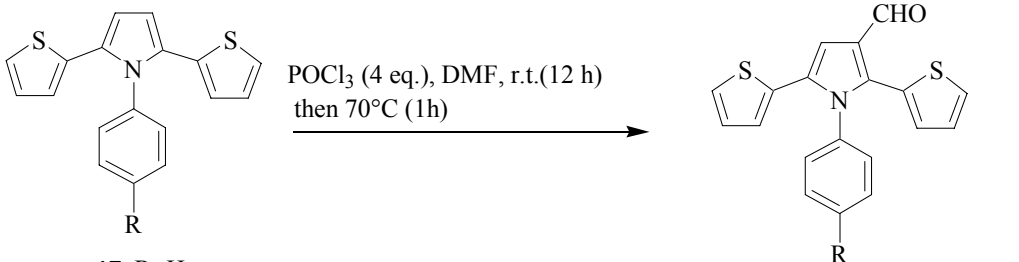

17, R=H
18, R=F
19, R=Me
20, R=Hex

21, R=F, 65%
22, R=Me, 52%
23, R=Hex, 60%
R= H, not obtained

Apart from NMR spectra, position of aldehyde was also verified by single crystal X-ray diffraction (XRD) analysis. Crystals of **21** and **22** were obtained by slow evaporation of their chloroform solution.

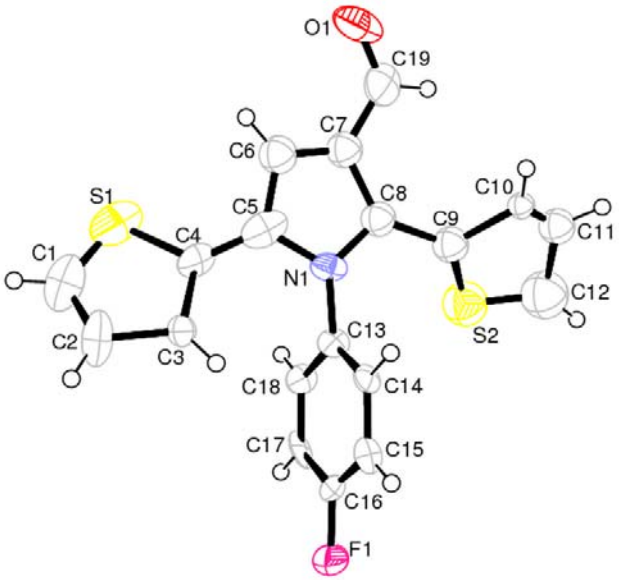

Figure 5.2: ORTEP diagram of **21**

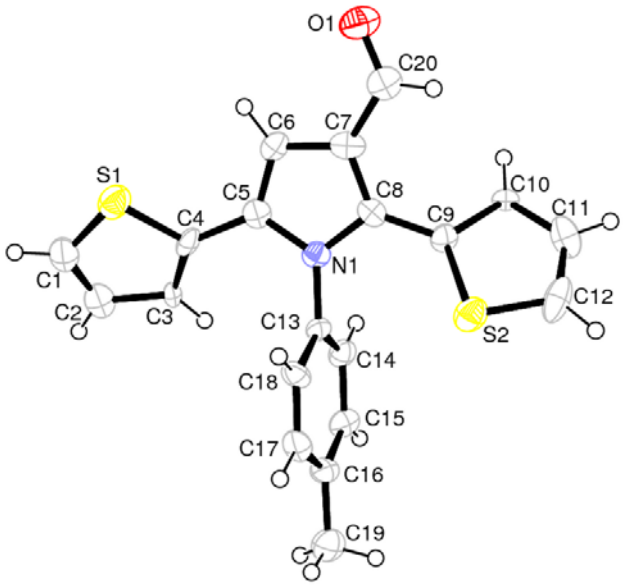

Figure 5.3: ORTEP diagram of **22**

(Coll. M. Ahmed, C. Jelsch, C. Lecomte; CRM2)

When **17** was reacted under the same conditions, previous trend was not repeated, an inseparable mixture containing desired aldehyde was obtained in this case that was revealed by ^{1}H NMR spectrum and GC-MS data of the crude product.

Same reaction was repeated by using 1 eq. of $POCl_3$ but mixture of aldehydes was obtained that were unable to be separated. Then an alternative route using **15** as a precursor was followed.

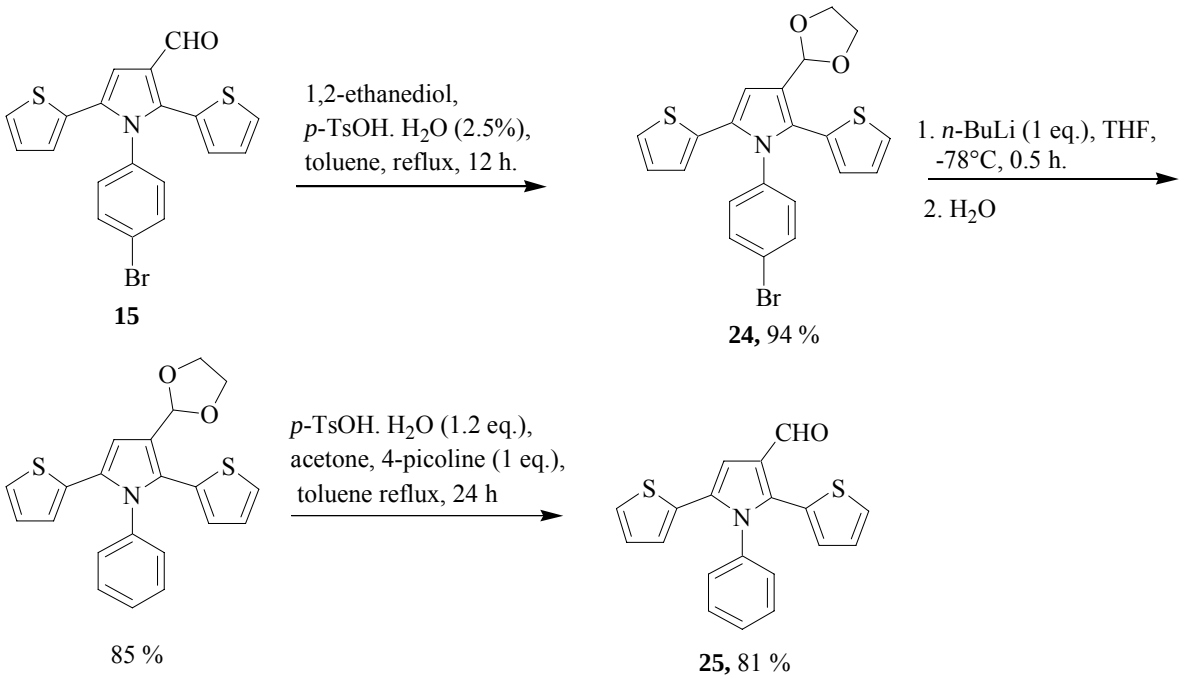

The aldehyde was first protected as a dioxolane (**24**, 94 %) by refluxing the solution of **15**, 1,2-ethanediol and catalytic amount of *p*-TsOH.H_2O (2.5 mol %) in toluene for 12 h. Then bromine was removed by treatment with BuLi. After deprotection under acidic conditions, **25** was obtained in 81% yield.

5.4.Synthesis of DTP_1 series bipyridine ligands

Wadsworth–Emmons reaction between aldehydes **(21-23 and 25)** and **16** in the presence of *t*-BuOK in THF at room temperature afforded the DTP_1-R series of ligands in good yields (31-75 %).

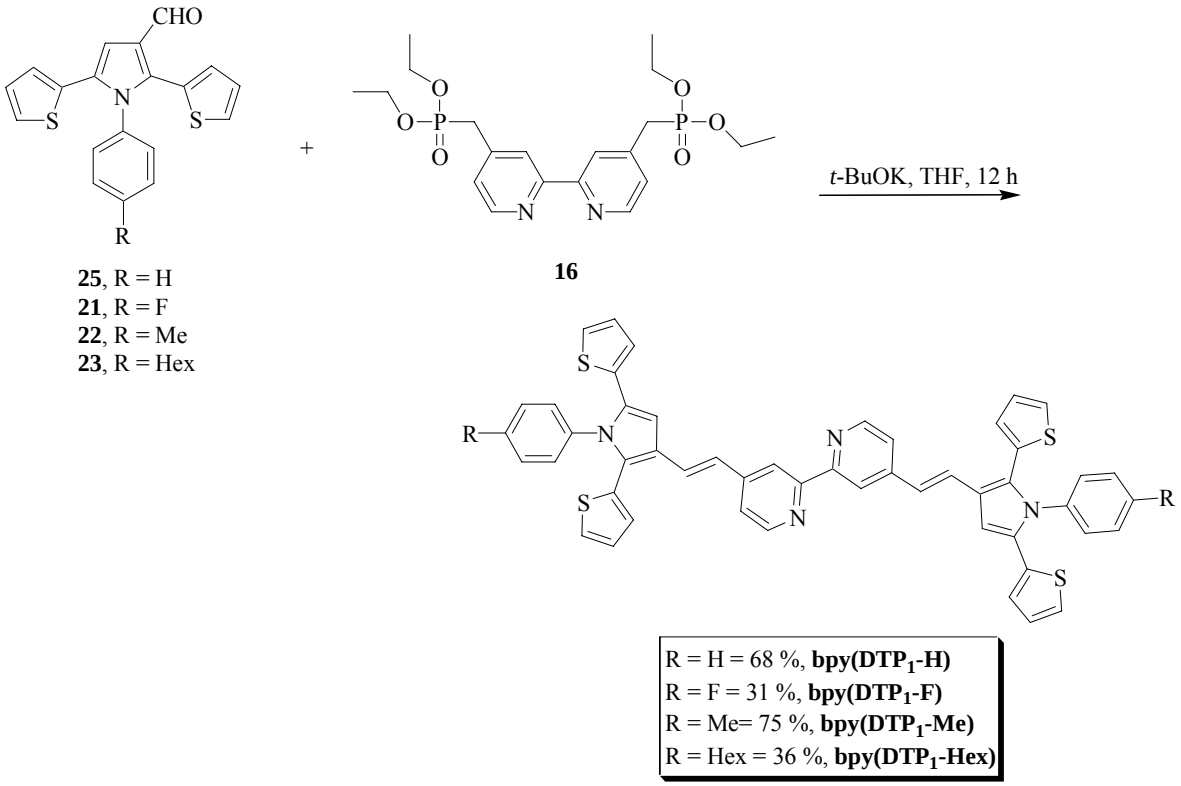

5.5. Synthesis of DTP_2 series bipyridine ligands

In order to obtain carboxaldehyde at thiophene ring to obtain DTP_2 series bipyridine ligands it was planned to prepare monobrominated diketone and then subject it to Paal-Knorr reaction with substituted anilines. Further bromine lithium exchange can be carried out by using *n*-BuLi followed by the formylation by using DMF.

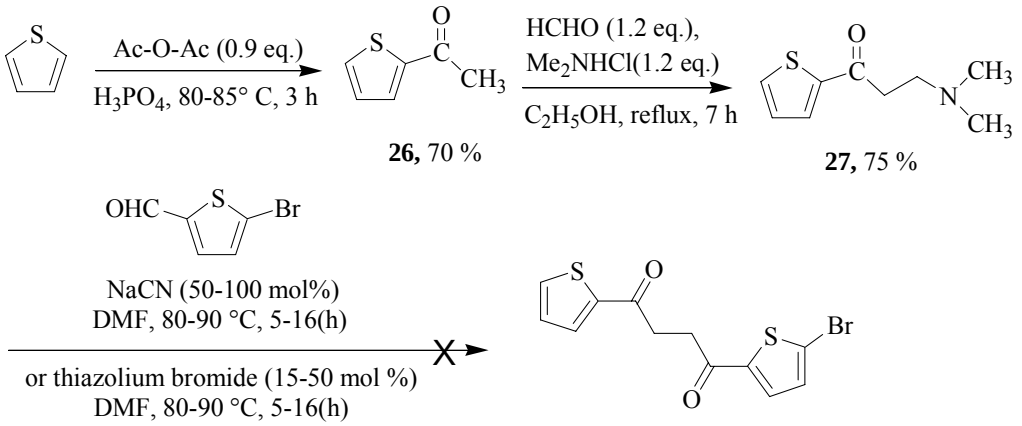

Thiophene in acetic anhydride was treated with a few drops of H_3PO_4 at 80-85° C for 3 hours and 2-acetylthiophene **(26)** was obtained in good yield (70 %) that further undergoes Mannich reaction to give Mannich base **(27)**. Stetter reaction **[39, 40]** was carried out between **27** and 5-bromo-2-thiophenecarbaldehyde in DMF by using NaCN as catalyst (1 eq. and then 50 mol %). But in both cases no reaction occurred. Degradation of starting materials took place.

Then Stetter reaction was tried by using 3-ethyl-5-(2-hydroxy ethyl)-4-methyl thiazolium bromide as catalyst instead of NaCN. In the mixture of **27** and thiazolium bromide (15 mol %) in DMF in presence of triethyamine the solution of 5-bromo-2-thiophenecarbaldehyde in DMF was added and reaction mixture was stirred at 80-90° C over a period of 5 hours. Degradation of starting materials was observed. Same reaction was repeated by using 20 mol % and 50 mol % of thiazolium bromide. GC-MS revealed that very complex mixture of unidentifiable products including the traces of target compound was present. And it was impossible to separate the product. So, it was impossible to obtain monobrominated diketone by following this route. So it was planned to introduce aldehyde at thiophene ring of substituted DTP moieties by using methods other than Vilsmeier-Haack formylation.

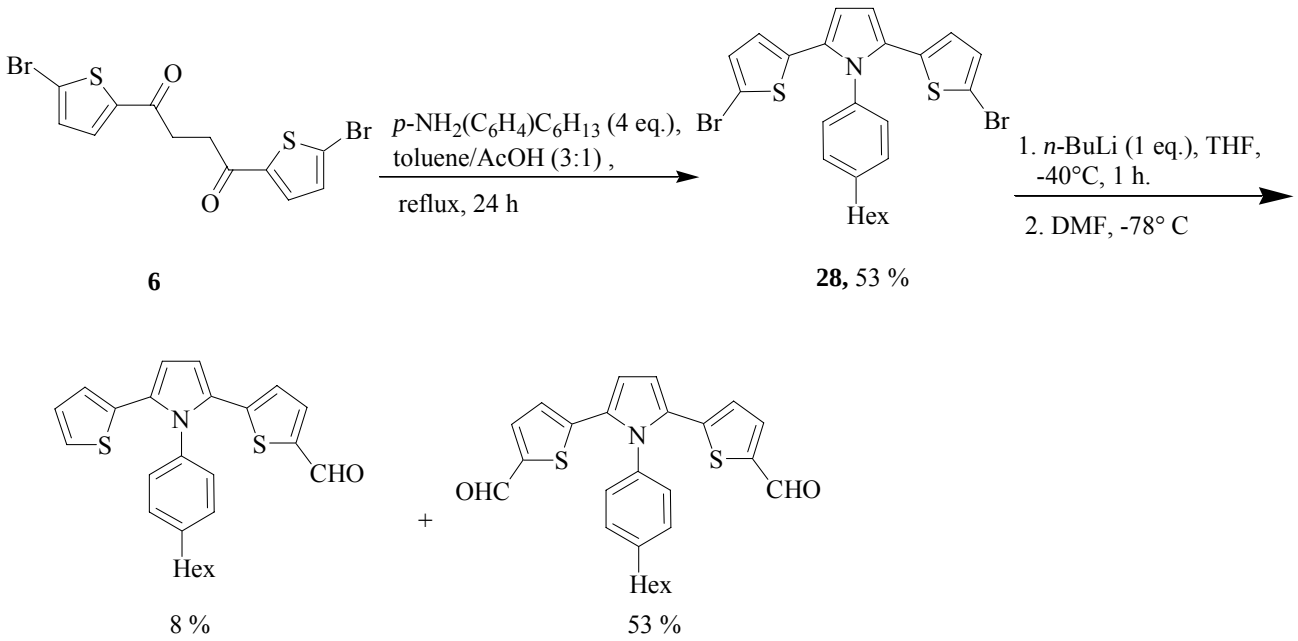

6 **28,** 53 %

8 % 53 %

6 was used as starting material and was subjected to Paal Knorr reaction in order to get **28** that was obtained in 53 % yield. To get target compound metallation was carried out first from **28** by using 2.5 eq. *n*-BuLi as metallating agent and THF as solvent at -40° C. Reaction progress

was monitored by TLC after one hour. Starting material was no more located that clearly indicated the completion of metallation. For formylation temperature of reaction mixture was decreased to -78° C and DMF was added. Temperature was gradually raised to room temperature and allowed to react overnight. Mixture was obtained that was separated by column chromatography. Major product was biformylated compound (53 %). To get exclusively monoformylated product same reaction was carried out by using 1 eq. of DMF but reaction was not selective this time as well.

Then it was planned to deprotonate **20** and then to carry out formylation.

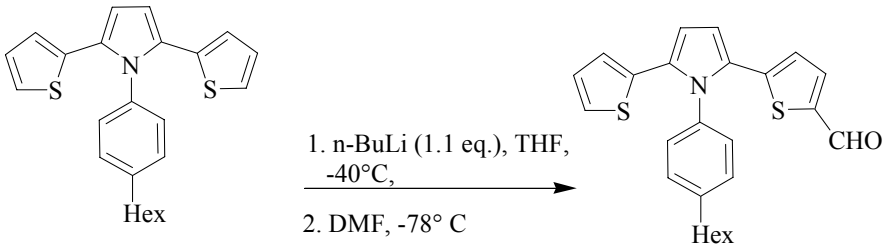

20

To deprotonate 1.1 eq. of *n*-BuLi was used at -40° C. After 1.5 hours DMF was added at -78° C. Then temperature was slowly raised to room temperature and reaction was further continued for 4 hours. At the end mixture of starting material **20**, monoformylated and biformylated product was obtained. Biformylated product was the major product. Selectivity was not obtained by any of above described route.

Then it was planned to carry out monobromination by using NBS that can be followed by lithiation to introduce aldehyde.

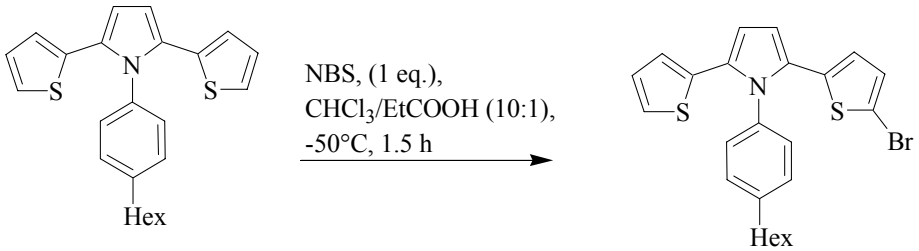

20 **29,** 66 %

When **20** was subjected to monobromination then as a result mixture of monobrominated, dibrominated product as well as starting material was obtained that was separated by column chromatography and **29** was obtained as a major product in good yield (66 %). By having successful monobromination on **20** same method was attempted on the other substituted DTP moieties e.g. **18** and **19**.

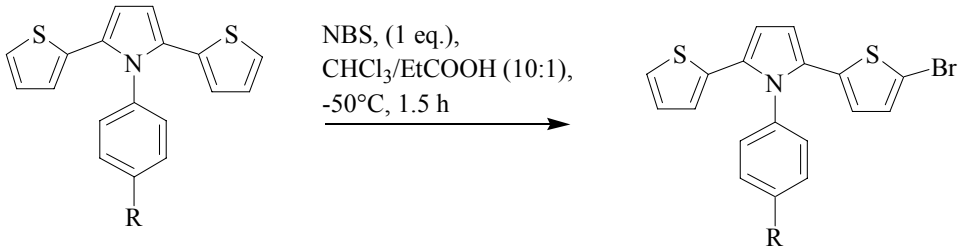

19, R= Me
18, R= F

30, R= Me, 60%
31, R= F, 68%

For the introduction of aldehyde group on thiophene ring of **29**, **30** and **31** monobrominated DTP moieties, bromine lithium exchange was carried out by using 1.1 eq. of *n*-BuLi at -40° C. Reaction progress was monitored by TLC. After 1.5 h when no more starting material was detected, DMF was introduced at -78° C and temperature was slowly raised to room temperature and allowed to react overnight. After aqueous treatment **32**, **33** and **34** were obtained in 43, 55 and 45 % yield respectively.

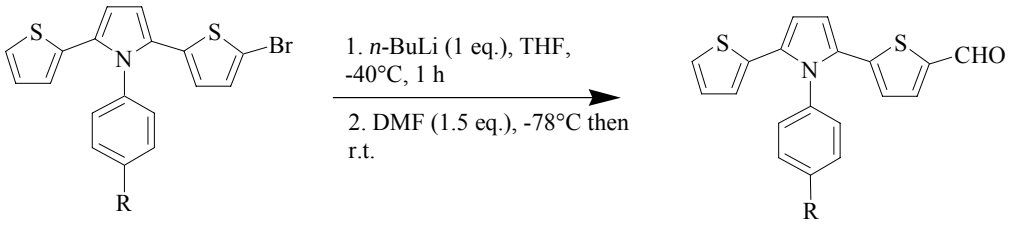

29, R= Hex
30, R= Me
31, R= F

32, R= Hex, 43%
33, R= Me, 55%
34, R= F, 45%

Finally, the Wadsworth–Emmons reaction between aldehydes **32- 34**, and phosphonate **16** in the presence of *t*-BuOK in THF at room temperature afforded the DTP_2-R series of ligands in acceptable yields (43-55 %). The general and rather easy work-up procedure gives an advantage to the Wadsworth–Emmons route for the synthesis of DTP_1-R and DTP_2-R series of ligands.

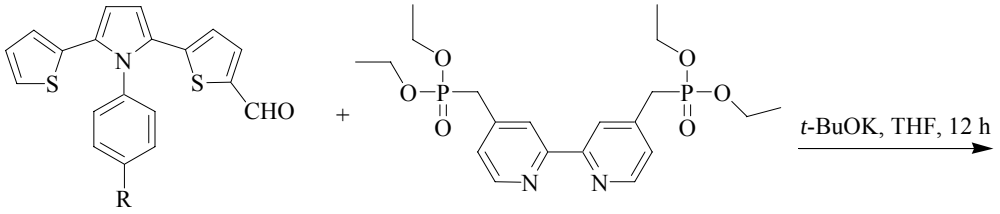

32, R= Hex
33, R= Me
34, R= F

16

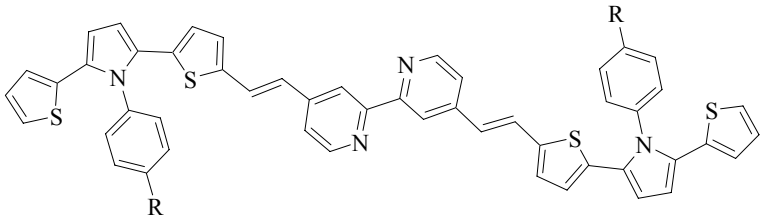

R = Hex = 40 %, **bpy(DTP$_2$-Hex)**
R = Me= 46 %, **bpy(DTP$_2$-Me)**
R = F = 73 %, **bpy(DTP$_2$-F)**

These resulting conjugated ligands are important in the sense that they can be aggregated in a polymeric unit simply by a (transition) metal ion resulting in coordination complexes that have potential to exhibit excellent absorption and emission properties due to intraligand charge transfer (ILCT) or metal-ligand charge transfer (MLCT) transition. Homoleptic and heteroleptic complexes can be prepared from these ligands. Optical properties of such ligands as well as metal complexes can be easily tuned through variation of substituents.

5.6. Properties of Ligands

For the purpose of comparison between ligands of **DTP$_1$-R** (DTP moiety attached to bipyridine via pyrrole) and **DTP$_2$-R** (DTP moiety attached to bipyridine via thiophene) series, spectroscopic, photophysical, electrochemical and computations were performed.

5.6.1. Absorption spectroscopy

As shown in Fig 5.4, all ligands of the **DTP$_1$-R** series exhibited absorption spectra of similar shape. No matter whether electron donating group (R = Hex, Me), electron withdrawing

(R = Br, F) or no substituent (R = H) is present. An intense band was observed in the range of 304-311 nm, followed by a less intense shoulder having the maximum in the 352-381 nm range. A significant red-shift (λ_{abs}=381 nm instead of 351-360 nm for the other ligands) was observed with **bpy(DTP$_1$-Hex)** that have an electron-donating hexyl group.

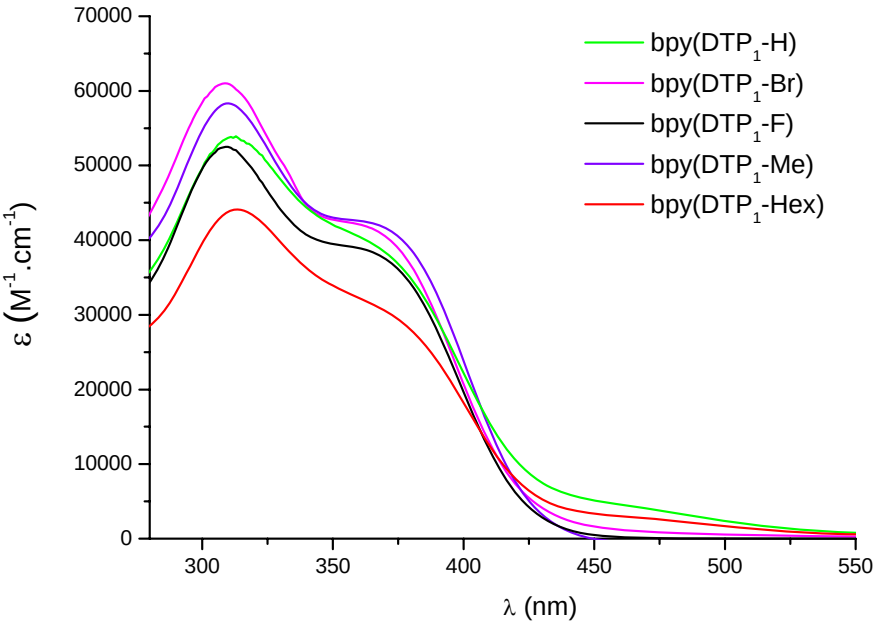

Figure 5.4: Absorption spectra of **bpy(DTP$_1$-R)** ligands in DMSO

Table 5.5: Absorption properties of bpy(DTP$_1$-R) Ligands

Ligand	**λabs-max (nm)[a]**	**ε 10^3 $M^{-1}cm^{-1}$**
bpy(DTP$_1$-H)	352 311	42.1 53.9
bpy(DTP$_1$-Br)	356 309	42.4 61.0
bpy(DTP$_1$-F)	360 310	39.0 52.5
bpy(DTP$_1$-Me)	360 310	42.6 58.3
bpy(DTP$_1$-Hex)	381 304	26.0 41.6

[a] Measured in DMSO at 25°C.

As it is clearly evident from table 5.5 the ε values were found to be dependent on the substitution, the best absorption was noticed for **bpy(DTP$_1$-Br)** and the least for **bpy(DTP$_1$-Hex)**. Surprisingly, **bpy(DTP$_1$-F)** (bearing the most electron-withdrawing fluorine group) and unsubstituted **bpy(DTP$_1$-H)** gave almost the same ε values.

In Comparison to **DTP$_1$-R**, absorption spectra of the **DTP$_2$-R** series (Fig 5.5) have shown two distinct changes.

(i) A strong red shift and broadening toward the visible domain was observed (λ_{max}= 432, 435 and 439 nm for **bpy(DTP$_2$-F), bpy(DTP$_2$-Me)** and **bpy(DTP$_2$-Hex)** respectively).

(ii) High intensity absorption in the range of 304-311 nm that was observed with **DTP$_1$-R** ligands was dramatically weakened in **DTP$_2$-R** series.

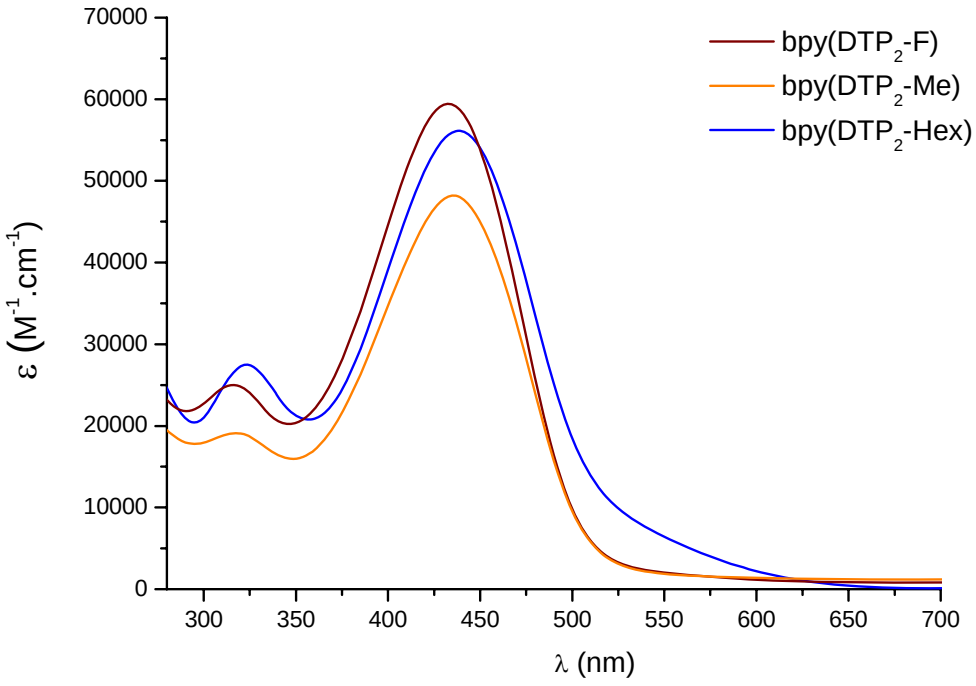

Figure 5.5: Absorption spectra of **bpy(DTP$_2$-R)** ligands in DMSO

Table 5.6: Absorption properties of bpy(DTP$_2$-R) Ligands

Ligand	λabs-max (nm)[a]	ε 10^3 $M^{-1}cm^{-1}$
bpy(DTP$_2$-F)	432 316	59.5 24.9
bpy(DTP$_2$-Me)	435 318	48.2 19.1
bp(DTP$_2$-Hex)	439 323	56.1 27.5

[a] Measured in DMSO at 25°C.

In this series, the nature of the substituent had a strong impact on the epsilon values (table 5.6), the fluorine substituted ligand **bpy(DTP$_2$-F)** led to the highest ε values (59500 $M^{-1}.cm^{-1}$) whereas 48200 and 56100 $M^{-1}.cm^{-1}$ were obtained for **bpy(DTP$_2$-Me)** and **bpy(DTP$_2$-Hex)** respectively. Such increase in ε value could be due to an increase in molecular dipole moment by the electron withdrawing fluorine group.

5.6.2. Electrochemical properties

The electrochemical properties of the ligands have been investigated by cyclic voltammetry, and the electrochemical data are summarized in Table 5.7.

As shown in Table, an irreversible oxidation of ligands occurred around 1V (vs. SCE) for the **DTP$_1$** series and at 0.8 V (vs. SCE) for the **DTP$_2$** series.

For the same concentration, **bpy(DTP$_1$-R)** series exhibited a current twice higher than the **bpy(DTP$_2$-R)** series. Therefore, this irreversible oxidation can be attributed to radical cation formation at the external thiophene. The comparison of potentials confirmed that the electronic interaction between the **DTP** group and the bipyridine via the styryl moiety is higher in the **bpy(DTP$_2$-R)** series as described above. In the negative potential part, the reduction mechanisms of the ligands are also irreversible. They correspond to the addition of an electron in the LUMO which is centered on the bipyridine group as shown in figure 5.14. In agreement with the electronic interaction, the LUMO potentials are 0.3V more negative in the **bpy(DTP$_1$-R)** series. Due to the pseudo-orthogonality of the dihedral angle between the phenyl ring and the pyrrole

group, the electron donating (Hex, Me) or withdrawing (F, Br) effects of the substituent on the phenyl are scarcely significant on the oxidation and reduction potential values. These small effects were also difficult to detect due to the irreversible nature of the electrochemical processes under investigation.

Table 5.7: Electrochemical properties of Ligands

Ligand	Epa (L^+/L) (V/SCE)[a]	Epc (L/L^-) (V/SCE)[b]
bpy(DTP_1-H)	1.02 (irrev.)	-1.90 (irrev.)
bpy(DTP_1-Br)	0.98 (irrev.)	-1.90 (irrev.)
bpy(DTP_1-F)	1.0 (irrev.)	-1.94 (irrev.)
bpy(DTP_1-Me)	0.97 (irrev.)	-1.92 (irrev.)
bpy(DTP_1-Hex)	0.96 (irrev.)	-1.92 (irrev.)
bpy(DTP_2-F)	0.84 (irrev)	-1.63 (irrev.)
bpy(DTP_2-Me)	0.80 (irrev)	-1.65 (irrev.)
bpy(DTP_2-Hex)	0.84 (irrev.)	-1.65 (irrev.)

[a,b]. First oxidation and reduction potentials respectively standardized with Fc^+/Fc as internal standard and converted into SCE scale by adding 0.47V ($E_{1/2}Fc^+/Fc$). Recorded in DMF using $Bu_4N^+PF_6^-$ as supporting electrolyte at 100mV/s.

5.6.3. Emission properties *(Coll. S. Caramori, C.A. Bignozzi, Ferrara, Italy)*

All the free ligands were found to be emitting in fluid solution of DMSO (Table 4.8), THF (Table 5.9) and DMF and (Table 5.10) in the nanosecond time scale.

λ_{em} for **bpy(DTP_1-R)** in DMSO were found in the 530-540 nm range while in agreement with absorption, whereas a notable red-shift was observed with **bpy(DTP_2-R)**. 580 nm λ_{em} was observed for **bpy(DTP_2-Hex)** (Table 5.8).

λ_{em} for **bpy(DTP_1-R)** in THF were blue shifted as compared to λ_{em} in DMSO *i.e* in the 497-501 nm range, whereas a notable red-shift of around 40 nm was observed with **bpy(DTP_2-R)** *i.e.* in the 538-541nm range (Table 5.9). But these values are clearly blue shifted again as compared to the λ_{em} maxima obtained in DMSO.

The emission kinetics were not trivial either, being biexponential for both the **bpy(DTP$_1$-R)** and **bpy(DTP$_2$-R)** series in DMF (Table 5.10 In the **bpy(DTP$_2$-R)** series the emission decays became mono-exponential in THF (Table 5.9) and were accompanied by a threefold increase in lifetime (from ca. 0.5 to 1.5 ns). In the case of the **bpy(DTP$_1$-R)** series, the bi-exponentiality of the decay was maintained also in THF, where two components weighing approximately 50 % with a respective lifetime of ca. 0.8 and 2 ns were observed. In such cases any attempt to fit the decay with a monoexponential function was, a failure, generating unacceptable $\chi^2 > 10$.

Table 5.8: Emission properties of the free ligands in DMSO

Ligand	**λem-max[a] (λexcit.) (nm)**
bpy(DTP$_1$-H)	542 (352) 542 (311)
bpy(DTP$_1$-Br)	531 (356)
bpy(DTP$_1$-F)	540 (310)
bpy(DTP$_1$-Me)	536 (375) 541 (309)
bpy(DTP$_1$-Hex)	540 (381) 540 (304)
bpy(DTP$_2$-F)	575 (432) 575 (316)
bpy(DTP$_2$-Me)	580 (435)
bp(DTP$_2$-Hex)	580 (438) 580 (322)

[a] Photomultiplier corrected emission maxima for the ligands in DMSO in the absence of O_2, A< 0.05.

Table 5.9: Emission properties of the free ligands in THF

Ligand	λem-max (nm)[a]	τ(ns)[b]
bpy(DTP$_1$-H)	501	1.25
bpy(DTP$_1$-Br)	497	1.64
bpy(DTP$_1$-F)	498	1.57
bpy(DTP$_1$-Hex)	498	1.68
bpy(DTP$_2$-F)	538	1.44
bpy(DTP$_2$-Me)	540	1.57
bpy(DTP$_2$-Hex)	541	1.57

[a] Emission maxima in THF . [b] In the case of biexponential decay (DTP$_1$ series) the average amplitude weighted lifetime was given.

Table 5.10: Emitting properties of the DTP$_2$ series in DMF

Ligand	λem-max (nm)[a]	(amplitude %) τ_1(ns) (amplitude %) τ_2(ns)	$\tau_{average}$(ns)[b]
DTP$_2$-F	570	(94.63) 0.32 (5.37) 2.213	0.420
DTP$_2$-Me	571	(91) 0.3704 (8.75) 2.07	0.519
DTP$_2$-Hex	571	(92.57) 0.39 (7.43) 2.08	0.517

[a] Emission maxima in DMF [b] The singlet excited state decay becomes biexponential in DMF. Here the average amplitude weighted lifetime is reported.

However, a change in the solvent did not cause a notable energy shift of the ground state absorption (Fig. 5.6), it resulted in an evident modification of the emission maxima, that underwent a 30-40 nm blue-shift passing from DMF to THF (Fig. 5.6 and 5.7), probably due to excited state destabilization in the less polar solvent, suggesting the presence of some degree of charge transfer/separation in the excited state.

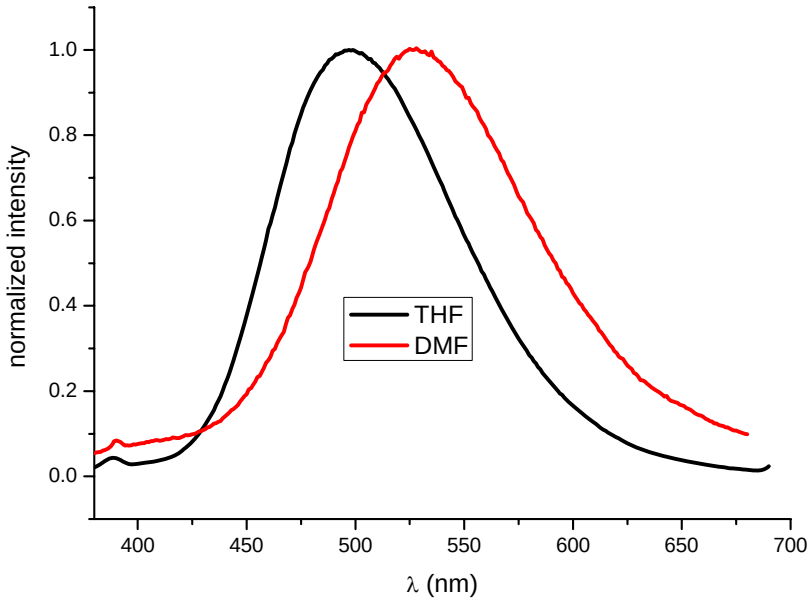

Figure 5.6: Typical bpy(DTP$_1$-R) ligand emission in DMF (red) and in THF (black). Above it is shown the **bpy(DTP$_1$- Br)**. A 30 nm red shift is generally observed.

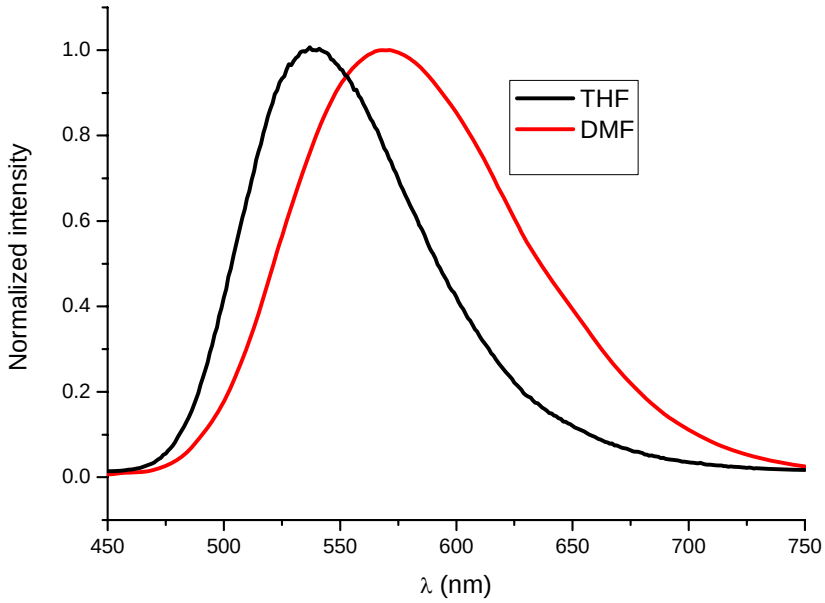

Figure 5.7: Typical bpy(DTP$_2$-R) ligand emission in DMF (red) and in THF (black). Above it is shown the **bpy(DTP$_2$-F)**.

The **bpy(DTP$_1$-R)** behavior was tentatively explained by the presence of two energetically close excited states, both contributing to the broad emission band. Indeed the excitation spectrum showed a dependence upon the observation wavelength, showing two reasonably well resolved bands (323 and 367 nm) (Fig. 5.8) whose relative intensity changed as a function of the observation wavelength. In particular it was observed that the excitation spectrum bear closer resemblance to the ground state absorption spectrum when the emission was observed at 430 nm (in the blue portion of the emission band), whereas the 367 nm band gradually gained intensity when the observation wavelength was moved to the red. The emission lifetime changed accordingly, undergoing, for example in the case of **bpy(DTP$_1$-F)**, a ≈ 20% shortening when measured at 430 nm (0.65 ns) with respect to the value obtained in the band maximum (500 nm, 0.84ns). On the other hand the excitation spectra of the **bpy(DTP$_2$-R)** family were generally in good agreement with the ground state absorption (Fig.5.9).

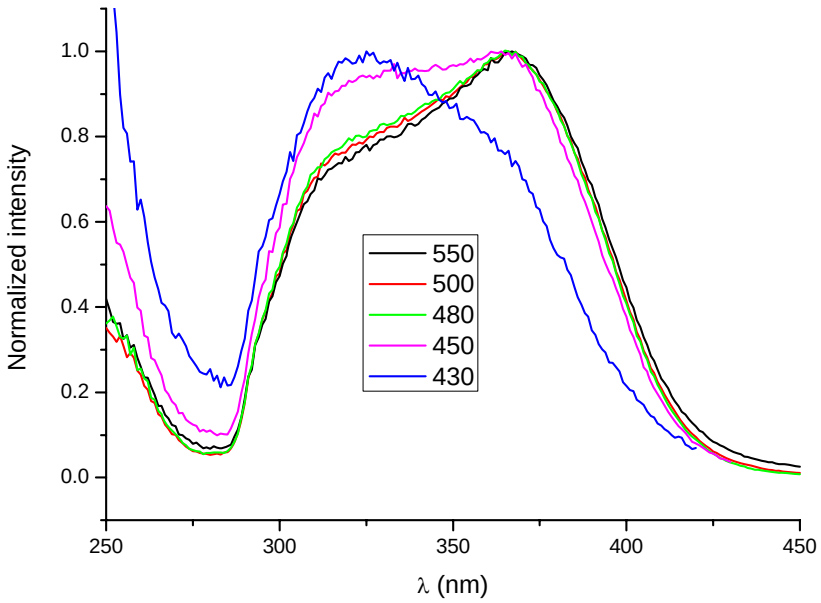

Figure 5.8: Typical excitation spectrum of **bpy(DTP$_1$-R)** series, bpy(DTP$_1$-F) is reported here as an example) in THF. The spectrum varies as a function of the observation wavelength. The 367 nm band gradually decreases in intensity with respect to the 323 nm as the the observation is moved from the red part of the emission band (550 nm) to the blue (430 nm).

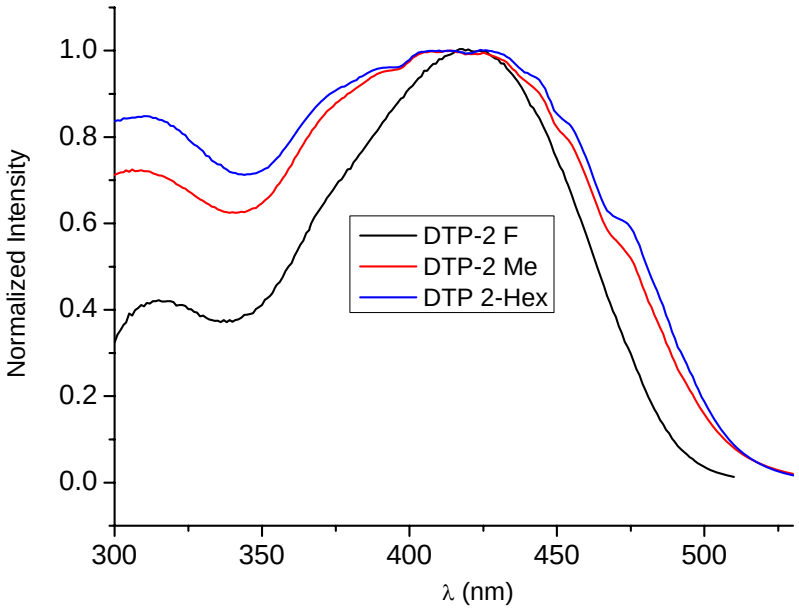

Figure 5.9: Typical excitation spectrum of the **bpy(DTP$_2$-R)** series in THF. A close agreement with the absorption spectrum can be noticed.

5.6.4. Laser Spectroscopy measurements *(Coll. S. Caramori, C.A. Bignozzi, Ferrara, Italy)*

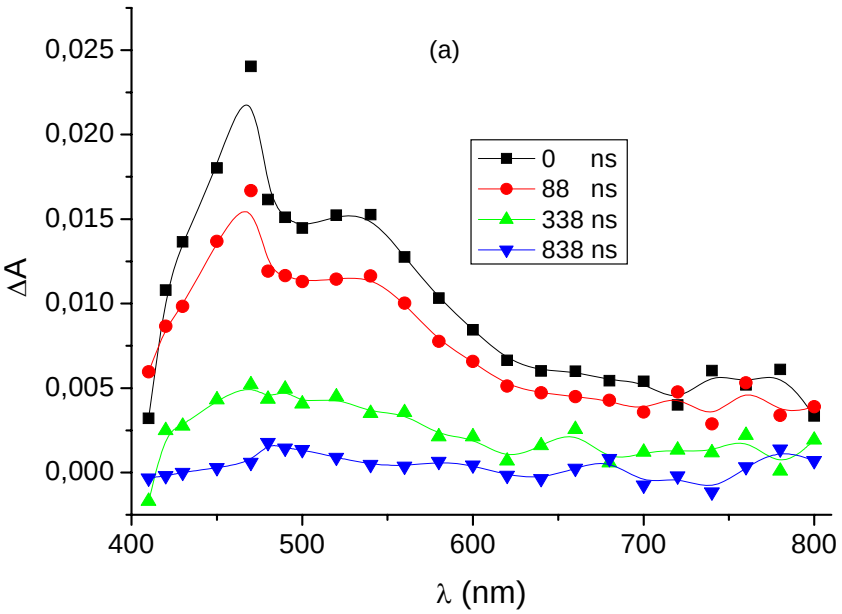

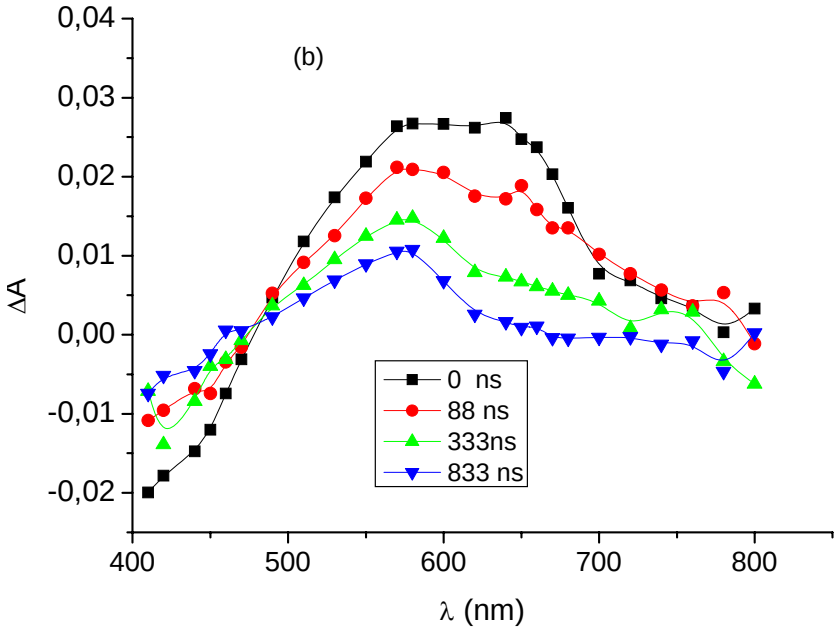

Figure 5.10: Transient triplet absorption of **bpy(DTP$_1$-F)** (a) and **bpy(DTP$_2$-F)** (b) in DMF ($\lambda_{exc.}$=355 nm, 0-838 ns interval). 0 delay corresponds to the initial absorption. The negative signal due to singlet bleaching and to laser induced emission is excluded here.

Upon 355 nm laser excitation the **bpy(DTP$_1$-R)** family originated a laser pulse-limited negative signal due to ground state bleaching and laser induced emission, followed by a relatively long lived triplet absorption (monoexponential, $\tau \approx 240$ ns) with a distinct 470 nm maximum, followed by a 540 nm shoulder (Fig.5.10(a)). The **bpy(DTP$_2$-R)** ligands were characterized by a relatively weak ground state bleaching in the 400-500 nm interval, followed by an intense and broad absorption (monoexponential $\tau \approx 300$ ns) with a plateau between 550 and 650 nm (Fig.5.10(b)).

5.6.5. Computational analysis *(Coll. A. Monari, X. Assfeld, CBT-SRSMC)*

From absorption studies it is evident that the way by which DTP moiety was attached to bipyridine dramatically affected the electronic properties of the corresponding ligand. This is probably due to the differences in the extent of π delocalization in the ligands In order to analyze the molecular structure and electron distribution into the ligands, *ab initio* calculations were performed. Geometries of all the ligands have thus been optimized at DFT level using B3LYP exchange correlation functional. A double zeta 6-31G basis was used throughout. In

order to assure a proper comparison all the possible systems obtained from **DTP_1** and **DTP_2** moieties were computed, making a total of **10** ligands. Optimized Geometries for **bpy(DTP_1-Hex)** and **bpy(DTP_2-Hex)** are given in Fig. 5.11.

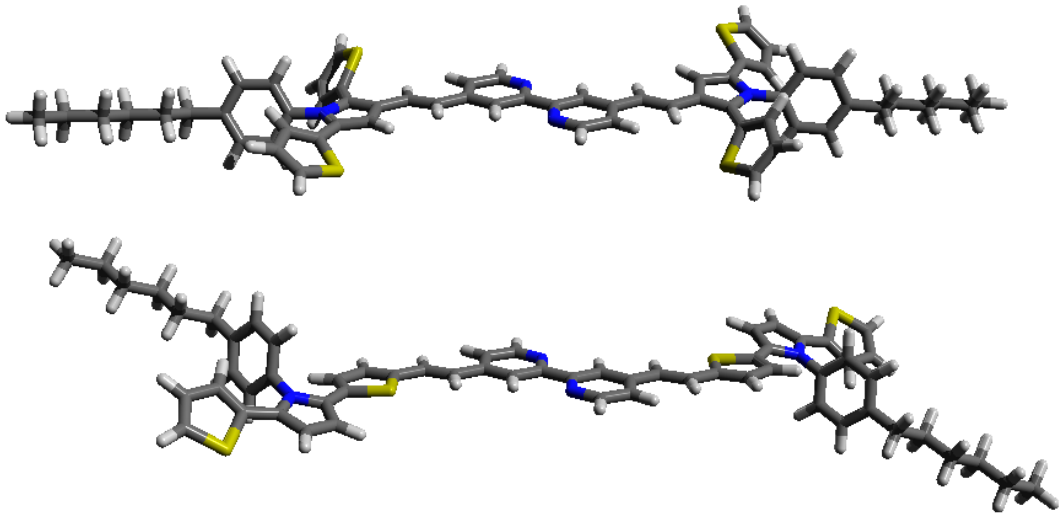

Figure 5.11: DFT optimized geometry of **bpy(DTP_1-Hex)** (top) and **bpy(DTP_2-Hex)** (bottom)

Dihedral angles between relevant pyrrole and thiophene rings were measured from the optimized structures (Fig. 5.12). In **bpy(DTP_1-Hex)**, the bipyridine-styryl-pyrrole sequence was found to be coplanar, while thiophene rings were distorted from the plane. The styryl moiety appeared to induce a beneficial effect on the dihedral angle with regard to planarity when thiophene was bound at the ortho position (147° *vs* 130° for the thiophene at the meta position). Thus, one thiophene could be expected to participate in the π-delocalization process. In **bpy(DTP_2-Hex)**, the loss of planarity was minimized when a thiophene was bound to both styryl and pyrrole (θ=157°). So, in case of **bpy(DTP_2-Hex)** where DTP was bound by the thiophene ring, a more extended delocalization was offered. Whereas, in **bpy(DTP_1-Hex)** the thiophene ring did not seem to participate to the delocalization.

This was in agreement that a more extended delocalized system favoured absorption at the longer wavelength (lower energy) domain.

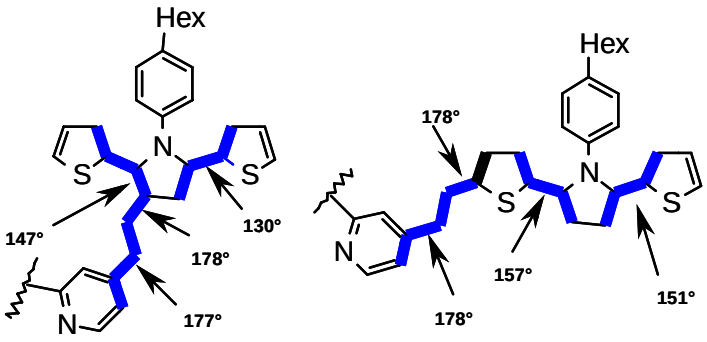

Figure 5.12: Calculated dihedral angles in **bpy(DTP$_1$-Hex)** (left) and **bpy(DTP$_2$-Hex)** (right) half of the molecule is depicted

The first 25 excited states have been computed by using TDDFT formalism for all the optimized ligands. CAM-B3LYP **[41]** functional has been used in order to better account for the long range corrections, a slightly larger augmented and polarized double zeta basis (6-31+g(d,p)) **[42]** has been used. The solvatochromic effect of the solvent has been taken into account by using the polarizable continuum model (PCM) model **[43]**. Note that the transoid structure presented in Fig. 5.11 appeared as the most stable ones in solution, anyway the computed spectra for cisoid structure showed slight deviation from the previous ones. Computed UV-Vis spectra for **bpy(DTP$_1$-Hex)** and **bpy(DTP$_1$-Hex)** is given in figure 5.13, and it matched well with the experimental one. Whereas computed wavelengths and oscillator strength are reported in Table 5.11. A fairly good agreement between experiment and theoretical values was observed

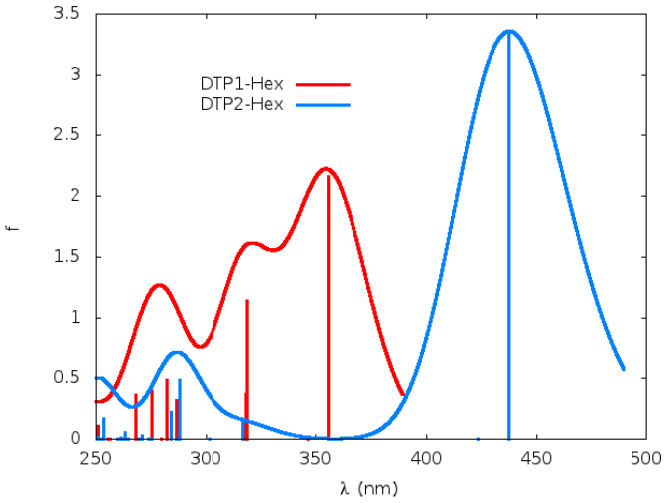

Figure 5.13: Computed spectra of **bpy(DTP$_1$-Hex)**and **bpy(DTP$_2$-Hex).**

Table 5.11: Ligands TDDFT computed principal excitation wavelengths and oscillator strength

X	**bpy(DTP$_1$-R)** λ(nm), (f) [a]	**bpy(DTP$_2$-R)** λ(nm), (f) [a]
H	355.51 (2.06) 318.48 (1.56)	433.66 (3.52) 318.44 (0.07) 286.07 (0.56)
Br	351.76 (2.20) 342.40 (0.01) 315.43 (1.02)	429.08 (3.51) 316.79 (0.06) 285.19 (0.55)
F	352.08 (2.11) 342.72 (0.01) 315.52 (0.93)	433.61 (3.52) 318.44 (0.07) 286.07 (0.56)
Me	355.77 (2.11) 346.33 (0.05) 318.56 (1.01)	433.61 (3.52) 318.44 (0.07) 286.07 (0.56)
Hex	355.79 (2.16) 346.34 (0.01) 318.60 (1.13)	437.65 (3.55) 316.73 (3.13) 287.91 (0.48)

[a] oscillator strength in parentheses

The **bpy(DTP$_2$-R)** structures confirmed the presence of a very important red-shift of about 80 nm as compared to **bpy(DTP$_1$-R)**. On the other hand, the different members of a same family gives quite reproducible spectra, confirming the small influence of the phenyl substituent as expected from its pseudo-orthogonality with regard to the pyrrole ring (Fig. 5.13). Interestingly enough the unsubstituted **bpy(DTP$_1$-R)** compounds do not show the small absorption at about 340 nm like the other members of that family, this is coherent with the less pronounced shoulder in the experimental spectrum evidenced in that region. A comparison of the computed spectra for the **bpy(DTP$_1$-Hex)** and the **bpy(DTP$_1$-Hex)** is shown in Fig 5.13, where the spectrum has been obtained enveloping each transition with a Gaussian function of fixed half length width of 0.06 eV. It is clearly evident that besides some difference in relative intensities the general structure of the spectrum is well reproduced in the longer wavelength region. All the computed transition for both class of compounds are of π–π* type as it is confirmed by an excited state analysis. The frontier Kohn-Sham orbitals are reported in Fig. 5.14 for **bpy(DTP$_1$-Hex)** and **bpy(DTP$_2$-Hex)**, although somehow difficult to glance from a simple (delocalized)

molecular orbital picture, but the more extended nature of the conjugated π system in case of **bpy(DTP$_2$-R)** appears to be confirmed.

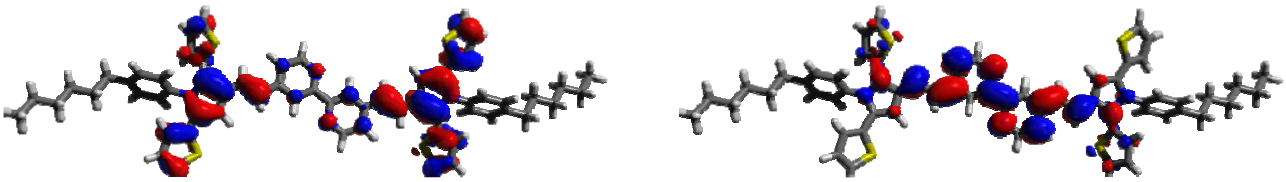

HOMO **LUMO**

Figure 5.14: (a) bpy(DTP$_1$-Hex) frontier orbitals isodensity contour

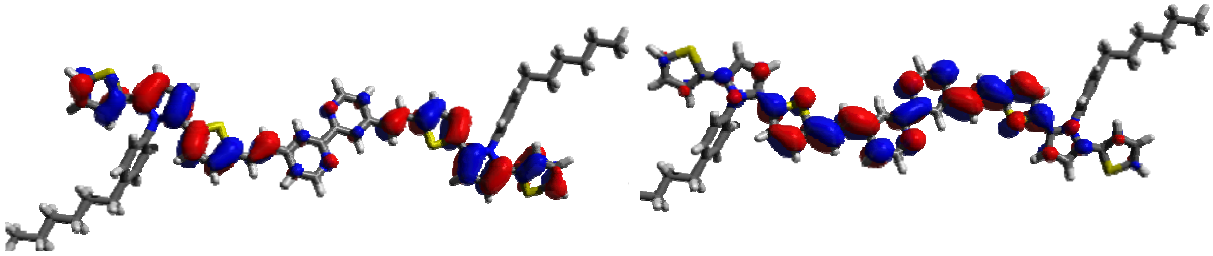

HOMO **LUMO**

Figure 5.14: (b) bpy(DTP$_2$-Hex) frontier orbitals isodensity contour

5.7. Conclusions

A new family of ligands has been obtained by binding bipyridine to dithienylpyrrole moieties (DTP). We have synthesized **bpy(DTP$_1$-R)** and **bpy(DTP$_2$-R)** series of ligands and carried out characterization by spectroscopic, photophysical, electrochemical and computational measurements.

The electronic properties are deeply modified with regard to the binding site of DTP. The absorption spectrum of **bpy(DTP$_2$-R)** ligand series is red shifted and broadened in comparison to that of **bpy(DTP$_1$-R)** series.

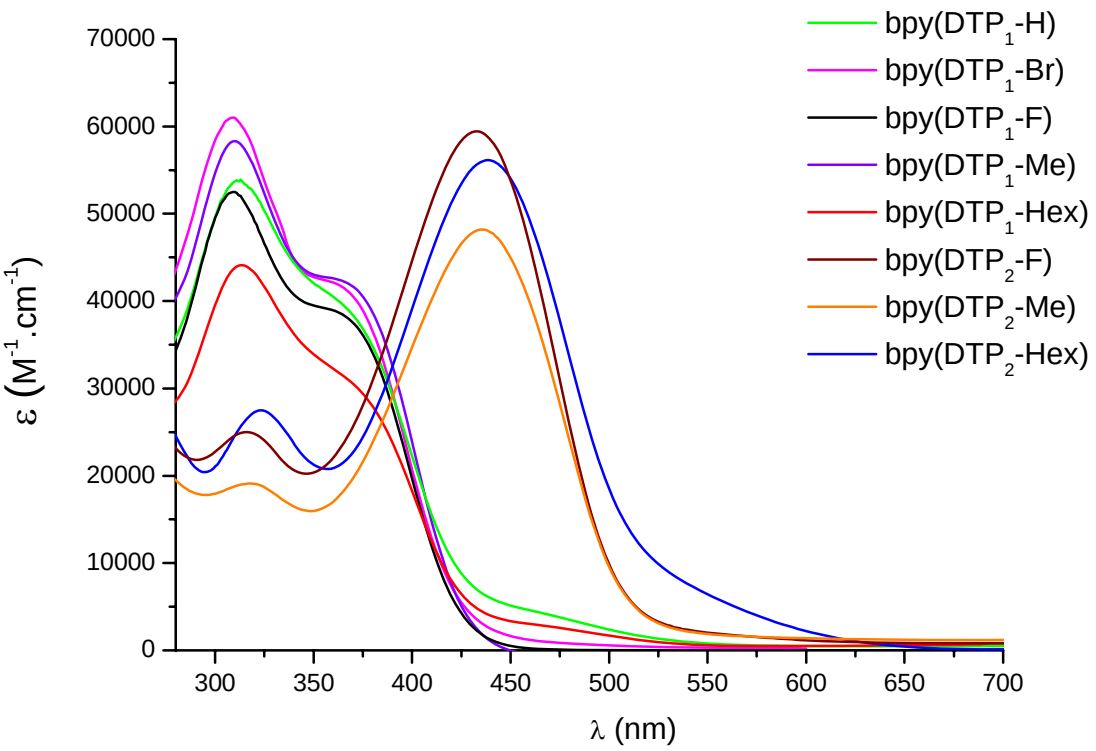

Figure 5.15: Absorption spectra of Ligands in DMSO

Computational calculations as well as transient spectroscopy were used to explain such differences by evidencing a larger π-delocalization extent in **bpy(DTP$_2$-R)** series. In summary DTP-containing ligands are promising candidates to carry out complexation with ruthenium metal in order to obtain homoleptic, bis-heteroleptic and tris-heteroleptic complex.

5.8. References

[1] Steel, P.J. *Coord. Chem. Rev.* 1990, **106**, 227.

[2] Balzani, V.; Juris, A.; Venturi, M.; Campagna, S.; Serroni, S. *Chem. Rev.* 1996, **96**, 759.

[3] Kaes, C.; Katz, A.; Hosseini, M.W. *Chem. Rev*. 2000, **100**, 3553.

[4] Smith, A.P.; Fraser, C.L. *Compr. Coord. Chem. II*, 2003, **1**, 1.

[5] Maury, O.; Guegan, J.-P.; Renouard, T.; Hilton, A.; Dupau, P.; Sandon, N.; Toupet, L.; Bozec, H.L. *New J. Chem.* 2001, **25**, 1553.

[6] Bouder, T.L.; Viau, L.; Guegan, J.-P.; Maury, O.; Bozec, H.L. *Eur. J. Org. Chem*. 2002, 3024.

[7] Maury, O.; Viau, L.; Senechal, K.; Corre, B.; Guegan, J.-P.; Renouard, T.; Ledoux, I.; Zyss, J.; Bozec, H.L. *Chem. Eur. J.* 2004, **10**, 4454.

[8] Maury, O.; Bozec, H.L. *Acc. Chem. Res.* 2005, **38**, 691.

[9] Coe, B.J.; Harris, J.A.; Brunschwig, B.S.; Asselberghs, I.; Clays, K.; Garin, J.; Orduna, J. *J. Am. Chem. Soc*. 2005, **127**, 13399. .

[10] Viau, L.; Maury, O.; Bozec, H.L. *Tetrahedron Lett*. 2004, **45**, 125.

[11] Lohio, O.; Viau, L.; Maury, O.; Bozec, H.L. *Tetrahedran Lett*. 2007, **48**, 1229.

[12] Berner, D.; Klein, C.; Nazeeruddin, M.K.; Angelis, F.D.; Castellani, M.; Bugnon, P.; Scopelliti, R.; Zuppiroli, L.; Gratzel, M. *J. Mater. Chem*. 2006, **16**, 4468.

[13] Juris, A.; Campagna, S.; Bidd, I.; Lehn, J.-M.; Ziesseli, R. *Inorg. Chem.* 1988, **7**, 4007.

[14] Aranyos, V.; Hjelm, J.; Hagfeldt, A.; Grennberg, H. *J. Chem. Soc., Dalton. Trans.* 2001, 1319.

[15] Karthikeyan, C.S.; Peter, K.; Wietasch, H.; Thelakkat, M.; *Solar Energy Mater.Solar Cells,* 2007, **91**, 432.

[16] Jiang, K.-J.; Xia, J.-B.; Masaki, N.; Noda, S.; Yanagida, S.; *Inorg. Chim. Acta*, 2008, **361**, 783.

[17] Fabregat-Santiago, F.; Bisquert, J.; Cevey, L.; Chen, P.; Wang, P.; Zakeeruddin, S.M.; Gratzel, M. *J. Am. Chem. Soc.* 2009, **131**, 558.

[18] Nakazaki, J.; Chung, I.; Matsushita, M.M.; Sugawara, T.; Watanabe, R.; Izuoka, A.; Kawada, Y. *J. Mater. Chem*, 2003, **13**, 1011.

[19] Smirnov, V.I.; Afanas'ev, A.V.; Belen'kii, L.I. *Chemistry of Heterocyclic Compounds,* 2011, **46 (10)**, 1199.

[20] Paal, C. *Ber. Dtsch. Chem. Ges.* 1885, **18**, 367.

[21] Knorr, L. *Ber. Dtsch. Chem. Ges.* 1884, **17**, 1635.

[22] Niziurski-Mann, R.E.; Cava, M.P.; *Adv. Mater.,* 1993, **5**, 547.

[23] Cava, M.P.; Parakka, J.P.; Lakshmikantham, M.V.; *Mater. Res. Soc. Symp. Soc*. 1994, **329**, 179.

[24] Ferraris, J.P.; Skiles, G.D. *Polymer*, 1987, **28**, 179.

[25] Merz, A.; Ellinger, F. *Synthesis*, 1991, **6**, 462.

[26] Mekhalif, Z.; Lazarescu, A.; Hevesi, L.; Pireaux, J.J.; Dehalle, J. *J. Mater. Chem*. 1998, **3**, 545.

[27] Ogura, K.; Zhao, R.; Yanai, H.; Maeda, K.; Tozawa, R.; Matsumoto, S.; Akazome, M. *Bull. Chem. Soc. Jpn*., 2002, **75**, 2359.

[28] Minetto, G.; Raveglia, L.F.; Sega, A.; Taddei, M. *Eur. J. Org. Chem.* 2005, 5277.

[29] Meeker, D.L.; Mudigonda, D.S.K.; Osbon, J.M.; Loveday, D.C.; Ferraris, J.P. *Macromolecules*, 1998, **31**, 2943.

[30] Rockel, B.; Huber, J.; Gleiter, R.; Schumann, W. *Adv. Mater*. 1994, **718**, 568.

[31] Ellinger, S.; Ziener, U.; Thewalt, U.; Landfester, K.; Moller, M. *Chem. Mater*., 2007, **19**, 1070.

[32] Oliva, M.M.; Pappenfus, T.M.; Melby, J.H.; Schwaderer, K.M.; Johnson, J.C.; McGee, K.A.; Filho, D.A.S.; Bredas, J.-L.; Casado, J.; Lopez Navarrete, J. T. *Chem. Eur. J.*, 2010, **16**, 6866.

[33] Vilsmeier, A.; Haack, A. *Ber. Dtsch. Chem. Ges.* 1927, **60**, 119.

[34] Marson, C.M. *Tetrahedron* ,1992, **48**, 3659.

[35] Majo, V.J.; Perumal, P.T. *J. Org. Chem.* 1998, **63**, 7136.

[36] Jones, G.; Stanforth, S.P. *Org. React.* 2000, **56**, 355.

[37] Fraser, C.L.; Anastasi N.R.; Lamba, J.J.S. *J. Org. Chem.*, 1997, **62**, 9314.

[38] Smith, A.P.; Lamba, J.J.S.; Fraser, C.L. *Org. Synth*. 2004, **10**, 107.

[39] Stetter, H. *Angew. Chem., Int. Ed. Engl.* 1976, **15**, 639.

[40] Stetter, H.; Kuhmann, H. *Chem. Ber.* 1976, **109**, 2890.

[41] Yanai, T.; Tew, D.; Handy, N. *Chem. Phys. Lett.*, 2004, **393**, 51.

[42] Krishnan, R.B.R.; Seeger, J.S.; Pople, R.; J. A. *J. Chem. Phys.*, 1980, **72**, 650.

[43] Miertus, S.; Scrocco, E.; Tomasi, J. *J. Chem. Phys.*, 1981, **55**, 117.

Chapitre No: 6

Synthèse et propriétés des Complexes Homolèptiques de Ruthenium

Résumé en français

Les complexes homoléptiques de type (**Ru[bpy(DTP-X)$_3$])$^{2+}$** ont été préparés par synthèse microonde (250W) entre $RuCl_2(DMSO)_4$ et 3 equiv. de ligand dans l'éthylène glycol. Les sont obtenus en 10 min avec de bons rendements (40-79 %).

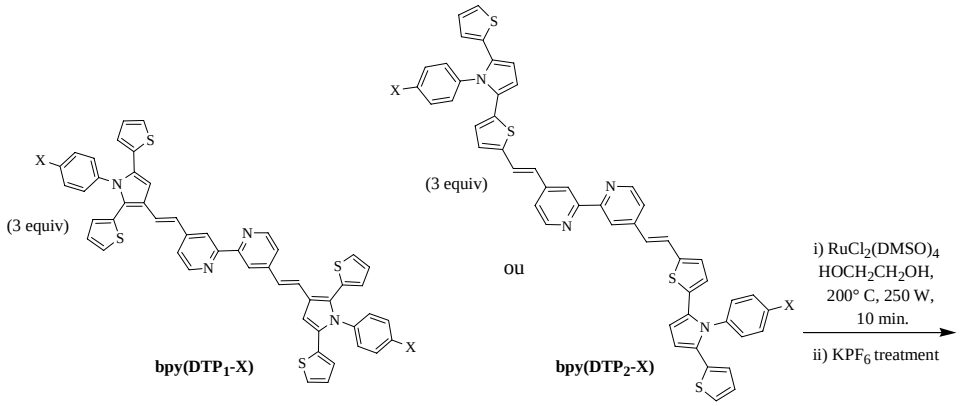

bpy(DTP$_1$-X) **bpy(DTP$_2$-X)**

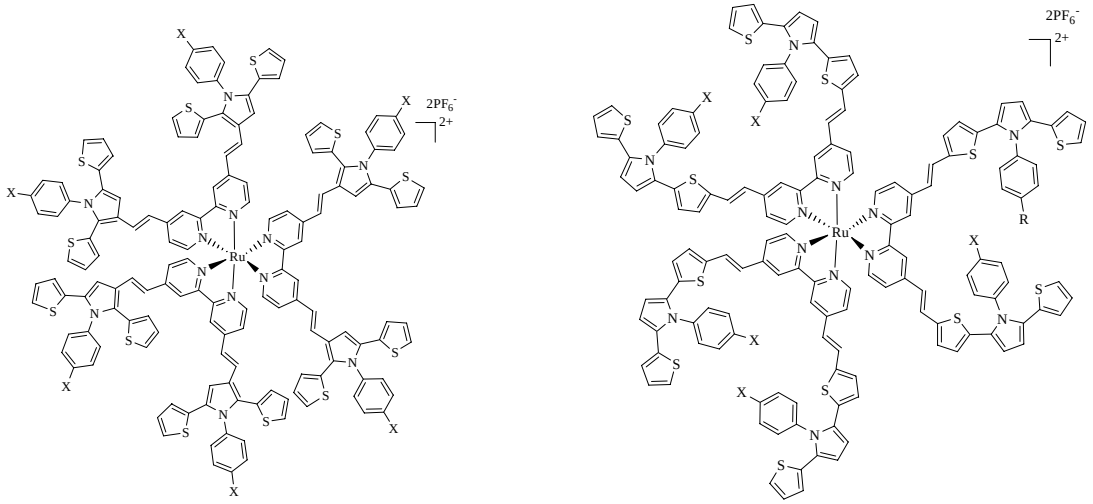

Ru[bpy(DTP$_1$-X)]$_3$(PF$_6$)$_2$ **Ru[bpy(DTP$_2$-X)]$_3$(PF$_6$)$_2$**

Les caractérisations réalisées au chapitre précédent pour les ligands ont été répétées ici. Les

complexes homoléptiques présentent des comportements similaires à ceux des ligands. Les spectres UV-Vis montrent que les complexes de la série **Ru[bpy(DTP$_2$-X)]$_3$(PF$_6$)$_2$** ont une fenêtre d'absorption très large dans domaine du visible avec un coefficient d'extinction molaire quasiment constant entre 400 et 600 nm ce qui est très prometteur pour la collecte de photons envisagée par la suite. Par contre la partie du spectre concernant les hautes énergies n'est pas absorbée. Les complexes de la série **Ru[bpy(DTP$_1$-X)]$_3$(PF$_6$)$_2$** présentent un spectre couvrant de façon efficace la zone 300-500 nm avec de bons coefficients d'extinction molaire ce qui est également très prometteur.

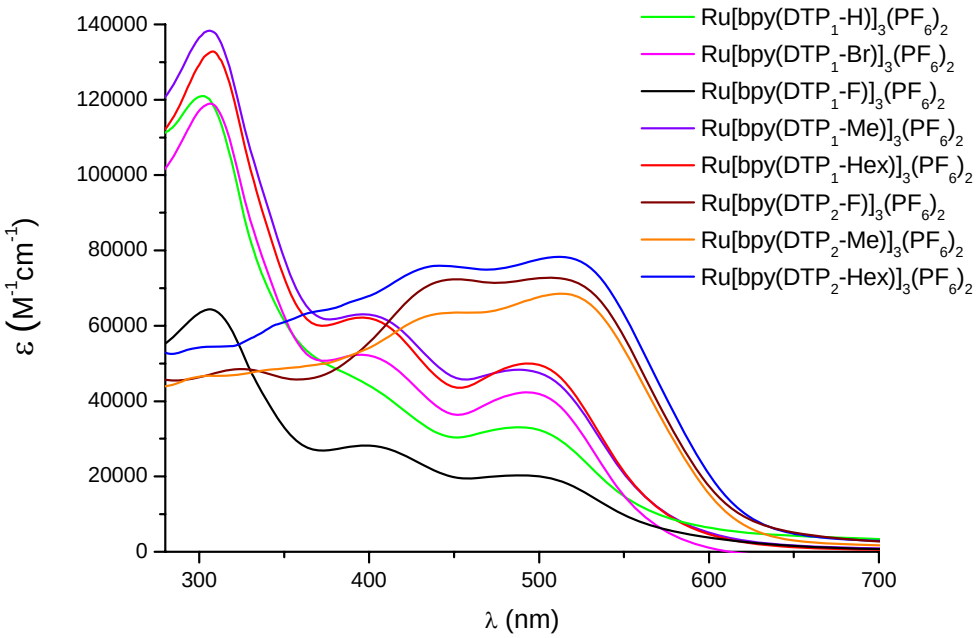

Les spectres d'émission et les mesures photophysiques (spectroscopie transitoire) montrent également des comportements très différents entre les deux type de complexes. Les spectres d'émission de la série **Ru[bpy(DTP$_2$-X)]$_3$(PF$_6$)$_2$** montrent clairement la présence d'une transition LC et d'une MLCT, il en va de même pour le spectre d'absorption transitoire. En revanche, aucune émission de type MLCT n'a été détectée mais seulement une émission de type LC pour la famille **Ru[bpy(DTP$_2$-X)]$_3$(PF$_6$)$_2$** pour laquelle a probablement un fort recouvrement entre les orbitales HOMO du métal et du ligand est suspecté. Cette caractéristique est également confirmée par le calcul DFT.

Chapter No: 6

Synthesis and Properties of Homoleptic Complexes

6.1. Homoleptic Complexes

6.1.1. Synthesis of Homoleptic Complexes

The symmetrically coordinated homoleptic complexes (**Ru[bpy(DTP-R)]$_3$)$^{2+}$** were prepared by reacting $RuCl_2(DMSO)_4$ with 3 equiv. of ligand in ethylene glycol under microwave irradiation (250 W). The complexes were obtained after 10 minutes of stirring in good yield (40-79 %). The resulting complexes were isolated by simple workup, i.e. precipitation with KPF_6 salt and washing with appropriate solvents which produced desired homoleptic complexes that were confirmed by ^1H NMR, and mass spectrometry.

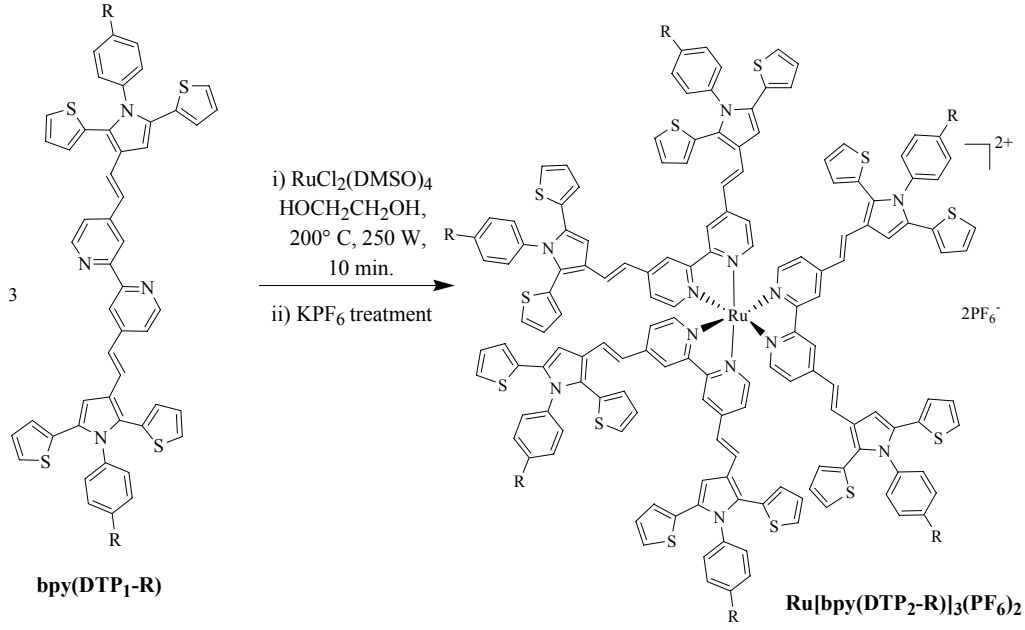

Scheme 6.1: Synthesis of Homoleptic complexes **Ru[bpy(DTP$_1$-R)]$_3$(PF$_6$)$_2$**

Starting ligands **bpy(DTP$_1$-R)**, their homoleptic complexes **Ru[bpy(DTP$_1$-R)]$_3$(PF$_6$)$_2$** and corresponding yields are reported in table 6.1.

Table 6.1: Homoleptic complexes [Ru[bpy(DTP$_1$-R)]$_3$(PF$_6$)$_2$ of DTP$_1$ ligand series

Ligand bpy(DTP$_1$-R)	Complex Ru[bpy(DTP$_1$-R)]$_3$ (PF$_6$)$_2$	Yield %
bpy(DTP$_1$-H)	**Ru[bpy(DTP$_1$-H)]$_3$ (PF$_6$)$_2$**	76
bpy(DTP$_1$-Br)	**Ru[bpy(DTP$_1$-Br)]$_3$ (PF$_6$)$_2$**	79
bpy(DTP$_1$-F)	**Ru[bpy(DTP$_1$-F)]$_3$ (PF$_6$)$_2$**	75
bpy(DTP$_1$-Me)	**Ru[bpy(DTP$_1$-Me)]$_3$ (PF$_6$)$_2$**	67
bpy(DTP$_1$-Hex)	**Ru[bpy(DTP$_1$-Hex)]$_3$ (PF$_6$)$_2$**	63

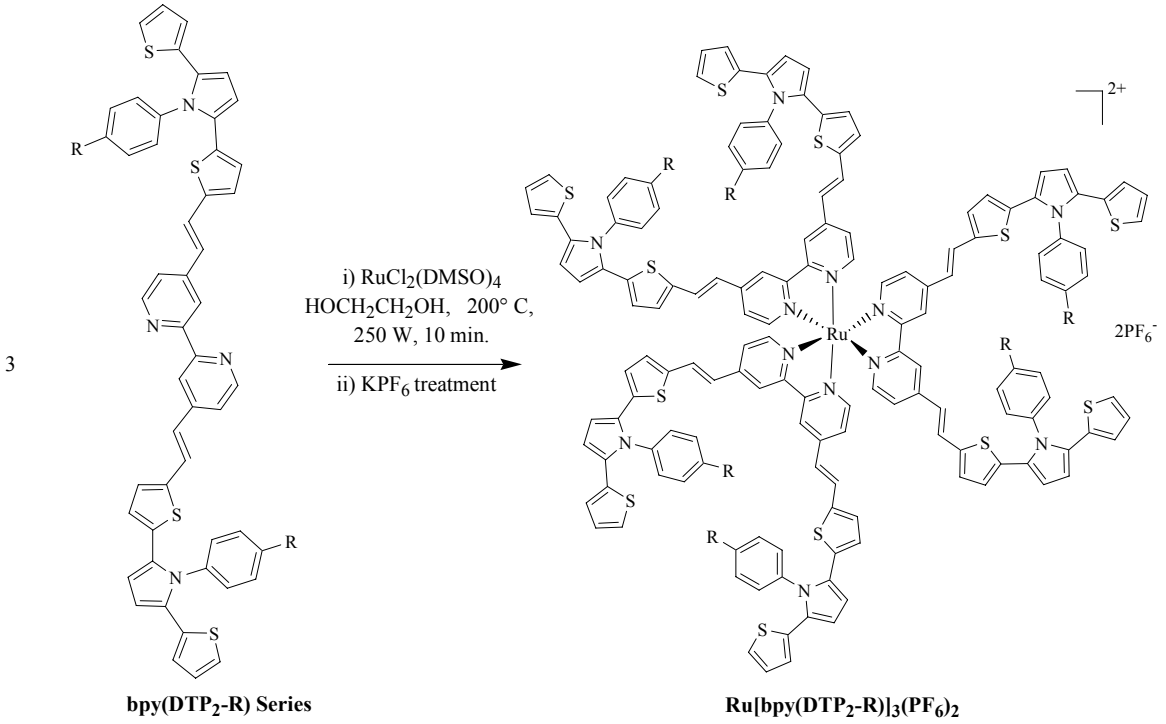

Scheme 6.2: Synthesis of Homoleptic complexes **Ru[bpy(DTP$_2$-R)]$_3$ (PF$_6$)$_2$**

Starting ligands **bpy(DTP$_2$-R)**, their homoleptic complexes **Ru[bpy(DTP$_2$-R)]$_3$ (PF$_6$)$_2$** and their corresponding yields are reported in table 6.2.

Table 6.2: Homoleptic complexes $[Ru(DTP_2\text{-}R)_3](PF_6)_2$ of DTP_2 ligand series

Ligand $bpy(DTP_2\text{-}R)$	Complex $Ru[bpy(DTP_2\text{-}R)]_3\ (PF_6)_2$	Yield %
$bpy(DTP_2\text{-}F)$	$Ru[bpy(DTP_2\text{-}F)]_3\ (PF_6)_2$	65
$bpy(DTP_2\text{-}Me)$	$Ru[bpy(DTP_2\text{-}Me)]_3\ (PF_6)_2$	40
$bpy(DTP_2\text{-}Hex)$	$Ru[bpy(DTP_2\text{-}Hex)]_3\ (PF_6)_2$	66

6.1.2. Properties of Homoleptic Complexes

6.1.2.1. Absorption properties

The absorption spectra of ruthenium homoleptic complexes **$Ru[bpy(DTP_1\text{-}R)]_3(PF_6)_2$** are reported in Fig. 6.1. Spectra featured three absorption bands, an intense absorption band in the UV region (302-308 nm) and two other moderately intense bands in the visible region near 395-398 nm and 488-494 nm. Bands in visible region that is in between 395-398 and 488-494 nm are due to metal-to-ligand charge transfer (MLCT) transitions. Whereas, the absorption bands at about 302-308 nm are assigned to the intra ligand ($\pi - \pi*$) transitions of bipyridine ligands.

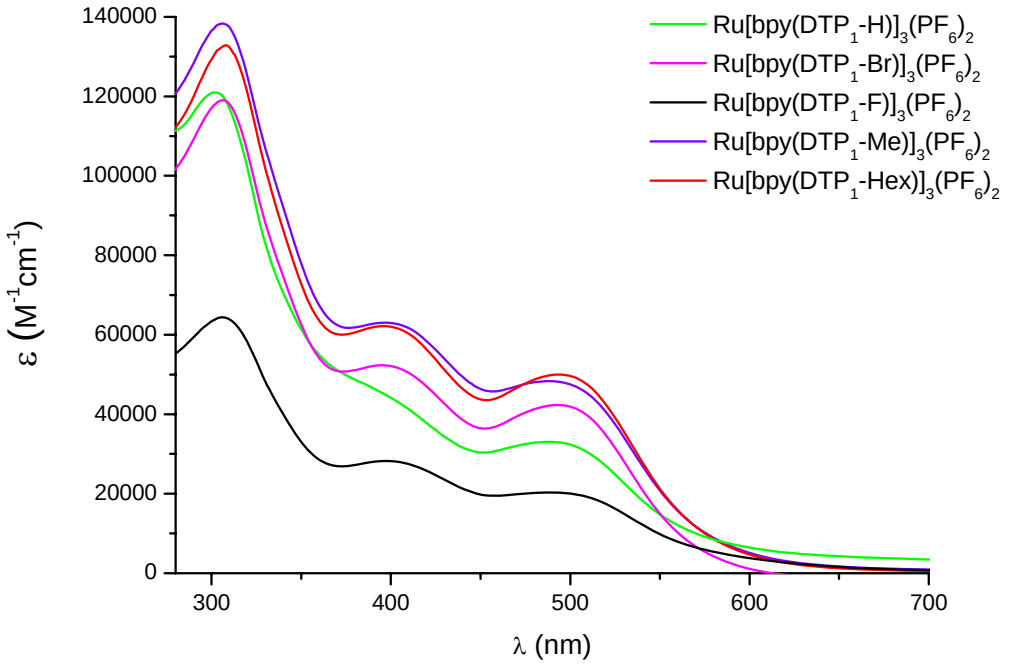

Figure 6.1: Absorption spectra of Homoleptic complexes $Ru[bpy(DTP_1\text{-}R)]_3(PF_6)_2$ in acetonitrile

Table 6.3. Absorption properties of bpy(DTP1$_1$-R) homoleptic complexes

Complex	λabs-max (nm)[a]	ε 10^3 $M^{-1}cm^{-1}$
Ru[bpy(DTP$_1$-H)]$_3$ (PF_6)$_2$	488 396 302	33.0 45.1 120.9
Ru[bpy(DTP$_1$-Br)]$_3$(PF_6)$_2$	494 395 307	42.3 52.3 118.9
Ru[bpy(DTP$_1$-F)]$_3$ (PF_6)$_2$	490 398 306	20.2 28.2 64.4
Ru[bpy(DTP$_1$-Me)]$_3$ (PF_6)$_2$	489 398 306	48.3 63.0 138.3
Ru[bpy(DTP$_1$-Hex)]$_3$ (PF_6)$_2$	493 396 308	49.9 62.1 132.8

[a] Measured in CH_3CN at 25°C

By examining spectra (Fig: 6.1) and table 6.3 it is clearly indicated that **Ru[bpy(DTP$_1$-Br)]$_3$(PF_6)$_2$**, **Ru[bpy(DTP$_1$-H)]$_3$(PF_6)$_2$**, **Ru[bpy(DTP$_1$-Me)]$_3$(PF_6)$_2$** and **Ru[bpy(DTP$_1$-Hex)]$_3$(PF_6)$_2$** bearing bromine, hydrogen, methyl and hexyl group respectively on the phenyl ring gave similar spectra with comparable ε values. Whereas in **Ru[bpy(DTP$_1$-F)]$_3$(PF_6)$_2$** bearing fluorine group the absorbance was decreased to almost half, the ε value was obtained (20200 $M^{-1}.cm^{-1}$(490 nm)) instead of 42300 $M^{-1}.cm^{-1}$ (493 nm) for **Ru[bpy(DTP$_1$-Br)]$_3$ (PF_6)$_2$.**

Optimized Geometries of all the ligands at DFT level have already confirmed that more extended system of delocalization is present in ligands of **bpy(DTP$_2$-R)** series. Complexes also follow the same trend. In Comparison to homoleptic complexes of **bpy(DTP$_1$-R)** series (Fig: 6.2), absorption spectra of the complexes of **bpy(DTP$_2$-R)** series have shown two distinct changes.

(i) A strong red shift and broadening toward the visible region was observed (λ_{max}= 490, 489 and 493 nm for the homoleptic complexes of **bpy(DTP$_2$-F), bpy(DTP$_2$-Me)** and **bpy(DTP$_2$-Hex)** ligands respectively). So, the absorption spectrum is dominated by MLCT transition in the visible region.

(ii) High intensity absorption in the range of 302-308 nm that was observed with **bpy(DTP$_1$-R)** complexes was extremely weakened in **bpy(DTP$_2$-R)** series complexes.

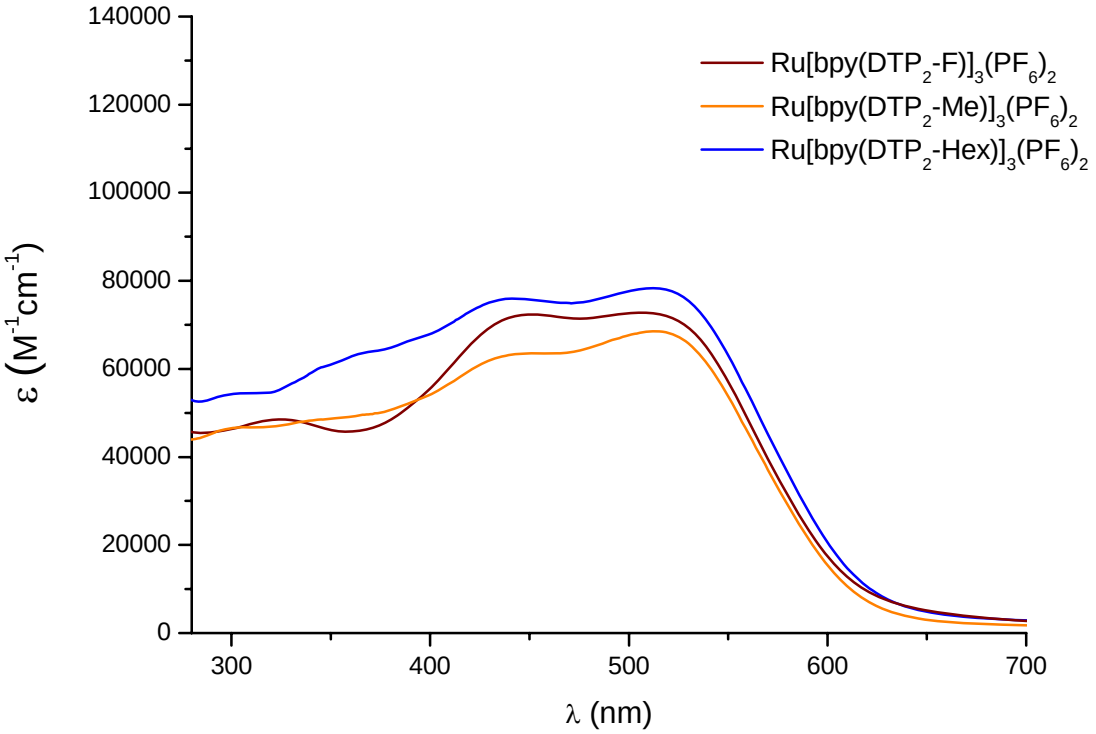

Figure 6.2: Absorption spectra of Homoleptic complexes Ru[bpy(DTP$_2$-R)]$_3$(PF$_6$)$_2$ in acetonitrile

The high molar extinction coefficients were almost constant along the visible domain (table: 6.4). In agreement with the ligands, switching from the methyl group Ru[bpy(DTP$_2$-Me)]$_3$(PF$_6$)$_2$ [48300 $M^{-1}.cm^{-1}$(489 nm)] to the hexyl group Ru[bpy(DTP$_2$-Hex)]$_3$(PF$_6$)$_2$ [49900 $M^{-1}.cm^{-1}$ (493 nm)] promoted a notable impact on the absorbance. The introduction of fluorine Ru[bpy(DTP$_2$-F)]$_3$(PF$_6$)$_2$ also notably increased the ε values up to 72700 $M^{-1}.cm^{-1}$ (508 nm).

Table 6.4. Absorption properties of bpy(DTP$_2$-R) homoleptic complexes

Complex	λabs-max (nm)[a]	ε 10^3 $M^{-1}cm^{-1}$
Ru[bpy(DTP$_2$-F)]$_3$ (PF$_6$)$_2$	508 453 326	72.7 72.3 48.4
Ru[bpy(DTP$_2$-Me)]$_3$ (PF$_6$)$_2$	512 451	68.5 63.5
Ru[bpy(DTP$_2$-Hex)]$_3$ (PF$_6$)$_2$	512 443 360	78.3 75.9 62.7

[a] Measured in CH_3CN at 25°C

It is a fact that most of ruthenium polypyridine complexes display relatively low molar absorptivity and particularly weak absorbance in the red part of the solar spectrum **[1]** but the extended π delocalization in **bpy(DTP$_2$-R)** series ligands created an increase in the molar extinction coefficient for these complexes. Therefore, very high molar extinction coefficients 68500-78300 $M^{-1}cm^{-1}$ (508-512 nm) of MLCT bands in the visible region were obtained for the homoleptic complexes of **bpy(DTP$_2$-R)** series.

6.1.2.2. Electrochemical properties

The electrochemical behavior of the homoleptic complexes was studied by cyclic voltammetry and reported in table 6.5. They show two oxidation waves, the first one is semi-reversible and corresponds to the Ru^{II}/Ru^{III} couple, the second one is irreversible and is attributed to the formation of radical cation on the thiophene as described for the ligands. The first reduction wave corresponds to the transfer of an electron in the bipyridine which is obviously easier in the complexes than in the ligands. The comparison of these potentials confirmed the electronic behaviour previously described for the ligands, i.e. a higher degree of conjugation in the **bpy(DTP$_2$)** compared to the **bpy(DTP$_1$)** series.

Table 6.5. Electrochemical properties of homoleptic complexes

Complex	$E_{1/2}$ Ru^{III}/Ru^{II} (V/SCE)[a]	Epa (L^+/L) (V/SCE) [a]	$E_{1/2}$ (L/L^-) (V/SCE)[b]
Ru[bpy(DTP$_1$-H)]$_3$(PF$_6$)$_2$	1.05 (ΔEp=0.18)	1.17 (irrev.)	-1.16 (ΔEp=0.08)
Ru[bpy(DTP$_1$-Br)]$_3$(PF$_6$)$_2$	0.98 (ΔEp=0.20)	0.95 (irrev.)	-1.17 (ΔEp=0.08)
Ru[bpy(DTP$_1$-F)]$_3$(PF$_6$)$_2$	0.98 (ΔEp=0.24)	1.07 (irrev.)	-1.17 (ΔEp=0.08)
Ru[bpy(DTP$_1$-Me)]$_3$(PF$_6$)$_2$	0.96 (ΔEp=0.20)	1.05 (irrev.)	-1.18 (ΔEp=0.08)
Ru[bpy(DTP$_1$-Hex)]$_3$(PF$_6$)$_2$	0.96 (ΔEp=0.20)	1.00 (irrev.)	n.d [c]
Ru[bpy(DTP$_2$-F)]$_3$(PF$_6$)$_2$	0.80 (ΔEp=0.120)	0.86 (irrev.)	-1.07 (ΔEp=0.08)
Ru[bpy(DTP$_2$-Me)]$_3$(PF$_6$)$_2$	0.77 (ΔEp=0.120)	0.82 (irrev.)	-1.10 (ΔEp=0.08)
Ru[bpy(DTP$_2$-Hex)]$_3$(PF$_6$)$_2$	0.76 (ΔEp=0.120)	0.82 (irrev.)	-1.11 (ΔEp=0.08)

[a] Oxidation potentials standardized with Fc^+/Fc as internal standard and converted into SCE scale by adding 0.47V ($E_{1/2}Fc^+/Fc$). Recorded in DMF using $Bu_4N^+PF_6^-$ as supporting electrolyte at 100mV/s. [b] First reduction potential. [c] n.d. = not detected.

6.1.2.3. Emission properties *(Coll. S. Caramori, C.A. Bignozzi, Ferrara, Italy)*

All homoleptic complexes of **bpy(DTP$_1$-R)** and **bpy(DTP$_2$-R)** series were emitting in fluid solution of DMF (Table 6.6 and 6.7).

Table 6.6. Emission properties of bpy(DTP$_1$-R) homoleptic complexes

Complex	λem-max[a] Ligand/ MLCT based	λ_{excit} (nm)	$\tau_{singlet}$ (ns)[b] $\tau_{triplet}$ (ns)
Ru[bpy(DTP$_1$-H)]$_3$(PF$_6$)$_2$	550 (Ligand) 687 (MLCT)	307 493	1.23 215
Ru[bpy(DTP$_1$-Br)]$_3$(PF$_6$)$_2$	541 (Ligand) 691 (MLCT)	400 500	1.64 217
Ru[bpy(DTP$_1$-F)]$_3$(PF$_6$)$_2$	476 (Ligand) 698 (MLCT)	300 500	1.57 212
Ru[bpy(DTP$_1$-Me)]$_3$(PF$_6$)$_2$	445 (Ligand) 671 (MLCT)	306 493	- -
Ru[bpy(DTP$_1$-Hex)]$_3$(PF$_6$)$_2$	541 (Ligand) 692 (MLCT)	410 510	1.68 220

[a] Photomultiplier corrected emission maxima for the complexes in DMF A< 0.05. [b] Ligand based singlet emission lifetime measured by TCSPC and triplet absorption lifetime upon 532 nm nanosecond (FWHM 7 ns) laser excitation. All measurements performed in deareated DMF.

Table 6.7. Emission properties of bpy(DTP$_2$-R) homoleptic complexes

Complex	λem-max[a] Ligand/ MLCT based	λ_{excit} (nm)	$\tau_{singlet}$ (ns)[b] $\tau_{triplet}$ (ns)
Ru[bpy(DTP$_2$-F)]$_3$(PF$_6$)$_2$	512 (Ligand) No MLCT emission	325 507	2.01 200
Ru[bpy(DTP$_2$-Me)]$_3$(PF$_6$)$_2$	554 (Ligand) No MLCT emission	435 512	0.58 200
Ru[bpy(DTP$_2$-Hex)]$_3$(PF$_6$)$_2$	577(Ligand) No MLCT emission	440 512	0.56 155

[a] Photomultiplier corrected emission maxima for the complexes in DMF A< 0.05. [b] Ligand based singlet emission lifetime measured by TCSPC and triplet absorption lifetime upon 532 nm nanosecond (FWHM 7 ns) laser excitation. All measurements performed in deareated DMF.

In DTP$_1$ series, when the ligand manifold was excited, two distinct emission bands were observed, one centered in the 480-550 nm region, depending on the ligand, bearing a close similarity in both energy and lifetime with the free ligand fluorescence, and one in the red part of the spectrum (centered around 690 nm) originated by the typical ^{3}MLCT radiative deactivation. Excitation of the lowest energy absorption band (490-505 nm in DMF) resulted only in the low energy emission (Fig. 6.3), whose maximum varied very little within the DTP$_1$ series. The excitation spectrum observed in correspondence of the low energy emission (687-692 nm) was in excellent agreement with the absorption spectrum of the complex, showing three distinct well resolved bands (Fig. 6.4)

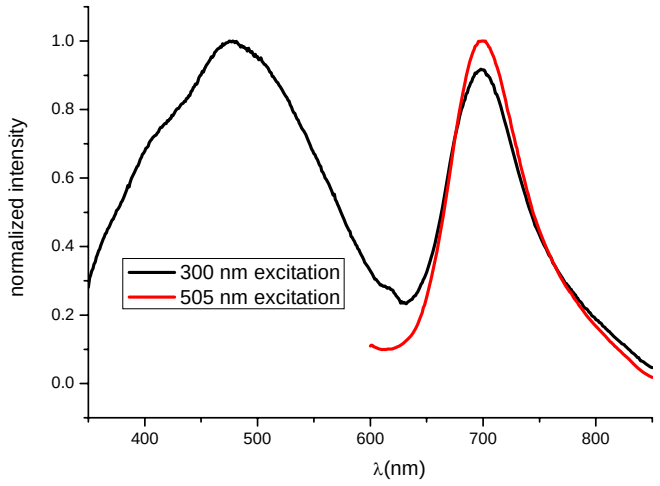

Figure 6.3: Typical emission spectrum of the Ru[bpy(DTP$_1$-R)]$_3$(PF$_6$)$_2$series: Ru[bpy(DTP$_1$-F)]$_3$(PF$_6$)$_2$ in DMF upon 300 nm and 505 nm excitation

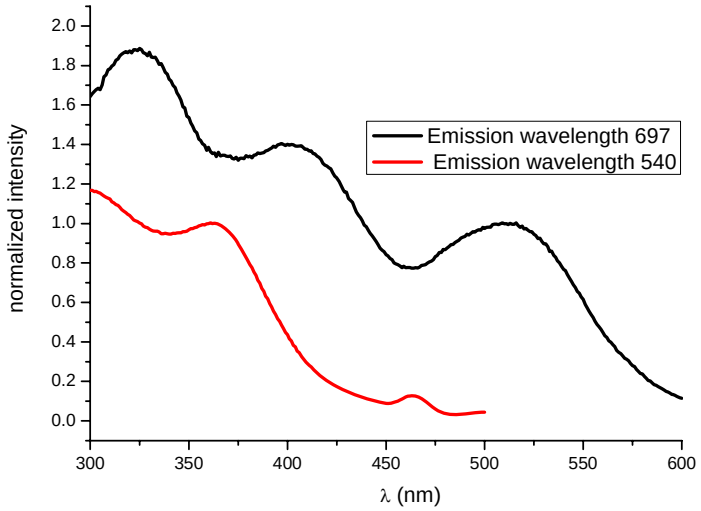

Figure 6.4: Excitation spectrum of Ru[bpy(DTP_1-F)]$_3$(PF_6)$_2$ in DMF recorded by observing at 540 nm (red) and at the 697 nm black.

In DTP_2 series, when the ligand manifold was excited, only one emission band was observed, centered in the 512-577 nm region, being that of the LC type. No MLCT emission was observed (Fig. 6.5 and Table. 6.7). Interestingly, compared to the parent free ligand, the Ru[bpy(DTP_2-F)]$_3$(PF_6)$_2$ emission was substantially blue shifted (512 vs 570 nm) and its lifetime increased (from 0.4 to 2 ns), probably due to destabilization caused by strong interaction with the dπ orbital of the metal.

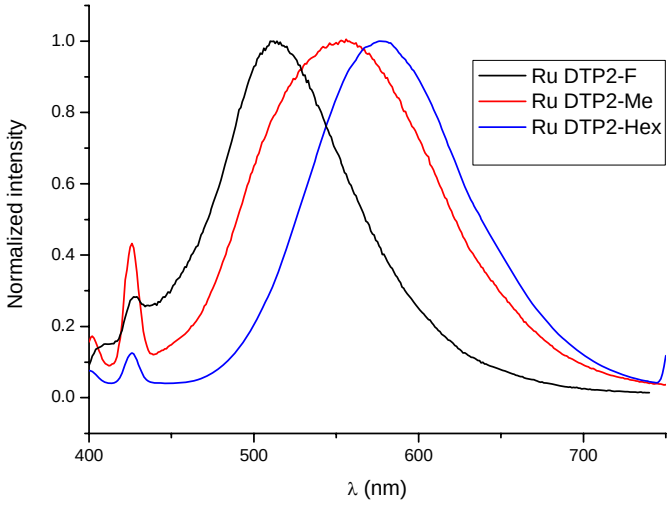

Figure 6.5: Emission spectra of the Ru-DTP_2 series upon 380 nm excitation. No emission was observed by direct excitation of the low energy band λ > 480 nm)

6.1.2.4. Laser Spectroscopy *(Coll. S. Caramori, C.A. Bignozzi, Ferrara, Italy)*

Transient absorption (TA) spectra of the **Ru[bpy(DTP$_1$-R)]$_3$(PF$_6$)$_2$** complexes in DMF by using a laser excitation at 532 nm (≈10 mJ /pulse) (Fig. 6.6) exhibited similar characteristics consistent with a long lived triplet MLCT excited state.

An intense absorption was observed in the blue region at 480 nm followed by an equally intense bleaching of the MLCT band with a minimum centered at 510 nm, followed by a strong featureless triplet absorption in the red part of the visible domain. The excited state lifetime was in the 200-220 ns range for all complexes and the decay was monoexponential. The excited/ground state isosbestic point was found at about 490 nm.

(a)

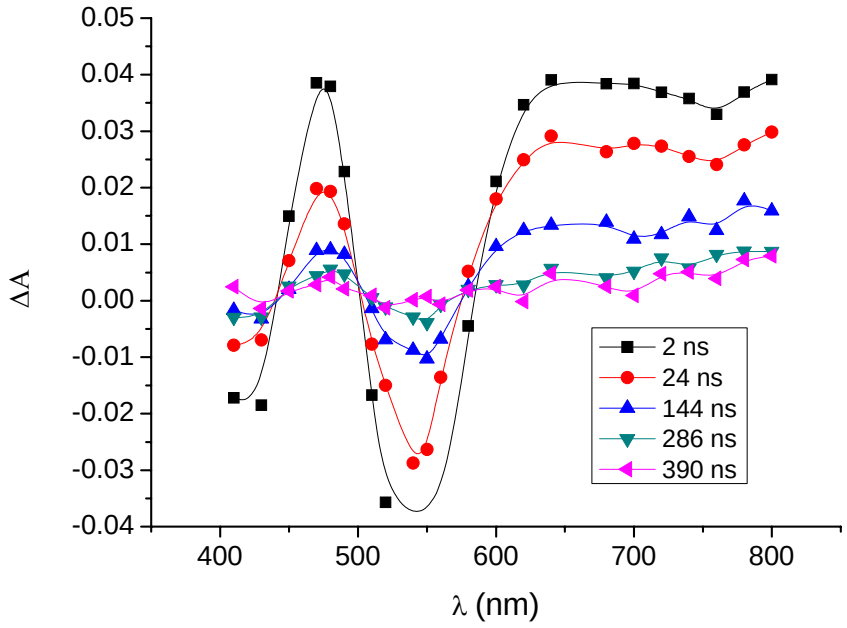

(b)

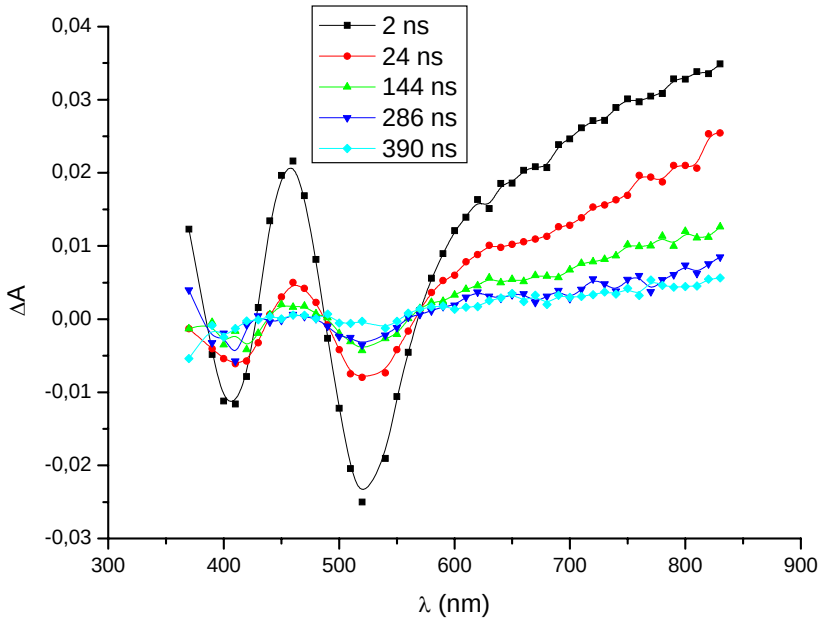
2 ns
24 ns
144 ns
286 ns
390 ns
ΔA
λ (nm)
0,04
0,03
0,02
0,01
0,00
-0,01
-0,02
-0,03
300
400
500
600
700
800
900

(c)

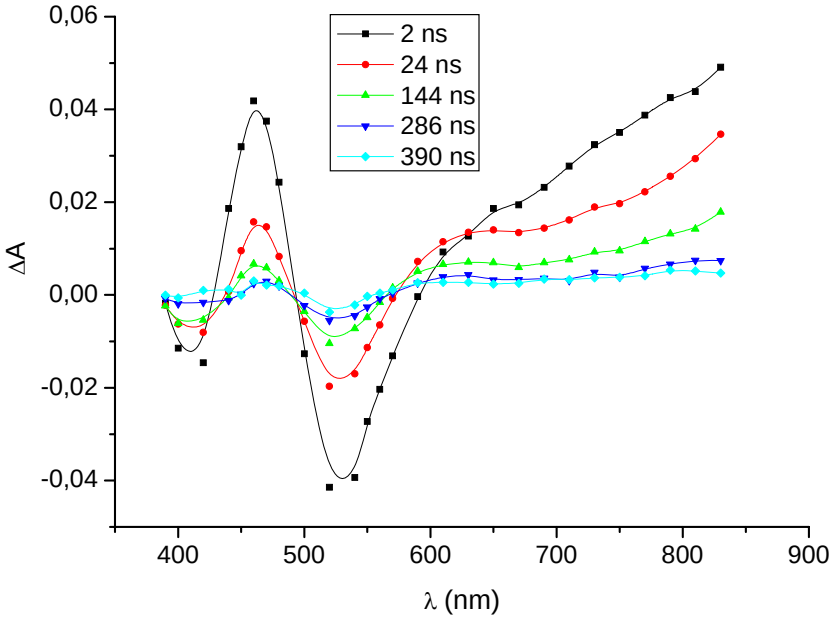
2 ns
24 ns
144 ns
286 ns
390 ns
ΔA
λ (nm)
0,06
0,04
0,02
0,00
-0,02
-0,04
400
500
600
700
800
900

(d)

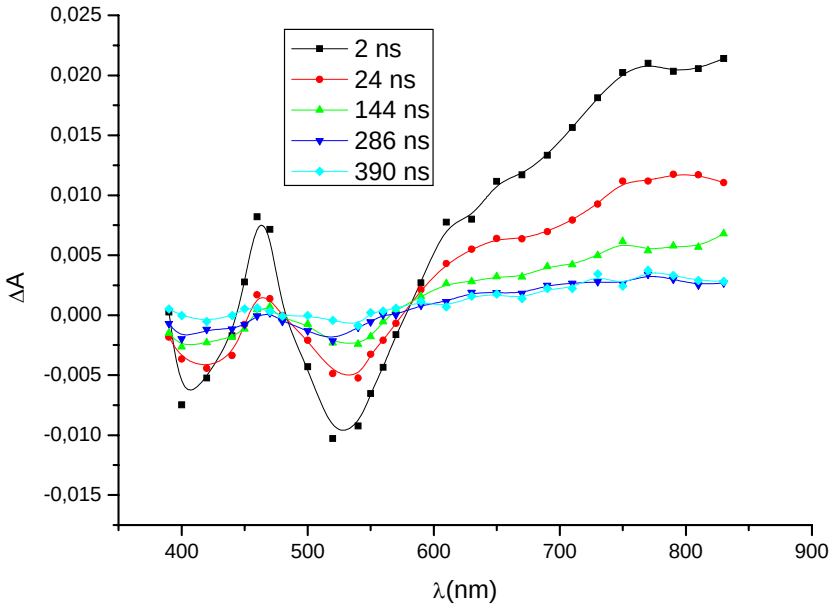

Figure 6.6: Transient absorption spectra of **Ru[bpy(DTP$_1$-R)]$_3$(PF$_6$)$_2$ series** in DMF ($\lambda_{exc.}$=532 nm). **Ru[bpy(DTP$_1$-H)]$_3$(PF$_6$)$_2$** (a), **Ru[bpy(DTP$_1$-Br)]$_3$(PF$_6$)$_2$** (b), **Ru[bpy(DTP$_1$-F)]$_3$(PF$_6$)$_2$** (c), **Ru[bpy(DTP$_1$-Hex)]$_3$(PF$_6$)$_2$** (d)

In order to check if the band could be assigned to a ligand centered transition. Zn adducts were prepared. Zinc-polypyridine complexes are known to display strong ILCT transitions and no MLCT due to the high third ionization potential of zinc and therefore are useful to identify ligand-based processes upon excitation in ruthenium complexes **[2]**.

Zinc^{2+} adducts were directly obtained in DMF solution, without isolation, by reacting the ligand with a ≈ 10 fold excess of solid $Zn(ClO_4)_2$. The reaction was instantaneous. No spectral changes were observed after prolonged laser flash photolysis experiments.

$$\text{bpy(DTP-R)} + 10\ Zn(ClO_4)_2 \xrightarrow{\text{DMF}} Zn^{+}\ \text{bpy(DTP-X)}$$

By comparison with the TA spectra of the free ligand and of the Zn^{2+} adduct, it was noticed that the same features were generally found in the transient spectra of the Zn^{2+}-ligand adducts (Fig. 6.7). So, the 480 nm band could be assigned to ligand-centred (LC) LUMO→LUMO+n absorption, populated by excitation of the charge transfer band.

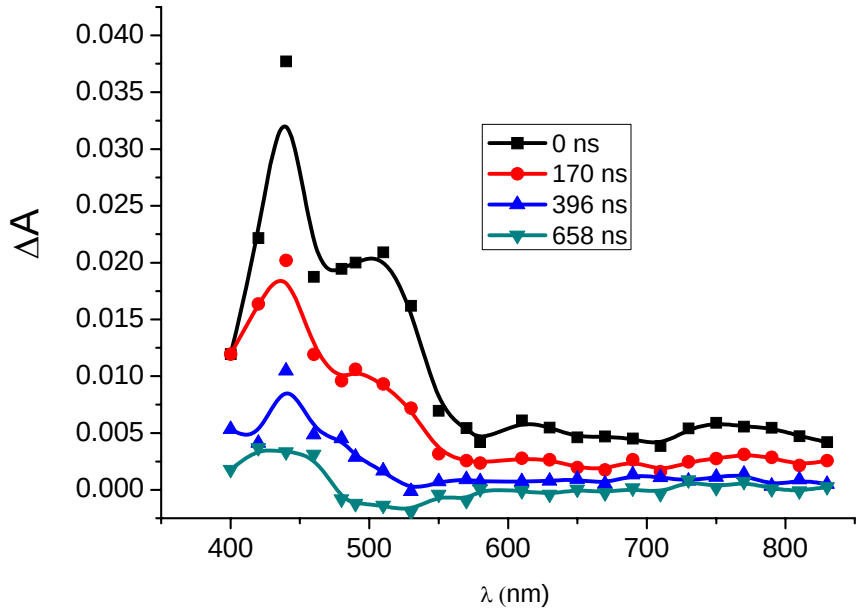

Figure 6.7: Transient triplet absorption of the Zn^{2+} bpy$(DTP_1\text{-}F)_3$ adduct following 355 nm laser excitation.

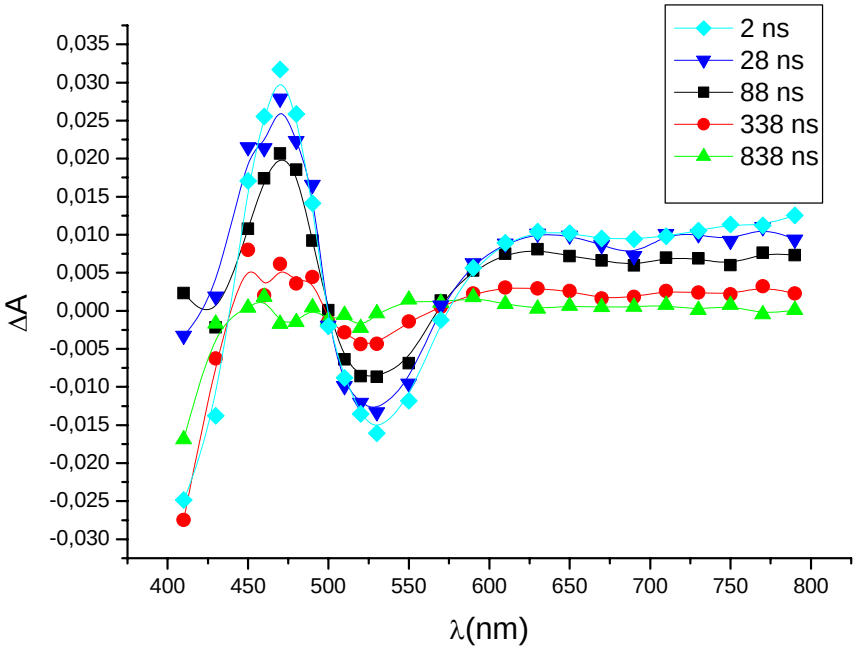

Figure 6.8: Transient spectrum of the **Ru[bpy$(DTP_1\text{-}F)]_3(PF_6)_2$** upon 355 nm laser excitation

Upon 355 nm (mainly ligand absorption manifold) excitation (Fig. 6.8) similar spectra were obtained, however, compared to that observed upon 532 nm excitation, the bleaching of the MLCT band was about half of the intensity of the characteristic 480 nm ligand-centered (LC) absorption, the low energy ($\lambda > 600$ nm) absorption was flat and of about half intensity, both characteristics recalling the spectral features of the parent ligand (Fig. 4.10 b) and of the relative Zn^{2+} adduct (Fig. 6.9) and indicating the persistence of the ligand-centered excited state and the incomplete relaxation to the MLCT state.

In DTP_2 series, The TA spectra obtained by following 532 nm excitation (Fig. 6.9) were generally characterized by a monoexponetial decay, with lifetimes in the 150-200 ns range. All TA spectra shared common features, summarized by the ground state bleaching, which mirrored the two overlapping bands of the ground state absorption, and by the strong triplet-triplet absorption with a maximum a 700 nm. The isosbestic point could be quite accurately individuated at 600 nm. The strong absorption into the red part of the spectrum is evident in the TA spectra of the free ligand and of the Zn^{2+} adduct (Fig. 6.10 and 6.11), although its maximum was blue shifted of about 100 nm, and probably originates by the LUMO→LUMO+n absorption. In this sense, the 100 nm red shift in the Ru(II) complexes may not be surprising, given that the LUMO π^* orbital may be more strongly destabilized upon interaction with the occupied $d\pi$ orbitals of the metal resulting in a decreased LUMO-LUMO+n energy gap. In this case, the TA spectra collected by following 355 nm excitation (Fig.6.9 (b)) were almost superimposable to those obtained with the 532 nm excitation, suggesting a strong coupling between the metal and the ligand. This fact and the lack of a distinct MLCT emission even upon direct excitation of the lowest energy band ($\lambda > 500$ nm) may suggest that the description of the excited state of the **$Ru[bpy(DTP_2\text{-}R)]_3(PF_6)_2$** complexes in terms of usual localized states (hole on the metal, electron on the LUMO orbital of the ligand) may not be entirely appropriate, and as a result of the strong mixing of the HOMOs of the metal and of the ligand, a photoexcited hole delocalization would result in a favoured deactivation of the lowest excited state by internal conversion.

(a)

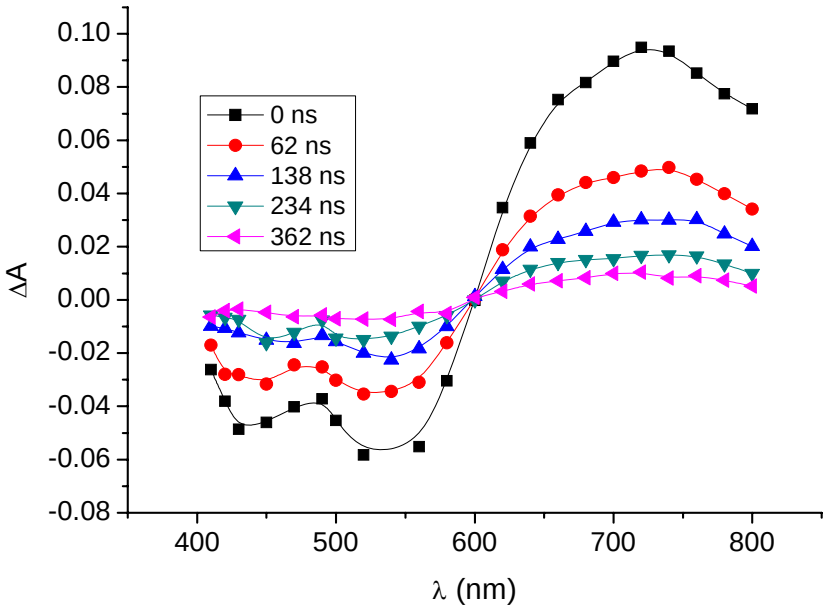
0.10
0.08
0.06
0.04
0.02
0.00
-0.02
-0.04
-0.06
-0.08
ΔA
400
500
600
700
800
λ (nm)
0 ns
62 ns
138 ns
234 ns
362 ns

(b)

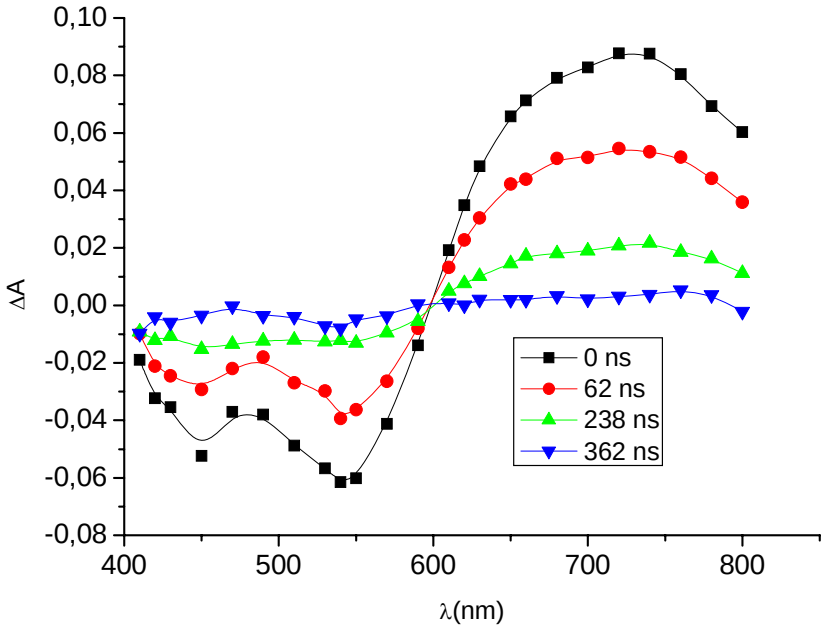
0,10
0,08
0,06
0,04
0,02
0,00
-0,02
-0,04
-0,06
-0,08
ΔA
400
500
600
700
800
λ(nm)
0 ns
62 ns
238 ns
362 ns

(c)

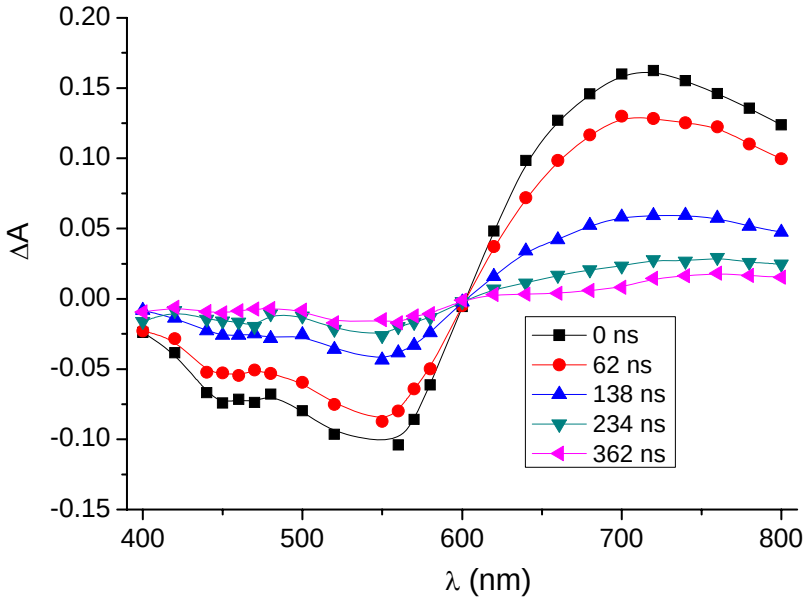

(d)

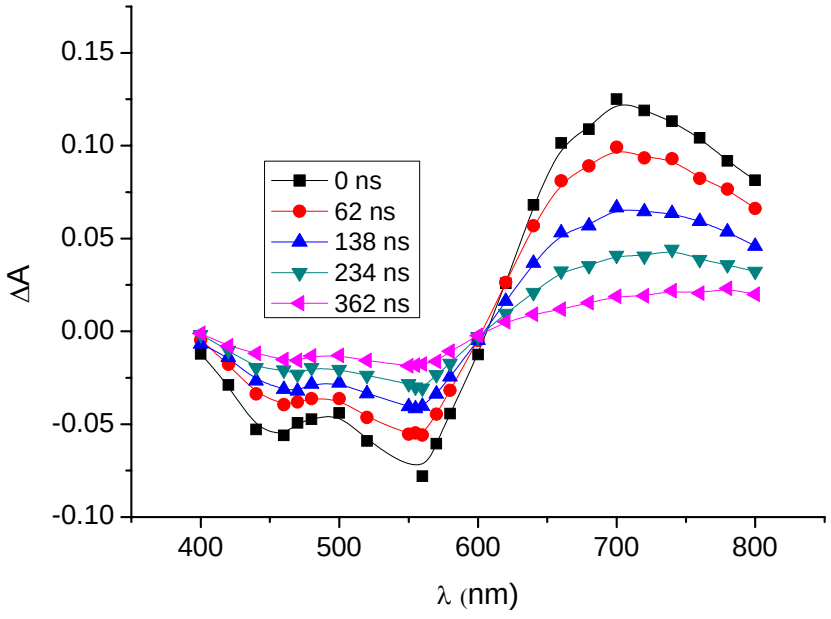

Figure 6.9: Transient absorption spectra of **Ru[bpy(DTP$_2$-R)]$_3$(PF$_6$)$_2$ series** in DMF ($\lambda_{exc.}$=532 nm). **Ru[bpy(DTP$_2$-Hex)]$_3$(PF$_6$)$_2$** (a), **Ru[bpy(DTP$_2$-Hex)]$_3$(PF$_6$)$_2$** ($\lambda_{exc.}$=355 nm) (b), **Ru[bpy(DTP$_2$-Me)]$_3$(PF$_6$)$_2$** (c), **Ru[bpy(DTP$_2$-F)]$_3$(PF$_6$)$_2$** (d)

Surprisingly, no MLCT type emission was observed within the **Ru[bpy(DTP$_2$-R)]$_3$(PF$_6$)$_2$**, the only emission being that of the LC type in the 512-580 nm region, as confirmed by the absorption spectra of the free ligand and of the Zn^{2+} adduct, similar energy, lifetime and by the excitation spectra obtained in correspondance of the emission maxima (Fig. 6.10 and 6.11).

Attempts to detect MLCT emission upon excitation at 532 nm at low temperature (77K) for **Ru[bpy(DTP$_2$-F)]$_3$(PF$_6$)$_2$** also failed, indicating that the non-radiative decay is dominant in the **Ru[bpy(DTP$_2$-X)]$_3$(PF$_6$)$_2$** series even in a frozen matrix.

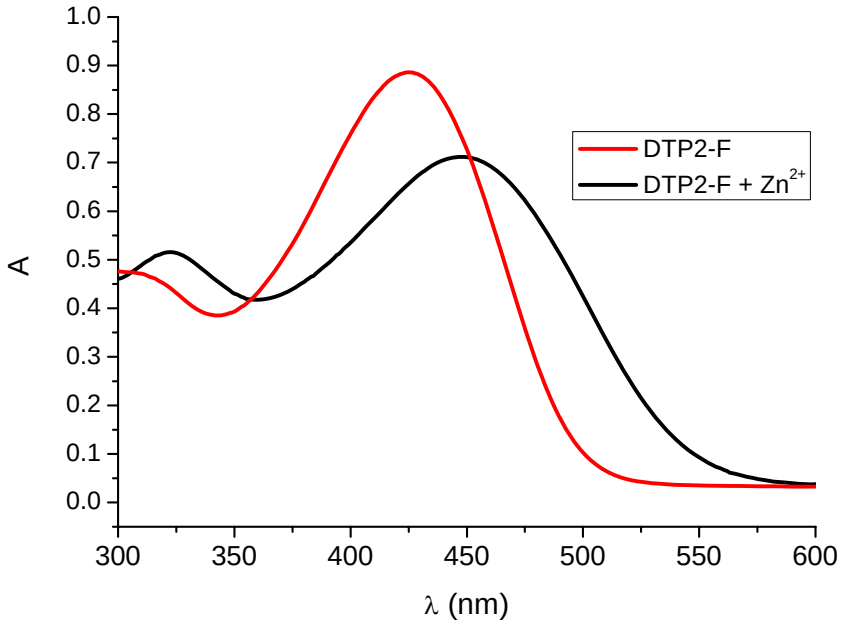

Figure 6.10: Absorption spectra of Zn^{2+} bpy(DTP$_2$-F)$_3$ adduct in concentrated solution (typical concentration used for laser flash photolysis experiments) compared to the absorption spectrum of the free ligand.

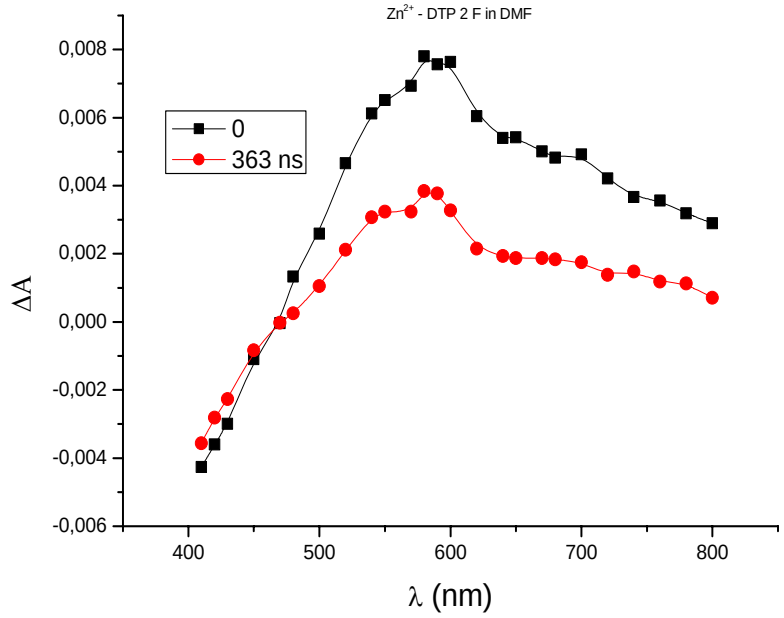

Figure 6.11: Transient triplet absorption of the Zn^{2+} **[Ru(DTP$_2$-F)$_3$](PF$_6$)$_2$]**adduct following 355 nm laser excitation

6.1.2.5. Computational analysis *(Coll. A. Monari, X. Assfeld, CBT-SRSMC)*

In order to interpret absorption and photophysical properties computational calculations were performed.

The homoleptic complexes have been optimized at DFT level with B3LYP functional. Excited states have been computed at TD-DFT level with CAM-B3LYP correlation exchange functional. In that case we used a LANL2DZ [**3]** basis allowing to treat Ru inner electrons with pseudopotentials. Due to the very high computational cost excited states have been computed using again the relatively small LANL2DZ basis. The latter is certainly not sufficient to provide a qualitative agreement with experimental data, but the main feature of the spectrum can be inferred and the nature of the transition can be easily interpreted. The computed principal transition in the lower energy region of the spectrum can be seen in Table 6.8 for the two families. Coherently with experimental results the **DTP$_2$** family is significantly red-shifted with respect to the **DTP$_1$** members, the intensities also appears much higher. Note also that the low lying spectrum of the **DTP$_2$** family is composed of a series of transition all having almost the same intensity, an occurrence that can be related to the extended plateau observed in the

experimental spectrum, although in the computed result the low frequency transition appears closer between them than in the experimental one.

Table 6.8: Complexes TDDFT computed principal excitation wavelengths and oscillator strength.

X	$Ru[bpy(DTP_1\text{-}R)]_3(PF_6)_2$ λ(nm), (f)[a]	$Ru[bpy(DTP_2\text{-}R)]_3(PF_6)_2$ λ(nm), (f)[a]
H	433.80 (0.99) 433.23 (1.02) 431.00 (0.70) 374.28 (2.42)	498.23 (1.94) 496.40 (1.81) 490.32 (3.30) 487.90 (2.47) 486.57 (1.92) 420.15 (0.50)
Br	433.03 (1.04) 432.39 (1.07) 430.62 (0.66) 371.89 (2.68)	492.86 (2.01) 492.15 (1.90) 484.81 (3.54) 483.02 (2.03) 482.30 (1.78) 419.08 (0.56)
F	432.32 (1.02) 431.97 (1.05) 429.98 (0.64) 371.58 (2.58)	492.09 (1.86) 491.50 (2.01) 483.75 (3.72) 482.19 (1.76) 481.61 (1.89) 419.13 (0.58)
Me	434.03 (0.95) 433.49 (1.01) 431.12 (0.73) 375.31 (1.77)	498.79 (1.81) 497.93 (1.98) 490.67 (3.86) 489.33 (1.82) 488.34 (1.98) 420.64 (0.49)
Hex	433.67 (0.85) 433.00 (0.90) 430.77 (0.78) 375.36 (2.51)	500.40 (1.91) 499.12 (1.94) 492.24 (3.58) 490.57 (1.98) 489.37 (2.05) 422.49 (0.49)

[a] oscillator strength in parentheses

The last occurrence, as well as the general blue shifting of the spectrum can be related to the small basis set used during computation due to the important size of the system. In order to better analyse the excited states nature we considered Natural Transition Orbitals (NTO) **[4, 5]**

representation of the electronic transition. NTOs are obtained by singular value decomposition (SVD) of the transition density matrix, and they can be considered as the optimal orbitals to represent an electronic transition in the TDDFT formalism. In contrast with Kohn-Sham molecular orbitals base, that require many occupied/virtual orbital couples, in NTO base only one or at maximum two couples entirely describe all the physics underlining the transition. Therefore, "occupied" NTO can be seen as the "hole" orbital, i.e. the orbital from which electron is removed during transition, while "virtual" NTO is the orbital in which electron is placed in the excited state.

NTOs for one of the low lying transition of the **Ru[bpy(DTP$_1$-F)]$_3$(PF$_6$)$_2$** and **Ru[bpy(DTP$_2$-F)]$_3$(PF$_6$)$_2$** are shown in Fig. 6.12 and 6.13, respectively (note that the other substituents do not qualitatively alter the orbitals). It can be seen easily that although in the two cases the transitions are mainly of MLCT nature, significant participation of the ligand in the occupied orbital is observed (especially for **Ru[bpy(DTP$_2$-F)]$_3$(PF$_6$)$_2$**). This effect can be extremely important in the case of their use as DSSC sensitizers, since such a transition will leave the "hole" far away from the semi-conductor surface, so diminishing recombination occurrence and facilitating the access of the redox mediator. One can also see that, as expected and coherently with the observed red shift the **Ru[bpy(DTP$_2$-F)]$_3$(PF$_6$)$_2$** shows a larger delocalization of the electronic density in the virtual orbital, leading to a stabilization of the excited state and hence to a red-shift.

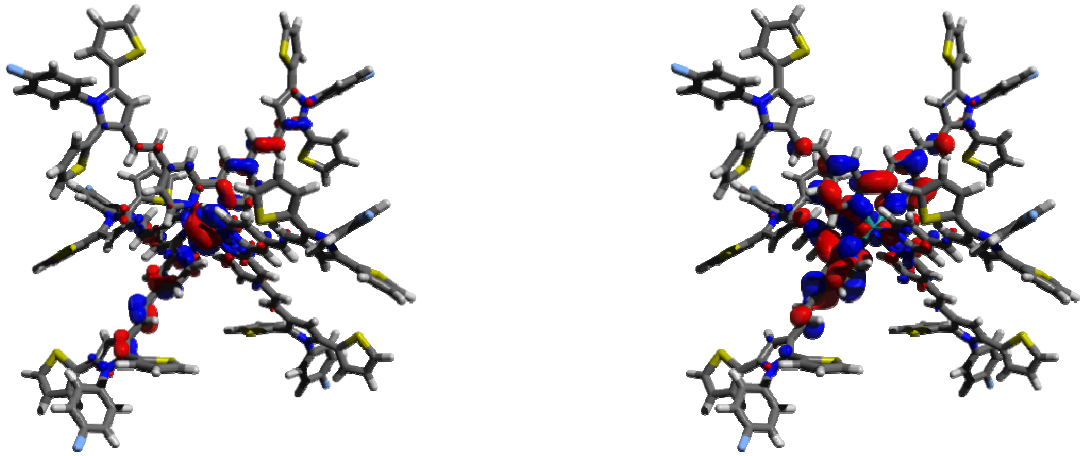

Occupied **Virtual**

Figure 6.12: NTOs isodensity surface of **Ru[bpy(DTP$_1$-F)]$_3$(PF$_6$)$_2$** at 432 nm. (Table 5.8 for transitions)

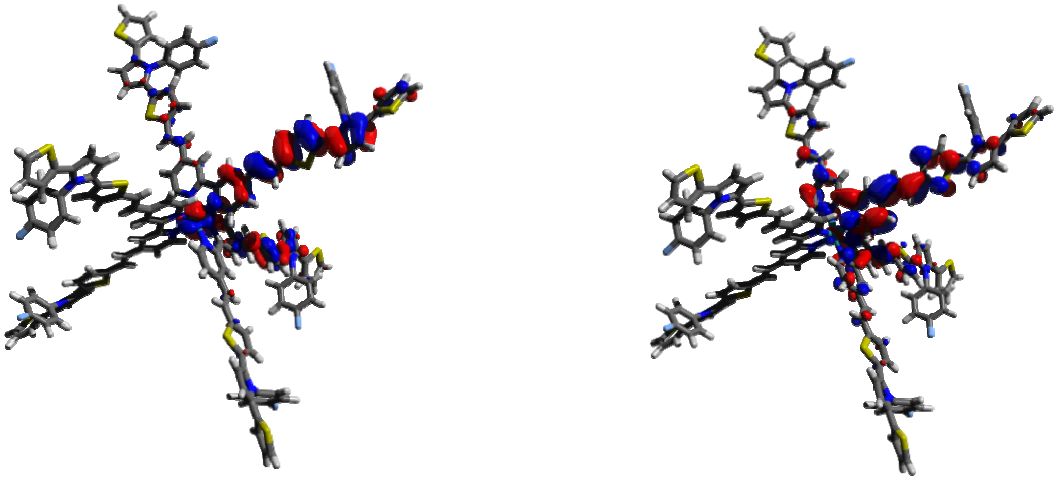

Occupied **Virtual**

Figure 6.13: NTOs isodensity surface of **Ru[bpy(DTP$_2$-F)]$_3$(PF$_6$)$_2$** at 492 nm. (Table 5.8 for transitions)

6.1.2.6. Conclusions

Dithienylpyrrole (DTP)-based bipyridine ligands **bpy(DTP$_1$-R)** and **bpy(DTP$_2$-R)** were coordinated with ruthenium metal to give the corresponding homoleptic complexes i.e. **Ru[bpy(DTP$_1$-R)]$_3$(PF$_6$)$_2$** and **Ru[bpy(DTP$_2$-R)]$_3$(PF$_6$)$_2$**. The homoleptic ruthenium complexes exhibited the same features like ligands. The **Ru[bpy(DTP$_2$-R)]$_3$(PF$_6$)$_2$** complexes offered a wide absorption range in the visible domain with a notable and constant molar extinction coefficient all along this domain (Fig: 6.14).

When the new homoleptic complexes were compared with the best homoleptic complex previously reported [**6**] by our group SOR, it is evident that strong red shift and broadening toward the visible region was observed for the homoleptic complexes of **bpy(DTP$_2$-R)** ligands with significantly higher molar extinction coefficient. So, the absorption spectrum is dominated by MLCT transition in the visible region that is important for light harvesting process. Quantum Calculations as well as transient spectroscopy were used to explain this behaviour by evidencing a larger π-delocalization extent in **Ru[bpy(DTP$_2$-R)]$_3$(PF$_6$)$_2$** complexes.

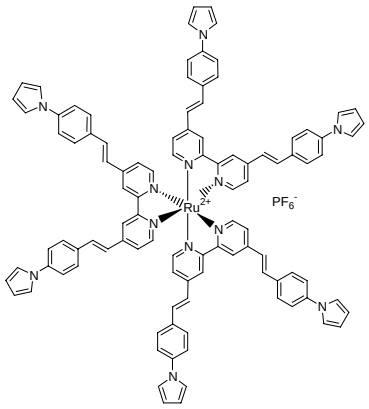

SOR Complex

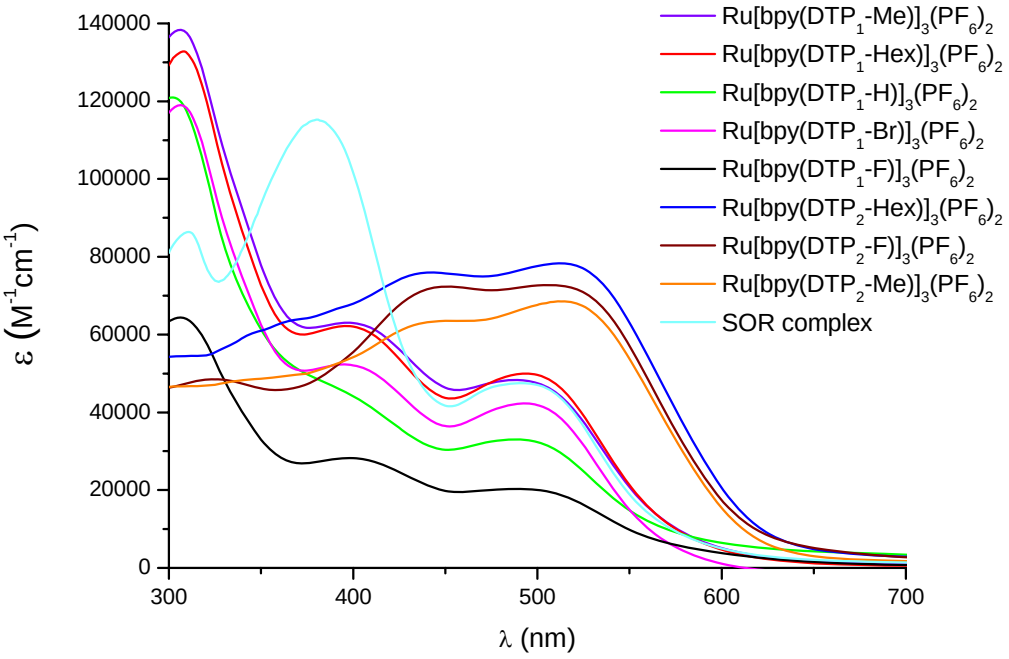

Figure 6.14: Absorption spectra of Homoleptic complexes in acetonitrile

In conclusion this new class of ruthenium complexes are promising as light harvesters and it would be interesting to prepare bis-heteroleptic and tris-heteroleptic complexes with the same ligands and introduce them as sensitizers for the photosensitization of semiconductor in dye-sensitized solar cells.

6.2. References

[1] Hara, K.; Sato, T.; Katoh, R.; Furube, A.; Ohga, Y.; Shinpo, A.; Suga, S.; Sayama, K.; Sugihara, H.; Arakawa, H. *J. Phys. Chem. B.* 2003, **107**, 597.

[2] Renouard, T.; Le Bozec, H. *Eur. J. Inorg. Chem.*, 2000, 229.

[3] Dunning Jr, T.H.; Hay, P.J. *In Modern Theoretical Chemistry; Schaefer, H. F., III, Ed.; Plenum; New York, 1976; Vol. 3, pp 1- 28.*

[4] Creutz, C.; Chou, M.; Netzel, T.L.; Okumura, M.; Sutin, N. *J. Am. Chem. Soc*. 1980, **102**, 1309.

[5] Monari, A.; Very, T.; Rivail J.-L.; Assfeld, X. *Comput. Theor. Chem.*, 2011, DOI: 10.1016/j.comptc.2011.1011.1026

[6] Martineau, D.; Beley, M.; Gros, P.C.; Cazzanti, S.; Caramori, S.; Bignozzi, C.A. *Inorg. Chem.* 2007, **46**, 2272.

Chapitre No: 7

Synthèse et propriétés des Complexes Hétéroleptiques de Ruthenium

Résumé en français

Dans ce chapitre, sont présentées la synthèse et la caractérisation de complexes hétéroleptiques portant les ligands bpy(DTP-R) et un ligand bipyridine à fonctions carboxyliques (dcbpy) nécessaires pour l'accrochage sur le semiconducteur et l'injection des électrons dans la bande de conduction après excitation.

Deux types de complexes ont été préparés :

Les complexes bishétéroleptiques **[Ru{bpy(DTP-R)}$_2$(dcbpy)](PF$_6$)$_2$** composés de deux ligands bpy(DTP-R) et d'un ligand dcbpy ont d'abord été préparés. Si les complexes ont été obtenus avec de bons rendements en série DTP$_1$-R (52-72%) en revanche tous nos essais pour les obtenir en série DTP$_2$-R on été vains. Nous n'avons pas d'explication à cet échec. Une gêne stérique plus importante créée par le substituant pourrait être une partie du problème.

Les complexes trishétéroleptiques **[Ru{bpy(DTP-R)}(dcbpy)(NCS)$_2$]** composés d'un ligand bpy(DTP-R), d'une dcbpy et de deux ligands NCS (pour apporter une transition supplémentaire et donc une absorption à plus faible énergie) ont en suite été préparés. La série **[Ru{bpy(DTP$_1$-R)}(dcbpy)(NCS)$_2$]** (R=H,Br,F,Me, Hex) a pu être obtenue avec des rendements acceptables (40-47%). En revanche, seul le complexe **[Ru{bpy(DTP$_2$-Me)}(dcbpy)(NCS)$_2$]** a pu être préparé avec un rendement de 47%.

La série DTP$_2$ pose beaucoup plus de problème que la série DTP$_1$ pour la synthèse de complexes hétéroleptiques.

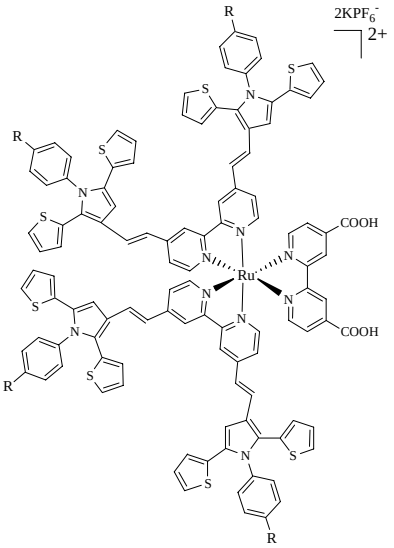

[Ru{bpy(DTP-R)}$_2$(dcbpy)](PF$_6$)$_2$

R=Me, Hex

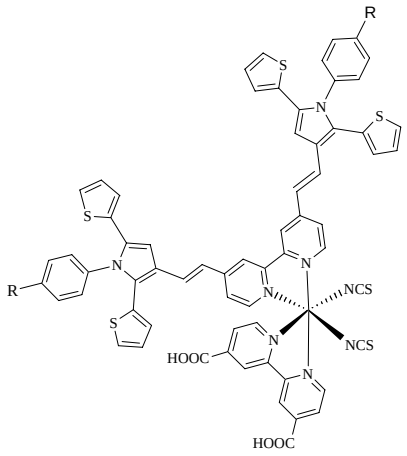

[Ru{bpy(DTP$_1$-R)}(dcbpy)(NCS)$_2$]

(R=H,Br,F,Me, Hex)

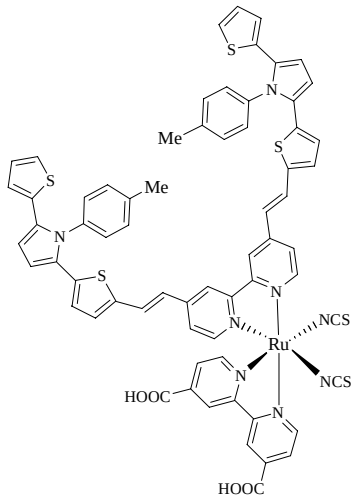

[Ru{bpy(DTP$_2$-Me)}(dcbpy)(NCS)$_2$]

Les spectres d'absorption des deux complexes bishétéroleptiques **[Ru{bpy(DTP$_1$-Me)}$_2$(dcbpy)](PF$_6$)$_2$** et **[Ru{bpy(DTP$_1$-Hex)}$_2$(dcbpy)](PF$_6$)$_2$** sont très similaires (Figure 7.2). Trois bandes d'absorptions sont observées : une intense dans la region des UV (308-311 nm) correspondant aux transitions $\pi - \pi^*$ localisées sur les bipyridines et deux autres à 400-406 nm et 461-479 nm correspondant à des transitions de type MLCT. Par comparaison avec les complexes homoleptiques, on observe des profils semblables avec une légère baisse du coefficient d'extinction molaire dans le cas du complexe bis-hétéroleptique. L'intensité des bandes semble ici en relation avec le nombre de ligands bpy(DTP-R) autour du métal. Cette série possède des caractéristiques très intéressantes pour une utilisation en cellule DSSC.

Les spectres des complexes tris-heteroleptiques (Fig.7.3) montrent des différences importantes entre la série **DTP$_1$** et **DTP$_2$-R** : i) La bande à 406-411 nm subit un effet bathochrome (468 nm) avec un très net élargissement dans le visible jusqu'à 625 nm. ii) Les bandes très intenses à 312-314 nm deviennent extrêmement faibles en série **DTP$_2$**.

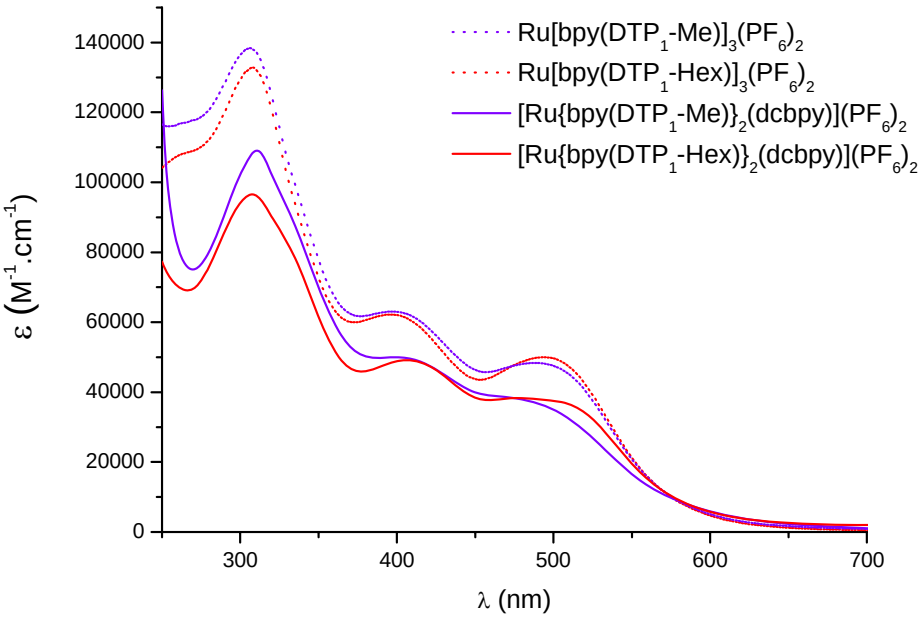

Figure 7.2: Comparaison des spectres d'absorption des complexes homo- et bishétéroleptiques

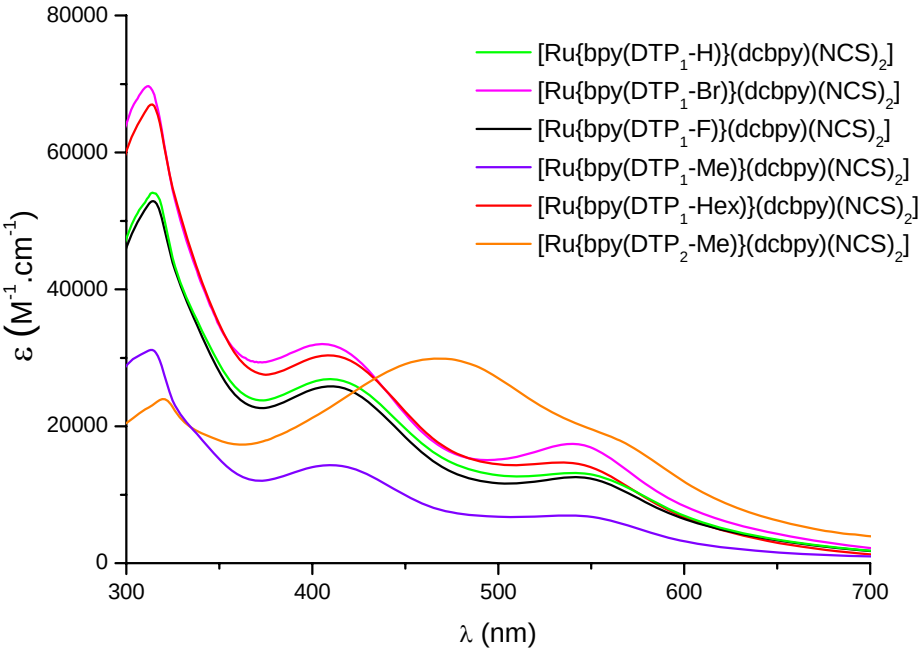

Figure 7.3: Comparaison des spectres d'absorption des complexes trishétéroleptiques

Les calculs théoriques DFT (NTO) effectués sur les complexes tris-hétéroleptiques montrent que l'orbitale occupée (trou créé après excitation) est localisée au niveau du métal et des ligands NCS

alors que l'orbitale virtuelle (là où arrive l'électron) se situe au niveau de la bipyridine carboxylique ce qui est favorable à l'injection. Le ligand bpy(DTP) n'est pas impliqué dans le processus ce que peut être gênant pour la recombinaison.

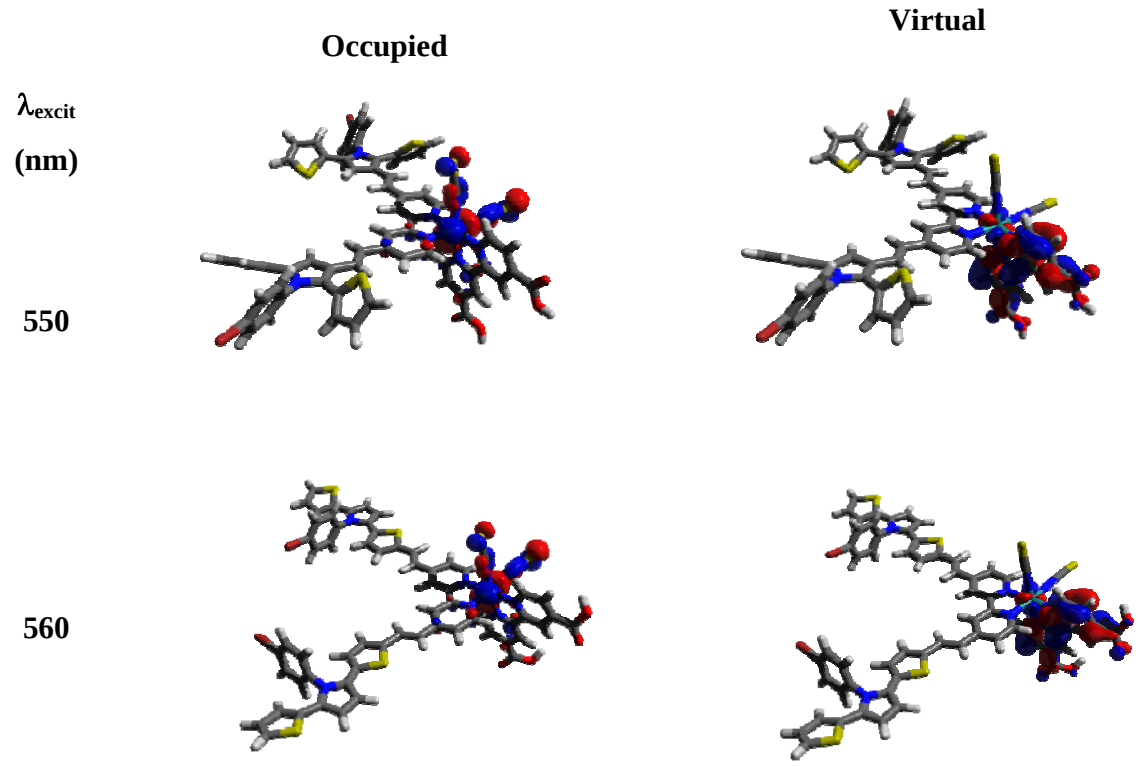

Les propriétés photovoltaïques ont été étudiées pour l'instant seulement sur 2 complexes **[Ru{bpy(DTP$_1$-Hex)}(dcbpy)(NCS)$_2$]** et **[Ru{bpy(DTP$_2$-Me)}(dcbpy)(NCS)$_2$]**. Les colorants ont été adsorbés sur électrode de TiO_2 et la photosensibilisation contôlée par spectroscopie UV-vis. Le deux complexes collectent le rayonnement solaire de façon très efficace. Des cellules DSSC ont ensuite été assemblées en utilisant les deux colorants. Deux médiateurs redox ont été testés, l'un à base d'iodures l'autre à base de complexes de cobalt. Dans tous les cas, même si un photo-courant est bien généré sous irradiation de la cellule, les performances sont modestes en comparaison de composés de référence. L'excellente collecte de photons et des potentiels redox très favorables à la régénération par le médiateur laissent penser à une limitation lors de l'injection dans la bande conduction du semiconducteur ou à des problèmes stériques empêchant l'accès du médiateur au centre ruthénium oxydé pour la régénération.

Chapter No: 7

Synthesis and Properties of Heteroleptic Complexes

Tris-heteroleptic complexes contain a 4,4'-dicarboxy-2,2'-bipyridine (dcbpy) ligand for anchoring on the titanium dioxide (TiO_2) surface, a second bipyridine ligand used as an antenna for improving the light harvesting performances and two thiocyanate ligands to tune the photo- and electrochemical properties of the dyes. Although the NCS is a suitable donor ligand, it can undergo photosubstitution or photodegradation reactions, which decrease the long-term stability of the complexes. The occurrence of these reactions can be reduced through the replacement of NCS ligands with other donor ligands, such as bidentate ligands. Thus approach of bisheteroleptic $[RuL_2(dcbpy)]^{2+}$ complexes is interesting to obtain stable and efficient dyes.
In this chapter we will describe the synthesis and characterization of bis-heteroleptic and tris-heteroleptic complexes prepared from our new series of ligands.

7.1. Bis-Heteroleptic Complexes

7.1.1. Synthesis of bis-heteroleptic Complexes

The bis-heteroleptic complexes were prepared from **bpy(DTP$_1$-R)** series of ligands. For this purpose we only focus on ligands that offer better solubility i.e. **bpy(DTP$_1$-Me)** and **bpy(DTP$_1$-Hex),** bearing methyl and hexyl groups respectively.

The complexes were obtained by following a two-step procedure (Scheme 7.1). The first step was the preparation of a dichloro complex **Ru[bpy(DTP$_1$-R)]$_2$Cl$_2$** by reaction of $RuCl_3.3H_2O$ with 2 equiv of ligand. The dichloro complexes were obtained quantitatively (as controlled by ^{1}HNMR) in a short time (10 minutes) under microwave irradiation in DMF (Scheme 7.1). In the second step, the dichloro ligands were substituted by the dicarboxybipyridine (dcbpy) ligand by reacting a stoichiometric amount of dcbpy in refluxing

acetic acid for 5-16 hours. Bis-heteroleptic complexes of bpy(DTP_1-R) series were obtained in good overall yields (52-72 %).

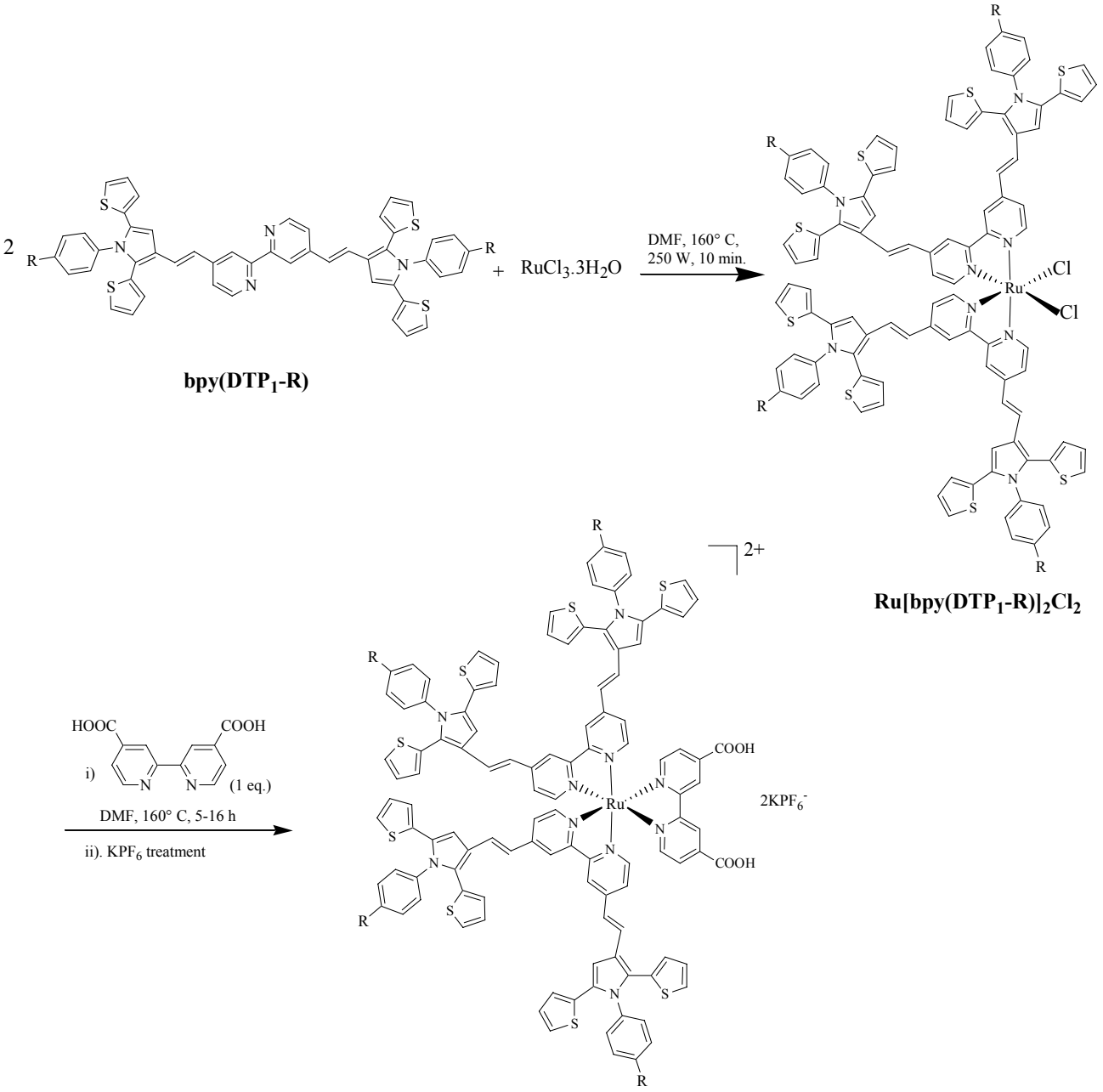

bpy(DTP_1-R)

Ru[bpy(DTP_1-R)]$_2Cl_2$

[Ru{bpy(DTP_1-Me)}$_2$(dcbpy)]$(PF_6)_2$, 52 %

[Ru{bpy(DTP_1-Hex)}$_2$(dcbpy)]$(PF_6)_2$, 72 %

Scheme 7.1: Synthesis of bis-heteroleptic complexes **[Ru{bpy(DTP_1-R)}$_2$(dcbpy)]$(PF_6)_2$**

Unfortunately, when we attempted the same synthesis with **bpy(DTP$_2$-R)** series of ligands (R = Me, Hex) we were unable to obtain target complexes. In each attempt we obtained mixture of unidentifiable products. An explanation of this failure is not easy but taking in account the structure of ligands, possibility exists that steric effect of alkyl substituents might be involved in it.

7.1.2. Properties of bis-heteroleptic Complexes

Bis-heteroleptic complexes were then subjected to a range of photophysical and electrochemical analyses.

7.1.2.1.Absorption properties

The electronic absorption spectra of bis-heteroleptic complexes were recorded in acetonitrile + DMSO (4:1) solution. DMSO was added to complete solubilization. The results are displayed in Fig. 7.1 and the data are summarized in Table 7.1.

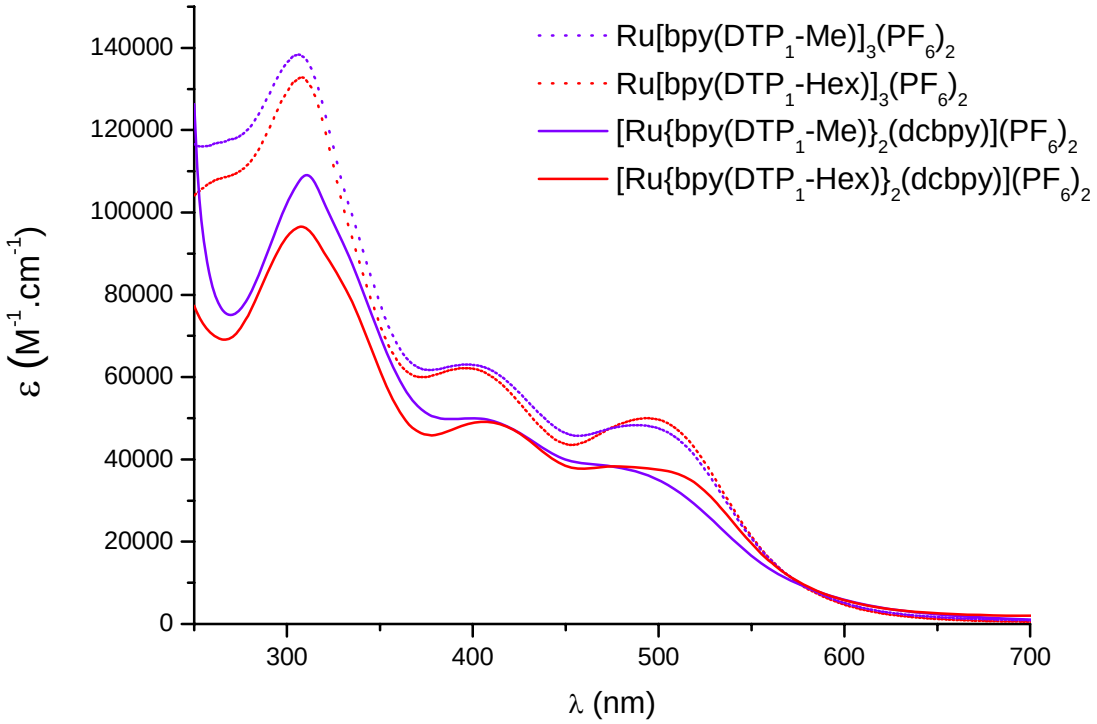

Figure 7.1: Comparison of absorption spectra of homoleptic and bis-heteroleptic complexes

Table 7.1: Absorption properties of Bis-Heteroleptic complexes

Complex	λabs-max (nm)[a]	ε 10^3 $M^{-1}cm^{-1}$
[Ru{bpy(DTP$_1$-Me)}$_2$(dcbpy)](PF$_6$)$_2$	461 400 311	38.9 49.9 109.0
[Ru{bpy(DTP$_1$-Hex)}$_2$(dcbpy)](PF$_6$)$_2$	479 406 308	38.2 49.1 96.5

[a] Measured in CH_3CN + DMSO (4:1) at 25°C.

Spectra featured three absorption bands, an intense absorption band in UV region (308-311 nm) and two other comparatively less intense bands in the visible region near 400-406 nm and 461-479 nm. The strong band in 308-311 nm range is attributed to intra-ligand π– π* transitions localized mainly on bipyridine whereas both bands in the visible region correspond to spin-allowed MLCT transitions. It is observed that spectra of both **[Ru{bpy(DTP$_1$-Me)}$_2$(dcbpy)](PF$_6$)$_2$** and **[Ru{bpy(DTP$_1$-Hex)}$_2$(dcbpy)](PF$_6$)$_2$** complexes are similar with comparable ε values.

The absorption spectra of bis-heteroleptic complexes have been compared with their homoleptic analogues. It is evident that molar extinction coefficient values for homoleptic complexes are higher than bis-heteroleptic complexes which are in agreement with the fact that the bands intensities grew as the number of ligands increased in the complex.

The bis-heteroleptic complexes exhibited slight red-shift for absorption band in the UV region and first MLCT band as compared with homoleptic complexes but no red shift was noticed for the second MLCT band.

7.1.2.2. Electrochemical properties

The electrochemical behaviour of the bis-heteroleptic complexes was studied by cyclic voltammetry and presented in table 7.2.

It is well known that Polypyridyl complexes of Ru^{II} exhibit rich and complex electrochemistry in non-aqueous solutions comprising both metal-centered oxidation Ru^{III}/Ru^{II} and bpy-centered reduction reactions. So, the bis-heteroleptic complexes also exhibited two

oxidation waves, the first one corresponding to the Ru^{III}/Ru^{II} couple, appears at 0.93 V/SCE for both $[Ru\{bpy(DTP_1\text{-}Me)\}_2(dcbpy)](PF_6)_2$ and $[Ru\{bpy(DTP_1\text{-}Hex)\}_2(dcbpy)](PF_6)_2$ which indicates that the inductive effects from the both substituents *i.e.* methyl and hexyl respectively are similar and do not affect the metal's redox potential. It is semi-reversible for $[Ru\{bpy(DTP_1\text{-}Me)\}_2(dcbpy)](PF_6)_2$ and irreversible for $[Ru\{bpy(DTP_1\text{-}Hex)\}_2(dcbpy)](PF_6)_2$. As the anodic sweep is continued to higher potentials, a second oxidation process is seen that is irreversible and is attributed to the formation of radical cation on the thiophene as described for the ligands and homoleptic complexes. The relative wave heights of the Ru- and bithienyl-based responses indicate that a single electron oxidation of the bithienyl group is taking place. Upon sweeping to low potential, most complexes undergo ligand-centered reduction refers to the transfer of an electron in the bipyridine which is also irreversible.

In comparison to related homoleptic complexes, the Ru^{III}/Ru^{II} redox couple in both bis-heteroleptic complexes is shifted to slightly lower potentials (0.93 V/SCE vs 0.96 V/SCE).

Table 7.2: Electrochemical properties of bis-heteroleptic complexes

Complex	$E_{1/2}$ or Epa (Ru^{III}/Ru^{II}) (V/SCE)[a,c]	Epa (L^+/L) (V/SCE)[a]	Epc (L/L^-) (V/SCE)[b]
$[Ru\{bpy(DTP_1\text{-}Me)\}_2(dcbpy)](PF_6)_2$	0.93 (ΔEp=0.20)	1.03 (irrev.)	-1.26 (irrev.)
$[Ru\{bpy(DTP_1\text{-}Hex)\}_2(dcbpy)](PF_6)_2$	0.93 (irrev.)	1.00 (irrev.)	-1.25 (irrev.)

[a] Oxidation potentials standardized with Fc^+/Fc as internal standard and converted into SCE scale by adding 0.47V ($E_{1/2}Fc^+/Fc$). Recorded in DMF using $Bu_4N^+PF_6^-$ as supporting electrolyte at 100mV/s. [b] First reduction potential. [c] When irreversible Epa should be considered.

7.1.2.3 Emission properties

Emission band maxima and lifetimes for all of the bis-heteroleptic complexes are presented in Table 7.3.

Table 7.3: Emission properties of bis-heteroleptic complexes

Complex	λem-max[a] Ligand/ MLCT based	λ_{excit} (nm)
[Ru{bpy(DTP$_1$-Me)}$_2$(dcbpy)](PF$_6$)$_2$	447 (Ligand) 674 (MLCT)	311 500
[Ru{bpy(DTP$_1$-Hex)}$_2$(dcbpy)](PF$_6$)$_2$	446 (Ligand) 677 (MLCT)	310 500

[a] Photomultiplier corrected emission maxima for the complexes in acetonitrile + DMSO (4:1) A< 0.05.

On excitation of bis-heteroleptic complexes at wavelengths given in table 7.3, two distinct emission bands were observed, one centered in the 446-447 nm region, being that of the LC type, and one in the red part of the spectrum in the 674-677 range originated by the typical ^{3}MLCT radiative deactivation.

When compared with related homoleptic complexes [Ru{bpy(DTP$_1$-Me)}$_2$(dcbpy)](PF$_6$)$_2$ exhibited almost same emission maxima as its homoleptic analogue. Whereas [Ru{bpy(DTP$_1$-Hex)}$_2$(dcbpy)](PF$_6$)$_2$ have blue shift (446 vs 541 in LC part; 677 vs 692 in MLCT region) as compared to homoleptic complex. These blue shifts can be attributed to the withdrawing electronic effect of the dcbpy ligand.

7.2. Tris-Heteroleptic Complexes

7.2.1. Synthesis of tris-heteroleptic Complexes

During current work we used microwave heating method to rapidly produce a variety of desirable ruthenium tris-heteroleptic complexes featuring good yields with brief workups. As our interest lie in the development of new Ru^{II} complexes of relevance to solar energy conversion in quite rapid and efficient manner.

The [Ru(p-cymene)Cl$_2$]$_2$ complex was chosen as metal source in microwave synthesis. This precursor is of utmost importance for the synthesis of a variety of the most promising next generation heteroleptic dyes including Z907 **[1]**, N-845 **[2]**, Z-910 **[3]** and K-19 **[4]**. As in [Ru(p-cymene)Cl$_2$]$_2$ different ligands on the metal can be introduced in a stepwise and controlled

manner, permitting the sequential stoichiometric addition of dcbpy, followed by a large excess of the ambidentate NCS^- ligands.

Tris-heteroleptic complexes were synthesized by following a one pot synthesis (Scheme 7.2.) under microwave irradiation, where $[Ru(p\text{-cymene})Cl_2]_2$ was initially reacted with one equivalent of bpy(DTP_1-R) ligand at 70° C in DMF solution for 10 minutes under microwave irradiation (250 W). To the resulting mixture, dcbpy was added and allowed to react at 160° C for 10 minutes. [Ru{bpy(DTP_1-R)}(dcbpy)Cl_2] was obtained, in which NH_4NCS was added in large excess and the reaction was further continued for 10 minutes at 160° C. At the end of the reaction, DMF was removed under reduced pressure and the crude product was purified by size exclusion separation on Sephadex LH-20 column to obtain the desired complex. Analytical and spectroscopic data obtained for complexes agreed well with the proposed structure for the respective complexes.

Starting ligands **bpy(DTP_1-R)**, their tris-heteroleptic complexes **[Ru{bpy(DTP_1-R)}(dcbpy)$(NCS)_2$]** with corresponding yields are reported in table 7.4.

Table 7.4: Tris-heteroleptic complexes [Ru{bpy(DTP_1-R)}(dcbpy)$(NCS)_2$] of DTP_1 ligand series

Ligand bpy(DTP_1-R)	**Complex [Ru{bpy(DTP_1-R)}(dcbpy)$(NCS)_2$]**	**Yield %**
bpy(DTP_1-H)	**[Ru{bpy(DTP_1-H)}(dcbpy)$(NCS)_2$]**	40
bpy(DTP_1-Br)	**[Ru{bpy(DTP_1-Br)}(dcbpy)$(NCS)_2$]**	42
bpy(DTP_1-F)	**[Ru{bpy(DTP_1-F)}(dcbpy)$(NCS)_2$]**	45
bpy(DTP_1-Me)	**[Ru{bpy(DTP_1-Me)}(dcbpy)$(NCS)_2$]**	47
bpy(DTP_1-Hex)	**[Ru{bpy(DTP_1-Hex)}(dcbpy)$(NCS)_2$]**	42

The microwave reactions generated the desired tris-heteroleptic products in acceptable yields (40-47 %).

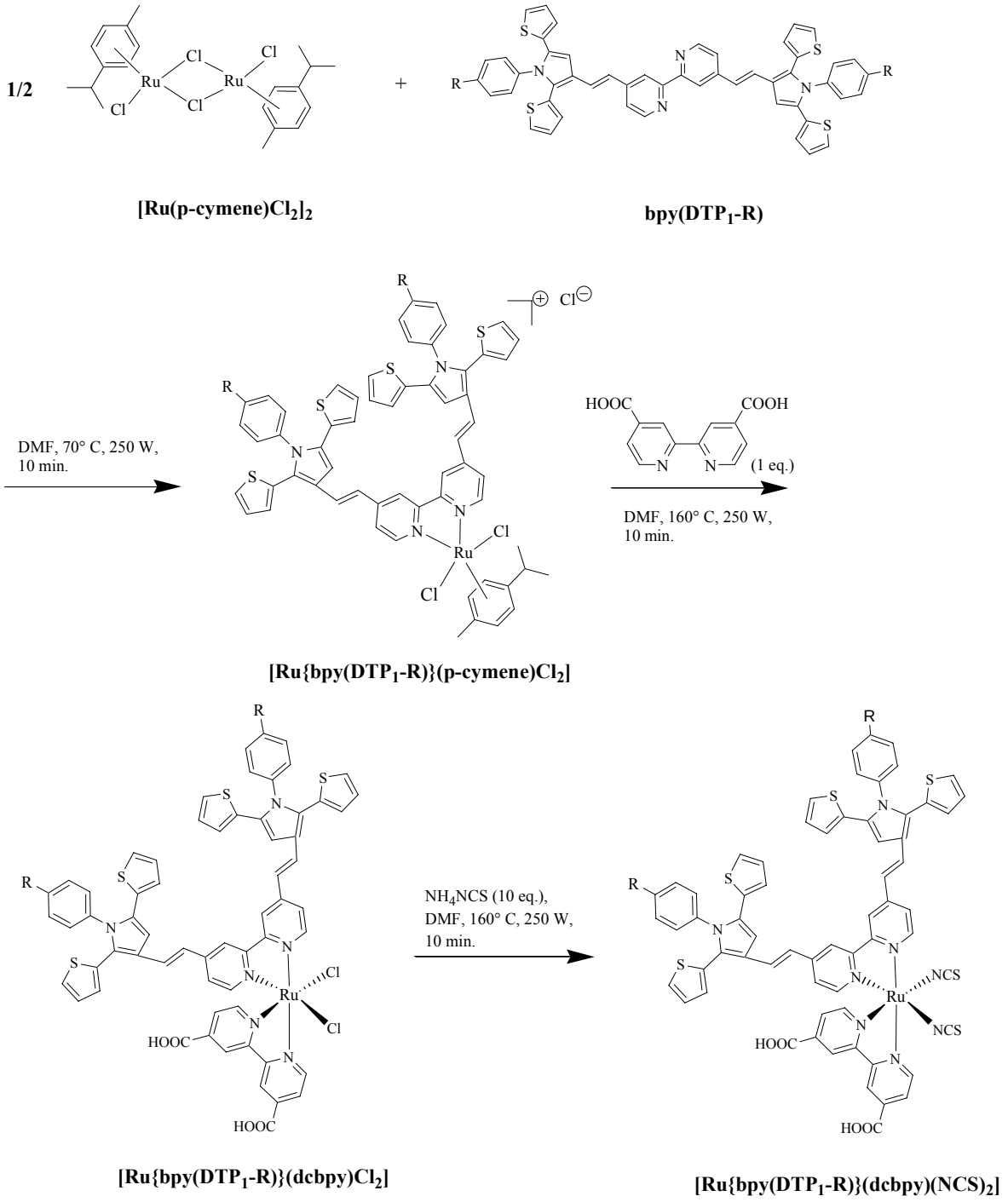

Scheme 7.2: Synthesis of Tris-Heteroleptic complexes **[Ru{bpy(DTP$_1$-R)}(dcbpy)(NCS)$_2$]** of **bpy(DTP$_1$-R)** ligand series

Same reaction conditions were used to prepare tris-heteroleptic complexes of bpy(DTP_2-R). Starting ligands **bpy(DTP_2-R)**, their tris-heteroleptic complexes **[Ru{bpy(DTP_2-R)}(dcbpy)$(NCS)_2$]** with the corresponding yields are reported in table 7.5.

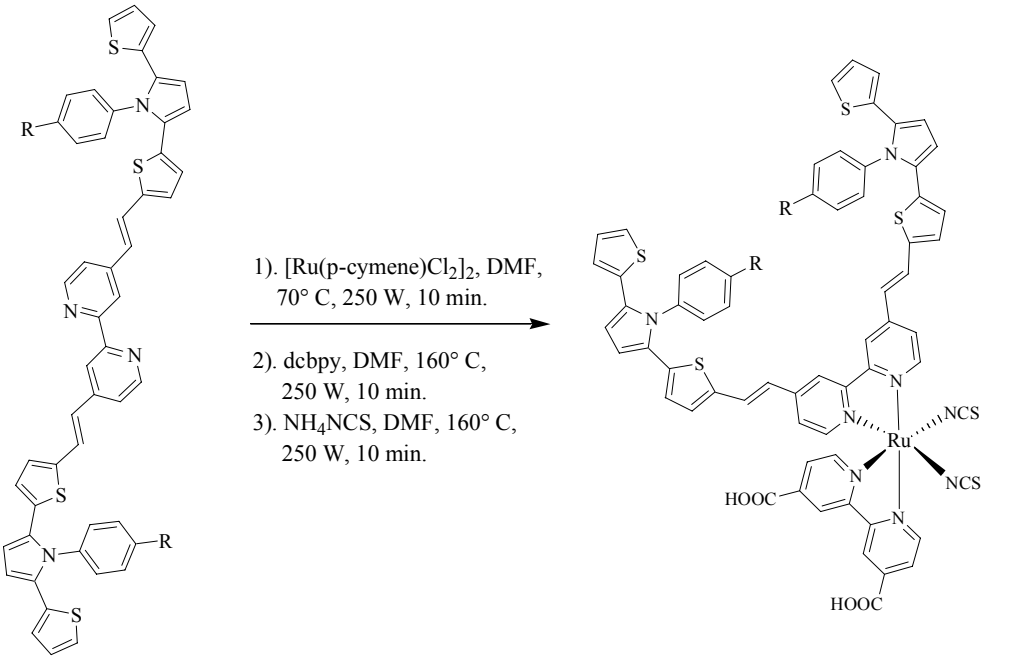

bpy(DTP_2-R) **[Ru{bpy(DTP_2-R)}(dcbpy)$(NCS)_2$]**

Scheme 7.3: Synthesis of Tris-Heteroleptic complexes **[Ru{bpy(DTP_2-R)}(dcbpy)$(NCS)_2$]** of **bpy(DTP_2-R)** ligand series

Table.7.5: Tris-heteroleptic complexes [Ru{bpy(DTP_2-R)}(dcbpy)$(NCS)_2$]

Ligand **bpy(DTP_2-R)**	**Complex** **[Ru{bpy(DTP_2-R)}(dcbpy)$(NCS)_2$]**	**Yield %**
bpy(DTP_2-F)	**[Ru{bpy(DTP_2-F)}(dcbpy)$(NCS)_2$]**	ui*
bpy(DTP_2-Me)	**[Ru{bpy(DTP_2-Me)}(dcbpy)$(NCS)_2$]**	47
bpy(DTP_2-Hex)	**[Ru{bpy(DTP_2-Hex)}(dcbpy)$(NCS)_2$]**	ui*

*ui = unidentified

In case of DTP_2 series only **[Ru{bpy(DTP_2-Me)}(dcbpy)$(NCS)_2$]** was obtained (47 %), whereas by using same reagents and by following the same reaction conditions, it was not possible to obtain other tris-heteroleptic complexes. In each case complex mixture was obtained whose constituents were impossible to identify. Conventional heating procedure instead of

microwave irradiation was employed. It involved the sequential addition of ligand, dcbpy and NH_4NCS, **[5-10]** to obtain $[Ru\{bpy(DTP_2\text{-}F)\}(dcbpy)(NCS)_2]$ and $[Ru\{bpy(DTP_2\text{-}Hex)\}(dcbpy)(NCS)_2]$ complexes but this approach was not successful and unidentified products were obtained.

$RuCl_2(DMSO)_4$ is also an important candidate to obtain tris-heteroleptic complexes as it can also be substituted in a stepwise and controlled manner, permitting the sequential stoichiometric addition of dcbpy followed by a large excess of the ambidentate NCS^- ligand. So $RuCl_2(DMSO)_4$ was used instead of $[Ru(p\text{-cymene})Cl_2]_2$. But unfortunately this approach was not successful as well and desired product was not obtained.

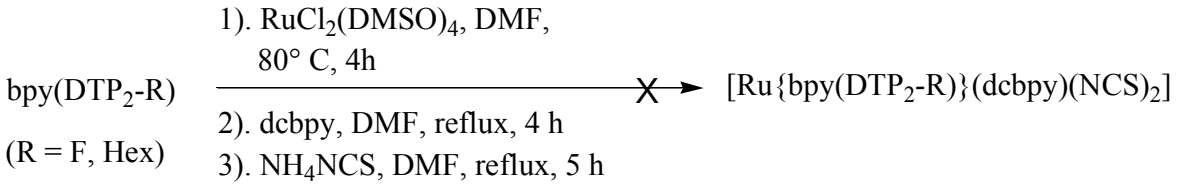

Scheme 7.4: Synthesis of Tris-Heteroleptic complexes **$[Ru\{bpy(DTP_2\text{-}R)\}(dcbpy)(NCS)_2]$** of DTP_2 ligand series by using $RuCl_2(DMSO)_4$ synthon

By taking in account the problem of free dcbpy acid group, we decided to protect carboxylate group of dcbpy as ester and this ester bipyridine complex was used instead of dcbpy. Microwave as well as conventional heating procedure were employed but targeted complexes were not achieved in any case.

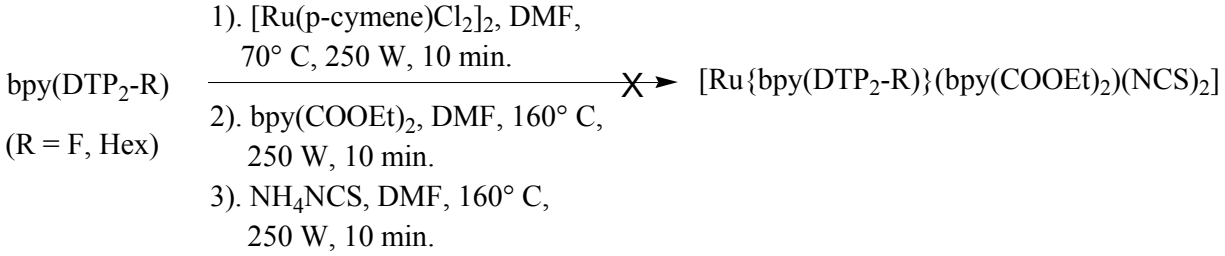

Scheme 7.5: Synthesis of Tris-Heteroleptic complexes **$[Ru\{bpy(DTP_2\text{-}R)\}(dcbpy)(NCS)_2]$** of DTP_2 ligand series by using ester bipyridine complex instead of dcbpy under microwave conditions.

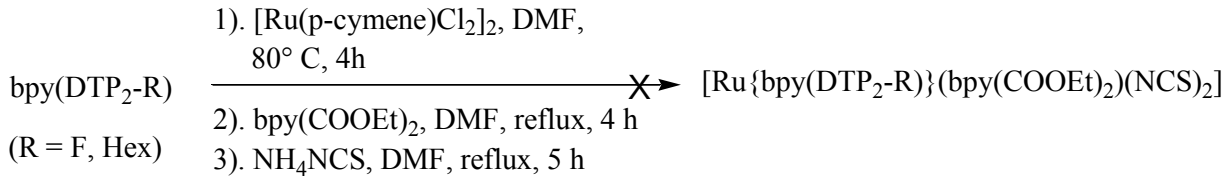

Scheme 7.6: Synthesis of Tris-Heteroleptic complexes **[Ru{bpy(DTP$_2$-R)}(dcbpy)(NCS)$_2$]** of DTP$_2$ ligand series by using ester bipyridine complex instead of dcbpy (conventional heating conditions).

Method of Kuang et al. [**11]** was carried out to obtain [Ru{bpy(DTP$_2$-F)}(dcbpy)(NCS)$_2$] and [Ru{bpy(DTP$_2$-Hex)}(dcbpy)(NCS)$_2$] complexes. This method is different from commonly employed one pot synthesis, so by following this method the mixture of ligand and [Ru(p-cymene)Cl$_2$]$_2$ was refluxed in ethanol for 4 hours to ensure the synthesis of [Ru{bpy(DTP$_2$-R)}(p-cymene)Cl$_2$], that was verified by ^{1}HNMR. Then next steps were carried out in DMF.

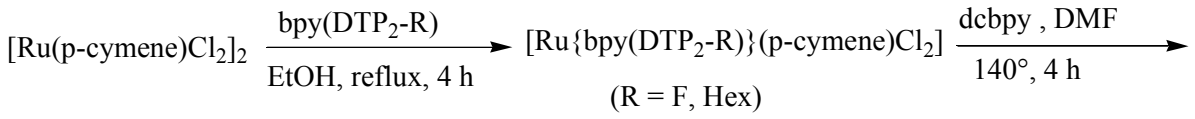

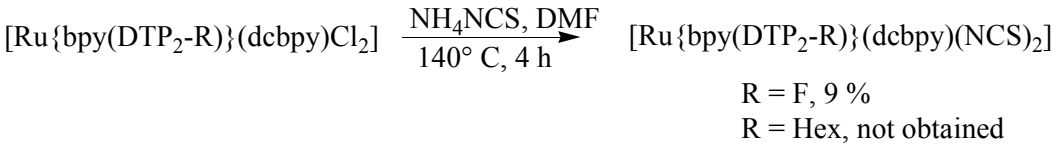

Scheme 7.7: Synthesis of Tris-Heteroleptic complexes **[Ru{bpy(DTP$_2$-R)}(dcbpy)(NCS)$_2$]** of DTP$_2$ ligand series by following the method of Kuang et al., 2006.

As a result [Ru{bpy(DTP$_2$-F)}(dcbpy)(NCS)$_2$] was obtained in low yield (9 %) whereas it was impossible to obtain [Ru{bpy(DTP$_2$-Hex)}(dcbpy)(NCS)$_2$] by following the same reaction conditions. Unidentifiable product was obtained at the end of reaction. As the synthesis of heteroleptic complexes of **bpy(DTP$_2$-R)** series remain problematic, we focused on the characterization of those complexes that we obtain in sufficient amount.

7.2.2. Properties of Tris-Heteroleptic Complexes

7.2.2.1. Absorption properties

UV-vis absorption spectra of complexes are shown in Figure 7.2 whereas the spectroscopic characteristics of all new complexes are gathered in Table 7.6.

The absorption spectra of tris-heteroleptic complexes of **bpy(DTP$_1$-R)** series consist of three bands. Generally the high energy bands in the UV region at 312-314 nm are assigned to intra ligand π-π* charge-transfer transitions of dcbpy. The bands in 406-411 nm region are the characteristic metal-to-ligand charge transfer i.e. dπ(Ru)-π*(bpy) bands. The low energy absorption band located in the range of 534-541 nm should be the result of MLCT arising from the participation of the NCS moieties.

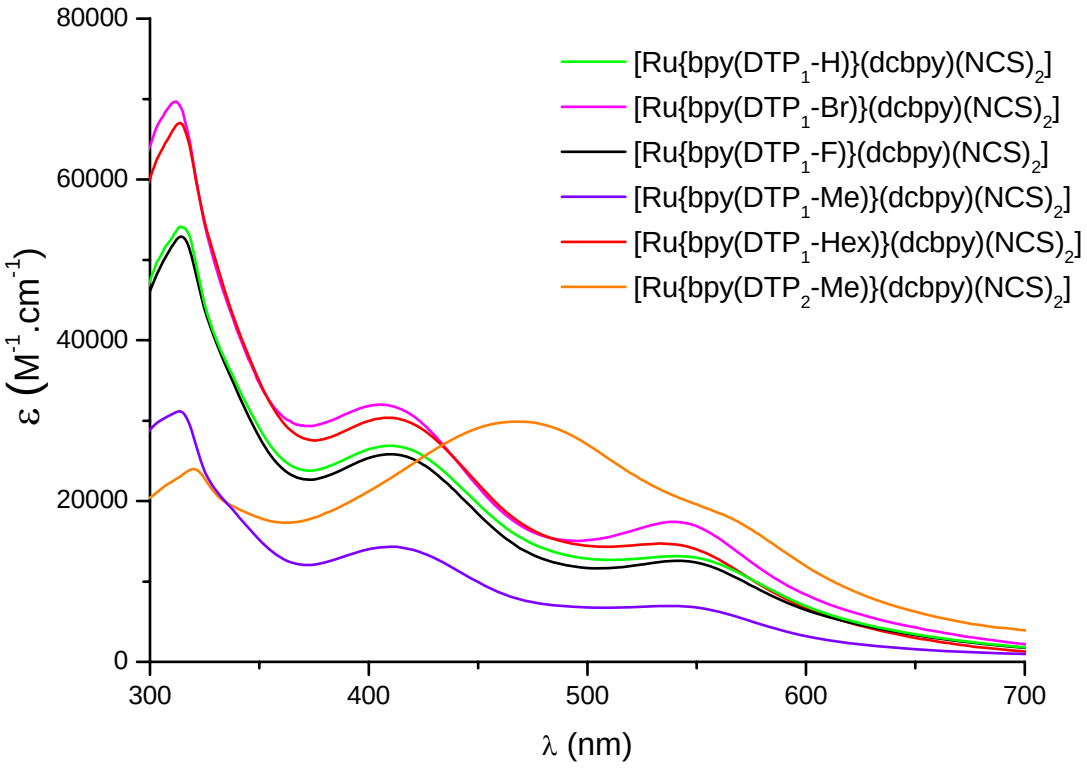

Figure 7.2: Absorption spectra of Tris-Heteroleptic complexes in acetonitrile+DMSO (4:1)

By examining spectra (Fig 7.2) and table 7.6, it is evident that all tris-heteroleptic complexes of bpy(DTP$_1$-R) series gave similar spectra with comparable ε values. [Ru{bpy(DTP$_1$-

Br)}(dcbpy)$(NCS)_2$] has a peak molar extinction coefficient of 69600 $M^{-1}.cm^1$ very closely followed by [Ru{bpy(DTP_1-Hex)}(dcbpy)$(NCS)_2$] that has ε value of 67000 $M^{-1}.cm^1$. [Ru{bpy(DTP_1-H)}(dcbpy)$(NCS)_2$] [Ru{bpy(DTP_1-F)}(dcbpy)$(NCS)_2$] showed 54100 and 52800 $M^{-1}.cm^1$ respectively. [Ru{bpy(DTP_1-Me)}(dcbpy)$(NCS)_2$] exhibited the same trend like other complexes of this series but showed ε value almost half (31100 $M^{-1}.cm^1$) than that of [Ru{bpy(DTP_1-Hex)}(dcbpy)$(NCS)_2$]. Electron donating and electron withdrawing substituents did not show any clear trend towards ε values.

Table 7.6: Absorption properties of Tris-Heteroleptic complexes

Complex	λabs-max (nm)[a]	ε (10^3 $M^{-1}cm^{-1}$)
[Ru{bpy(DTP_1-H)}(dcbpy)$(NCS)_2$]	541 410 314	13.1 26.8 54.1
[Ru{bpy(DTP_1-Br)}(dcbpy)$(NCS)_2$]	540 406 312	17.4 32.0 69.6
[Ru{bpy(DTP_1-F)}(dcbpy)$(NCS)_2$]	540 410 314	12.5 25.8 52.8
[Ru{bpy(DTP_1-Me)}(dcbpy)$(NCS)_2$]	541 411 313	6.9 14.3 31.1
[Ru{bpy(DTP_1-Hex)}(dcbpy)$(NCS)_2$]	534 409 314	14.7 30.3 67.0
[Ru{bpy(DTP_2-Me)}(dcbpy)$(NCS)_2$]	468 320	29.8 23.9

[a] Measured in CH_3CN + DMSO (4:1) at 25°C.

In tris-heteroleptic complex of DTP_2 series, only two distinct absorption bands could be observed: weak band at 320 nm and a broad band from 375 to 600 nm, centered at 468 nm.

In comparison to tris-heteroleptic complexes of **bpy(DTP_1-R)** series (Fig: 7.2), absorption spectra of the complexes of **bpy(DTP_2-R)** series have shown two distinct changes.

(i) 406-411 nm band was significantly red shifted to 468 nm and broadening toward the visible region. That broad band is extended to 625 nm. So, the absorption spectrum is dominated by MLCT transition in the visible region.

(ii) High intensity absorption in the range of 312-314 nm that was observed with **bpy(DTP$_1$-R)** complexes was extremely weakened in **bpy(DTP$_2$-R)** series complexes

The molar extinction coefficient of tris-heteroleptic complex is higher in the MLCT region as compared to the tris-heteroleptic complexes of DTP_1 series. The π delocalization in more conjugated DTP_2 series ligands caused an increase in the molar extinction coefficient.

The absorption spectra of tris-heteroleptic complexes have been compared with their bis-heteroleptic analogues (Fig 7.3).

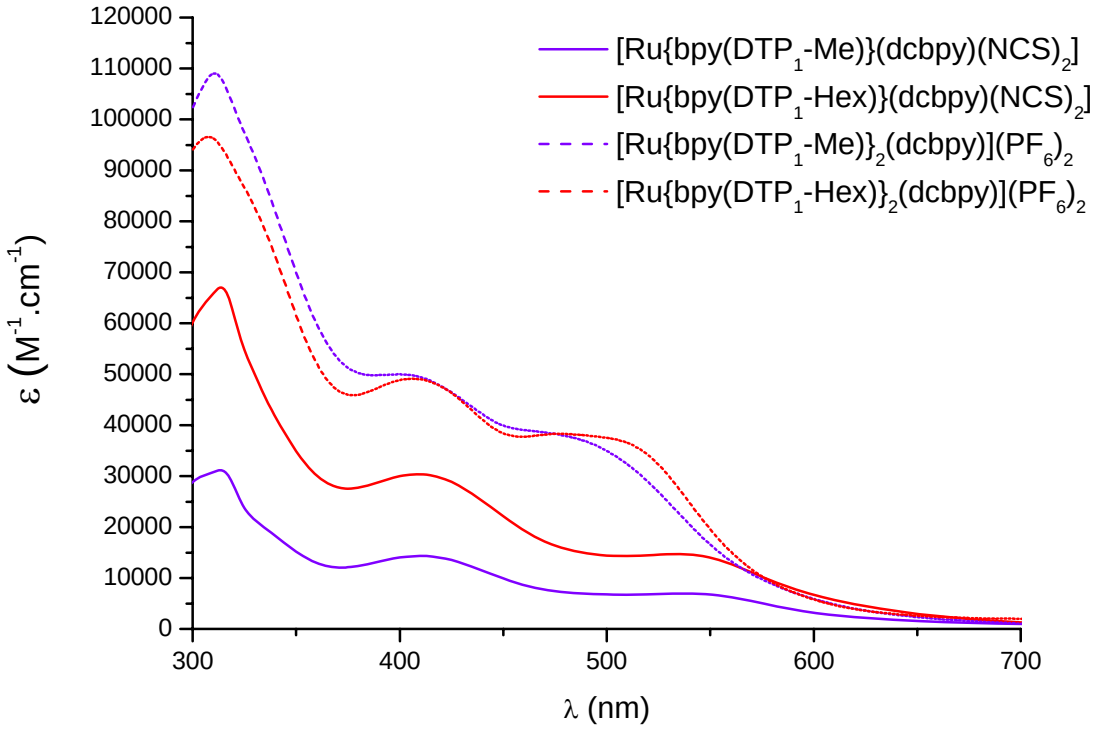

Fig. 7.3: Comparison of absorption spectra of bis-heteroleptic and tris-heteroleptic complexes in acetonitrile + DMSO (4:1)

It is evident that molar extinction coefficient values for bis-heteroleptic complexes are higher than tris-heteroleptic complexes, which are in quite good agreement with the fact that the bands intensities increased with increased number of ligands in the complex.

Both type of complexes showed the first two bands in the same range. But the low energy absorption band located in 534-541 nm MLCT band arising from the participation of the

NCS moieties, did not appear in related bis-heteroleptic complexes without an NCS ligand. In bis-heteroleptic complexes blue shifted band appeared at 461-479 nm.

7.2.2.2. Electrochemical properties

The redox properties of the prepared tris-heteroleptic complexes were monitored by cyclic voltammetry and are given in table 7.7. They show two oxidation waves, the first one corresponds to the Ru^{II}/Ru^{III} couple and is semi-reversible only for [Ru{bpy(DTP_1-F)}(dcbpy)$(NCS)_2$] and irreversible for all other complexes of **bpy(DTP_1)** and **bpy(DTP_2)** series, the second one is irreversible and is attributed to the formation of radical cation on the thiophene as described for the ligands. The oxidation potentials of the Ru^{II}/Ru^{III} couple were found at lower values i.e. at 0.70 V/SCE for the **bpy(DTP_2)** series as a consequence of the expected higher degree of conjugation in the **bpy(DTP_2)** compared to the **bpy(DTP_1)** series.

Table 7.7: Electrochemical properties of Tris-Heteroleptic complexes

Complex	$E_{1/2}$ or Epa (Ru^{III}/Ru^{II}) (V/SCE)[a,d]	Epa (L^+/L) (V/SCE) [a]	$E_{1/2}$ or Epc (L/L^-) (V/SCE)[b,e]
[Ru{bpy(DTP_1-H)}(dcbpy)$(NCS)_2$]	1.00 (irrev.)	1.00 (irrev.)	-1.26 (irrev.)
[Ru{bpy(DTP_1-Br)}(dcbpy)$(NCS)_2$]	1.00 (irrev.)	1.00 (irrev.)	-1.24 (ΔEp=0.160)
[Ru{bpy(DTP_1-F)}(dcbpy)$(NCS)_2$]	0.78 (ΔEp=0.110)	1.08 (irrev.)	-1.27 (ΔEp=0.08)
[Ru{bpy(DTP_1-Me)}(dcbpy)$(NCS)_2$]	0.8 (irrev.)	1.02 (irrev.)	-1.42 (irrev.)
[Ru{bpy(DTP_1-Hex)}(dcbpy)$(NCS)_2$]	0.8 (irrev.)	1.00 (irrev.)	n.d [c]
[Ru{bpy(DTP_2-Me)}(dcbpy)$(NCS)_2$]	0.70 (irrev.)	0.85 (irrev.)	n.d [c]

[a] Oxidation potentials standardized with Fc^+/Fc as internal standard and converted into SCE scale by adding 0.47V ($E_{1/2}Fc^+/Fc$). Recorded in DMF using $Bu_4N^+PF_6^-$ as supporting electrolyte at 100mV/s. [b] First reduction potential. [c]n.d. = not detected. [d]when irreversible Epa should be considered. [e]when irreversible Epc should be considered.

At negative potentials ligand -based reduction was observed, which refers to the transfer of an electron into the bipyridine which is also irreversible. In case of reduction potential complexes bearing electron-donating substituents [Ru{bpy(DTP_1-Me)}(dcbpy)$(NCS)_2$] result in comparatively higher electron density at Ru^{II}, increasing back-bonding and destabilizing the π^* orbitals of the ligands, thereby shifting their reduction potentials to more negative values (-1.42 V/SCE). Whereas the complexes bearing electron-withdrawing substituents [Ru{bpy(DTP_1-Br)}(dcbpy)$(NCS)_2$] and [Ru{bpy(DTP_1-F)}(dcbpy)$(NCS)_2$] result in comparatively less electron density at Ru^{II}, thereby shifting their reduction potentials to comparatively less negative values (-1.24 to -1.27 V/SCE).

In comparison to related homoleptic and bis-heteroleptic complexes, the Ru^{III}/Ru^{II} redox couple in all the examined tris-heteroleptic complexes is shifted to slightly lower potentials. In DTP_1 series, 0.78-1.00 V/SCE for tris-heteroleptic complexes whereas 0.96-1.05 V/SCE in case of homoleptic analogues. In DTP_2 series, 0.78-1.00 V/SCE for tris-heteroleptic complexes whereas 0.96-1.05 V/SCE in homoleptic analogues. In DTP_2 series, 0.70 V/SCE for tris-heteroleptic complexes whereas 0.76-0.80 for the related homoleptic complexes. Same trend of shifting towards lower potentials is noticed when comparison was carried out with bis-heteroleptic analogues (0.80 V/SCE vs 0.93 V/SCE). This behaviour corresponds to the monoanionic nature of ligands, which destabilize the t_{2g} orbitals of the Ru^{II} ion, making it comparatively easier to oxidize.

As follows from the preceding discussion, the oxidation is facilitated for tris-heteroleptic complexes in contrast to bis-heteroleptic and homoleptic analogues.

7.2.2.3. Emission properties

All tris-heteroleptic complexes of **bpy(DTP_1-R)** and **bpy(DTP_2-R)** series were emitting in fluid solution of acetonitrile+DMSO (4:1) (Table 7.8) at room temperature. In DTP_1 series, when the complex was excited at at wavelengths given in table 7.8, two distinct emission bands were observed in most of the cases, one centered in the 450-510 nm region, depending on the ligand, bearing a close resemblance in both energy and lifetime with the free ligand fluorescence, and one in the red part of the spectrum in the 542-770 range originated by the typical ^{3}MLCT radiative deactivation. In **[Ru{bpy(DTP_1-H)}(dcbpy)$(NCS)_2$], [Ru{bpy(DTP_1-**

Hex)}(dcbpy)(NCS)$_2$] and **[Ru{bpy(DTP$_1$-Me)}(dcbpy)(NCS)$_2$]** only LC type emission was observed. No MLCT emission was observed. In **[Ru{bpy(DTP$_1$-Br)}(dcbpy)(NCS)$_2$]** and **[Ru{bpy(DTP$_1$-F)}(dcbpy)(NCS)$_2$]** significantly red shifted ^{3}MLCT emission maxima (750-770 nm *vs* 691-698 nm) was observed as compared to the corresponding homoleptic complexes. So, it can be concluded that in this series, the nature of the substituent had a strong impact on the emission maxima, the ligand with electron withdrawing substituents led to the highest emission maxima. Such increase could be due to an increase in molecular dipole moment by the electron withdrawing bromine and fluorine groups. Another explanation could be the increase of the inter-system crossing yield due to the bromine or fluorine groups.

Table 7.8: Emission properties of tris-heteroleptic complexes

Complex	λem-max[a] Ligand/ MLCT based	λ_{excit} (nm)
[Ru{bpy(DTP$_1$-H)}(dcbpy)(NCS)$_2$]	510 (Ligand) No MLCT emission	410 540
[Ru{bpy(DTP$_1$-Br)}(dcbpy)(NCS)$_2$]	450 (Ligand) 750 (MLCT)	320 530
[Ru{bpy(DTP$_1$-F)}(dcbpy)(NCS)$_2$]	475 (Ligand) 770 (MLCT)	315 540
[Ru{bpy(DTP$_1$-Me)}(dcbpy)(NCS)$_2$]	453 (Ligand) No MLCT emission	315 540
[Ru{bpy(DTP$_1$-Hex)}(dcbpy)(NCS)$_2$]	475 (Ligand) No MLCT emission	310 530
[Ru{bpy(DTP$_2$-Me)}(dcbpy)(NCS)$_2$]	435 (Ligand) No MLCT emission	320 470

[a] Photomultiplier corrected emission maxima for the complexes in acetonitrile + DMSO (4:1) A< 0.05.

In DTP$_2$ series, after excitation at wavelengths given in table 7.8, two emission bands were observed, one centered in the 435 nm region, being that of the LC type. Whereas, no MLCT emission was observed.

7.2.2.4. Computational analysis *(Coll. A. Monari, X. Assfeld, CBT-SRSMC)*

To elucidate the electronic structure and gain further insight into the electrochemical and photophysical properties of tris-heteroleptic complexes quantum mechanical calculations were performed.

The tris-heteroleptic complexes have been optimized at DFT level with B3LYP functional. Excited states have been computed at TD-DFT level with CAM-B3LYP correlation exchange functional. The solvatochromic effects due to the environment have been taken into account by polarizable continuum model (PCM) with dielectric constant of acetonitrile. Geometry optimizations were performed with LANL2DZ [**12]** basis. Ru inner electrons were described with pseudopotentials. For excited state computations the quality of the basis was checked against a triple zeta one. The computed UV/Vis. spectrum of bpy(DTP_1-F) complex was superimposable with the experimental one. We decided to use relatively small LANL2DZ basis. The latter is certainly not sufficient to provide a qualitative agreement with experimental data, but the main feature of the spectrum can be inferred and the nature of the transition can be easily interpreted. The computed principal transition in the lower energy region of the spectrum can be seen (Table 7.9) for the two families. Coherently with experimental results the **DTP_2** series is comparatively red-shifted with respect to the **DTP_1** members, the intensities in visible region are also higher. Note also that the low lying spectrum of the **DTP_2** family is composed of a series of transition all having almost the same intensity, an occurrence that can be related to the extended plateau observed in the experimental spectrum, although in the computed result the low frequency transition appears closer between them than in the experimental one.

Table 7.9: Complexes TDDFT computed principal excitation wavelengths and oscillator strength

X	[Ru{bpy(DTP_1-R)(dcbpy)$(NCS)_2$] λ(nm), (f)[a]	[[Ru(DTP_2-R)(dcbpy)$(NCS)_2$] λ(nm), (f)[a]
H	539.28 (0.03) 456.82 (0.29) 429.96 (0.19) 398.98 (0.29)	546.83 (0.03) 464.03 (0.71) 444.60 (1.30) 423.22 (1.15) 413.41 (0.94)
Br	538.58 (0.03) 456.61 (0.29) 430.69 (0.19) 399.09 (0.30)	545.94 (0.04) 462.20 (0.69) 441.15 (1.06) 420.04 (1.14) 410.18 (1.12)
F	538.65 (0.03) 456.63 (0.29) 430.56 (0.18) 399.02 (0.30)	546.23 (0.03) 465.12 (0.88) 449.95 (1.60) 427.35 (1.15) 417.37 (0.60)
Me	539.52 (0.03) 456.89 (0.30) 429.75 (0.20) 399.00 (0.33)	546.88 (0.03) 464.28 (0.75) 445.94 (1.37) 424.32 (1.15) 414.02 (0.87)
Hex	539.50 (0.03) 456.89 (0.29) 429.74 (0.20) 399.00 (0.33)	546.57 (0.03) 464.32 (0.76) 445.41 (1.35) 423.98 (1.17) 414.06 (0.83)

[a] oscillator strength in parentheses

In order to better analyse the excited states nature we considered Natural Transition Orbitals (NTOs) [**13]** representation of the electronic transition as we have already done for homoleptic complexes. “Occupied” NTO can be seen as the “hole” orbital, i.e. the orbital from which electron is removed during transition, while “virtual” NTO is the orbital in which electron is placed in the excited state.

NTOs for transition in **[Ru{bpy(DTP$_1$-F)(dcbpy)(NCS)$_2$]** at different wavelengths are shown in table 7.10, (note that the other substituents do not qualitatively alter the orbitals). An analysis of transitions at 550 and 500 nm clearly indicated the shifting of electron density from from Ru with strong participation of NCS, to dcbpy. In both cases the transitions are mainly of MLCT nature and electron density in excited state is driven towards reactions favourable for the injection of electrons into semiconductor. Two occupied/virtual orbital couples were required to entirely describe the transition occurring at 460 nm. This transition seems a mixture of MLCT and LLCT transitions, from that MLCT part might be useful for light harvesting process. At 430 nm the charge density is shifting from Ru with strong participation of NCS, to ancillary ligand, making injection from this transition more problematic. Transition at 400 nm is described by two occupied/virtual orbital couples and is the mixture of MLCT and LLCT transitions. In LLCT transition charge density that initially lies on NCS ligand with weak contribution of ancillary ligand shifted completely to the ancillary ligand. Whereas in MLCT contribution it is shifted from NCS ligand to dcbpy and could play role in injection of the excited state electrons into semiconductors to carry out light harvesting process.

Table 7.10: NTOs isodensity surface of [Ru{bpy(DTP$_1$-F)(dcbpy)(NCS)$_2$] at different wavelengths

Transition Wavelength (nm)	Occupied	Virtual
550	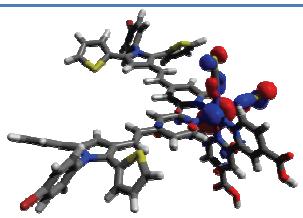	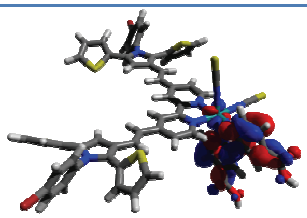
500	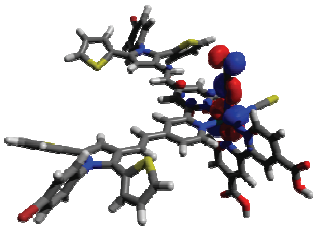	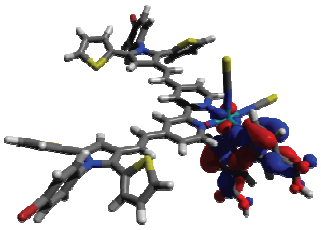
460	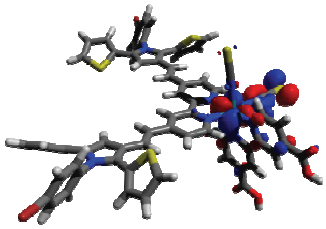 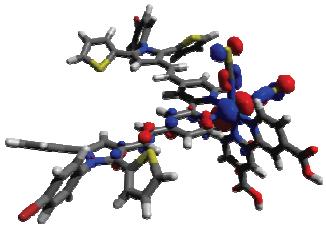	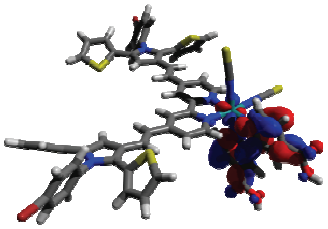 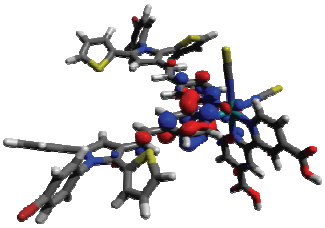

430	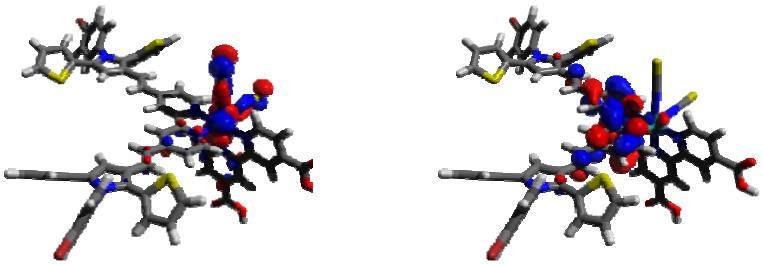
400	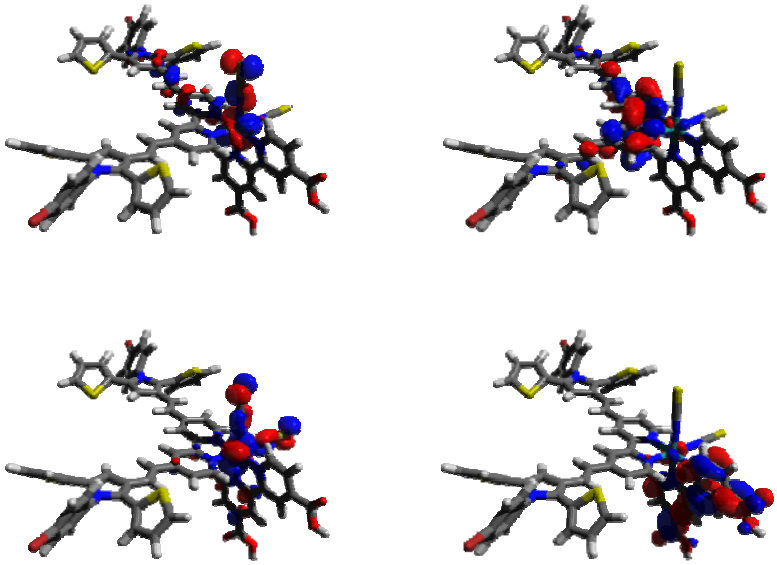

NTOs for transition of **[Ru{bpy(DTP$_2$-F)(dcbpy)(NCS)$_2$]** at different wavelengths are shown in Table 7.11, At 560 and 505 nm, the electron density shifted from Ru with strong participation of NCS, to dcbpy. So both these transitions can be useful in sensitization process. Transition at 475 nm is described by two occupied/virtual orbital couples and is the mixture of MLCT and LLCT transitions. In LLCT transition electron density is shifted from dcbpy to ancillary ligand. At 465 nm intraligand charge transfer (ILCT) is noticed in both couples of occupied/virtual orbital. The electron density seems to be delocalized at ancillary ligand. At 440 nm one occupied/virtual orbital couple showed the electron density at NCS ligand with involvement of ancillary ligand that completely shifted to the ancillary ligand during transition. Whereas the other orbital couple showed the useful transfer of charge from one NCS to dcbpy. At 425 nm

both orbital couples showed LLCT, where electron density located at NCS ligand with involvement of ancillary ligand as well shifted completely on the ancillary ligand as a result of transition.

Table 7.11: NTOs isodensity surface of [Ru{bpy(DTP$_2$-F)(dcbpy)(NCS)$_2$] at different wavelengths

Transition Wave length (nm)	Occupied	Virtual
560	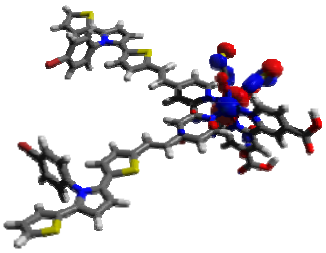	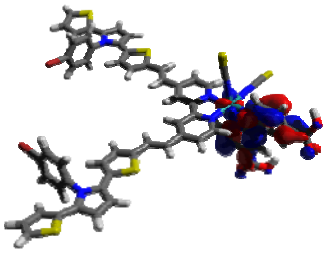
505	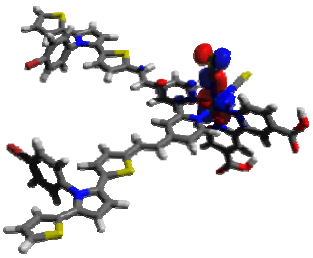	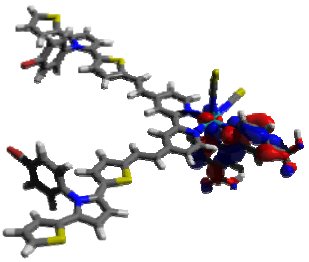

475

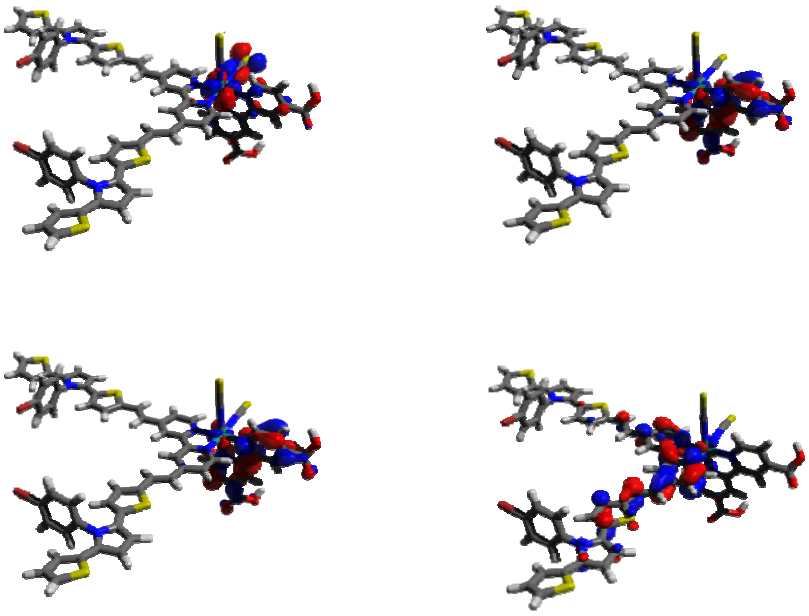

465

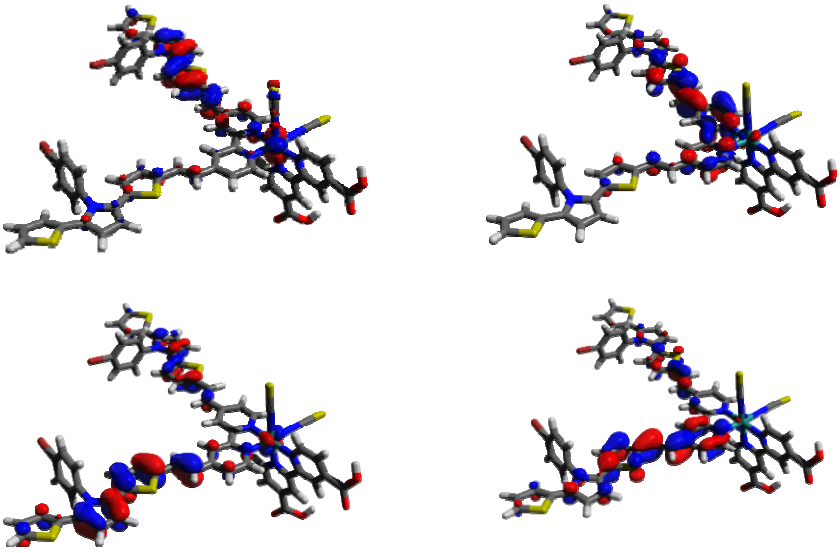

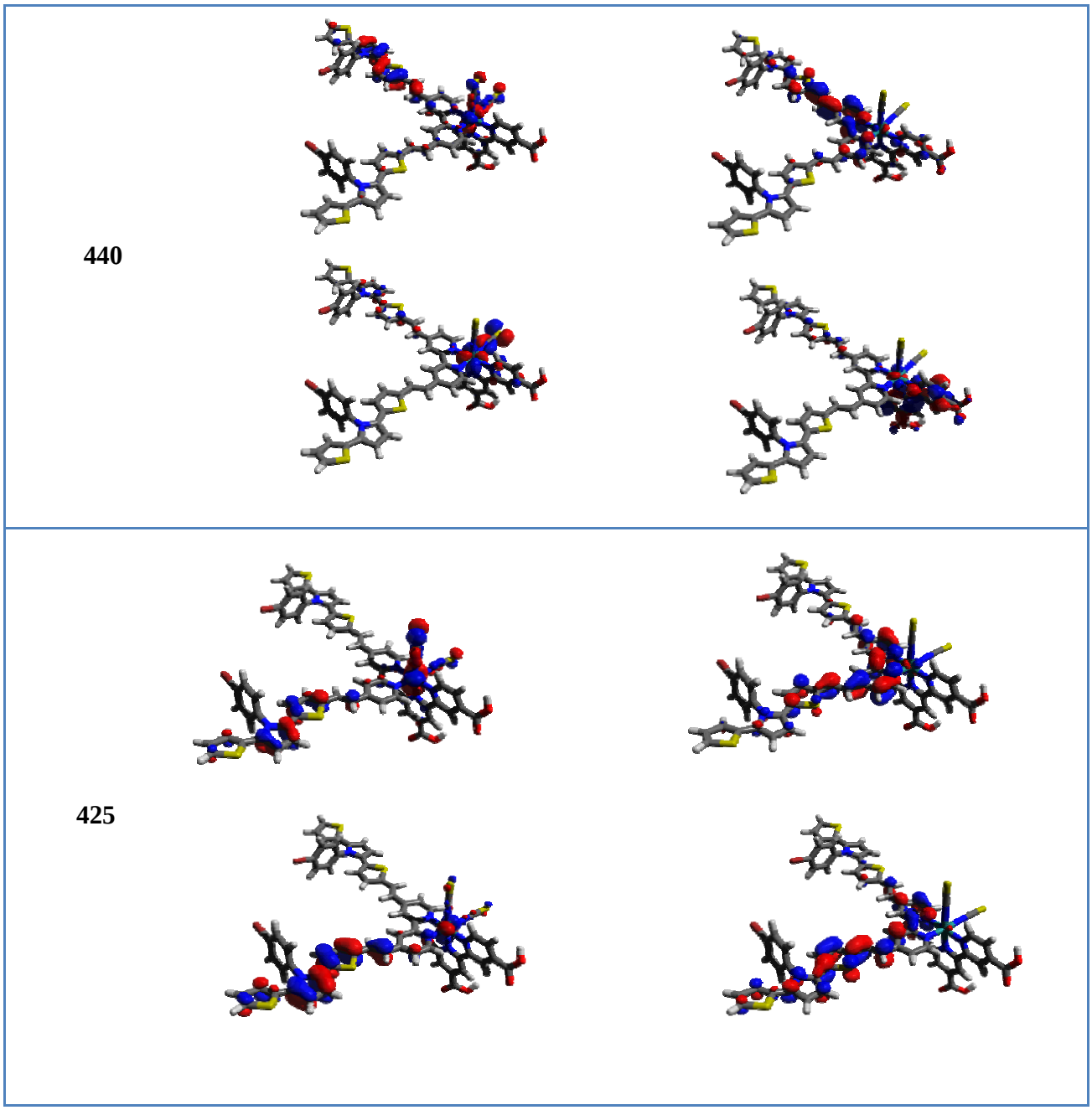

By detailed analysis and comparison of NTOs for transition of the **[Ru{bpy(DTP$_1$-R)(dcbpy)(NCS)$_2$]** and **[Ru{bpy(DTP$_2$-R)(dcbpy)(NCS)$_2$]** at different wavelengths. It is noticed that in heteroleptic complexes of DTP$_2$ series only low energy transitions which have a weak oscillator strength, may involve in injection of excited state electrons to the semiconductor surface, so can be useful in sensitization process. Most of high energy transitions are ligand based.

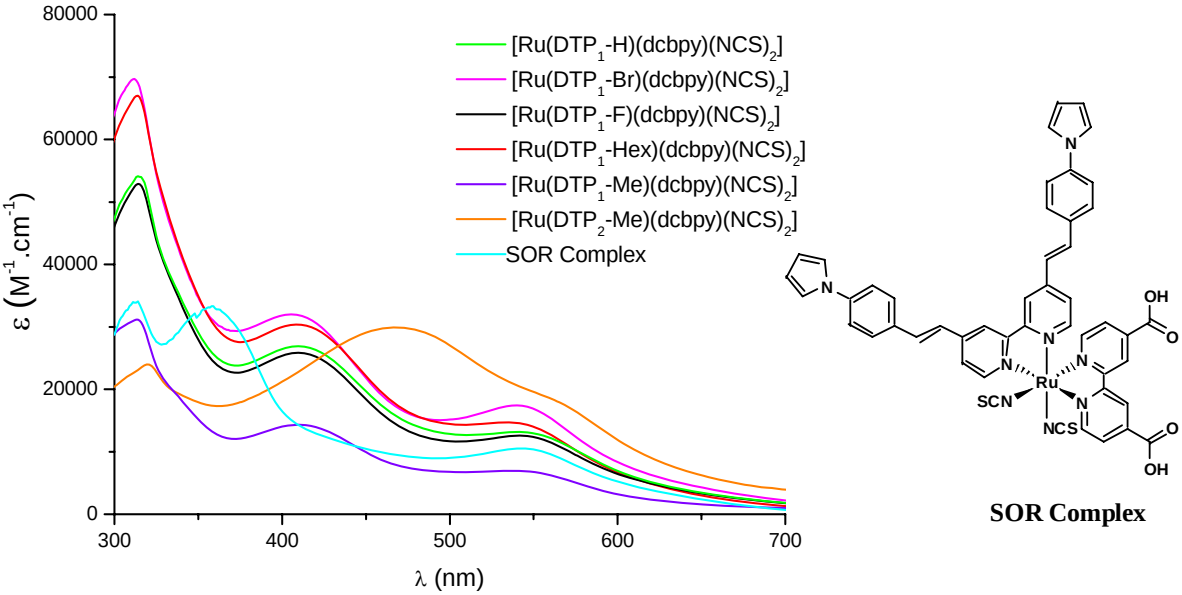

Figure 7.4: Absorption spectra of Tris-Heteroleptic complexes

So the new tris-heteroleptic complexes have the advantage of wide absorption range in visible domain with higher molar extinction coefficients.

7.4.Preliminary photovoltaic measurements *(Coll. S. Caramori, C.A. Bignozzi, Ferrara, Italy)*

7.4.1. Absorption Study of sensitized TiO_2

Due to time constraint, the photovoltaic properties have been measured only for two tris-heteroleptic complexes: **[Ru{bpy(DTP$_1$-Hex)(dcbpy)(NCS)$_2$]** and **[Ru{bpy(DTP$_2$-Me)(dcbpy)(NCS)$_2$]**. The dyes were chemisorbed on TiO_2 films from a solvent mixture (EtOH/CH_3CN/THF/*t*BuOH (1/1/1/1)) and the sensitization was controlled by UV-Vis spectroscopy. **Z907** [**15**,**16]** was used as reference dye (Figure 7.5).

In heteroleptic complexes of DTP_1 ligands low energy as well some of high energy transitions are of MLCT nature, so can play significant role in light harvesting process.

It can be concluded that extended π-delocalization in DTP_2 ligand series is a hindrance for the injection process and it delocalized the electronic density at the ancillary ligand and do not shift it towards the anchoring ligand.

7.3.Conclusions about the properties of heteroleptic complexes

It is noticed that the molar extinction coefficient values for bis-heteroleptic complexes are quite higher than tris-heteroleptic complexes (Figure 7.3). Both classes of complexes showed the first two bands in almost the same range whereas the low energy MLCT band located in 534-541 nm arising from the participation of the NCS moieties did not appear in related bis-heteroleptic complexes that are without an NCS ligand. In bis-heteroleptic complexes blue shifted band 461-479 nm was appeared. From these observations it can be concluded that bis-heteroleptic complexes are very promising in terms of molar extinction coefficient values, absorption domain and stability.

In tris-heteroleptic complexes [Ru{bpy(DTP_2-R)(dcbpy)$(NCS)_2$] series offered a promising absorption range in the visible domain with significantly higher molar extinction coefficient all along MLCT region as compared to [Ru{bpy(DTP_1-R)(dcbpy)$(NCS)_2$] (Fig: 7.4). When the new tris-heteroleptic complexes were compared with the best tris-heteroleptic complex so far reported [**14]** by our group SOR, [Ru{bpy(DTP_1-R)(dcbpy)$(NCS)_2$] series showed much higher molar extinction coefficients in the UV-Vis region (312-314 nm) and second MLCT band region (534-541 nm). Whereas very useful red shift was observed in first MLCT region (406-411 nm vs 358 nm) with comparable ε value. [Ru{bpy(DTP_2-R)(dcbpy)$(NCS)_2$] complex also exhibited promising absorption range in the visible domain with significantly higher ε value as compared to SOR complex.

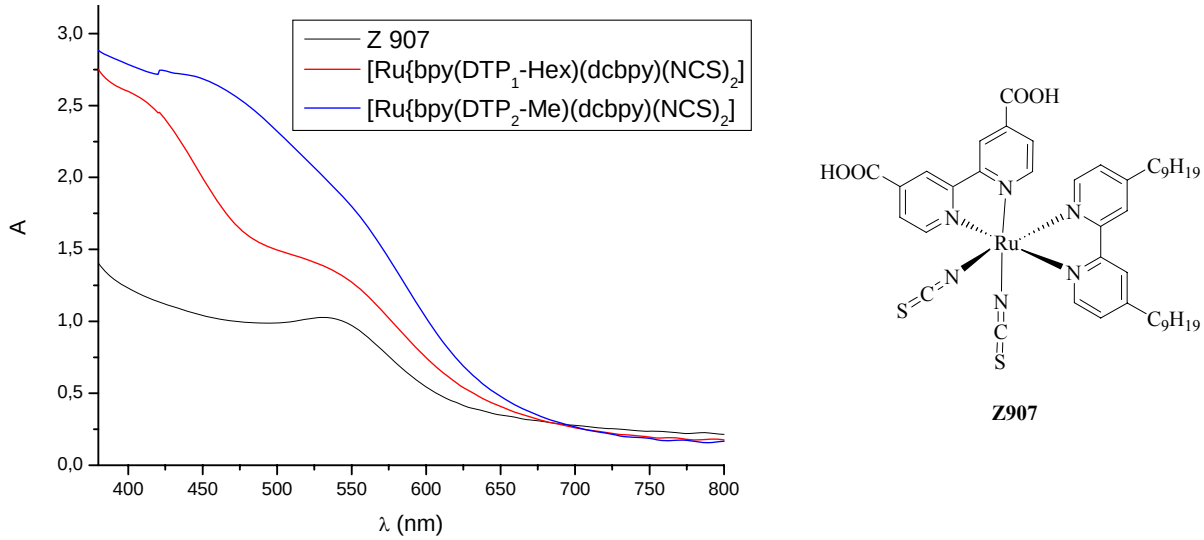

Figure 7.5: Absorption spectra of TiO_2 thin films sensitized with **[Ru{bpy(DTP$_1$-Hex)(dcbpy)(NCS)$_2$]**, **[Ru{bpy(DTP$_2$-Me)(dcbpy)(NCS)$_2$]** and **Z907**.

Consistently with their higher molar extinction coefficients, the electrodes sensitized by our heteroleptic dyes exhibit much higher optical densities than the reference compound (**Z 907**), reaching values close to 3 in the case of **[Ru{bpy(DTP$_2$-Me)(dcbpy)(NCS)$_2$]**. The light harvesting in the 400-600 nm region can be considered almost complete (>90%) for both **[Ru{bpy(DTP$_1$-Hex)(dcbpy)(NCS)$_2$]** and **[Ru{bpy(DTP$_2$-Me)(dcbpy)(NCS)$_2$]**.

7.4.2. J/V Curves

DSSCs were then assembled using the new dyes. A mediator made of 1-propyl-3-methly-imidazolium iodide (PMII, 0.6 M), LiI (0.1 M) and I_2 (0.2 M) in methoxypropionitrile was used. The J/V curves for each dye along with their efficiency are given in fig. 7.6; Table 7.12 and 7.13.

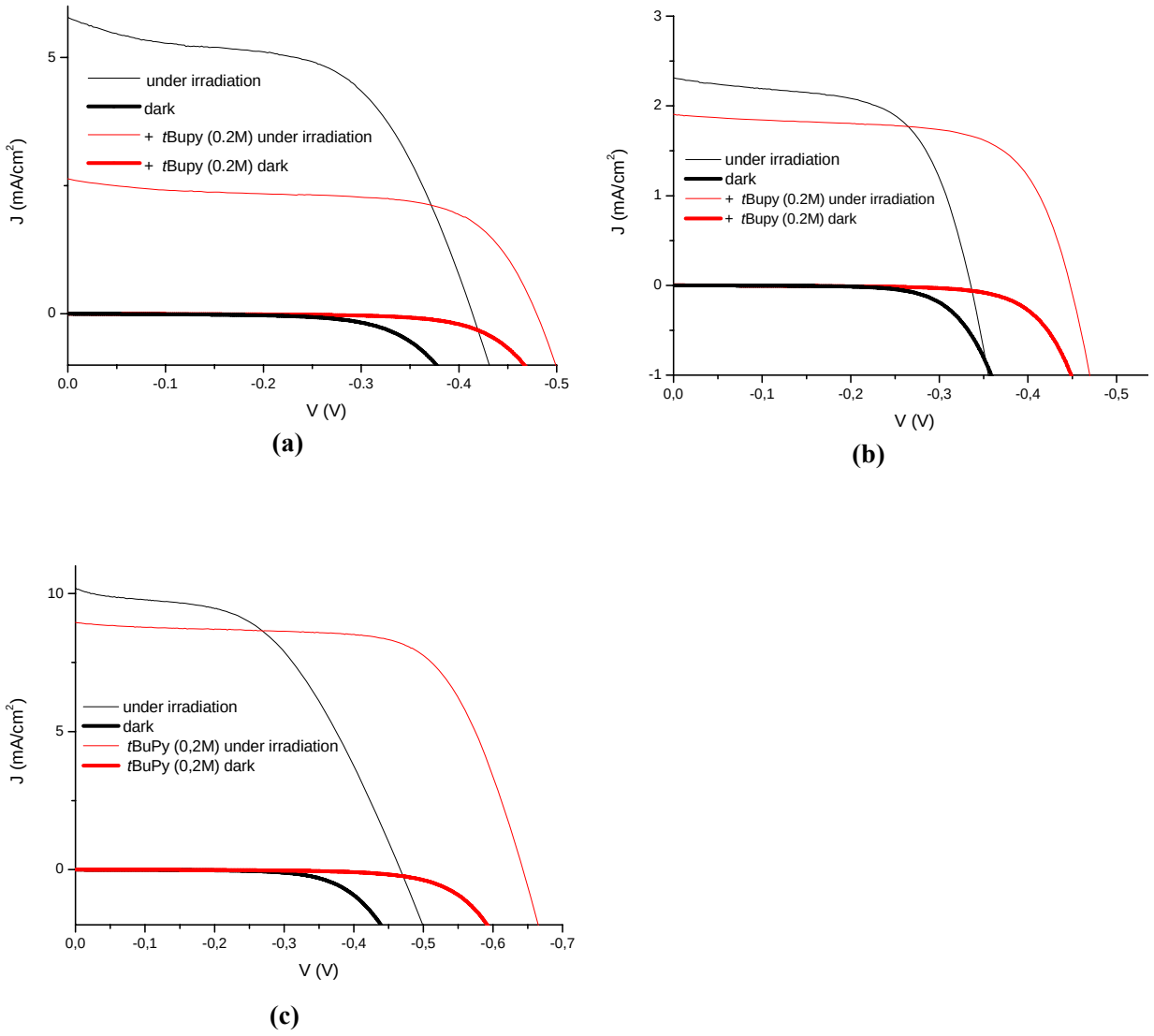

Figure 7.6: J/V curves for (a) **[Ru{bpy(DTP$_2$-Me)(dcbpy)(NCS)$_2$]** (b) **[Ru{bpy(DTP$_1$-Hex)(dcbpy)(NCS)$_2$]** (c) **Z907**

Table 7.12: J/V values and efficiency of dyes in presence of electrolyte (0.6 M PMII) + 0.1 M LiI + 0.2 M I_2

Dye	J (mA/cm^2)	Voc (V)	FF	η
[Ru{bpy(DTP$_1$-Hex)(dcbpy)(NCS)$_2$]	2.3	0.34	0.6	0.47
[Ru{bpy(DTP$_2$-Me)(dcbpy)(NCS)$_2$]	5.7	0.41	0.56	1.3
Z907	10.2	0.46	0.5	2.37

Table 7.13: J/V values and efficiency of dyes in presence of electrolyte (0.6 M PMII) + 0.1 M LiI + 0.2 M I_2 + 0.2 M *t*Bupy

Dye	J (mA/cm^2)	Voc (V)	FF	η
[Ru{bpy(DTP$_1$-Hex)(dcbpy)(NCS)$_2$]	1.91	0.45	0.66	0.57
[Ru{bpy(DTP$_2$-Me)(dcbpy)(NCS)$_2$]	2.63	0.41	0.62	0.62
Z907	8.94	0.64	0.66	3.8

The performance of both **[Ru{bpy(DTP$_2$-Me)(dcbpy)(NCS)$_2$]** and **[Ru{bpy(DTP$_1$-Hex)(dcbpy)(NCS)$_2$]** are lower than those of Z907 when employed with the standard electrolyte (PMII, LiI, I_2).

Since we suspected a possible recombination of injected electrons with the oxidized form of the mediator (I_3^-) at the surface of TiO_2, the sensitized anode was treated with a solution of 4-*t*Bu-pyridine (*t*Bupy) [**17]** known to prevent this recombination process. The addition of *t*Bupy (0.2 M) greatly enhanced the relative performance in the case of Z907 and **[Ru{bpy(DTP$_1$-Hex)(dcbpy)(NCS)$_2$]** (Fig. 7.6). A large improvement in photovoltage (Voc) (from 0.34 to 0.45 V for the later dye) and fill factor at the price of a marginal diminution in photocurrent. In the case of **[Ru{bpy(DTP$_2$-Me)(dcbpy)(NCS)$_2$]**, the addition of *t*Bupy was detrimental, since the enhancement in photovoltage was offset by a nearly halved photocurrent. The slight decrease of photocurrent occurring using *t*Bupy is a consequence of concomitant raising of conduction band edge of TiO_2. The lowered photocurrent is generally compensated by an increase of the Voc. This occurred for Z907 and **[Ru{bpy(DTP$_1$-Hex)(dcbpy)(NCS)$_2$]** but not for **[Ru{bpy(DTP$_2$-Me)(dcbpy)(NCS)$_2$]** indicating a possible competition between excited state deactivation and charge injection with latter dye.

In order to improve the performance, a cobalt based electrolyte, optimized for bulky donor/acceptor organic dyes was employed to verify whether the blocking effect of the DTP moieties could be exploited in the case of non corrosive electrolytes. The $Co(bpy)_3^{2+}$/ $Co(bpy)_3^{3+}$ couple was used instead of the usual $Co(DTB)_3^{2+}$/$Co(DTB)_3^{3+}$ (DTB = 4,4-ditertiobutyl-2,2'-bipyridine) [**18]** for the following reasons : 1) $Co(bpy)_3^{2+}$ is smaller and less prone to diffusional limitations 2) dye reduction is faster as compared to $Co(DTB)_3^{2+}$ 3) it leads to a slightly better Voc than $Co(DTB)_3^{2+}$ due to its higher $E_{1/2}$. However $Co(bpy)_3^{2+}$ gives rise to fast recombination processes and requires a dye with good passivating properties to be successfully employed. Thus this electrolyte represents a demanding test to prove the passivating abilities of the new dyes. It

must be noted that in this case Z907 does not represent an optimal reference. The best results with this kind of cobalt electrolytes are obtained with bulky donor/acceptor dyes of the type D35 [**18**].

As shown in Fig.7.7, Z907 is considerably superior. The photocurrent and Voc generated in this case from irradiation of both **[Ru{bpy(DTP$_2$-Me)(dcbpy)(NCS)$_2$]** and **[Ru{bpy(DTP$_1$-Hex)(dcbpy)(NCS)$_2$]** are lower than using the iodide-based mediator.

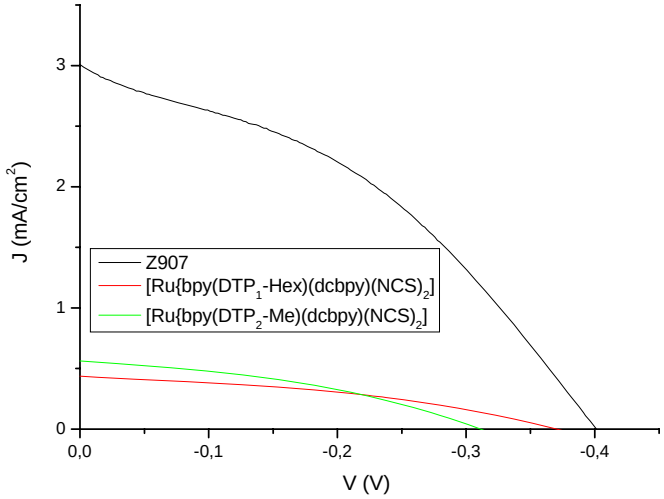

Figure 7.7: J/V curves for heteroleptic complexes and Z907 in presence of $Co(Bpy)_3^{2+}$/ $Co(Bpy)_3^{3+}$ couple. $Co(Bpy)_3^{2+}$ (0.18 M), $Co(Bpy)_3^{3+}$ (0.056 M), Li+ (0.1 M), *t*Bupy (0.2 M) in acetonitrile.

7.4.3. IPCE Measurements

The IPCE spectra were then realized. The performance of both **[Ru{bpy(DTP$_2$-Me)(dcbpy)(NCS)$_2$]** and **[Ru{bpy(DTP$_1$-Hex)(dcbpy)(NCS)$_2$]** are lower than those of Z907 that is quite consistent with the observations made from the J/V curves.

The addition of 0.2 M *t*BuPy only causes a small decrease in the photoconversion of Z907 and **[Ru{bpy(DTP$_1$-Hex)(dcbpy)(NCS)$_2$]**, but a considerable reduction in the case of **[Ru{bpy(DTP$_2$-Me)(dcbpy)(NCS)$_2$]**. Nevetheless **[Ru{bpy(DTP$_2$-Me)(dcbpy)(NCS)$_2$]** was always superior to **[Ru{bpy(DTP$_1$-Hex)(dcbpy)(NCS)$_2$].**

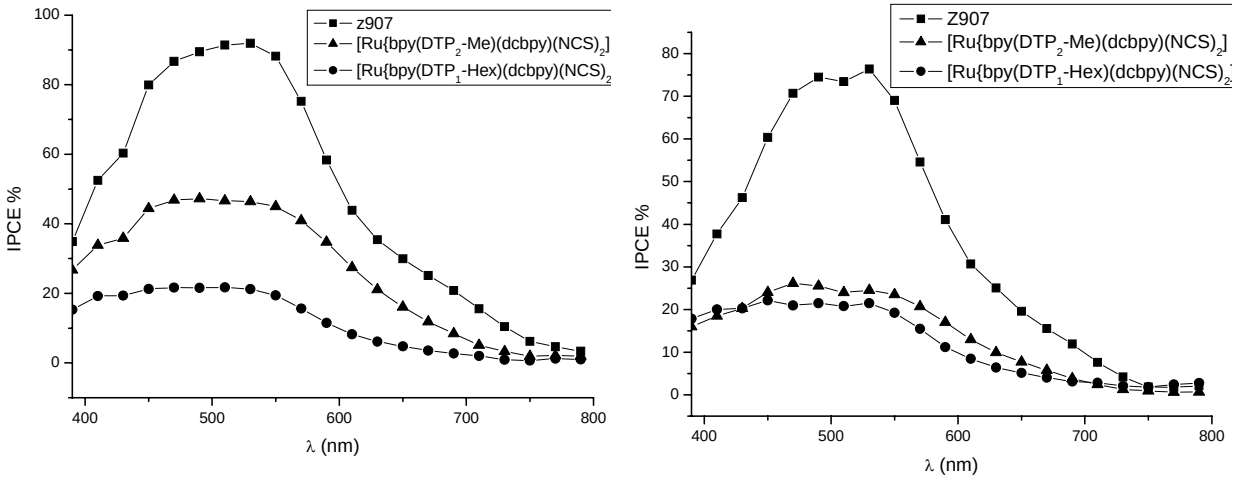

(a) **(b)**

Figure 7.8: IPCE spectra **(a)** heteroleptic complexes and Z907 **(b)** heteroleptic complexes and Z907 in presence of 0.2 M *t*BuPy

7.5. Conclusions

As demonstrated above, the new tris-heteroleptic complexes especially **[Ru{bpy(DTP_2-Me)(dcbpy)$(NCS)_2$]** act as strong light absorbers in the visible region with higher molar extinction coefficients. The orbital energies of these complexes seemed to be appropriately positioned with respect to the conduction band of TiO_2 and the redox potential of the electrolyte on the basis of electrochemistry results. So, according to these results the new complexes were supposed to be potential candidates for light-harvesting applications, in particular for DSSCs.

Consistently with their higher molar extinction coefficients, the electrodes sensitized by heteroleptic dyes exhibit much higher optical densities than the reference compound (**Z 907**). But preliminary photovoltaic measurements showed quite different behaviour. The J/V values and performance of both **[Ru{bpy(DTP_2-Me)(dcbpy)$(NCS)_2$]** and **[Ru{bpy(DTP_1-Hex)(dcbpy)$(NCS)_2$]** are lower than those of Z907 when employed with the standard electrolyte (PMII, LiI, I_2). IPCE spectra is also consistent with these observations

The reasons of the relatively poor performance of the new dyes are not fully understood and further investigations are needed. Limitations arising from poor light harvesting are obviously ruled out. Thermodynamic limitations in dye regeneration kinetics should not be probable based on the oxidation potentials of the dyes (> 0.6 V vs SCE see Table 7.7). In

contrast, electronic/steric effects could be involved since the bulky DTP moiety could impede an efficient access of iodide to Ru(III) centers. This may also explain the unexpectedly low performance with the cobalt electrolyte.

7.6. References

[1] Wang, P.; Zakeeruddin, S.M.; Moser, J.E.; Nazeeruddin, M.K.; Sekiguchi, T.; Grätzel, M. *Nat. Mater.* 2003, **2**, 402.

[2] Hirata, N.; Lagref, J.-J.; Palomares, E.J.; Durrant, J.R.; Nazeruddin, M.K.; Grätzel, M.; Di Censo, D. *Chem. Eur. J*. 2004, **10**, 595.

[3] Wang, P.; Zakeeruddin, S.M.; Moser, J.E.; Humphry-Baker, R.; Comte, P.; Aranyos, V.; Hagfeldt, A.; Nazeeruddin, M.K.; Grätzel, M. *Adv. Mater*. 2004, **16**, 1806.

[4] Wang, X.-Y.; Del Guerzo, A.; Schmehl, R.H. *J. Photochem. Photobiol. C: Photochem. Rev*. 2004, **5**, 55.

[5] Kim, J.-J.; Choi, H.; Kim, C. Kang, M.-S.; Kang, H.S.; Ko, J. *Chem. Mater.* 2009, **21**, 5719.

[6] Song, H.-K.; Park, Y.H.; Han, C.-H.; Jee, J.-G. *J. Ind. Eng. Chem.* 2009, **15**, 62.

[7] Willinger, K.; Fischer, K.; Kisselev, R.; Thelakkat, M. *J. Mater. Chem.* 2009, **19**, 5364.

[8] Yin, J.-F.; Chen, J.-G..; Lu, Z.-Z.; Ho, K.-C.; Lin, H.-C.; Lu, K.-L. *Chem. Mater.* 2010, **22**, 4392.

[9] Chandrasekharam, M.; Rajkumar, G.; Rao, C.S.; Suresh, T.; Reddy, M.A.; Reddy, P.Y.; Soujanya, Y.; Takeru, B., Ho, Y. J.; Nazeeruddin, M.K.; Grätzel, M. *Synt. Met.* 2011, **161**, 1098.

[10] Han, W.-S.; Han, J.-K.; Kim, H.-Y.; Choi, M.J.; Kang, Y.-S. ; Pac, C.; Kang, S.O. *Inorg. Chem*. 2011, **50**, 3271.

[11] Kuang, D.; Ito, S.; Wenger, B.; Klein, C.; Moser, J.-E.; Humphry- Baker, R.; Zakeeruddin, S.M.; Grätzel, M. *J. Am. Chem. Soc.* 2006, **128,** 4146.

[12] Dunning Jr, T.H.; Hay, P.J. *In Modern Theoretical Chemistry; Schaefer, H. F., III, Ed.; Plenum; New York, 1976; Vol. 3, pp 1- 28.*

[13] Monari, A.; Very, T.; Rivail J.-L.; Assfeld, X. *Comput. Theor. Chem.*, 2011, DOI: 10.1016/j.comptc.2011.1011.1026

[14] Grabulosa, A.; Martineau, D.; Beley, M.; Gros, P.C.; Cazzanti, S.; Caramori, S.; Bignozzi, C.A. *Dalton Trans.* 2009, 63.

[15] Wang, P.; Zakeeruddin, S.M.; Exnar, I.; Grätzel, M. *Chem. Commun.* 2002, 2972.

[16] Wang, P.; Zakeeruddin, S.M.; Humphry-baker, R.; Moser, J.E.; Grätzel, M. *Adv. Mater. (Weinheim, Ger.)* 2003, **15**, 2101.

[17] Huang, S.Y.; Schlichtho1rl, G.; Nozik, A.J.; Grätzel, M.; Frank, A.J. *J. Phys. Chem. B*, 1997, **101**, 2576.

[18] Feldt, S.M.; Gibson, E.A.; Gabrielsson, E.; Sun, L.; Boschloo, G.; Hagfeldt, A. *J. Am. Chem. Soc.* 2010, **132(46)**, 16714.

Chapitre No: 8

Conclusion Générale et Perspectives

Au cours de ce travail de thèse, nous avons synthétisé et caractérisé une nouvelle famille de ligands bipyridiniques portant des motifs dithiénylpyrroles (DTP). La bipyridine a été liée au pyrrole (série DTP_1) ou thiophene (série DTP_2). Une série de complexes de ruthénium homoleptiques, bis- et tris-hétéroleptiques a été préparée à partir des nouveaux ligands.

Il est clairement montré que les propriétés électroniques des ligands et complexes sont très dépendantes du fait que la bipyridine soit liée au pyrrole ou au thiophène. Ceci a été mis en evidence par spectroscopie UV-vis, électrochimie, photophysique. En série DTP_1, les ligands absorbent dans la partie UV du spectre. En revanche, en série DTP_2 un très fort effet bathochrome est observé avec une absorption de forte intensité dans la partie visible. Les spectres des complexes homoleptiques, bis-hétéroleptiques et tris-hétéroleptiques suivent la même tendance. Les calculs théoriques ainsi que la spectroscopie transitoire ont été utilisées pour mettre en évidence une plus forte π-délocalisation en série DTP_2.

Deux complexes ont pu être étudiés en cellule DSSC, en accord avec leur coefficient d'extinction molaire élevés **[Ru{bpy(DTP_2-Me)(dcbpy)$(NCS)_2$]** et **[Ru{bpy(DTP_1-Hex)(dcbpy)$(NCS)_2$]** opèrent une collecte très efficace de la lumière solaire (>90% dans la zone 400-600 nm) supérieure à celle du colorant standard **Z907** (portant une chaîne butyle sur chaque pyridine du ligand ancillaire).

En employant un médiateur redox standard (PMII, LiI, I_2) les valeurs de J/V et l'efficacité des deux colorants sont inférieures à celle de Z907. L'utilisation d'autres régénérateurs n'a pas permis d'améliorer ce résultat. Les courbes IPCE sont en parfait accord avec les courbes J/V. Cependant **[Ru{bpy(DTP_2-Me)(dcbpy)$(NCS)_2$]** est plus performant que **[Ru{bpy(DTP_1-Hex)(dcbpy)$(NCS)_2$]**.

Les calculs DFT sur les complexes homoleptiques montrent bien une participation du ligand ancillaire dans l'orbitale occupée (en particulier en série **DTP_2**).

En revanche ces mêmes calculs en série tris-hétéroleptique montrent qu'un certain nombre de transitions correspondent à une localisation du trou sur les ligands NCS (en particulier pour **DTP_1**) ce qui augmente les risques de recombinaison. En série DTP_2 la

majeure partie des transitions sont de type ILCT. La charge reste localisée essentiellement sur le ligand ancillaire et n'est pas transférée au ligand 4,4-dicarboxy-2,2'bipyridine (dcbpy) devant assurer l'injection dans la bande de conduction du TiO_2. Ces transitions sont donc néfastes pour une injection efficace .

Les raisons expliquant les modestes performances des nouveaux colorants sont encore peu claires et nécessiteront des études complémentaires. Les limitations liées à la collecte de photons sont à exclure car nos colorants absorbent de façon optimale dans le domaine du visible après adsorption sur TiO_2. Thermodynamiquement, Les potentiels redox sont également très bien adaptés à la régénération par les médiateurs envisagés. En revanche, des effets stereo-électroniques liés à l'encombrement créé par les groupes DTP peut limiter l'accès notamment des ions iodures du médiateur au centre métallique oxydé (Ru(III)). Ceci pourrait expliquer les très faibles performances obtenues avec le médiateur à base de cobalt plus encombré que les ions iodures.

Perspectives

L'utilisation de chromophores organiques dans les cellules DSSC a récemment focalisé de nombreux travaux de recherche et des efficacités de 5 à 9% ont pu être atteintes. Ils sont constitués d'un donneur, d'un lien conjugué et d'un accepteur (D-π-A).

En considérant, la forte capacité des composes à base DTP à collecter les photons nous souhaitons les tester comme groupes donneurs dans les colorants organiques. Quelques exemples sont donnés ci-dessous.

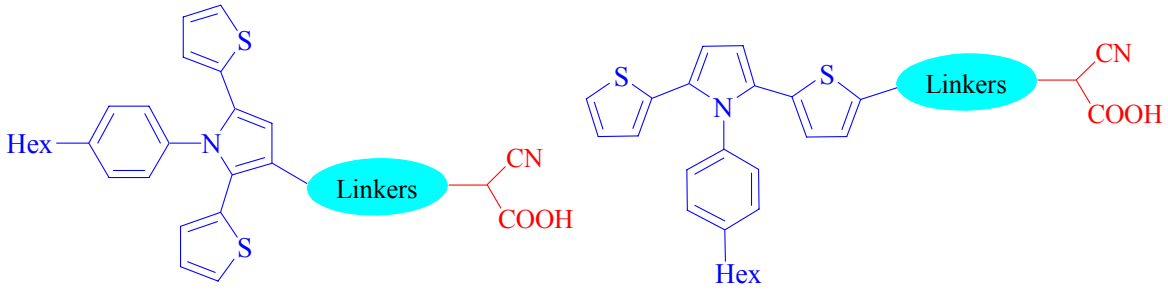

Les motifs DTP à chaîne lipophile seront privilégiés afin d'obtenir une solubilité optimale lors de l'adsorption sur le semi-conducteur. De plus, la structure du DTP avec le phényle placé hors du plan devrait contribuer à supprimer l'agrégation. Ce problème est récurrent en série organique et est responsable de la désactivation des états excites et donc de pertes de performances.

Chapter No: 8

General Conclusions and Perspectives

During current study we have designed, synthesized and characterized DTP based 2,2'-bipyridine ligands. Bipyridine was bound at pyrrole (DTP_1 series) or thiophene (DTP_2 series) ring. Variety of ruthenium polypyridyl complexes were prepared from both series of ligands.

There are clear indications that the points of attachment have significant effects upon the absorption, photophysical and electrochemical properties of the ligands and their corresponding homoleptic, bis-heteroleptic and tris-heteroleptic complexes. In DTP_1 series, the ligands absorbed in the UV part of the spectrum whereas when bipyridine was bound to the thiophene (DTP_2 series) ring, a strong bathochromic effect was observed leading to a strong absorption in the visible region. The corresponding homoleptic, bis-heteroleptic and tris-heteroleptic ruthenium complexes also exhibited the same features. The complexes from the DTP_2 series offered a promising absorption range in the visible domain with a notable and constant molar extinction coefficient all along this domain. Calculations as well as transient spectroscopy were used to explain such differences by evidencing a larger π-delocalization extent in DTP_2 series.

Consistently with their higher molar extinction coefficients, the electrodes sensitized by new heteroleptic dyes exhibit much higher optical densities than the reference compound (**Z 907**), reaching values close to 3 in the case of **[Ru{bpy(DTP_2-Me)(dcbpy)$(NCS)_2$]**. The light harvesting in the 400-600 nm region can be considered almost complete (>90%) for both **[Ru{bpy(DTP_1-Hex)(dcbpy)$(NCS)_2$]** and **[Ru{bpy(DTP_2-Me)(dcbpy)$(NCS)_2$]**.

When employed with the standard electrolyte (PMII, LiI, I_2) the J/V values as well as efficiency of both **[Ru{bpy(DTP_2-Me)(dcbpy)$(NCS)_2$]** and **[Ru{bpy(DTP_1-Hex)(dcbpy)$(NCS)_2$]** were lower than those of Z907. No improvement was found even by using cobalt based electrolyte. The IPCE spectra were consistent with the observations made from the J/V curves.

As demonstrated by the DFT calculations of homoleptic complexes, transition are mainly of MLCT nature with a significant participation of the ligand in the occupied orbital

(especially for **DTP_2**). This effect can be extremely important in the case when such ligands will be employed in tris-heteroleptic complexes that can be directly used as sensitizers in DSSC, since such a transition will leave the "hole" far from the semi-conductor surface, diminishing recombination occurrence and facilitating the access of the redox mediator.

But DFT calculations of tris-heteroleptic complexes revealed the fact that in some transitions the hole is localized on the NCS ligand (especially for **DTP_1**) that increases the chances of charge recombination. Whereas in case of tris-heteroleptic complexes of **DTP_2** series majority of transitions are ILCT based. Charge remains delocalized at ancillary ligand and not transferred to dcbpy, diminishing charge injection. So such transitions are quite useless for light harvesting process.

From above mentioned results it can be concluded that the reasons of the relatively poor performance of the new dyes are not fully understood and further investigations are required for this purpose. Limitations arising from poor light harvesting are obviously ruled out as demonstrated above, the Ru complexes of DTP based ligands act as strong light absorbers in the visible region. Electrochemical behavior is also appropriate for regeneration and not a hindrance at all. In contrast, electronic/steric effects could be involved since the bulky DTP moiety could impede an efficient access of iodide to Ru(III) centers. This may also explain the unexpectedly low performance with the cobalt electrolyte.

Perspectives

Organic chromophores for the DSSC, have drawn the attention of many research groups in the last couple of years. They have reached efficiencies in the range of 5-9 % so far. The organic dyes commonly consist of donor, linker, and acceptor groups (i.e., a D - π- A molecular structure). Introduction of π-conjugated moieties is carried out to expand the π-conjugation system and sustain the stability of the dye molecule. Various properties of organic dyes could be finely tuned by alternating independently or matching the different groups of D-π-A dyes.

Various varieties of organic dyes, such as perylene, cyanine, xanthenes, merocyanine, coumarin, hemicyaine, indoline, and triphenylamine dyes, have been reported, making organic dyes fruitful in the application of DSSCs.

By considering promising effects of DTP based compounds on light harvesting we plan to incorporate these moieties as donor groups in organic dyes. Cyanoacrylic acid could be used as the electron-withdrawing/anchoring moiety, and different types of thiophene

groups (i.e., thiophene, bithiophene, (E)-1,2-bis(2-thienyl)ethene, and thieno-thiophene) as π-conjugation bridges.

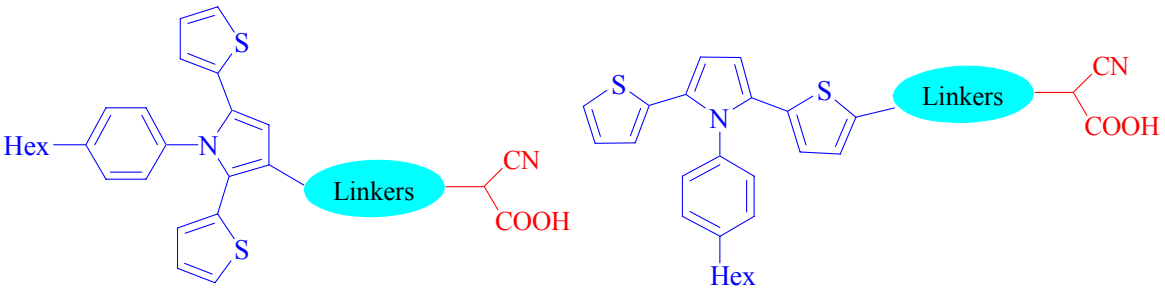

Model DTP-based organic dyes

DTP moiety substituted with hexyl group is chosen to obtain better solubility of final organic dye. Additionally, the structure of DTP with the out of plane configuration of the phenyl group could be useful to prevent aggregation. This is a current problem to be faced with π-delocalized plane organic dyes and responsible for excited state deactivation.

Chapter No: 9

Material and Methods

9.1. Materials

9.1.1. Synthesis

All reactions were carried out under an argon atmosphere, whereas workup procedures were done in air. THF and toluene were purified through an MBraun solvent purification system (MB SPS-800) prior to use. *N*, *N*-Dimethylformamide (DMF) was purified by distillation under reduced pressure. Deuterated solvents and commercially available reagents were used as received. Thin layer chromatography (TLC) was performed by using silica gel 60 F-254 (Merck) plates and visualized under UV light. Chromatographic purification of all compounds was performed by using silica gel 60, (0.063–0.2 mm/70–230 mesh) MACHEREY NAGEL, Germany. Microwave synthesis was performed on CEM Discover device fitted with infrared probe temperature control.

9.1.2. Measurements

^{1}H and ^{13}C NMR spectra were taken on AC200, AC250, or DRX400 Bruker spectrometers at ambient temperature. The chemical shifts (δ), were calibrated by using either tetramethylsilane (TMS) or signals from the residual protons of the deuterated solvents and are reported in parts per million (ppm) from low to high field. Standard abbreviations indicating multiplicity are used as: s = singlet; d = doublet; t = triplet; m = multiplet; dd = doublet of doublet. All coupling constants are reported in hertz.

High-resolution mass spectrometry (HRMS) data was obtained by using Bruker micrOTOF-Q spectrometer. Elemental analysis was performed by using Thermo Finnigan EA 1112. UV-vis spectra were recorded in a 1 cm path length quartz cell on a LAMBDA 1050 (Perkin Elmer), spectrophotometer. Emission and Excitation spectra were obtained on optically diluted solutions by using a Fluoromax 2 (Jobin Yvon) Spectrofluorometer.

Singlet emission lifetimes were acquired by using a Picoharp 300 time correlated single photon counting (TCSPC) apparatus by using the 380 nm excitation generated by a nano-led with a repetition rate of 10 MHz. The maximum reliable time resolution of the apparatus was 300 ps. The average number of fluorescence counts per seconds (cps) in optically diluted solutions ($A_{380} \approx 0.2$) were in the range 10^3-10^4. The emission decay was deconvolved and statistically elaborated by means of the Fluofit® dedicated program. The fitting was deemed satisfactory when $0.99<\chi^2<1.02$ and the residues were homogeneously distributed around 0 along the whole time interval under consideration (typically 20 ns). In the case of multiexponential decay, the amplitude weighted average lifetime was considered.

Transient absorption spectroscopy experiments were carried out by using a nanosecond transient absorption apparatus. If necessary, in the case of weak signals (ligand based triplet absorption), to obtain a satisfactory S/N ratio, oscillographic traces were averaged over 5-10 laser shots.

Cyclic voltammetry was performed on a Radiometer PST006 potentiostat using a conventional three-electrode cell. The saturated calomel electrode (SCE) was separated from the test compartment using a bridge tube. The test solution was DMF containing 0.1 M tetrabutylammonium hexafluorophosphate as supporting electrolyte. The working electrode was a 10 mm Pt wire and the counter-electrode was a 1 cm^2 vitreous carbon disc. The solutions were purged with argon before each measurement. A 0.5 mM solution of the studied compound (ligand/complex) dissolved in DMF containing 0.1 M tetrabutylammonium hexafluorophosphate as the supporting electrolyte was generally used. After the measurement, ferrocene was added as the internal reference for calibration. All potentials were quoted versus SCE. In these conditions the redox potential of the couple Fc^+/Fc was found at 0.47V. In all the experiments the scan rate was 100mV/s.

IPCE measurements were performed by illumination of the cell by using an Osram 150W Xenon lamp coupled to an Applied Photophysics monochromator. The irradiated surface was 0.5 cm^2. Photocurrents were measured under short circuit conditions by a digital Agilent 34410A multimeter. Incident irradiance was measured with a 1 cm^2 Centronic OSD100-7Q calibrated silicon photodiode.

9.1.3. Computations

All quantum chemistry calculations were performed by using gaussian09suite of code **[1]**. In case of ligands geometry optimization was done by using 6-31G basis set and B3LYP exchange correlation functional. Subsequently UV/Vis. spectrum was simulated by computing 25 excited states at TD-DFT level using CAM-B3LYP functional and 6-31G+(d,p) basis set. In case of complexes geometry optimization was performed using LANL2DZ basis and B3LYP functional, again 25 excited states were computed by using the same LANL2DZ basis and CAM-B3LYP functional. Excited states analysis in terms of NTOs was performed by using a locally produced and free downloadable code NancyEX (see hhttp/www.nancyex.sourceforge.net/)

9.2. Synthesis of diketones

1, 4- Bis(2'-thienyl)-1,4-butanedione, (1) [2]

To a suspension of $AlCl_3$ (101 mmol, 13.52 g) in 42 mL of dichloromethane, a solution of thiophene (100 mmol, 8 mL) and succinyl chloride (41.96 mmol, 4.7 mL) in 17 mL of dichloromethane was added dropwise at 15-20° C, and the mixture was stirred for 4 h at this temperature. The suspension was poured into a mixture of 250 g of ice and 10 mL of hydrochloric acid, and further stirred for 30 minutes. The organic layer was separated and the aqueous layer was extracted with dichloromethane. The organic layer and the extract were combined and washed with water and saturated aqueous $NaHCO_3$, dried over anhydrous $MgSO_4$, and evaporated to dryness. The crude product was suspended overnight in cold ethanol, filtered and dried to afford the product as light brown solid (68 %).

^{1}H NMR-(200 MHz, $CDCl_3$), δ (ppm): 7.83 (*d*, *J* = 3.5Hz, 2H); 7.64 (*d*, *J* = 4.8Hz, 2H); 7.26 (*t*, *J* = 3.9Hz, 2H); 3.40 (*s*, 4H)

1,4-Bis(5-bromo-2- thienyl)-1,4-butanedione, (5) [3]

To a suspension of $AlCl_3$ (75 mmol, 10 g) in 15 mL of CH_2Cl_2, a solution of 2-bromothiophene (25 mmol, 2.42 mL) and succinyl chloride (10 mmol, 1.1 mL) in 5 mL of CH_2Cl_2 was added dropwise at 40° C for 12 hours. After cooling the suspension was poured into 150 g ice and 2 mL HCl. The mixture was stirred for 30 minutes. Organic phase was separated

and washed with saturated aqueous $NaHCO_3$ solution and water, dried over $MgSO_4$. Solvent was removed under reduced pressure resulting brown powder. It was suspended overnight in ethanol, filtered and washed with excess of ethanol afforded brown powder (68 %).

^{1}H NMR-(200 MHz, $CDCl_3$), δ (ppm): 7.68 (*d*, *J* = 3.8 Hz, 2H); 7.26 (*d*, *J* = 3.8 Hz, 2H); 3.44 (*s*, 4H)

2,2'-(1,2-ethanediyl)bis[2-(5-bromo-2-thienyl)-1,3-Dioxolane, (6) [3]

5 (2.5 mmol, 1.0 g) was dissolved in 50 mL of hot toluene. After complete dissolution of diketone, *p*-toluenesulfonic acid (*p*-TosH) (1.1 mmol, 200 mg) and ethylene glycol (179.3 mmol, 10 mL) were added. Then the mixture was stirred and heated at 115° C for 48 hours by using Dean Stark trap. After cooling saturated aqueous $NaHCO_3$ was added. Organic phase was separated and the aqueous phase was extracted with toluene three times. The combined organic phases were dried over anhydrous $MgSO_4$, filtered, evaporated to dryness and purified by fractioned recrystallization by using cyclohexane to give title product (48 %).

^{1}H NMR-(200 MHz, $CDCl_3$), δ (ppm): 6.9 (*d*, *J* = 3.8 Hz, 2H); 6.74 (*d*, *J* = 3.8 Hz, 2H); 3.98 (*m*, 8H); 2.08 (*s*, 4H)

1,4- Bis(5-hexyl-2-thienyl)-1,4-butanedione, (7) [4]

To a suspension of $AlCl_3$ (11.8 mmol, 1.57 g) in 4 mL of CH_2Cl_2, a solution of of 2-n-hexylthiophene (5.94 mmol, 1 g) and succinyl chloride (2.6 mmol, 0.28 mL) in 1 mL dichloromethane was added dropwise at 0° C. The resultant red mixture was stirred for 48 h at room temperature and cooled with an ice bath. The reaction mixture was quenched with conc. HCl (0.2 mL) and water (1.8 mL). Additional CH_2Cl_2 was added and the mixture was filtered. The organic layer was separated and washed with 3 M HCl, neutralized with saturated aqueous $NaHCO_3$ solution, dried over anhydrous $MgSO_4$, and evaporated to dryness. The crude product was suspended in cyclohexane and filtered to afford title compound as light yellow solid (30 %).

^{1}H NMR-(250 MHz, $CDCl_3$), δ (ppm): 7.64 (*d*, *J* = 3.8 Hz, 2H); 6.82 (*d*, *J* = 3.7 Hz, 2H); 3.43 (*s*, 4H); 2.94 (*t*, 4H); 1.80 (*m*, 4H); 1.44 (*m,* 12H); 1.00 (*m*, 6H)

^{13}C NMR-(250 MHz, $CDCl_3$), δ (ppm): 195.9, 156.3, 141.6, 132.7, 125.8, 33.2, 31.8, 31.7, 31.0, 29.1, 22.9, 14.4

9.3. Synthesis of DTP moiety

Method A: A 250 mL round-bottomed flask equipped with a Dean-stark trap, a reflux condenser and a nitrogen-filled balloon was charged with **1**(2.00 mmol, 500 mg) and the corresponding aniline derivative (8.00 mmol) in 30 mL of 3:1 (v/v) toluene-acetic acid solution.
The reaction mixture was refluxed at 140–150 °C (oil bath temperature) for suitable times (monitored the reaction progress with TLC) and then cooled to room temperature. After the dark brown solution was transferred to a 300 mL beaker, a saturated Na_2CO_3 aqueous solution was added to make the reaction mixture basic. The organic layer was separated and then the aqueous layer was extracted with toluene (10 mL × 2). The combined organic layers were washed with water, dried over anhydrous $MgSO_4$ and then concentrated in vacuo. The residue was purified by column chromatography on silica gel (eluent: dichloromethane : cyclohexane 2:1).

Method B: To a suspension of **1** (2.00 mmol, 500 mg) and corresponding aniline derivative (2.4 mmol) in 150 mL xylene, *p*-TsOH.H_2O (30 mol %) was added and the mixture was stirred under reflux for 12 h with removal of water via Dean Stark trap. On completion of reaction, the mixture was washed with saturated aqueous $NaHCO_3$ and 2N HCl, dried over Na_2SO_4, concentrated in vacuo and purified by column chromatography

1-(*p*-Bromophenyl)-2,5-di(2-thienyl) pyrrole, (2) [5]

Method A: Yellow powder was obtained (65 %).
^{1}H NMR-(250 MHz, $CDCl_3$), δ (ppm): 7.53 (*dd*, *J* = 2.8 and 8.6 Hz, 2H); 7.16 (*dd*, *J* = 2.8 and 8.6 Hz, 2H); 7.09 (*dd*, *J* =1.1 and 5.1 Hz, 2H); 6.85 (*dd, J* = 3.6 and 5.1 Hz, 2H); 6.56 (*dd*, *J* = 1.1 and 3.6 Hz, 2H); 6.53 (s, 2H)
^{13}C NMR-(250 MHz, $CDCl_3$), δ (ppm): 138.1, 135.2, 132.9, 130.6, 127.5, 125.2, 124.8, 123.6, 110.6

1-(*p*-Cyanophenyl)-2,5-di(2-thienyl) pyrrole, (3) [2]

Method B: Light yellow powder was obtained (60 %).

^{1}H NMR-(200 MHz, $CDCl_3$), δ (ppm): 7.68 (*d*, *J* = 8.2 Hz, 2H); 7.36 (*d*, *J* = 8.2 Hz, 2H); 7.13 (*d*, *J* = 4.5 Hz, 2H); 6.87 (*t, J* = 4.5 Hz, 2H); 6.53 (*m*, 4H)

1-Phenyl-2,5-di(2-thienyl)pyrrole, (17) [5]

Method B: Yellowish brown powder was obtained (94 %).

^{1}H NMR-(250 MHz, $CDCl_3$), δ (ppm): 7.43 (*dt*, *J* = 1.8 and 6.4 Hz, 3H); 7.21 (*dd*, *J* = 1.4 and 6.4 Hz, 2H); 7.04 (*dd*, *J* =1.1 and 3.6 Hz, 2H); 6.80 (*dd*, *J* = 3.6 and 1.5 Hz, 2H); 6.53 (*dd*, *J* = 1.1and 1.5 Hz, 2H); 6.51 (*s*, 2H)

1-(*p*-Fluorophenyl)-2,5-di(2-thienyl) pyrrole, (18) [5]

Method A: Light yellow powder was obtained (68 %).

^{1}H NMR-(250 MHz, $CDCl_3$), δ (ppm): 7.30 (*dd*, *J* = 8.3 and 3.9 Hz, 2H); 7.12 (*d*, *J* = 4.0 and 8.3 Hz, 2H); 7.08 (*dd*, *J* =1.0 and 5.1 Hz, 2H); 6.84 (*dd, J* = 3.6 and 5.1 Hz, 2H); 6.56 (*dd*, *J* = 1.0 and 3.1Hz, 2H); 6.54 (*s*, 2H)

^{13}C NMR-(250 MHz, $CDCl_3$), δ (ppm): 135.1, 132.2, 132.0, 130.6, 127.6, 125.2, 124.9, 117.1, 116.6, 110.6.

1-*p*-Tolyl-2,5-di(2-thienyl) pyrrole, (19) [5]

Method A: Yellow powder was obtained (70 %).

^{1}H NMR-(250 MHz, $CDCl_3$), δ (ppm): 7.20 (*m*, 4H); 7.04 (*dd*, *J* = 5.1 and 1.1 Hz, 2H); 6.80 (*dd, J* = 5.1 and 3.6 Hz, 2H); 6.5 (*m*, 4H); 2.42 (*s*, 3H)

^{13}C NMR-(250 MHz, $CDCl_3$), δ (ppm): 139.6, 136.3, 135.5, 130.6, 130.3, 130.1, 127.3, 124.6, 124.3, 110.2, 21.7

1-(*p*-Hexylphenyl)-2,5-di(2-thienyl) pyrrole, (20) [5]

Method A: Light yellow powder was obtained (55 %).

^{1}H NMR-(250 MHz, $CDCl_3$), δ (ppm): 7.20 (*m*, 4H); 7.02 (*dd*, *J* = 1.0 and 5.1 Hz, 2H); 6.80 (*dd*, *J* = 5.1 and 3.6 Hz, 2H); 6.52 (*s*, 2H); 6.52 (*d*, *J* = 1.0 Hz, 2H); 2.71 (*t*, 2H); 1.68 (*m*, 2H); 1.35 (*m*, 6H); 0.96 (*t*, *J* = 6.5 Hz, 3H)

^{13}C NMR-(250 MHz, $CDCl_3$), δ (ppm): 144.6, 136.3, 135.5, 130.6, 130.1, 129.6, 127.2, 124.1, 123.9, 109.8, 36.1, 32.1, 31.6, 29.1, 23.1, 14.5.

9.4. Synthesis of functionalized DTP moiety

1-(*p*-cyanophenyl)-2,5-di((5,5'-bis-*n*hexyl)-2-thienyl) pyrrole (8)

Instead of **1**, **7** was used as starting material.

Method B: Light yellow powder was obtained (2 %).

^{1}H NMR-(200 MHz, $CDCl_3$), δ (ppm): 7.64 (*d*, *J* = 8.3 Hz, 2H); 7.32 (*d*, *J* = 8.3 Hz, 2H); 6.91 (*d*, *J* = 4.4 Hz, 2H); 6.73 (*t*, *J* = 4.2 Hz, 2H); 6.42 (*m*, 4H); 2.98(*t*, 4H); 1.81 (*m*, 4H); 1.57 (*m*, 12H); 1.09 (*m*, 6H)

1-(*p*-bromophenyl)-2,5-di((5,5'-bis-*n*hexyl)-2-thienyl) pyrrole (9)

Instead of **1**, **7** was used as starting material and eluent was dichloromethane-cyclohexane (1:1).

Method A: Yellow powder was obtained (5 %).

^{1}H NMR-(250 MHz, $CDCl_3$), δ (ppm): 7.54 (*dd*, *J* = 1.9 and 4.7 Hz, 2H); 7.18 (*dd*, *J* = 1.9 and 4.7 Hz, 2H); 6.53 (*d*, *J* = 3.6 Hz, 2H); 6.47 (*s*, 2H); 6.31 (*d*, *J* = 3.6 Hz, 2H); 3.10 (*t*, 4H); 1.95 (*m*, 4H); 1.69 (*m*, 12H); 1.27 (*m*, 6H)

1-(*p*-*n*hexylphenyl)-2,5-di((5,5'-bis-*n*hexyl)-2-thienyl) pyrrole (10) [4]

Instead of **1**, **7** was used as starting material and eluent was dichloromethane-cyclohexane (1:1).

Method A: Yellow powder was obtained (55 %).

^{1}H NMR-(250 MHz, $CDCl_3$), δ (ppm): 7.32 (*d*, *J* = 8.5 Hz, 2H); 7.20 (*d*, *J* = 8.3 Hz, 2H); 6.51 (*d*, *J* = 3.9 Hz, 2H); 6.43 (*s*, 2H); 6.33 (*d*, *J* = 3.6 Hz, 2H); 2.73 (*t*, 2H); 2.66 (*t*, 4H); 1.68 (*m*, 2H); 1.55 (*m*, 4 H); 1.28 (*m*, 18H); 0.88 (*m*, 9H)

1-(*p*-*n*hexylphenyl)-2,5-di((5,5'-dibromo)-2-thienyl) pyrrole (28)

Instead of **1**, **5** was used as starting material.
Method A: Light brown powder was obtained (53 %).
^{1}H NMR-(250 MHz, $CDCl_3$), δ (ppm): 7.49 (*d*, *J* = 8.5 Hz, 2H); 7.18 (*d*, *J* = 8.5 Hz, 2H); 6.11 (*d*, *J* = 3.9 Hz, 2H); 6.23 (*s*, 2H); 6.30 (*d*, *J* = 3.9 Hz, 2H); 2.41 (*t*, 2H); 1.68 (*m*, 2H); 1.35 (*m*, 6H); 0.96 (*t*, *J* = 6.5 Hz, 3H)

4-[2,5-bis(5-bromothiophen-2-yl)-1*H*-pyrrol-1-yl]benzonitrile (11)

Instead of **1**, **5** was used as starting material.
Method B: Yellow powder was obtained (50 %).
^{1}H NMR-(250 MHz, $CDCl_3$), δ (ppm): 7.72 (*d*, *J* = 8.5 Hz, 2H); 7.36 (*d*, *J* = 8.5 Hz, 2H); 6.83 (*d*, *J* = 3.9 Hz, 2H); 6.51 (*s*, 2H); 6.30 (*d*, *J* = 3.9 Hz, 2H)

Synthesis of 4, 4'-bis [(trimethylsilyl)methyl]-2,2'-bipyridine, (bpysi) [6,7]

In 250 mL tri neck flask diisopropylamine (10 mmol, 1.6 mL) was dissolved in 15 mL THF at -78° C under argon. n-BuLi (0.96 M solution in hexanes), (11 mmol, 11.4 mL) was added dropwise and the mixture was stirred for 20 minutes at -40° C. 4,4'-dimethyl-2,2'-bipyridine (4.05 mmol, 0.75 g) was dissolved in 15 mL THF and was introduced dropwise into previous mixture at -78° C. The brown colored mixture was obtained that was stirred for 20 minutes at -78°C and then for further 25 minutes at -10° C. Chlorotrimethylsilane (8.5 mmol, 1.09 mL) was added dropwise at -78° C and exactly after 10 seconds, 3 mL methanol and 10 mL saturated $NaHCO_3$ solution was added to quench the reaction. When ambient temperature was obtained then 30 mL of ethyl acetate was added. Separation of two phases took place. Organic phase was washed three times with water. Saturated NaCl solution was used where it was required for the

separation of two phases. After washing with water organic phase was dried over $MgSO_4$, filtered and evaporated under vacuum. Light yellow powdered product was obtained (99 %).
^{1}H NMR-(200 MHz, $CDCl_3$), δ (ppm): 8.61 (*d*, *J* = 4.7 Hz, 2H); 8.20 (*s*, 2H); 7.09 (*d*, *J* = 4.6 Hz, 2H); 2.35 (*s*, 4H), 0.35 (*s*, 18H)

Synthesis of 4,4'-bis(chloromethyl)-2,2'-bipyridine, (bpyCl) [6,7]

In 100 mL three necked flask **bpysi** (2.74 mmol, 0.9 g) was dissolved in 15 mL of acetonitrile. Hexachloromethane (10.9 mmol, 2.62 g) and cesium fluoride (10.9 mmol, 1.66 g) was also added. The resultant solution was stirred at 60° C for 16 h. After this 20 mL of ethyl acetate and 20 mL of water was added. Organic phase was separated and washed three times with water. Dried over $MgSO_4$, filtered and dried in vacuo. Light yellow powder was obtained after recrystallization with ethanol (85 %).
^{1}H NMR-(200 MHz, $CDCl_3$), δ (ppm): 8.76 (*d*, *J* = 4.7 Hz, 2H); 8.52 (*s*, 2H); 7.48 (*d*, *J* = 4.2Hz, 2H); 4.72 (*s*, 4H).

Synthesis of Tetraethyl(4,4'-diphosphonate-2,2'-bipyridine), (16) [6,7]

In 100 mL three necked flask sodium hydride (10 mmol, 0.24 g) was washed with THF two times under argon. Then 4 mL of toluene was introduced and in resultant suspension $HPO(OEt)_2$ (6 mmol, 0.77 mL) was added dropwise. Quick reaction take place and clear solution was obtained that was stirred for 1 h at 80° C. **bpyCl** (1 mmol, 253 mg) was dissolved in 5 mL toluene and was introduced in the reaction mixture. That was further stirred for 6 h at 80° C. After cooling 15 mL of ethyl acetate and 15 mL of saturated aqueous NaCl were added, the organic phase was separated, washed three times with water and dried over $MgSO_4$. After filteration solvent was evaporated under vacuum. Light yellow powder was obtained (55 %).
^{1}H NMR-(200 MHz, $CDCl_3$), δ (ppm): 8.90 (*d*, *J* = 4.8 Hz, 2H); 8.63 (*s*, 2H); 7.62 (*d*, *J* = 4.8 Hz, 2H); 4.38 (*t*, *J* = 6.8 Hz, 8H); 3.29 (*d*, *J* = 22.1 Hz, 4H); 3.29 (*t*, *J* = 7.1 Hz, 12H)

2-Acetylthiophene (26)

Thiophene (125 mmol, 10 mL) in acetic anhydride (115 mmol, 10.6 mL) was treated with a few drops of H_3PO_4 at 80-85° C for 3 hours. The reaction mixture was cooled to room temperature and poured into water, extracted with CH_2Cl_2, separated organic layer was washed with 10 % NaOH solution and water, dried over $MgSO_4$. Solvent was removed under vacuo to afford light brown oil (70 %).

^{1}H NMR-(200 MHz, $CDCl_3$), δ (ppm): 7.71(*d*, *J* = 2.9 Hz, 1H); 7.65 (*d*, *J* = 4.4 Hz, 1H); 7.15 (*t*, *J* = 4.4 Hz, 1H); 2.85 (*s*, 3H)

3-(dimethylamino)-1-(thiophen-2-yl)propan-1-one (27)

Paraformaldehyde (48 mmol, 1.44 g), dimethylamine hydrochloride (48 mmol, 3.9 g) and **26** (40 mmol, 5 g) were dissolved in 8 mL ethanol. 0.5 mL of HCl (35 %) was added and the mixture was refluxed for 7 hours. After cooling the yellowish solution was diluted with cold acetone and chilled at 0° C for several hours. White crystals were formed that were filtered, washed with acetone, dissolved in water and extracted in ethyl acetate. The aqueous layer was treated with potassium carbonate (pH = 10) and extracted in ethyl acetate. The combined organic phases were dried over anhydrous $MgSO_4$ and concentrated under reduced pressure to give title product as yellow oil (75 %).

^{1}H NMR-(200 MHz, $CDCl_3$), δ (ppm): 7.75 (*d*, *J* = 4.5 Hz, 1H); 7.65 (*d*, *J* = 4.5 Hz, 1H); 7.2 (*t*, *J* = 4.0 Hz, 1H); 3.12 (*t*, *J* = 6.8 Hz, 2H); 2.79 (*t*, *J* = 6.8 Hz, 2H); 2.29 (*s*, 6H)

9.5. Monobromination of DTP moiety

DTP moiety (1 mmol) was dissolved at -50° C in a mixture of 15 mL chloroform and 1.5 mL propanoic acid. To this solution *N*-bromosuccinimide (1.05 mmol) was added. The reaction mixture was stirred at this temperature for 1.5 h. After that reaction was quenched by adding water. Reaction mixture was washed with 1 % aqueous NaOH solution and water respectively and then dried over anhydrous $MgSO_4$. Solvent was evaporated and crude product was purified by column chromatography on silica gel.

1-(*p*-*n*hexylphenyl)-2,5-di((5-bromo)-2-thienyl) pyrrole (29)

20 was used as starting material. dichloromethane:cyclohexne (1:8) was used as eluent. Light yellow powder was obtained (66 %).

^{1}H NMR-(250 MHz, $CDCl_3$), δ (ppm): 7.25 (*dd*, *J* = 5.1 and 1.1 Hz, 1H); 7.11-7.23 (*m,* 5H); 6.93-7.04 (*m,* 2 H); 6.87 (*dd*, *J* = 5.1 and 3.7 Hz, 1H); 6.66 (*s*, 1H); 6.61 (*dd*, *J* = 3.6 and 1.0 Hz; 1H); 2.71 (*t*, 2H); 1.69 (*m*, 2H); 1.35 (*m,* 6H); 0.96 (*t*, *J* = 6.5 Hz, 3H)

^{13}C NMR-(250 MHz, $CDCl_3$), δ (ppm):144.6, 135.9, 134.2, 132.0, 130.2, 129.5, 129.1, 128.8, 127.0, 126.5, 126.4, 125.1, 124.8, 112.4, 36.0, 32.1, 31.5, 29.2, 23.1, 14.6

1-(*p*-tolyl)-2,5-di((5-bromo)-2-thienyl) pyrrole (30)

19 was used as starting material and crude product was purified by flash column chromatography on silica gel (eluent: : 0.5 % solution of ethyl acetate in cyclohexane) to afford off white powder (60 %).

^{1}H NMR-(250 MHz, $CDCl_3$), δ (ppm): 7.21 (*dd*, *J* = 4.9 and 1.3 Hz, 1H); 7.04-7.17 (*m,* 5H); 6.90-6.96 (*m,* 2 H); 6.83 (*dd*, *J* = 5.1 and 3.6 Hz, 1H); 6.60 (s, 1H); 6.56 (*dd*, *J* = 3.7 and 1.0 Hz); 2.37 (*s*, 3H)

^{13}C NMR-(250 MHz, $CDCl_3$), δ (ppm):139.4, 135.7, 134.2, 131.9, 130.0, 129.8, 129.4, 129.2, 127.3, 126.9, 126.8, 125.6, 125.2, 112.8, 22.0

1-(*p*-fluoro)-2,5-di((5-bromo)-2-thienyl) pyrrole (31)

18 was used as starting material and crude product was tried to purify by flash column chromatography on silica gel (eluent: dichloromethane:cyclohexne 1:8) but complete purification was not possible so mixture was subjected to next step.

9.6. Synthesis of aldehydes

1,(4'-Formylphenyl)-2,5-di(2"-thienyl)pyrrole, (4) [5]

To a solution of **3** (3 mmol, 1 g) in 90 mL toluene, diisobutylaluminium hydride (1.2 M solution in toluene), (3.6 mmol, 3 mL) was added dropwise at -60° C, and the mixture was stirred for 1 h at that temperature. After removal of the cooling bath 2.5 mL of saturated aqueous NH_4Cl was added dropwise at -20° C, 17 mL of 3 N HCl was added at room temperature and the mixture was stirred for further 3 h. The mixture was extracted with toluene and water, and the organic layer was dried over Na_2SO_4. Solvent was removed under vacuo to afford light yellow powder (92 %).

^{1}H NMR-(200 MHz, $CDCl_3$), δ (ppm): 10.39 (*s*, 1H); 7.92 (*d*, *J* = 8.2 Hz, 2H); 7.44 (*d*, *J* = 8.2 Hz, 2H); 7.11 (*d*, *J* = 5.0 Hz, 2H); 6.84 (*t*, *J* = 5.0 Hz, 2H); 6.58 (*s*, 2H); 6.54 (*d*, *J* = 3.0 Hz, 2H)

4-[2,5-bis(5-bromothiophen-2-yl)-1*H*-pyrrol-1-yl]benzaldehyde (12)

Same procedure was used as for **4, 11** was used as starting material instead of **3**. Yellow powder was obtained (95 %).

^{1}H NMR-(250 MHz, $CDCl_3$), δ (ppm): 10.17 (*s*, 1 H); 7.95 (*d*, *J* = 8.3 Hz, 2H); 7.42 (*d*, *J* = 8.3Hz, 2H); 6.78 (*d*, *J* = 3.8 Hz, 2H); 6.48 (*s*, 2H); 6.28 (*d*, *J* = 3.9 Hz, 2H)

9.6.1. General procedure for preparation of 15, 21, 22, 23, 25

Phosphorus oxychloride (4 mmol) was added to 10 mL of DMF at 0° C and the mixture was stirred for 15 minutes. DTP moiety (1 mmol) was dissolved in 8 mL of DMF and this solution was added to previous solution over a period of 30 minutes at 0° C. The red coloured mixture was stirred overnight and then heated at 70° C for 1 h, after which the reaction mixture was cooled and poured into ice. The yellow precipitated product was filtered, dried over $MgSO_4$ and purified by column chromatography on silica gel.

1-(*p*-bromophenyl)-2,5-di(2-thienyl)-4-carboxaldehyde-pyrrole (15)

2 was used as starting material. The crude product was purified by column chromatography on silica gel by using cyclohexane: ethyl acetate (4:1) as mobile phase. The title product was obtained as yellow powder (50%).

^{1}H NMR- (250 MHz, $CDCl_3$), δ (ppm): 9.90 (*s*, 1H); 7.51 (*dd*, *J* = 8.7 and 2.8 Hz, 2H); 7.38 (*dd*, *J* = 5.0 and 1.3 Hz, 1H); 7.19 (*dd*, *J* = 5.2 and 1.1 Hz, 1H); 7.09 (*dd*, *J* = 8.6 and 2.8 Hz, 2H); 7.02 (*s*, 1H); 6.97 (*m*, 2H); 6.89 (*dd*, *J* = 5.1 and 3.7 Hz, 1H); 6.64 (*dd*, *J* = 3.7 and 1.1 Hz, 1H).

^{13}C NMR-(250 MHz, $CDCl_3$), δ (ppm): 186.5, 132.9, 131.6, 131.4, 129.4, 127.7, 127.6, 126.9, 126.4, 125.5, 108.5.

1-(*p*-fluorophenyl)-2,5-di(2-thienyl)-4-carboxaldehyde-pyrrole (21)

18 was used as starting material. Purification was carried out by column chromatography on silica gel (eluent: cyclohexne: ethyl acetate 2:1). Yellow powder was obtained (65 %).

^{1}H NMR-(250 MHz, $CDCl_3$), δ (ppm): 9.91 (*s*, 1H); 7.36 (*dd*, *J* = 4.5 and 1.8 Hz, 1H); 7.21 (*dd*, *J* = 2.8 and 1.8 Hz, 1H); 7.18 (*dd*, *J* = 3.5 and 2.2 Hz, 2H); 7.08 (*dd*, *J* = 3.5 and 2.2 Hz, 2H); 7.05 (*s*, 1H); 6.98 (*m*, 2H); 6.88 (*dd*, *J* = 5.1 and 3.6 Hz, 1H); 6.65 (*dd*, *J* = 3.6 and 1.1 Hz, 1H).

^{13}C NMR-(250 MHz, $CDCl_3$), δ (ppm): 188.3, 166.1, 162.0, 138.3, 133.0, 131.6, 131.4, 131.3, 131.1, 129.2, 129.0, 127.3, 127.1, 126.4, 125.6, 126.0, 125.3

1-(*p*-tolyl)-2,5-di(2-thienyl)-4-carboxaldehyde-pyrrole (22)

19 was used as starting material. Crude product was purified by column chromatography on silica gel (eluent: cyclohexne: ethyl acetate 2:1). Yellow powder was obtained (52 %).

^{1}H NMR-(250 MHz, $CDCl_3$), δ (ppm): 9.92 (*s*, 1H); 7.33 (*dd*, *J* = 3.5 and 0.7 Hz, 1H); 7.15 (*m*, 5H); 7.07 (*s*, 1H); 6.98 (*m*, 2H); 6.86 (*dd*, *J* = 5.0 and 1.2 Hz, 1H); 6.62 (*dd*, *J* = 3.6 and 2.7 Hz, 1H); 2.44 (*s*, 3H).

^{13}C NMR-(250 MHz, $CDCl_3$), δ (ppm): 186.6, 139.9, 134.6, 133.6, 134.9, 131.2, 130.2, 129.5, 129.0, 127.4, 127.2, 126.3, 125.8, 125.4, 107.4, 21.4

1-(*p*-*n*hexylphenyl)-2,5-di(2-thienyl)-4-carboxaldehyde-pyrrole (23)

20 was used as starting material. Crude product was purified by column chromatography on silica gel (eluent: cyclohexne: ethyl acetate 2:1). Yellow powder was obtained (60 %).
^{1}H NMR-(250 MHz, $CDCl_3$), δ (ppm): 9.84 (*s*, 1H); 7.36 (*dd*, *J* = 3.4 and 0.7 Hz, 1H); 7.16 (*m*, 5H); 7.06 (*s*, 1H); 6.96 (*m*, 2H); 6.84 (*dd*, *J* = 5.0 and 1.2 Hz, 1H); 6.61 (*dd*, *J* = 3.5 and 2.7 Hz, 1H), 2.69 (*t*, *J* = 7.6 Hz, 2H); 1.63 (*m*, 2H); 1.35 (*m,* 6H); 0.93 (*m*, 3H).
^{13}C NMR-(250 MHz, $CDCl_3$), δ (ppm): 186.8, 131.7, 131.0, 129.3, 128.7, 127.2, 127.0, 126.0, 125.6, 125.1, 107.7, 36.0, 32.1, 31.5, 29.2, 23.1, 14.6

1-(4-bromophenyl)-3-(1,3-dioxolan-2-yl)-2,5-di(thiophen-2-yl)-1*H*-pyrrole (24)

15 (1 mmol, 414 mg), ethylene glycol (6 mmol, 0.33 mL) and *p*-TsoH.H_2O (0.025 mmol, 4.75 mg) were dissolved in 30 mL of toluene. The reaction mixture was refluxed for 16 h under Dean-Stark conditions and then washed three times with 1 % aqueous NaOH solution and water respectively. The organic phase was dried over anhydrous $MgSO_4$, filtered and evaporated under vacuum to afford **24** (94 %).
^{1}H NMR-(250 MHz, $CDCl_3$), δ (ppm): 7.44 (*d*, *J* = 8.6 Hz, 2H); 7.25 (*dd*, *J* = 4.1 and 1.9 Hz, 1 H); 7.11 (*dd*, *J* = 5.9 and 1.0 Hz, 1 H); 7.05 (*d*, *J* = 8.6 Hz, 2H); 6.93 (*m*, 2 H); 6.85 (*dd*, *J* = 5.1 and 3.6 Hz, 1H); 6.71 (*s*, 1H); 6.57 (*dd*, *J* = 3.6 and 1.0, 1H); 5.78 (*s*, 1H); 4.21 (*m*, 2H); 4.01 (*m*, 2H).

1-(phenyl)-2,5-di(2-thienyl)-4-carboxaldehyde-pyrrole (25)

24 (0.80 mmol, 370 mg) was dissolved in 12 mL of THF. To this solution *n*-BuLi (1.5 M solution in hexanes) (0.96 mmol, 0.64 mL) was added dropwise at -40° C. Reaction progress was monitored by TLC, after completion of metallation (about 2 hours) the reaction mixture was hydrolyzed by adding water and extracted with CH_2Cl_2, separated organic layer was washed with water. Dried over $MgSO_4$ and evaporated under vacuum to afford a green product that was

subjected to further step without purification. (0.66 mmol, 250 mg) of the above obtained product, 10 mL water and and *p*-TsoH.H_2O (0.79 mmol, 150.6 mg) were dissolved in 25 mL of acetone. Then 0.06 mL of 4-picoline was added and reaction mixture was refluxed for 24 h. Then it was cooled and extracted with CH_2Cl_2 and washed with saturated aqueous $NaHCO_3$ and water respectively. Dried over $MgSO_4$, concentrated in vacuo and purified by column chromatography on silica gel (eluent: cyclohexane: ethyl acetate 4:1) to afford green powdered product (81 %).

^{1}H NMR-(250 MHz, $CDCl_3$), δ (ppm): 9.90 (*s*, 1H); 7.39 (*m*, 3H); 7.34 (*d*, *J* = 3.3 Hz, 1 H); 7.22 (*d*, *J* = 7.0 Hz, 2H); 7.14 (*d*, *J* = 5.0 Hz, 1H); 7.04 (*s*, 1H); 6.96 (*d*, *J* = 3.1 Hz, 2H); 6.85 (*t*, *J* = 3.8 Hz, 1H); 6.61 (*d*, *J* = 3.3 Hz, 1H).

^{13}C NMR-(250 MHz, $CDCl_3$), δ (ppm): 186.6, 137.4, 137.2, 133.4, 131.7, 131.0, 129.6, 129.2, 128.8, 127.2, 127.0, 126.2, 125.7, 125.2, 108.0.

9.6.2. General procedure for preparation of 32, 33, 34

Monobrominated DTP moiety (1 mmol) was dissolved in 15 mL of THF. To this solution n-BuLi (1.5 M solution in hexanes) (1.2mmol) was added dropwise at -40° C. Reaction progress was monitored by TLC, after completion of metallation (about 1.5 hours) the temperature was lowered till -78° C. And DMF (1.5 mmol) was added dropwise in form of solution in THF. Temperature was slowly raised to room temperature and was allowed to stir overnight. Then reaction was quenched by adding water and extracted with CH_2Cl_2, separated organic layer was washed with water and dried over $MgSO_4$. The crude product was purified by column chromatography on silica gel (eluent: ethyl acetate: cyclohexne 1:4).

1-(*p*-*n*hexylphenyl)-2,5-di((5-carboxaldehyde)-2-thienyl) pyrrole (32)

29 was used as starting material. Green oily product was obtained (43 %).

^{1}H NMR-(250 MHz, $CDCl_3$), δ (ppm): 9.75 (*s*, 1H); 7.43 (*d*, *J* = 4.1 Hz, 1H); 7.26 (*m*, 4H); 7.07 (*d*, *J* = 5.1Hz, 1H); 6.81 (*dd*, *J* = 5.0 and 3.7 Hz, 1H), 6.76 (*d*, *J* = 4.0 Hz, 1H); 6.60 (*m*, 3 H), 2.72(*t*, *J* = 7.4 Hz, 2H); 1.69 (*m*, 2H); 1.34 (*m*, 6H); 0.92 (*t*, *J* = 6.7 Hz, 3H).

^{13}C NMR-(250 MHz, $CDCl_3$), δ (ppm): 182.7, 145.8, 140.8, 137.3, 135.7, 134.8, 133.3, 130.4, 129.9, 127.7, 125.3, 124.4, 112.8, 110.9, 36.4, 32.4, 31.9, 29.5, 23.3, 14.8

1-(*p*-tolyl)-2,5-di((5-carboxaldehyde)-2-thienyl) pyrrole (33)

30 was used as starting material. Dark orange oily product was obtained (55 %).

^{1}H NMR-(250 MHz, $CDCl_3$), δ (ppm): 9.69 (*s*, 1H); 7.44 (*d*, *J* = 4.1 Hz, 1H); 7.25 (*m*, 4H); 7.09 (*dd*, *J* = 5.1 and 1.1 Hz, 1H); 6.83 (*dd*, *J* = 5.1 and 3.7 Hz, 1H); 6.77 (*d*, *J* = 4.0 Hz, 1H); 6.66 (*d*, *J* = 4.1 Hz, 1H); 6.59 (*m*, 2H); 2.51 (*s*, 3H).

^{13}C NMR-(250 MHz, $CDCl_3$), δ (ppm): 182.3, 145.7, 140.7, 137.3, 135.4, 133.2, 130.9, 130.1, 129.6, 127.4, 125.1, 124.2, 112.7, 110.8, 21.8

1-(*p*-fluoro)-2,5-di((5-carboxaldehyde)-2-thienyl) pyrrole (34)

31 was used as starting material. Yellow powder was obtained (45 %).

^{1}H NMR-(200 MHz, $CDCl_3$), δ (ppm): 9.86 (*s*, 1H); 7.57 (*d*, *J* = 4.0 Hz, 1H); 7.40 (*d*, *J* = 8.6 Hz, 2H); 7.34 (*d*, *J* = 8.6 Hz, 2H); 7.21 (*dd*, *J* = 5.2 and 0.9 Hz, 1H); 6.94 (*dd*, *J* = 4.8 and 3.7 Hz, 1H); 6.86 (*d*, *J* = 4.0 Hz, 1H); 6.78 (*d*, *J* = 4.0 Hz, 1H); 6.71 (*dd*, *J* = 2.5 and 1.0 Hz, 1H); 6.68 (*d*, *J* = 3.9 Hz, 1H).

^{13}C NMR-(200 MHz, $CDCl_3$), δ (ppm): 182.4, 144.9, 140.9, 136.9, 133.9, 133.1, 132.0, 129.6, 127.4, 125.4, 123.3, 117.6, 117.0, 112.8, 111.1

9.7. Protection of Aldehydes

[4-[2,5-bis(5-bromothiophen-2-yl)-1*H*-pyrrol-1-yl]benzaldehyde] dimethylacetal (13)

Solution of **12** (0.4 mmol, 200 mg) and *p*-TsoH.H_2O (0.04 mmol, 7.6 mg) in 20 mL methanol was refluxed for 15 h. On completion of reaction, the mixture was allowed to cool. Yellow precipitates were filtered, dissolved in CH_2Cl_2 and neutralized by saturated aqueous $NaHCO_3$. Organic layer was extracted, washed with water and was dried over $MgSO_4$. Solvent was removed under vacuo to afford yellow powder (97 %).

^{1}H NMR-(250 MHz, $CDCl_3$), δ (ppm): 7.57 (*d*, *J* = 7.6 Hz, 2H); 7.32 (*d*, *J* = 7.3Hz, 2H); 6.78 (*d*, *J* = 3.7 Hz, 2H); 6.49 (*d*, *J* = 3.8 Hz, 2H); 6.33 (*d*, *J* = 3.9 Hz, 2H); 5.59 (*s*, 1H); 3.35 (*s*, 6 H)

2-[4-[2,5-bis(5-bromothiophen-2-yl)-1*H*-pyrrol-1-yl] phenyl-1.3-dioxolane (14)

12 (0.5 mmol, 246 mg), ethylene glycol (3 mmol, 0.17 mL) and *p*-TsoH.H_2O (0.01 mmol, 1.90 mg) were dissolved in 20 mL of toluene. The reaction mixture was refluxed overnight under Dean-Stark conditions and then washed three times with 1 % aqueous NaOH solution and water respectively. The organic phase was dried over anhydrous $MgSO_4$, filtered and evaporated under vacuum to afford yellow product (90 %).

^{1}H NMR-(200 MHz, $CDCl_3$), δ (ppm): 7.57 (*d*, *J* = 9.5 Hz, 2H); 7.31 (*d*, *J* = 9.6 Hz, 2H); 6.79 (*d*, *J* = 3.6 Hz, 2H); 6.50 (*d*, *J* = 3.7 Hz, 2H); 6.25 (*d*, *J* = 3.9 Hz, 2H); 5.92 (*s*, 1H); 4.16 (*m*, 4 H)

9.8. Synthesis of Ligands

Aldehyde (1 mmol) and **16** (0.5 mmol) were dissolved in 15 mL of deoxygenated anhydrous THF. Solid potassium *tert*-butoxide (1.5 mmol) was added rapidly. The resultant solution was stirred at room temperature overnight. Afterwards the methanol was added in reaction mixture, precipitates were formed that were filtered and washed with excess of methanol.

bpy(DTP_1-H)

25 was used as starting material. Brown powder was obtained (68 %).

^{1}H NMR-(250 MHz, DMSO-*d6*), δ (ppm): 8.64 (*d*, *J* = 4.8 Hz, 2H); 8.43(*s*, 2H); 7.63 (*d*, *J* = 4.5 Hz, 2H); 7.54 (*m*, 12H); 6.32(*m*, 6H); 7.19 (*s*, 2H); 7.10 (*t*, *J* = 3.4 Hz , 2H); 6.97 (*m*, 4H); 6.74 (*d*, *J* = 2.7 Hz, 2H).

^{13}C NMR-(250 MHz, DMSO-*d6*), δ (ppm): 155.8, 149.8, 146.1, 137.3, 133.4, 130.8, 130.4, 129.9, 129.4, 128.5, 127.3, 127.0, 125.9, 125.4, 124.2, 121.9, 120.5, 117.1, 106.6.

HRMS (APCI) calculated for $C_{50}H_{34}N_4S_4$ $[M+H]^+$: 819.1666. Found: 819.1734.

Anal. Calcd. for $C_{50}H_{34}N_4S_4$: C, 73.32; H, 4.18; N, 6.84; S, 15.66%. Found: C, 72.95; H, 4.17; N, 6.54; S, 15.31%.

UV-vis (DMSO), λmax/nm (ε/10^3 $M^{-1}cm^{-1}$) = 311 (53.9) and 352 (42.1).

bpy(DTP_1-Br)

15 was used as starting material. Yellow powder was obtained (38 %).

^{1}H NMR-(400 MHz, $CDCl_3$), δ (ppm): 8.58 (*d*, *J* = 5.1Hz, 2H); 8.35 (*s*, 2H); 7.46 (*dd*, *J* = 8.6 and 1.8 and Hz, 4H); 7.42 (*d*, *J* = 16.1, 2H); 7.33 (*m*, 4H); 7.18 (*dd*, *J* = 5.1 and 1.0 Hz, 2H); 7.07 (*dd*, *J* = 8.6 and 1.9 Hz, 4H); 7.0 (*m*, 4H); 6.90(*dd*, *J* = 5.1 and 1.4 Hz, 2H); 6.87(*s*, 2H); 6.85(*dd*, *J* = 3.5 and 1.0 Hz, 2H); 6.61 (*dd*, *J* = 3.6 and 1.0 Hz, 2H)**.**

^{13}C NMR- (400 MHz, $CDCl_3$), 157.2, 149.7, 146.9, 137.4, 134.2, 132.3, 131.5, 131.2, 131.0, 130.7, 129.8, 129.4, 129.0, 127.8, 127.3, 127.1, 125.8, 125.3, 124.5, 122.9, 120.3, 118.7, 107.0.

HRMS (APCI) calculated for $C_{50}H_{32}Br_2N_4S_4$ $[M+H]^+$: 974.9873. Found: = 974.9933.

Anal. Calcd. for $C_{50}H_{32}Br_2N_4S_4$: C, 61.48; H, 3.30; N, 5.73; S, 13.13%. Found: C, 61.16; H, 3.47; N, 5.42; S, 12.76%.

UV-vis (DMSO), λmax/nm ($\varepsilon/10^3$ $M^{-1}cm^{-1}$) = 309 (61.0) and 356 (42.4).

bpy(DTP_1-F)

21 was used as starting material. Yellow powder was obtained (31 %).

^{1}H NMR-(250 MHz, $CDCl_3$), δ (ppm): 8.60 (*d*, *J* = 5.3 Hz, 2H); 8.45 (*s*, 2H); 7.39 (*d*, *J* = 16.1 Hz, 2H); 7.33 (*dd*, *J* = 4.1 and 1.0 Hz, 2H); 7.19 (*m*, 8H); 7.03 (*m*, 10H); 6.89(*m*, 4H); 6.64 (*dd*, *J* = 2.6 and 1.0 Hz, 2H).

^{13}C NMR-(250 MHz, $CDCl_3$), δ (ppm): 165.0, 161.1, 149.0, 133.9, 133.8, 133.8, 131.4, 131.3, 131.0, 130.1, 129.9, 127.7, 127.2, 127.1, 125.7, 125.4, 124.0, 122.6, 120.5, 119.3, 116.4, 116.1, 106.8.

HRMS (APCI) calculated for $C_{50}H_{32}F_2N_4S_4$ $[M+H]^+$: 855.1478. Found: 855.1551.

Anal. Calcd. for $C_{50}H_{32}F_2N_4S_4$: C, 70.23; H, 3.77; N, 6.55; S, 15.00%. Found: C, 69.92; H, 3.96; N, 6.85; S, 15.06%.

UV-vis (DMSO), λmax/nm ($\varepsilon/10^3$ $M^{-1}cm^{-1}$) = 309 (52.5) and 360 (39.0).

bpy(DTP_1-Me)

22 was used as starting material. Yellow powder was obtained (75 %).

^{1}H NMR-(250 MHz, $CDCl_3$), δ (ppm): 8.58 (*d*, *J* = 5.0 Hz, 2H); 8.36 (*s*, 2H); 7.48 (*d*, *J* = 16.1

Hz, 2H); 7.31 (*m*, 4H); 7.12 (*m*, 10H); 7.01(*m*, 4H); 6.88(*s*, 2H); 6.86(*t*, *J* = 4.1 Hz, 4H); 6.60 (*d*, *J* =3.4 Hz, 2H); 2.42 (*s*, 6H).

^{13}C NMR-(250 MHz, $CDCl_3$), 157.3, 149.8, 147.2, 139.3, 135.9, 134.8, 132.4, 131.3, 129.7, 127.2, 126.2, 125.4, 124.9, 124.1, 122.4, 120.2, 118.7, 106.7, 21.9

HRMS (APCI) calculated for $C_{52}H_{38}N_4S_4$ $[M+H]^+$: 847.1979. Found: 847.2049.

Anal. Calcd for $C_{52}H_{38}N_4S_4$: C, 73.72; H, 4.52; N, 6.61; S, 15.14%. Found: C, 73.56; H, 4.51; N, 6.63; S, 15.06 %.

UV-vis (DMSO), λmax/nm ($\varepsilon/10^3\ M^{-1}cm^{-1}$) = 310 (58.3) and 360 (42.6).

bpy(DTP$_1$-Hex)

23 was used as starting material. Yellow powder was obtained (36 %).

^{1}H NMR-(400 MHz, $CDCl_3$), δ (ppm): 8.60 (*d*, *J* = 5.0 Hz, 2H); 8.38 (*s*, 2H); 7.35 (*d*, *J* = 16.1 Hz, 2H); 7.30 (*d*, *J* = 5.1Hz, 2H); 7.15 (*m*, 12H); 6.98(*m*, 4H); 6.93(*s*, 2H); 6.86(*t*, *J* = 4.1 Hz, 4H); 6.61 (*dd*, *J* = 2.6 and 0.9 Hz, 2H); 2.67 (*t*, *J* = 7.6 Hz, 4H); 1.63 (*m*, 4H); 1.31 (*m*, 12H); 0.90 (*m*, 6H).

^{13}C NMR-(250 MHz, $CDCl_3$), 157.1, 149.8, 147.1, 144.3, 135.8, 134.8, 131.3, 130.9, 129.5, 129.1, 127.4, 127.2, 126.9, 126.2, 125.2, 124.8, 124.1, 122.3, 120.2, 118.7, 106.4, 35.9, 32.1, 31.51, 29.1, 23.0, 14.5.

HRMS (APCI) calculated for $C_{62}H_{58}N_4S_4$ $[M+H]^+$: 987.3617. Found: 987.3544.

Anal. Calcd. for $C_{62}H_{58}N_4S_4$: C, 75.41; H, 5.92; N, 5.67; S, 12.99%. Found: C, 75.14; H, 5.53; N, 5.59; S, 12.64%.

UV-vis (DMSOλmax/nm ($\varepsilon/10^3\ M^{-1}cm^{-1}$) = 304 (41.6) and 381 (26.0).

bpy(DTP$_2$-F)

34 was used as starting material. Yellow powder was obtained (73 %). Due to poor solubility in organic solvents, NMR spectra could not be obtained.

HRMS (APCI) calculated for $C_{50}H_{32}F_2N_4S_4$ $[M+H]^+$: 855.1478. Found: 855.1551.

Anal. Calcd. for $C_{50}H_{32}F_2N_4S_4$: C, 70.23; H, 3.77; N, 6.55; S, 15.00%. Found: C, 69.96; H, 3.74; N, 6.36; S, 14.94%.

UV-vis (DMSO), λmax/nm ($\varepsilon/10^3\ M^{-1}cm^{-1}$) = 316 (24.9) and 433 (59.5).

bpy(DTP_2-Me)

33 was used as starting material. Brown powder was obtained (46 %). Due to poor solubility in organic solvents, NMR spectra could not be obtained.

HRMS (APCI) calculated for $C_{52}H_{38}N_4S_4$ $[M+H]^+$: 847.1979. Found: 847.2052.

Anal. Calcd for $C_{52}H_{38}N_4S_4$: C, 73.72; H, 4.52; N, 6.61; S, 15.14%. Found: C, 73.34; H, 4.53; N, 6.43; S, 15.01%.

UV-vis (DMSO), λmax/nm ($\varepsilon/10^3\ M^{-1}cm^{-1}$) = 318 (19.1) and 435 (48.2).

bpy(DTP_2-Hex)

32 was used as starting material. Light brown powder was obtained (40 %).

^{1}H NMR-(400 MHz, $CDCl_3$), δ (ppm): 8.59 (*d*, *J* = 5.1 Hz, 2H); 8.43 (*s*, 2H); 7.42 (*d*, *J* = 16.0 Hz, 2H); 7.27 (*m*, 12H); 7.05 (*dd*, *J* = 5.0 and 0.7 Hz, 2H); 6.85 (*d*, *J* = 3.84 Hz, 2H); 6.82 (*dd*, *J* = 4.9 and 3.7 Hz, 2 H), 6.71 (*d*, *J* = 16.0 Hz, 2H); 6.62 (*d*, *J* = 3.8 Hz, 2H); 6.56 (*dd*, *J* = 6.6 and 3.8 Hz, 2H); 6.39 (*d*, *J* = 3.8 Hz, 2H); 2.75 (*t*, *J* = 7.5 Hz, 4H); 1.71 (*m*, 4H); 1.35 (*m,* 12H); 0.91 (*t*, *J* = 6.7 Hz, 6H).

^{13}C NMR-(400 MHz, $CDCl_3$), δ (ppm): 156.89, 149.95, 146.11, 145.15, 139.96, 136.46, 136.21, 135.14, 131.40, 130.31, 129.95, 129.71, 128.71, 127.18, 126.57, 124.63, 124.42, 124.20, 120.86, 117.78, 110.42, 110.05, 36.14, 32.14, 31.67, 29.22, 23.08, 14.56.

HRMS (APCI) calcd for $C_{62}H_{58}N_4S_4$ $[M+H]^+$:987.3617. Found: 987.3614.

Anal. Calcd. for $C_{62}H_{58}N_4S_4$: C, 75.41; H, 5.92; N, 5.67; S, 12.99%. Found: C, 75.14; H, 5.62; N, 5.46; S, 12.61%.

UV-vis (DMSO), λmax/nm ($\varepsilon/10^3\ M^{-1}cm^{-1}$) = 323 (27.5) and 439 (56.1).

9.9. Synthesis of Homoleptic Complexes

Ligand (0.030 mmol) and $RuCl_2(DMSO)_4$ (0.01 mmol, 4.84 mg) were suspended in10 mL ethylene glycol. The mixture was irradiated in the microwave oven (180° C, 250 W, 5 minutes).

On cooling the red solution was poured into saturated aqueous solution of KPF_6. Few drops of acetone were also added and left at room temperature overnight. The dark red solid was formed that was filtered and washed with water and excess of diethyl ether and was dried in desiccator.

$Ru[bpy(DTP_1\text{-}H)]_3 (PF_6)_2$

bpy(DTP_1-H) was used as starting material. Dark red solid was obtained (76 %).

^{1}H NMR-(400 MHz, DMF-*d7*), δ (ppm): 9.03 (*s*, 6H); 7.92 (*d*, *J* = 5.9 Hz, 6H); 7.69 (*m*, 12H); 7.50 (*m*, 24H); 7.38 (*d*, *J* = 6.7 Hz 12H); 7.25 (*d*, *J* = 15.9 Hz , 6H); 7.12 (*s*, 6H); 7.03 (*m*, 12H); 6.97 (*t*, *J* = 4.5 Hz, 6H); 6.75 (d, *J* = 2.8 Hz , 6H).

HRMS (ESI): calculated for $C_{150}H_{102}N_{12}RuS_{12}$ m/z = 1278.2016 $[M - 2PF_6]^{2+}$. Found: 1278.1987.

UV-vis (CH_3CN), λmax/nm (ε/10^3 $M^{-1}cm^{-1}$) = 302 (120.9), 396 (45.1) and 488 (33.0).

$Ru[bpy(DTP_1\text{-}Br)]_3 (PF_6)_2$

bpy(DTP_1-Br) was used as starting material. Dark red solid was obtained (79 %).

^{1}H NMR-(400 MHz, CD_3CN), δ (ppm): 8.43 (s, 6H), 7.56 (m, 24H); 7.46 (m, 12H); 7.32 (m, 12H); 7.19 (d, *J* = 8.2 Hz, 12H), 7.10 (d, *J* = 16.5 Hz, 6H); 7.01 (s, 6H); 6.93 (m, 12H); 6.74 (d, *J* = 2.6 Hz, 6H).

HRMS (ESI): calcd for $C_{150}H_{96}Br_6N_{12}RuS_{12}$ m/z = 1515.9319 $[M - 2PF_6]^{2+}$. Found: 1515.9256.

UV-vis (CH_3CN), λmax/nm (ε/10^3 $M^{-1}cm^{-1}$) = 307 (118.9), 395 (52.3) and 494 (42.3).

$Ru[bpy(DTP_1\text{-}F)]_3 (PF_6)_2$

bpy(DTP_1-F) was used as starting material. Dark red solid was obtained (75 %).

^{1}H NMR-(400 MHz, DMF-*d7*), δ (ppm): 9.06 (s, 6H), 7.93 (d, *J* = 6.0 Hz, 6H); 7.69 (m, 12H); 7.48 (m, 24 H); 7.35 (t, *J* = 8.4 Hz, 12H), 7.20 (d, *J* = 16.0 Hz, 6H); 7.14 (s, 6H); 7.08 (m, 12H); 7.03 (dd, *J* = 5.1 and 1.4 Hz, 6H); 6.85 (d, *J* = 3.6 Hz, 6H).

HRMS (ESI): calculated for $C_{150}H_{96}F_6N_{12}RuS_{12}$ m/z = 1332.1751 $[M - 2PF_6]^{2+}$. Found: 1332.1518.

UV-vis (CH_3CN), λmax/nm (ε/10^3 $M^{-1}cm^{-1}$) = 306 (64.4), 398 (28.2) and 490 (20.2).

$Ru[bpy(DTP_1\text{-}Me)]_3(PF_6)_2$

bpy(DTP_1-Me) was used as starting material. The resultant product was not pure so crude product was purified by column chromatography on silica gel. In the beginning acetone was used as eluent to elute out unreacted ligand then acetone: water: saturated KNO_3 (6:1:0.1) was used to elute out the complex. 75 % of solvent was evaporated and rest was poured into saturated aqueous solution of KPF_6. Few drops of acetone were also added and was left at room temperature overnight. The red solid formed that was filtered and washed with water and diethyl ether and was dried in desiccator (67 %).

^{1}H NMR-(400 MHz, DMF-*d7*), δ (ppm): 9.15 (s, 6H); 7.92 (d, *J* = 5.5 Hz, 6H); 7.68 (m, 16H); 7.53 (d, *J* = 4.8 Hz, 6H); 7.31 (m, 32 H); 7.18 (s, 6H); 7.04 (m; 12H); 7.81 (*m*, 6H); 6.93 (d; *J* = 3.1Hz , 6H); 2.91 (s; 18H).

HRMS (ESI): calculated for $C_{156}H_{114}N_{12}RuS_{12}$ m/z = 1320.2502 $[M - 2PF_6]^{2+}$. Found: 1320.2502.

UV-vis (CH_3CN), λmax/nm (ε/10^3 $M^{-1}cm^{-1}$) = 306 (138.3), 398 (63.0) and 489 (48.3).

$Ru[bpy(DTP_1\text{-}Hex)]_3(PF_6)_2$

bpy(DTP_1-Hex) was used as starting material. The resultant product was not pure so crude product was purified by column chromatography on silica gel. In the beginning acetone was used as eluent to elute out unreacted ligand then acetone: water: saturated KNO_3 (6:1:0.1) was used to elute out the complex. 75 % of solvent was evaporated and rest was poured into saturated aqueous solution of KPF_6. Few drops of acetone were also added and was left at room temperature overnight. The red solid formed that was filtered and washed with water and diethyl ether and was dried in desiccator (63 %).

^{1}H NMR-(400 MHz, DMF-*d7*), δ (ppm): 9.20 (s, 6H); 8.09 (d, *J* = 6 Hz, 6H); 7.82 (m, 12H); 7.62 (d, *J* = 4.8 Hz, 6H); 7.48 (m, 36H); 7.28 (s, 6H); 7.20 (m; 12H); 7.13 (*t*, *J* = 4.8 Hz, 6H); 6.93 (d; *J* = 3.1Hz , 6H); 2.85 (t; *J* = 7.0 Hz; 12H); 1.78 (m; 12H); 1.46 (m; 36H); 1.04 (m; 18H).

HRMS (ESI): calculated for $C_{186}H_{174}N_{12}RuS_{12}$ m/z = 1530.4833 $[M - 2PF_6]^{2+}$. Found:

1530.4938.

UV-vis (CH_3CN), λmax/nm ($\varepsilon/10^3\ M^{-1}cm^{-1}$) = 308 (132.8), 396 (62.1) and 493 (49.9).

$Ru[bpy(DTP_2\text{-}F)]_3\ (PF_6)_2$

bpy(DTP_1-F) was used as starting material. Some unreacted ligand was present along with the complex. In order to remove unreacted ligand the resultant solid was dissolved in acetone. Complex was soluble whereas ligand remained insoluble. The solution was filtered and complex was again precipitated with saturated aqueous solution of KPF_6. Dark red precipitates were obtained that were filtered and washed with water and diethyl ether (65 %).

^{1}H NMR-(400 MHz, DMF-*d7*), δ (ppm): 9.25 (s, 6H); 8.15 (m, 12H); 7.82 (m, 12H); 7.65 (t, *J* = 7.4 Hz, 12H); 7.58 (d, *J* = 4.7 Hz, 12H); 7.38 (d, *J* = 2.9 Hz, 6H); 7.15 (m, 12H); 7.00 (dd, *J* = 8.0 and 3.7 Hz, 12H); 6.92 (dd, *J* = 8.1 and 3.6 Hz, 12H).

HRMS (ESI): calculated for $C_{150}H_{96}F_6N_{12}RuS_{12}$ m/z = 1332.1751 $[M - 2PF_6]^{2+}$. Found: 1332.1698.

UV-vis (CH_3CN), λmax/nm ($\varepsilon/10^3\ M^{-1}cm^{-1}$) = 326 (48.4), 453 (72.3) and 508 (72.7).

$Ru[bpy(DTP_2\text{-}Me)]_3\ (PF_6)_2$

bpy(DTP_2-Me) was used as starting material. Some unreacted ligand was present along with the complex at the end. In order to remove unreacted ligand, the resultant solid was dissolved in acetone. Complex was soluble whereas ligand remained insoluble. The solution was filtered and complex was again precipitated with saturated aqueous solution of KPF_6. Dark red precipitates were obtained that were filtered and washed with water and diethyl ether (40 %).

^{1}H NMR-(400 MHz, DMF-*d7*), δ (ppm): 9.07 (s, 6H); 8.01 (m, 12H); 7.64 (m, 6H); 7.38 (m, 30H); 7.15 (d, *J* = 3.8 Hz, 6H); 6.92 (m, 6H); 6.86 (d, *J* = 15.5 Hz, 6H); 6.76 (m; 12H); 6.69 (d, *J* = 3.3 Hz, 6H); 6.63 (d, *J* = 3.3 Hz, 6H); 2.46 (s, 18H).

HRMS (ESI): calculated for $C_{156}H_{114}N_{12}RuS_{12}$ m/z = 1320.2502 $[M - 2PF_6]^{2+}$. Found: 1320.2426.

UV-vis (CH_3CN), λmax/nm ($\varepsilon/10^3\ M^{-1}cm^{-1}$) = 451 (63.5) and 512 (68.5).

$Ru[bpy(DTP_2\text{-}Hex)]_3 (PF_6)_2$

bpy(DTP_1-Hex) was used as starting material. Dark red solid was obtained (66 %).

^{1}H NMR-(400 MHz, DMF-*d7*), δ (ppm): 9.12 (s, 6H); 7.95 (m, 12H); 7.66 (d, *J* = 5.9 Hz, 6H); 7.44 (m, 30H); 7.15 (d, *J* = 3.7 Hz, 6H); 6.90(t, *J* = 4.7 Hz, 6H); 6.85 (d, *J* = 15.8 Hz, 6H); 6.80 (m; 12H); 6.73 (d, *J* = 3.7 Hz, 6H); 6.70 (d, *J* = 3.7 Hz, 6H); 2.75 (m, 12H); 1.71 (m; 12H); 1.27 (m; 36H); 0.77 (t; *J* = 6.4 Hz 18H).

HRMS (ESI): calculated for $C_{186}H_{174}N_{12}RuS_{12}$ m/z = 1530.4833 $[M - 2PF_6]^{2+}$. Found: 1530.4808.

UV-vis (CH_3CN), λmax/nm ($\varepsilon/10^3\ M^{-1}cm^{-1}$) = 360 (62.7), 443 (75.9) and 513 (78.3).

9.10. Synthesis of Bis-Heteroleptic Complexes

$[Ru\{bpy(DTP_1\text{-}Hex)\}_2(dcbpy)](PF_6)_2$

bpy(DTP_1-Hex) (0.030 mmol, 30 mg), $RuCl_3.3H_2O$ (0.015 mmol, 3.97 mg) and 3 drops of N-ethylmorpholine were suspended into 10 mL DMF. The mixture was irradiated in the microwave oven (160° C, 250 W, 10 minutes). Green solution was obtained. Solvent was evaporated and the solid residue and 4,4′-dicarboxy-2,2′-bipyridine (0.015 mmol, 3.66 mg) was dissolved in 10 mL acetic acid. The mixture was refluxed for 16 h. Then the solution was filtered over celite and filterate was evaporated. The crude solid was dissolved in DMF:methanol (50:50) and subjected to a sephadex LH-20 column by using 30 % DMF solution in methanol as eluting agent. The colored bands were collected. Solvent was evaporated and water was added into resulting solid. Few drops of dilute HNO_3 were added to adjust the pH 3. Saturated aqueous solution of KPF_6 was added in this mixture. Few drops of acetone were also added and left at room temperature overnight. The red solid was formed that was filtered, washed with water and diethyl ether and was dried in desiccator (25.1g; 72 %).

^{1}H NMR-(400 MHz, DMF-*d7*), δ (ppm): 9.55 (brs, 2H), 9.06 (s, 4H), 7.87 (m, 6H), 7.71 (m, 12H), 7.47 (m, 4H), 7.34 (m, 20H), 7.14 (d, *J* = 4.4 Hz, 4H), 6.93 (m, 14H), 6.78 (t, *J* = 2.8 Hz, 4H), 1.63 (brt, 8H), 1.32 (m, 32H), 0.88 (t, *J* = 6.1 Hz, 12H).

HRMS (ESI): calculated for $C_{136}H_{124}N_{10}O_4RuS_8$ m/z = 1160.0562$[M - 2PF_6]^{2+}$. Found:

1160.3252.

UV-vis [CH_3CN:DMSO (4:1)], λmax/nm (ε/10^3 $M^{-1}cm^{-1}$) = 308 (96.5), 406 (49.1) and 479 (38.2).

[Ru{bpy(DTP$_1$-Me)}$_2$(dcbpy)](PF$_6$)$_2$

bpy(DTP$_1$-Me) (0.035 mmol, 30 mg), $RuCl_3.3H_2O$ (0.017 mmol, 4.63 mg) and 3 drops of N-ethylmorpholine were suspended into 10 mL DMF. The mixture was irradiated in the microwave oven (160° C, 250 W, 10 minutes). Green solution was obtained. Solvent was evaporated and the solid residue and 4,4′-dicarboxy-2,2′-bipyridine (0.017 mmol, 4.15 mg) was dissolved in 10 mL acetic acid. The mixture was refluxed for 7 h. Then the solution was filtered over celite and filterate was evaporated. The crude solid was dissolved in 10 % triethylamine solution of methanol and subjected to a sephadex LH-20 column by using 10 % triethylamine solution of methanol as eluting agent. The colored bands were collected. Solvent was evaporated and water was added into resulting solid. Few drops of dilute HNO_3 were added to adjust the pH 3. Saturated aqueous solution of KPF_6 was added in this mixture. Few drops of acetone were also added and left at room temperature overnight. The red solid was formed that was filtered, washed with water and diethyl ether and was dried in desiccator (52 %).

^{1}H NMR-(400 MHz, DMF-*d7*), δ (ppm): 9.73 (brs, 2H), 9.03 (s, 4H), 7.86 (m, 6H), 7.61 (m, 12H), 7.46 (t, *J* = 4.2 Hz, 4H), 7.29 (m, 20H), 6.98 (m, 18H), 6.78 (t, *J* = 3.3 Hz, 4H), 2.39 (s, 12H).

HRMS (ESI): calculated for $C_{116}H_{84}N_{10}O_4RuS_8$ m/z = 1019.1750[M - $2PF_6$]$^{2+}$. Found: 1019.1702.

UV-vis [CH_3CN:DMSO (4:1)], λmax/nm (ε/10^3 $M^{-1}cm^{-1}$) = 311 (109.0), 400 (49.9) and 461 (38.9).

9.11. Synthesis of Tris-Heteroleptic Complexes

Ligand (0.024 mmol) and $[Ru(Cl)_2(p\text{-cymene})]_2$ (0.012 mmol) were suspended in 10 mL of DMF. The mixture was irradiated in microwave oven (70° C, 250 W, 10 minutes), a clear yellow solution was obtained. Once cold, solid 4, 4′-dicarboxy-2,2′-bipyridine (0.024 mmol, 5.86

mg) was added and the mixture was irradiated again (160° C, 250 W, 10 minutes), dark green solution was obtained. On cooling, NH_4NCS (0.24 mmol, 18.26 mg) was added and irradiation was repeated (160° C, 250 W, 10 minutes) that gave dark purple solution. Once cold most of the solvent was evaporated and the flask was filled with water and left it for several hours at room temperature. The dark purple solid was formed that was filtered and washed with water. To purify the product, it was dissolved 10 % triethylamine solution of methanol, and was subjected to a sephadex LH-20 column by using 10 % triethylamine solution in methanol as eluting agent. The major purple band was collected and mixed with 8 mL of water. The methanol was carefully evaporated and in the aqueous solution few drops of dilute HNO_3 were added to obtain pH 3. At this point immediate precipitation was observed that was filtered and washed with water and diethyl ether.

[Ru{bpy(DTP$_1$-H)}(dcbpy)(NCS)$_2$]

bpy(DTP$_1$-H) was used as starting material. Dark purple solid was obtained (40 %).

^{1}H NMR-(400 MHz, DMF-*d7*), δ (ppm): 9.68 (d, *J* = 5.7 Hz, 1H), 9.27 (m, 2H), 9.12 (s, 1H), 8.82 (s, 1H), 8.42 (d, *J* = 5.7 Hz, 1H), 8.28 (s, 1H), 8.19 (d, *J* = 5.7 Hz, 1H), 7.81 (m, 4H), 7.48 (m, 18H), 7.24 (s, 2H), 7.08 (m, 8H), 6.82 (d, *J* = 3.4 Hz, 1H), 6.75 (d, *J* = 3.4 Hz, 1H).

HRMS (ESI): calculated for $C_{64}H_{39}Br_2N_8O_4RuS_6$ $[M - H]^{1-}$ m/z = 1279.5322. Found: 1279.0637$[M - H]^{1-}$

UV-vis [CH_3CN: DMSO (4:1)], λmax/nm (ε/10^3 $M^{-1}cm^{-1}$) = 314 (54.1), 410 (26.8), 540 (13.1)

[Ru{bpy(DTP$_1$-Br)}(dcbpy)(NCS)$_2$]

bpy(DTP$_1$-Br) was used as starting material. Dark purple solid was obtained (42 %).

^{1}H NMR-(400 MHz, DMF-*d7*), δ (ppm): 9.61 (d, *J* = 5.7 Hz, 1H), 9.42 (m, 2H), 9.28 (s, 2H), 8.94 (s, 1H), 8.36 (d, *J* = 5.2 Hz, 1H), 8.29 (d, *J* = 5.8 Hz, 1H), 7.82 (m, 4H), 7.73 (m, 8H), 7.47 (m, 4H), 7.26 (s, 2H), 7.17 (m, 4H), 7.05 (m, 6H), 6.92 (d, *J* = 3.2 Hz, 1H), 6.84 ((d, *J* = 3.2 Hz, 1H).

HRMS (ESI): calculated for $C_{64}H_{39}Br_2N_8O_4RuS_6$ $[M - H]^{1-}$ m/z = 1437.3245. Found: 1437.8731 $[M - H]^{1-}$

UV-vis [CH_3CN: DMSO (4:1)], λmax/nm (ε/10^3 $M^{-1}cm^{-1}$) = 312 (69.6), 406 (32.0), 540 (17.4)

[Ru{bpy(DTP$_1$-F)}(dcbpy)(NCS)$_2$]

bpy(DTP$_1$-F) was used as starting material. Dark purple solid was obtained (45 %).
^{1}H NMR-(400 MHz, DMF-*d7*), δ (ppm): 9.85 (d, *J* = 5.7 Hz, 1H), 9.44 (m, 2H), 9.28 (s, 2H), 9.01 (s, 1H), 8.59 (d, *J* = 5.2 Hz, 1H), 8.38 (d, *J* = 5.8 Hz, 1H), 8.28 (d, *J* = 5.7 Hz, 1H), 7.99 (m, 2H), 7.86 (d, *J* = 4.9 Hz, 1H), 7.80 (d, *J* = 5.6 Hz, 1H), 7.64 (m, 8H), 7.52 (m, 8H), 7.42 (s, 2H), 7.31 (m, 5H), 7.08 (d, *J* = 3.2 Hz, 1H), 7.01 (d, *J* = 3.2 Hz, 1H).
HRMS (ESI): calculated for $C_{64}H_{39}F_2N_8O_4RuS_6$ $[M - H]^{1-}$ m/z = 1315.5131. Found: 1315.0464 $[M - H]^{1-}$
UV-vis [CH_3CN: DMSO (4:1)], λmax/nm (ε/10^3 $M^{-1}cm^{-1}$) = 314 (52.8), 410 (25.8), 540 (12.5)

[Ru{bpy(DTP$_1$-Me)}(dcbpy)(NCS)$_2$]

bpy(DTP$_1$-Me) was used as starting material. Dark purple solid was obtained (47 %).
^{1}H NMR-(400 MHz, DMF-*d7*), δ (ppm): 9.69 (d, *J* = 5.8 Hz, 1H), 9.25 (m, 2H), 9.10 (s, 2H), 8.82 (s, 1H), 8.43 (d, *J* = 5.1 Hz, 1H), 8.21 (d, *J* = 5.8 Hz, 1H), 7.83 (m, 2H), 7.72 (d, *J* = 6.9 Hz, 1H), 7.67 (d, *J* = 4.9 Hz, 1H), 7.45 (m, 6H), 7.32 (m, 8H), 7.16 (m, 3H), 7.03 (m, 4H), 6.91 (d, *J* = 8.7 Hz, 1H), 6.85 (d, *J* = 3.1 Hz, 1H), 6.77 (d, *J* = 3.1 Hz, 1H), 2.43 (s, 3H), 2.38 (s, 3H).
HRMS (ESI): calculated for $C_{76}H_{65}N_8O_4RuS_6$ $[M - H]^{1-}$ m/z = 1308.5953. Found: 1307.0950 $[M - H]^{1-}$.
UV-vis [CH_3CN: DMSO (4:1)], λmax/nm (ε/10^3 $M^{-1}cm^{-1}$) = 313 (31.1), 411(14.3), 541 (6.9)

[Ru{bpy(DTP$_1$-Hex)}(dcbpy)(NCS)$_2$]

bpy(DTP$_1$-Hex) was used as starting material. Dark purple solid was obtained (42 %).
^{1}H NMR-(400 MHz, DMF-*d7*), δ (ppm): 9.69 (d, *J* = 5.9 Hz, 1H), 9.26 (m, 2H), 9.11 (s, 1H), 8.99 (s, 1H), 8.84 (s, 1H), 8.44 (d, *J* = 5.2 Hz, 1H), 8.24 (d, *J* = 5.8 Hz, 1H), 8.12 (d, *J* = 5.7 Hz, 1H), 7.80 (m, 2H), 7.58 (m, 4H), 7.45 (m, 6H), 7.37 (m, 16H), 7.03 (m, 5H), 6.84 (d, *J* = 3.1 Hz, 1H), 6.76 (d, *J* = 3.1 Hz, 1H), 1.64 (m, 4H), 1.32 (m, 16H), 0.91 (m, 3H).

HRMS (ESI): calculated for $C_{76}H_{65}N_8O_4RuS_6$ $[M - H]^{1-}$ m/z = 1147.8523. Found: 1147.2502 $[M - H]^{1-}$.

UV-vis [CH_3CN: DMSO (4:1)], λmax/nm (ε/10^3 $M^{-1}cm^{-1}$) = 314 (67.0), 409 (30.3), 534 (14.7)

[Ru{bpy(DTP$_2$-F)}(dcbpy)(NCS)$_2$]

bpy(DTP$_2$-F) (0.023 mmol, 20 mg) and $[Ru(Cl)_2(p\text{-cymene})]_2$ (0.0115 mmol, 7.04 mg) in 10 mL of ethanol was refluxed for 4 h under argon. After evaporation of solvent, orange colored oil was obtained. Then this crude product and 4,4′-dicarboxy-2,2′-bipyridine (0.023mmol, 5.61 mg) were suspended in 10 mL of DMF and refluxed for 4 h under argon in the dark. Then to the green reaction mixture NH_4NCS (0.51 mmol, 38.51 mg) was added and the mixture for refluxed further for 4 h. The reaction mixture was cooled to room temperature. DMF was evaporated and water was added. Purple precipitates were obtained that were filtered and dissolved in small volume of 30 % DMF solution of methanol and subjected to a sephadex LH-20 column to purify. 30 % DMF solution of methanol was used as eluting agent. The major purple band was collected and mixed with 10 mL of water. The methanol was carefully evaporated and in the aqueous solution few drops of dilute HNO_3 were added to obtain pH 3. At this point immediate precipitation was occurred that was filtered and washed with water and diethyl ether (28 %).

^{1}H NMR-(400 MHz, DMF-*d7*), δ (ppm): 9.58 (d, *J* = 5.8 Hz, 1H), 9.23 (m, 2H), 9.09 (s, 1H), 8.38 (d, *J* = 5.8 Hz, 1H), 8.28 (s, 1H), 8.16 (d, *J* = 5.8 Hz, 1H), 7.79 (m, 3H), 7.61(m, 4H), 7.32 (m, 14H), 6.86 (m, 4H), 6.73 (m, 6H).

HRMS (ESI): calculated for $C_{64}H_{41}F_2N_8O_4RuS_6$ $[M + H]^{1+}$ m/z = 1317.5290. Found: 1317.0594$[M + H]^{1+}$.

UV-vis [CH_3CN:DMSO (4:1)], λmax/nm (ε/10^3 $M^{-1}cm^{-1}$) = 314 (52.8), 410 (25.8), 540 (12.5)

[Ru{bpy(DTP$_2$-Me)}(dcbpy)(NCS)$_2$]

bpy(DTP$_2$-Me) was used as starting material. To purify the product, it was dissolved in DMF, and subjected to a sephadex LH-20 column by using DMF: methanol (1:1) as eluting agent. The major purple band was collected. The solvent was evaporated and the flask was half

filled with water. Few drops of acetone were also added. Few drops of dilute HNO_3 were added to obtain pH 3. At this point immediate precipitation was occurred that was filtered and washed with water and diethyl ether (52 %).

^{1}H NMR-(400 MHz, DMF-*d7*), δ (ppm): 9.64 (d, *J* = 5.8 Hz, 1H), 9.21 (m, 2H), 9.07 (s, 1H), 8.36 (d, *J* = 5.8 Hz, 1H), 8.27 (s, 1H), 8.15 (d, *J* = 5.8 Hz, 1H), 7.76 (m, 2H), 7.38 (m, 16H), 6.94 (m, 4H), 6.73 (m, 9H), 2.49 (s, 3H), 2.45 (s, 3H).

HRMS (ESI): calculated for $C_{76}H_{65}N_8O_4RuS_6$ $[M - H]^{1-}$ m/z = 1308.5953. Found: 1308.0949 $[M - H]^{1-}$.

UV-vis [CH_3CN: DMSO (4:1)], λmax/nm (ε/10^3 $M^{-1}cm^{-1}$) = 320 (23.9), 468(29.8)

9.12. Photovoltaic measurement

9.12.1. TiO_2 electrode preparation

TiO_2 colloidal paste was prepared by hydrolysis of Ti(IV) isopropoxide. The nanocrystalline TiO_2 photoelectrodes were prepared by depositing the paste onto transparent conducting FTO glass (either Delta Technologies or IBE, 7Ω/Square) according to the well known "scotch tape" method. The thin films were allowed to dry at room temperature for 20 min. and finally fired at 450°C for 40 minutes. The still hot electrodes were immersed in the dye solution and kept at 80°C for 5 hours, after which the absorption was deemed complete. The efficiency of absorption was evaluated by UV-Vis spectroscopy: photoelectrodes characterized by an optical density ≥1 at the MLCT maximum of the sensitizer were commonly obtained. Dye solutions were prepared by dissolving a small amount of the Ru(II) complex in solvent mixture [EtOH/CH_3CN/THF/*t*BuOH (1/1/1/1)]. The solutions were sonicated and filtered to remove suspended undissolved dye.

9.12.2. Counter electrodes preparation

Platinum coated counter electrodes were obtained by spraying a 5 x 10-3 M H_2PtCl_6 (Fluka) solution in isopropanol on the well cleaned surface of an FTO glass. This procedure was repeated from 5 to 10 times to obtain a homogeneous distribution of H2PtCl6 droplets. The

electrodes were dried under a gentle air flow and treated in an oven at 380°C for 15 min obtaining the formation of stable platinum clusters. Gold coated electrodes, used with cobalt-based mediators were obtained by thermal vapour deposition on FTO of a 5-7 nm thick chromium adhesion layer followed by a 30-35 nm thick gold layer. The average pressure of the vacuum chamber of the evaporator was about 9×10^{-6} torr.

9.12.3. Photoelectrochemical cell assembly [8, 9, 10]

Parafilm® sealed cells were built by pressing the sensitized photoanode against a counter electrode equipped with a parafilm® frame used to confine the liquid electrolyte inside the cell. The thickness of liquid layer corresponded roughly to the thickness of the frame borders (≅120 μm). In this configuration the cell was stable towards solvent evaporation and leaking for several days even using volatile solvents like acetonitrile. In both cases metallic clamps were used to hold firmly the two electrodes together. The Cobalt-based mediators were prepared according to published procedures.

References

[1] Frisch, M.J.; Trucks, G.W.; Schlegel, H.B.; Scuseria, G.E.; Robb, M.A.; Cheeseman, J.R.; Scalmani, G.; Barone, V.; Mennucci, B.; Petersson, G.A.; Nakatsuji, H.; Caricato, M.; Li, X.; Hratchian, H.P.; Izmaylov, A.F.; Bloino, J.; Zheng, G.; Sonnenberg, J.L.; Hada, M.; Ehara, M.; Toyota, K.; Fukuda, R.; Hasegawa, J.; Ishida, M.; Nakajima, T.; Honda, Y.; Kitao, O.; Nakai, H.; Vreven, T.; Montgomery Jr J.A.; Peralta, P.E.; Ogliaro, F.; Bearpark, M.; Heyd, J.J.; Brothers, E.; Kudin, K.N.; Staroverov, V.N.; Kobayashi, R.; Normand, J.; Raghavachari, K.; Rendell, A.; Burant, J.C.; Iyengar, S.S.; Tomasi, J.; Cossi, M.; Rega, N.; Millam, N.J.; Klene, M.; Knox, J.E.; Cross, J.B.; Bakken, V.; Adamo, C.; Jaramillo, J.; Gomperts, R.; Stratmann, R.E.; Yazyev, O.; Austin, A.J.; Cammi, R.; Pomelli, C.; Ochterski, J.W.; Martin, R.L.; Morokuma, K.; Zakrzewski, V.G.; Voth, G.A.; Salvador, P.; Dannenberg, J.J.; Dapprich, S.; Daniels, A.D.; Farkas, O.; Ortiz, J.V.; Cioslowski, J.; Fox, D.J. *Gaussian 09, revision A.1; Gaussian, Inc.: Wallingford, CT, 2009.*

[2] Nakazaki, J.; Chung, I.; Matsushita, M.M.; Sugawara, T.; Watanabe, R.; Izuoka, A.; Kawada, Y. *J. Mater. Chem*, 2003, **13**, 1011.

[3] Ellinger, S.; Ziener, U.; Thewalt, U.; Landfester, K.; Moller, M. *Chem. Mater*., 2007, **19**, 1070.

[4] Oliva, M.M.; Pappenfus, T.M.; Melby, J.H.; Schwaderer, K.M.; Johnson, J.C.; McGee, K.A.; Filho, D.A.S.; Bredas, J.-L.; Casado, J.; Lopez Navarrete, J. T. *Chem. Eur. J.*, 2010, **16**, 6866.

[5] Ogura, K.; Zhao, R.; Yanai, H.; Maeda, K.; Tozawa, R.; Matsumoto, S.; Akazome, M. *Bull. Chem. Soc. Jpn*., 2002, **75**, 2359.

[6] Fraser, C.L.; Anastasi N.R.; Lamba, J.J.S. *J. Org. Chem.*, 1997, **62**, 9314.

[7] Smith, A.P.; Lamba, J.J.S.; Fraser, C.L. *Org. Synth*. 2004, **10**, 107.

[8] Zabri, H.; Gillaizeau, I.; Bignozzi, C.A.; Caramori, S.; Charlot, M.-F.; Cano Boquera, J.C.; Odobel, F. *Inorg Chem,* 2003, **42**, 6656.

[9] Sapp, S. A.; Elliott, C.M.; Contado, C.; Caramori, S.; Bignozzi, C.A. *J. Am. Chem. Soc.* , 2002, **124**, 11215.

[10] Cazzanti, S.; Caramori, S.; Argazzi, R.; Elliott, C.M.; Bignozzi, C.A. *J. Am. Chem. Soc.*, 2006, **128**, 9996

Résumé

Les cellules solaires à colorant (DSSC) sont une alternative sérieuse aux cellules à base de silicium. Le principe de fonctionnement repose sur la photosensibilisation d'un semi-conducteur par un colorant qui est en général un complexe polypyridinique du ruthénium (II). La modulation des propriétés de ces complexes permet d'optimiser les performances des cellules solaires correspondantes.
Dans cette thèse, nous avons synthétisé et étudié l'effet de nouveaux ligands bipyridiniques à substituants électro-donneurs π-délocalisés à base de dithiénylpyrroles (DTP). Ces motifs induisent, dans les complexes homoleptiques, bis- et tris-hétéroleptiques du Ru(II), des effets bathochromes (lorsque les motifs DTP sont liés par leur cycle thiophénique à la bipyridine) et d'importantes augmentations des coefficients d'extinction molaires. Les nouveaux composés ont été caractérisés par spectroscopies, électrochimie, photophysique et calcul théorique.
Deux complexes hétéroleptiques ont été testés en cellule DSSC. Si la collecte de photons est excellente, les performances restent en dessous de celles de colorants de référence. Comme en attestent les courbes J/V et les courbes IPCE. Ce résultat peut-être dû à une limitation lors de l'injection dans la bande de conduction ou encore à une gêne stéréo-électronique provoquée par le ligand lors de la réduction du colorant oxydé (Ru(III) par le médiateur.

Mots clés
Dithiénylpyrroles, complexes de ruthénium, photosensibilisateurs, effets électroniques, π-délocalisation, cellules solaires à colorants (DSSC).

Abstract

Dye-sensitized Solar Cells (DSSC) appear to be promising devices. Operation principle relies on the photosensitization of a wide-gap semiconductor with a dye, the latter typically being a polypyridinyl ruthenium(II) complex. Modulation of the properties of such complexes enables the optimization of the corresponding solar cells' performances.
In the present work, we synthesized and investigated the effect of new bipyridine ligands bearing electron-donating dithienylpyrroles (DTP). These moieties induced red-shifts of the absorption spectra in homoleptic, bis- and tris-heteroleptic Ru(II) complexes especially when the DTP was bound by its thiophene unit to the bipyridine ligand. A notable increase of the molar extinction coefficients was also obtained. All new compounds have been characterized by using spectroscopic, electrochemical, photophysical and computational chemistry techniques.
Two heteroleptic complexes have been tested in DSSCs. Despite excellent light harvesting properties, performances were found lower than those of standard dyes as revealed by J/V and IPCE curves. Stereoelectronic effects could be involved since the bulky DTP moiety could impede an efficient access of the mediator to Ru(III) centers.

Keywords
Dithienylpyrroles, ruthenium complexes, photosensitization, electronic effects, π-delocalization, Dye-Sensitized-solar cells (DSSC).